ILLINOIS

UNIVERSITY OF ILLINOIS AT URBANA-CHAMPAIGN

PRODUCTION NOTE

University of Illinois at
Urbana-Champaign Library
Large-scale Digitization Project, 2007.

UNIVERSITY OF ILLINOIS
COLLEGE OF ENGINEERING

ENGINEERING EXPERIMENT STATION
BULLETIN 497

INVESTIGATION OF PRESTRESSED REINFORCED CONCRETE FOR HIGHWAY BRIDGES, PART V: ANALYSIS AND CONTROL OF ANCHORAGE-ZONE CRACKING IN PRESTRESSED CONCRETE

by
W. A. Welsh, Jr.
M. A. Sozen

ENGINEERING EXPERIMENT STATION
BULLETIN 497

INVESTIGATION OF PRESTRESSED REINFORCED CONCRETE FOR HIGHWAY BRIDGES, PART V: ANALYSIS AND CONTROL OF ANCHORAGE-ZONE CRACKING IN PRESTRESSED CONCRETE

by

W. A. Welsh, Jr.
Assistant Professor of Civil Engineering
Clemson University

M. A. Sozen
Professor of Civil Engineering
University of Illinois

Price: $3.00

Prepared as part of an investigation
conducted by
The Engineering Experiment Station
University of Illinois
in cooperation with
The State of Illinois
Division of Highways
and
The U.S. Department of Transportation
Federal Highway Administration
Bureau of Public Roads
Project IHR-10
Investigation of Prestressed Reinforced Concrete
for Highway Bridges
Illinois Cooperative Highway Research Program
Series No. 85

Edited by
Ann C. Riggins

REQUESTS FOR THIS PUBLICATION should be addressed to Engineering Publications Office, 112 Engineering Hall, University of Illinois, Urbana 61801. On your order refer to the Bulletin number on the front cover.

UNIVERSITY OF ILLINOIS BULLETIN
Volume 66, Number 17; September 13, 1968. Published twelve times each month by the University of Illinois. Entered as second-class matter December 11, 1912, at the post office at Urbana, Illinois, under the Act of August 24, 1912. Office of Publication, 114 Altgeld Hall, Urbana, Illinois 61801.

ABSTRACT

THIS REPORT SUMMARIZES THE INFORMATION ON ANCHORAGE-ZONE CRACKING OBTAINED IN THE COURSE OF A RESEARCH PROGRAM CARRIED OUT DURING THE PERIOD 1960 THROUGH 1966.

AN ANALYTICAL SOLUTION IS DEVELOPED AND PRESENTED FOR PREDICTING THE POSSIBILITY OF ANCHORAGE-ZONE CRACKING AND FOR THE DESIGN OF TRANSVERSE REINFORCEMENT TO CONTROL SUCH CRACKING. THE IMPLICATIONS OF THE THEORETICAL SOLUTION ARE CHECKED AGAINST RESULTS FROM A TOTAL OF 177 TESTS, 66 OF WHICH WERE CARRIED OUT AS A PART OF THIS RESEARCH PROGRAM. THE VARIABLES COVERED WERE: (A) SIZE AND SHAPE OF CROSS SECTION, (B) ECCENTRICITY OF THE PRESTRESSING FORCE, (C) RATIO OF THE LOADED AREA TO THE CROSS-SECTIONAL AREA, (D) DISTRIBUTION OF THE PRESTRESSING FORCE, (E) TYPE OF PRESTRESSING (POST- OR PRETENSIONED), (F) CONCRETE QUALITY, (G) AMOUNT, TYPE, AND LOCATION OF THE TRANSVERSE REINFORCEMENT AND, (H) TIME-DEPENDENT EFFECTS.

DESIGN RECOMMENDATIONS ARE PRESENTED ALONG WITH A NUMERICAL EXAMPLE IN CHAPTER VI WHICH CAN BE STUDIED INDEPENDENTLY OF THE REST OF THE REPORT.

ACKNOWLEDGMENTS

This study was carried out as a part of the research under the Illinois Cooperative Highway Research Program Project IHR-10, "Investigation of Prestressed Reinforced Concrete for Highway Bridges." The work on the project was conducted by the Department of Civil Engineering of the University of Illinois in cooperation with the Division of Highways, State of Illinois, and the U.S. Department of Transportation, Bureau of Public Roads.

At the University, the work covered by this report was carried out under the general administrative supervision of W. L. Everitt, Dean of the College of Engineering, Ross J. Martin, Director of the Engineering Experiment Station, N. M. Newmark, Head of the Department of Civil Engineering, and Ellis Danner, Director of the Illinois Cooperative Highway Research Program and Professor of Highway Engineering.

At the Division of Highways of the State of Illinois, the work was under the administrative direction of Virden E. Staff, Chief Highway Engineer, and J. E. Burke, Engineer of Research and Development.

The program of investigation has been guided by a Project Advisory Committee consisting of the following:

Representing the Illinois Division of Highways:

J. E. Burke, Engineer of Research and Development, Illinois Division of Highways

Floyd K. Jacobsen, Bureau of Design, Illinois Division of Highways

C. E. Thunman, Jr., Engineer of Bridge and Traffic Structures, Bureau of Design, Illinois Division of Highways

Representing the Bureau of Public Roads:

E. L. Erickson, Chief, Bridge Division, Bureau of Public Roads

Representing the University of Illinois:

C. E. Kesler, Professor of Theoretical and Applied Mechanics

Narbey Khachaturian, Professor of Civil Engineering

W. J. Mackay, Illinois Division of Highways, also participated in the meetings of the Advisory Committee and contributed materially to the guidance of the program.

The investigation was directed by Dr. C. P. Siess, Professor of Civil Engineering, as Project Supervisor and as ex-officio chairman of the Project Advisory Committee. Immediate supervision of the investigation was provided by Dr. M. A. Sozen, Professor of Civil Engineering, as Project Investigator.

Acknowledgment is due to R. J. Lenschow for his assistance in the modification of the analysis for the design of transverse reinforcement.

This report was written as a thesis under the direction of Professor M. A. Sozen.

Appreciation is also extended to the reviews of this Bulletin: F. K. Jacobsen, Illinois Division of Highways; Professor W. L. Gamble, University of Illinois; and Dr. Peter Gergely, Cornell University.

CONTENTS

This page is intentionally blank.

FIGURES

This page is intentionally blank.

TABLES

This page is intentionally blank.

I. INTRODUCTION

1.1 INTRODUCTORY REMARKS

Longitudinal cracking in the anchorage zones of prestressed concrete beams has been reported in field studies[10,16]* and in laboratory investigations. The cracks have been observed in both post-tensioned and pretensioned girders with rectangular, I-shaped or T-shaped cross sections.

Longitudinal cracks in the anchorage zone result from the transverse tensile stresses produced as the prestress force "flows" from the region of force concentration to the region in which the longitudinal stresses are linearly distributed. Two zones in which longitudinal cracking may occur have been identified (Figure 1). The first zone is the bursting stress zone which occurs a short distance from the beam end on the axis of the applied force. The second zone is the spalling stress zone. Cracks in the spalling zone start on the end face of the beam at some distance from the point of application of the applied force and propagate parallel to the axis of the beam.

Transverse reinforcement has been used to restrain the development of spalling cracks and to postpone the formation of bursting cracks. The formation of a bursting crack generally occurs simultaneously with the failure of the anchorage zone. However, spalling cracks are not detrimental to the performance of the beam as long as they are restrained by the transverse reinforcement.

1.2 OBJECT AND SCOPE

The main object of the investigation described in this report was to develop an understanding of the need for and action of transverse reinforcement in the anchorage zone of prestressed concrete beams. The investigation included both theoretical and experimental work leading to a design procedure.

The results of experimental investigations at four laboratories are presented and discussed. These investigations are: (1) tests at the University of Illinois by Gergely[12] and by Welsh, (2) tests at the Portland Cement Association Research and Development Laboratories (Skokie) by Marshall and Mattock[28] and by Kriz and Raths,[23] (3) tests at the University of Glasgow by Arthur and Ganguli,[1] and (4) tests at the Cement and Concrete

*Superscript numbers in parentheses refer to entries in References, Chapter VIII.

Association by Zielinski and Rowe.[48]

The primary variables included in these test programs were: (1) shape of cross section, (2) eccentricity of the prestressing force, (3) type of prestressing (post- or pretensioned), (4) ratio of loaded area to cross-sectional area, (5) distribution of the prestressing force, (6) concrete quality, (7) time-dependent effects, and (8) amount, location, and properties of the transverse reinforcement.

The object of the theoretical investigation was the development of a simple and accurate solution for the transverse stresses produced by the prestress force. This analysis was modified to apply to cracked sections reinforced with transverse stirrups.[24] A design procedure incorporating this analysis is proposed in Chapter VI and some numerical examples are given.

1.3 NOTATION

a = $\frac{1}{2}\sqrt{2\sqrt{S}+R}$

A = total area of cross section

A_1, A_2, A_3, A_4 = constants

A_b = area of section below the reference plane

A_m = amplitude of a sine function

A_s = cross-sectional area of one reinforcing bar

b = width of cross section at the reference plane

b' = width of loaded area

b_{eq} = average width of the cross section over the distance c

B, B_1, B_2, B_3, B_4 = constants

c = distance from the reference plane to the centroid of the section below the reference plane

C, C_1, C_2, C_3, C_4 = constants

D_1, D_2, D_3, D_4 = constants

e = eccentricity of the total prestressing force measured from the centroid of the cross section

e_1 = eccentricity of prestressing force acting on the section below the reference plane measured from the centroid of the same section

e_2 = distance between the reference plane and the centroid of the section below the reference plane

E = modulus of deformation

E_c = modulus of deformation for concrete

E_s = modulus of deformation for steel

f'_c = compressive strength of concrete (6 x 12-in. cylinder)

f_{te} = effective tensile strength of concrete

f_o = force per unit length of beam in transverse reinforcement (distributed load)

f_{oc} = force per unit length of beam in transverse reinforcement (concentrated load)

F = spring force per unit length

F_o = stirrup force with no tensile strength in concrete

F_1 = stirrup force with tensile strength in concrete

g = $\frac{1}{2}\sqrt{2\sqrt{S}-R}$ and unit bond force

G = shear modulus

h = height of cross section

h_b = distance of reference plane above the bottom edge of the cross section in rectangular beams

I = moment of inertia of the whole cross section

I_b = moment of inertia of the section below the reference plane

k = spring stiffness

M = moment

M_{cr} = value of M_o at cracking

M_o = moment applied to the section above or below the reference plane

M_{pb} = moment produced by load applied to section below the reference plane about the centroid of the same section

M_{pt} = moment produced by load applied to section above the reference plane about the centroid of the same section

M_v = moment of the shear force on the reference plane about the centroid of the section below the reference plane

M_t = moment of the total prestressing force about the centroid of the section

P = total applied prestressing force

P_o = portion of the prestressing force applied to the symmetrically loaded portion of the physical analog

P_1 = portion of the prestressing force applied to the bottom part of the analog in the unsymmetrical case

P_2 = portion of the prestressing force applied to the top part of the analog in the unsymmetrical case

Q = shear force

r = $\frac{1}{2}\sqrt{R-2\sqrt{S}}$

R = $\frac{\gamma k}{A_b G}$

S = $\frac{k}{E_c I_b}$

t = height of loaded area

T = strand transfer length

V = total shear force on the reference plane

V_o = shear force on the reference plane of the analog in the symmetrical case

V_1 = shear force on the reference plane of the analog in the unsymmetrical case

W = width of crack

x = distance measured along the beam

y = deflection of the springs

Z = length of spalling crack

Z_o = crack length assuming no tensile strength in the concrete

Z_1 = crack length assuming tensile strength in the concrete

α = argument

β = angle

γ = shape factor for shear deflection

Δ = displacement

ε_y = transverse strain

η = real axis

λ = one-half wave length of a sine function

μ = Poisson's ratio

ξ = imaginary axis

σ_{bc} = bursting stress under a concentrated load

σ_b = bursting stress under a distributed load

σ_{end} = transverse stress at beam end

σ_s = spalling stress

σ_t = transverse stress

σ_x = longitudinal stress

σ_y = transverse stress

τ, τ_{xy} = shear stress

ϕ = Airy's stress function

II. ANALYSIS OF THE ANCHORAGE-ZONE PROBLEM

2.1 INTRODUCTORY REMARKS

Previous investigators of the anchorage-zone problem in prestressed concrete beams or of other related concentrated-load problems have used a variety of analytical methods. The majority of analyses have been two-dimensional in nature and have been confined to the investigation of the stresses in post-tensioned beams of homogeneous, isotropic, and linearly elastic materials. Several investigators have considered anchorage-zone stresses in three dimensions. In the past few years only a few attempts have been made to develop an analysis that considers the problems arising in pretensioned beams.

The analytical methods used in previous investigations can be classified into five main groups:

(1) In the first group, the anchorage-zone problem is considered to be a problem in elasticity. The two-dimensional Airy stress function is used to obtain a solution. The majority of the analytical investigations belong in this group. Bleich,[3] Guyon,[14,15] Iyengar,[22] Schleeh,[40] Douglas and Trahair,[8] and Som and Ghosh[43] have expressed the results of their analyses in terms of infinite series. Schleeh bases his method of analysis on Fadle's tables for the elastic stresses in a plate loaded with planar forces.[9] Huang,[20] Sargious,[38,39] Gergely,[12] and Gerstner and Zienkiewicz[13] used finite differences to express the results of their analyses.

(2) In the second group, photoelasticity was used to obtain the elastic stress distributions for specific arrangements of the prestressing force. Photoelastic investigations of the stresses in the anchorage zone have been made by Christodoulides,[4,5,6] Mahajan,[26] Sargious,[38,39] Srinivasagopalan,[44] and Hiltscher and Florin.[18,19] Both two-and three-dimensional investigations have been conducted.

(3) The analytical methods in the third group were based on a lattice analogy to the problem. Lattice analogies were used by Ross[34] and by Ramaswamy and Goel.[32] This method of analysis requires lengthy numerical calculations and is at best a check on the theory of elasticity solutions rather than a general approach.

(4) In the fourth group are the analyses that are based on the equations for beams on elastic foundations. Lenschow[24] and Dodge[7] have presented analyses that belong to this group. Lenschow has extended his analysis to permit both the calculation

of the transverse stresses in an uncracked anchorage zone and the determination of the stirrup force in a cracked anchorage zone.

(5) The fifth group of analytical methods contains what may be referred to as the "simplified methods." These analyses use an equilibrium approach with some approximate assumptions that make a relatively simple solution possible. Sievers[41,42] proposed an approximate method to determine the transverse stresses along the longitudinal axis of a symmetrically loaded post-tensioned beam. Morsch[31] used a truss analogy to find the stresses in eccentrically loaded concrete blocks. Magnel[25] developed an approximate solution for the stresses in the anchorage zone of a post-tensioned beam by assuming that the distribution of transverse stresses on any longitudinal plane could be represented by a cubic parabola. Garay[11] proposed a model to simulate the behavior of the anchorage zone. The model consisted of three longitudinal stringers, representing the flanges and web of the beam, connected by a plate. The stringers were assumed to support only longitudinal stresses while the plate carried the shear and transverse stresses. A simplified method for the design of transverse reinforcement was proposed by Gergely.[12] He assumed that the transverse tensile force in the concrete could be neglected and that the centroid of the transverse compressive stresses was at a distance h from the beam end (h is the height of the cross section). The principal disadvantage of the simplified methods of analysis is that, in effect, they assume the solution to the problem before they start. They are, however, simple to apply in specific cases.

The majority of previous investigations of the anchorage-zone problem have had two objectives in common. The first objective was to develop an analysis for the calculation of the prestress force which would produce longitudinal cracking in the anchorage zone. The second objective was to develop a procedure for the design of transverse reinforcement to restrain the propagation of the longitudinal cracks. Thus, the most general method of analysis for the anchorage-zone problem would be an analysis that gives both an estimation of the stress distribution before cracking and an approximation of the behavior after cracking.

All but one of the analyses mentioned above are concerned with the calculation of the elastic stress distribution in homogeneous, isotropic, and linearly elastic materials. The elastic distribution of stress can be used to predict, within reasonable limits, the cracking load of a concrete anchorage zone even though concrete is not a homogeneous, isotropic, and elastic material. However, the methods of analysis based on the elastic stress distribution cannot be used for the design of transverse reinforcement. The concrete must be cracked before the reinforcement can be used effectively. The formation of a crack invalidates the elastic stress distribution. Only Gergely[12] and Lenschow[24] have proposed analyses for the design of reinforcement which take into consideration the formation of longitudinal

cracks. Of these two analyses, Lenschow's analysis is the most versatile because it can be used to calculate the cracking load as well as the amount of transverse reinforcement needed to restrain the cracks. Furthermore, it can be extended to cover the cases of three-dimensional problems and pretensioned beams after cracking. Consequently, it will be used in order to analyze the test results reported. The method is described in the following sections.

2.2 THE PHYSICAL ANALOG

The distribution of the transverse stresses in the anchorage zone of a beam subjected to a concentrated load acting parallel to the longitudinal axis is pictured in Figure 1. The deflections of the fictitious springs inserted across the longitudinal cuts in the beam are related to the transverse stresses. The transverse tensile stress across the axis of the load will be referred to as the "bursting stress," while the transverse tensile stress across any other longitudinal plane will be called the "spalling stress." The distribution of the bursting and spalling stresses can be visualized from this figure. The physical analog representing the anchorage zone is related to the approach shown in Figure 1.

The physical analog for the anchorage zone of a post-tensioned beam is shown in Figure 2. The prismatic beam shown in Figure 2a is subjected to a concentrated load P. The transverse stresses across a longitudinal plane called the reference plane are to be found. The beam in Figure 2a can be represented by the beams in Figure 2b and 2c. The loading and introduced cuts in Figure 2b are symmetrical about the beam centroid. One of the cuts is along the reference plane. Fictitious springs inserted in the cuts represent the concrete and resist the deflection of the outer parts of the beam. The cut in Figure 2c is at the level of the reference plane. The loading in this figure is adjusted so that the two parts of the cut beam have the same curvature. Therefore, fictitious springs are not required.

The loading conditions in Figure 2b and 2c when superimposed should yield the loading in Figure 2a. To satisfy this criterion:

$$P_o - P_2 = 0 , \qquad (1)$$

$$P_o + P_1 = P , \qquad (2)$$

$$V_o + V_1 = V , \qquad (3)$$

where V is the shear that would exist on the reference plane. The sign convention for a portion of the beam below the reference plane is shown in Figure C1.* Positive moment produces compression in the top fibers, while positive shear produces a clockwise rotation of the element. The transverse stress is considered positive when in tension. The applied bending moment in Figure 2b can be written as:

$$M_o = -P_o e_1 - V_o e_2 , \qquad (4)$$

*Figure numbers beginning with A, B, and C refer to figures associated with the Appendix; however, they are located in the center of the book after the figures which deal directly with the main text.

where M_o is the equivalent moment applied to the section below the reference plane. The curvature of the bottom portion of the beam in Figure 2c conforms with the curvature of the whole beam in Figure 2a if (ignoring end disturbances):

$$(P_1 e_1 + V_1 e_2)/E_c I_b = Pe/E_c I \qquad (5)$$

in which I_b is the moment of inertia of the portion of the beam below the reference plane, I is the moment of inertia for the whole beam, and E_c is the modulus of deformation for concrete.

Combining Equations (1) through (5):

$$P_o e_1 + V_o e_2 = Pe_1 + Ve_2 - PeI_b/I \qquad (6)$$

or

$$M_o = M_{pb} + M_v - M_t I_b/I, \qquad (7)$$

where M_{pb} and M_v refer to the moments produced by the load and shear acting on the section of the beam below the reference plane. M_t is the moment on the entire beam. The moments M_{pb}, M_v, and M_t are assumed to act in the direction of positive moment. Equation (7) is a general equation for the moment applied to the analog and is valid for pretensioned as well as post-tensioned beams. The procedures for determining the quantities M_{pb}, M_v, and M_t and the assumptions on which they are founded are given in Sections 2.3 and 2.4 for post-tensioned and pre-tensioned beams.

The portion of the analog below the reference plane may now be treated as a beam on an elastic foundation. The major problem involved is the determination of the spring stiffness, k, so that the response of the analog is the same as that of the intact beam. The derivation of the spring constant k is given in Appendix C. The spring force per unit of length is:

$$F = ky, \qquad (8)$$

where y is the deflection of the springs.

The deflection of a beam on an elastic foundation can be expressed as:

$$y = e^{-ax}(C_3 \cos gx + C_4 \sin gx) \qquad (9)$$

in which x is the distance from the beam end. The terms a and g are related to the stiffnesses of the beam and springs. The constants C_3 and C_4 are determined from the boundary conditions. Equation (9) is derived in Appendix C. The transverse stress can be found from Equations (8) and (9) and is:

$$\sigma_t = F/b$$

$$= \frac{ke^{-ax}}{b}\left(C_3 \cos gx + C_4 \sin gx\right). \qquad (10)$$

The magnitude of the applied load at the initiation of longitudinal cracking in the anchorage zone can be determined from Equation (10) if the maximum value of the stress σ_t is equated to the effective tensile strength of the concrete. The effective tensile strength of the concrete may vary along the length of the beam as shown in Figure 3. Figure 3a shows the uniform distribution of effective tensile strength that was assumed by Lenschow. Figure 3b shows how shrinkage stresses may modify the effective tensile strength envelope in a real beam. The effect of small variations in the effective tensile strength envelope on the behavior of the test specimens described in Chapter III will be discussed in Sections 5.1, 5.2, and 5.3.

2.3 ANALYSIS FOR POST-TENSIONED BEAMS

The forces applied to the portion of the analog below the reference plane in a post-tensioned beam are shown in Figure 4a. The shear, V, acting along the reference plane is determined by considering a free body of the section. The stresses σ_x shown in Figure 4a represent the linear longitudinal stress distribution calculated from the applied load and the section properties of the whole beam. The shear, V, is assumed to be concentrated at the beam end. The error involved in this assumption is on the safe side and is small as long as the loads are concentrated in a group. The shear distribution is discussed in Appendix C.

The constants in Equation (10) are determined in Appendix C. Substituting the constants into Equation (10) gives:

$$\sigma_t = \frac{-M_o}{b}\sqrt{\frac{k}{E_c I_b}}\, e^{-ax}\left(\cos gx - \frac{a}{g}\sin gx\right). \quad (11)$$

It can be seen pictorially in Figure 1 that the maximum spalling stress occurs at the end of the beam, i.e., at x = 0 for Equation (11). Thus, the maximum spalling stress on a given reference plane is:

$$\sigma_s = \frac{-M_o}{b}\sqrt{\frac{k}{E_c I_b}} \; . \quad (12)$$

The maximum bursting stress occurs a short distance from the beam end. The value of x corresponding to the position of the maximum bursting stress produced by a concentrated load is:

$$x = \frac{1}{g}\,\text{artan}\left(\frac{4ag}{R}\right) . \quad (13)$$

Substituting Equation (13) into Equation (11) gives the maximum value of the bursting stress. This can be done without difficulty although the calculations may be laborious. Lenschow, therefore, proposed the simplified expression given below for the maximum bursting stress produced by a concentrated load.

$$\sigma_{bc} = \frac{1}{2\sqrt{6}}\,\frac{M_o}{b}\sqrt{\frac{k}{E_c I_b}} \; . \quad (14)$$

The spring constant, k, is derived in Appendix C. It can be taken as:

$$k = \frac{b_{eq} E_c}{c} \; , \quad (15)$$

where c is the distance from the reference plane to the centroid of the portion of the physical analog below the reference plane. The term b_{eq} is the imaginary width of the beam at the reference plane. It is equivalent to the real geometric form with respect to the spring constant. The term b_{eq} may be taken as the average effective thickness over the distance c. The effective thickness is determined from the assumption that the transverse stresses spread out at a 45-degree angle wherever there is a change in section.

For a beam of rectangular section, $b_{eq} = b$ and $c = h_b/2$, where h_b is the height of the section below the reference plane. The expressions for the maximum spalling and bursting stresses given in Equations (12) and (14) become:

$$\sigma_s = \frac{-M_o\, 2\sqrt{6}}{b\, h_b^2} \quad (16)$$

and

$$\sigma_{bc} = \frac{M_o}{b\, h_b^2} \; . \quad (17)$$

Substituting Equation (13) into Equation (11) gives the following for the maximum bursting stress in a rectangular beam.

$$\sigma_{bc} = \frac{0.72M_o}{b\,h_b^2} \quad . \qquad (18)$$

The bursting stress given by Equation (18) is 28 per cent less than that given by Lenschow's approximation in Equation (17).

The quantities on the right-hand side of the preceding equations are for a given position of the reference plane. The reference plane on which the spalling stress is a maximum can be found in a few trials. For a rectangular section subjected to a single load at an eccentricity e, the following expression locates the reference plane on which the spalling stress is a maximum.

$$\frac{2eh_b^3}{h^4} - \frac{h_b}{h} + \left(1 - \frac{2e}{h}\right) = 0 . \qquad (19)$$

This expression can be solved by trial and error for h_b for any given value of e. A simplified approximation of Equation (19) is given by Lenschow.

$$\frac{h_b}{h} = \frac{1}{2} - \frac{1}{3}\left(\frac{7e}{h} - 2\right) . \qquad (20)$$

The ratio h_b/h given by Equation (20) is very close to that given by Equation (19) for $e/h > 0.2$. For $e/h < 0.2$ the spalling stress is small compared to the bursting stress, and Equation (20) underestimates the ratio of h_b/h.

The influence of the load distribution on the spalling stresses is usually negligible and is not reflected by the analog. The distribution of load, however, does influence the bursting stress. If the centroids of the loaded area and cross section do not coincide, part of the distributed load has to be applied to the portion of the analog above the reference plane. Since this portion of the analog is to have no curvature, this would violate the basic assumption on which the analysis of the analog was based. This problem was solved by observing Guyon's values for the variation in bursting stress caused by a uniform load as compared with that caused by a concentrated load. This variation could be approximated closely by a linear expression having the form

$$\frac{\sigma_b}{\sigma_{bc}} = 1 - \frac{bt}{A}\left(3 - 4\,\frac{A_b}{A}\right) , \qquad (21)$$

where σ_b is the bursting stress under a distributed load, σ_{bc} is the bursting stress under a concentrated load, A_b is the area of the section below the reference plane, and A is the area of the whole cross section.

2.4 ANALYSIS FOR PRETENSIONED BEAMS

In a pretensioned beam the prestressing force is transferred by bond from the prestressing steel to the concrete. The bond force distribution along the strand is a complex problem in itself, but from the work of Rusch and Rehm[37] it seems justified to assume that it is uniform over the transfer length T. The assumed distribution of prestressing force in a pretensioned beam is shown in Figure 4b.

The assumption that the shear force on the reference plane is concentrated at the end of the beam is on

the safe side for post-tensioned beams, but is too conservative for pretensioned beams. The shear on the reference plane in a pretensioned beam is assumed to be distributed uniformly over the transfer length as shown in Figure 4b.

The applied moments from the prestressing force and from the shear have the same distribution. Thus, the total applied moment is:

$$M = M_o \, x/T \text{ for } 0 \leq x \leq T \qquad (22)$$

and

$$M = M_o \text{ for } x \geq T \, . \qquad (23)$$

The moment M is equivalent to the moment produced by two equal transverse forces M_o/T applied to the portion of the analog below the reference plane (Figure C2). If the shearing deflection is included, the deflection at x = 0 for a beam supported by a series of springs (stiffness k) and subjected to a moment M can be found using Maxwell's law of reciprocity and Equation (9) with suitable boundary conditions. The deflection at x = 0 is:

$$y_o = \frac{-2aM_o}{kT}\left(1-e^{-aT}\cos gT\right) - \frac{RM_o}{2gkT} e^{-aT} \sin gT. \qquad (24)$$

The spalling stress at x = 0 for a pretensioned beam is then:

$$\sigma_s = \frac{-M_o}{bT}\left[2a(1-e^{-aT}\cos gT) + \frac{R}{2g} e^{-aT} \sin gT\right], \qquad (25)$$

where a, g, and M_o are as defined in Section 2.3 for post-tensioned beams. In the discussion in Section C.2.2 in the Appendix, it is shown that Equation (25) should be used only for T > h/2. If T is less than h/2, Equation (12) should be used. In most practical cases the terms containing e^{-aT} are negligible. Therefore, Equation (25) can be simplified to:

$$\sigma_s = \frac{-2aM_o}{bT} \, , \qquad (26)$$

with the additional requirement that the spalling stress given by Equation (26) not exceed that given for a post-tensioned beam in Equation (12).

2.5 THE PHYSICAL ANALOG FOR THE CRACKED BEAM

It was mentioned in Section 2.1 that a longitudinal crack must form in the anchorage zone before the transverse reinforcement can be used effectively. Thus, the analog previously described must be modified to admit a crack if it is to be used to design reinforcement. Figure 5 shows a portion of the analog containing a crack and one line of transverse reinforcement. The springs along the length of the crack have been removed. The maximum stress in the concrete at the end of the crack is equal to the effective tensile strength of the concrete.

The equations pertaining to the analog for the cracked beam are derived in Appendix C. The following paragraphs will present the main expressions for the design of stirrup reinforcement, and will show the procedure to be used in comparing the analysis with the test results.

It is shown in Appendix C that the relationship between crack length and

crack width is:

$$d_1 Z^3 + d_2 Z^2 + d_3 Z + d_4 = 0 , \quad (27)$$

where

$$d_1 = \frac{f_{te} b \sqrt{S}}{3} - \frac{M_o S}{6} , \quad (28)$$

$$d_2 = 2 f_{te} b a - M_o a \sqrt{S} , \quad (29)$$

$$d_3 = f_{te} b \frac{2R + \sqrt{S}}{\sqrt{S}} - M_o (\sqrt{S} - R) - \frac{Wk}{2} , \quad (30)$$

$$d_4 = \frac{-Wak}{\sqrt{S}} , \quad (31)$$

in which Z is the crack length, W is the crack width, and f_{te} the effective tensile strength of the concrete. If the effective tensile strength varies along the length of the beam, it may be expressed as a function of Z and substituted into Equations (28), (29), and (30). In the following discussion it will be assumed that the effective tensile strength is constant along the beam unless specifically stated otherwise. The stirrup force can be obtained from the following equation once the crack length is known:

$$F_1 = \frac{f_{te} b - M_o \sqrt{S}}{2a + Z \sqrt{S}} . \quad (32)$$

For a given beam and given values of the applied load, effective tensile strength, and modulus of deformation for concrete, the relationships between crack length, crack width, and stirrup force given by Equations (27) and (32) may be plotted as shown in Figure 6. Also shown in Figure 6 is a force-slip curve for the stirrup reinforcement. The intersection of the force-slip curve and the curve given by Equations (27) and (32) gives the stirrup force and crack width that would be expected to occur in a beam. The procedure illustrated in Figure 6 will be used to analyze the test results in Chapter V. Some simplification of Equations (27) and (32) for design are given in Chapter VI.

2.6 COMPARISON OF LENSCHOW'S ANALYSIS WITH THE RESULTS OF OTHER SOLUTIONS

The major investigations of the anchorage-zone problem were described briefly in Section 2.1. The purpose of this section is to compare the results from Lenschow's analysis with the results from some of the well known solutions for some specific cases of loading.

The bursting stress distribution under a concentric load is shown in Figure 7 as given by Guyon, Magnel, Schleeh, and Lenschow. It can be seen that the distributions are similar and that the magnitude of the maximum stress does not vary greatly. The bursting stress distribution under a concentrated eccentric load is shown in Figure 8 as given by Guyon and Lenschow. The drastic reduction in the number of curves shown reflects the fact that few solutions have been obtained for eccentrically loaded specimens.

The spalling stresses given by Guyon, Gergely, and Lenschow are compared in Figure 9. Comparisons of the stresses on other reference planes show the same trends. It can be seen in Figure 9 that all three solutions give the same general distribution of transverse stress and also approximately the same maximum values.

III. TESTS AT THE UNIVERSITY OF ILLINOIS

3.1 INTRODUCTORY REMARKS

The objectives of the investigation described in this chapter were twofold: (1) to obtain an understanding of the need for transverse reinforcement and (2) to observe the effect of reinforcement on the anchorage zone of post-tensioned beams. The total number of 66 test specimens was divided into three groups: specimens without transverse reinforcement in the anchorage zone, specimens with transverse reinforcement, and reinforced specimens subjected to sustained loads. The dimensions of the specimens are shown in Figure A3 and data on the properties of the specimens are given in Tables 8 and 9.

The controlled variables investigated were: (1) shape of specimen cross section, (2) amount of transverse reinforcement, (3) contribution of the concrete tensile force at the level of the expected crack, (4) concrete shrinkage, and (5) effect of sustained load. Strains in the concrete were measured in three rectangular specimens and in one I-specimen. Transverse reinforcement strains were measured in ten rectangular and eight I-specimens. The width and propagation of spalling cracks were measured in 42 rectangular and eleven I-specimens. The testing arrangement for the specimens is shown in Figure A8. The test procedure is described in Section A.4 in the Appendix.

3.2 SPECIMENS WITHOUT TRANSVERSE REINFORCEMENT

3.2.1 Concrete Strains in Rectangular Beams

Transverse concrete strains were measured across longitudinal lines in the bursting and spalling zones of three rectangular specimens. In particular, transverse strains across the axis of the load and the center line were used to compare some aspects of the phenomena in the two zones.

The variation of transverse strain across the load axis is shown in Figures 10, 11, and 12 for specimens R1, R2, and R3. Specimens R1 and R3 failed in bearing at loads of 38.8 and 47 kips. Specimen R2 carried a load of 53.5 kips without failure. It can be seen that nonlinear response started at a load of about 15 kips in specimen R1 and 25 kips in specimens R2 and R3. This observation was consistent with the lower failure load in R1.

The measured distribution of transverse strain along the axis of the

applied load is typical of bursting strains. Representative curves in Figure 13 show that a maximum value was reached approximately one in. from the end of the beam. The tensile strains decrease toward the end face and center of the specimen.

The relationships between load and transverse strain measured across the center lines of specimens R2 and R3 are shown in Figure 14. The strain reversal must indicate cracking elsewhere in the specimen. The progress of the crack is shown by the reversal of strain in the gage nearest the end followed in turn by the other gages. The cracks in both beams became visible about 0.5 in. from the center line at a load of approximately 24 kips. The contraction indicated is attributable to the transverse shrinkage stresses which were released when the crack formed near the gages. Tensile shrinkage stresses were produced on the surface of the specimen as a result of the differential-shrinkage strains throughout the specimen cross section. When the shrinkage stresses were released by cracking, the area of the specimen which was in tension contracted producing the compressive strains observed in the tests.

The distribution of transverse strains along the center line are typical of spalling strains. Representative curves in Figure 13 show that the strains decrease steadily toward the center of the specimen.

Comparison of Figures 11 and 14 indicates that cracking in the spalling zone had little effect on the load-strain relationships in the bursting zone.

3.2.2 Concrete Strains in I-Specimens

The load-strain curves for the transverse strains across the line of the load in specimen I3 are given in Figure 15. The curves give information similar to that previously presented for rectangular beams. The strains in the I-specimen were approximately equal to those measured in the rectangular beams. The distribution of strains along the line of the load was typical of bursting strains.

The variation of transverse strains across the center line and across a line 1.5 in. from the center line of specimen I3 are shown in Figure 16. The spalling crack became visible 0.5 in. from the center line at 15 kips. This corresponded to the early reversal of transverse strains across the center line. The strains were small and erratic at points 1.5 in. from the center line. The transverse strain distribution along the center line resembled the typical spalling strain distribution.

3.2.3 Spalling Crack Propagation in I-Specimens

The development of spalling cracks was observed with a magnifying glass in six I-specimens. A typical development is shown in Figure 17. The three-inch high loading block covering half the tapered part of the flange at the right-hand end of the specimen produced the longer cracks observed at this end. The cracks occurred 5.5 in. from the bottom in specimens I3, I4, I5, and I6 and at 4.5 in. in specimens I1 and I2. In all specimens, failure occured under

the 1.5-in. loading block at the left-hand end.

3.2.4 Spalling Crack Propagation in Rectangular Beams

The widths and lengths of the spalling cracks in ten rectangular specimens were determined from deformation measurements taken across the cracks. A typical gage point layout for the deformation readings is shown in Figure A6. The results for these tests are presented in the form of crack profiles. A crack profile shows the width and length of the spalling crack as indicated by the deformation measurements made at one stage of the test. Each profile represents the average of the deformations measured on two sides of the specimen. The individual measurements did not differ by more than 10 per cent from the average. Figure A18 presents the crack profiles for specimen R19 and is representative for rectangular beams. Crack profiles for all ten beams are given in Appendix A.

The total number of ten specimens was divided into two groups. The first group of four beams was tested with the secondary purpose of determining the effect of a crack starter on the cracking load. The crack starter forced the crack to occur between the gage points making it possible to measure the crack width as described in Section A.4. The dimensions and position of the crack starter in the anchorage zone are given in Figures A4 and A5. The choice of the position for the crack starter was influenced by the location of the maximum spalling stress and by the difficulty of measuring the crack width on the end face if the crack formed too close to the loading plate.

A crack starter was placed in specimens R19 and R22 and omitted in specimens R20 and R21. The shape of the crack, which was identical in paired specimens, is shown in Figure 18. The first visible crack in beams R19 and R22 appeared during the load increment from 20 to 25 kips. In beams R20 and R21 the crack appeared between the loads of 25 and 30 kips. At a load of 30 kips, the visible crack was approximately two in. long in all four specimens. Since the behavior of the beams was not seriously affected by the crack starter, it was used throughout the remainder of the test series.

Figures A18 and A19 present the crack profiles for specimens R19 and R22. Figure A20 shows the relationships between the load and the transverse deformations measured at the beam end. The two specimens behaved similarly. The crack propagated slowly with increasing load for loads below 30 kips. As the applied load was increased above 30 kips, a large increase in the crack dimensions occurred for a small increment of load.

In both specimens there was a tendency for the crack to grow with time when the load was held constant. The instability of the crack was noticed in specimen R22 at a load of 25 kips.

The second group of specimens contained six beams. They were tested to study the effect of differential

shrinkage on the cracking load and crack propagation. The amount of differential shrinkage in the specimens was varied by using the curing procedures described below. All the beams were removed from their forms one day after casting. Specimens R43, R45, and R47 were then allowed to dry in the laboratory until the time of testing, while specimens R44, R46, and R48 were immediately coated with a thin layer of epoxy as described in Section A.3. Gage points were glued on all specimens at the positions shown in Figure A7 approximately twelve hours after the forms were removed. The gage reading at this time was used as a reference point to determine the shrinkage deformation from the gage reading made at a later date. The gage readings were made with a Whittemore gage that had a 10-in. gage length. Figure 19 shows the development of the shrinkage deformations in both the air-dried and epoxy-coated specimens. The curves in Figure 19 are the averages of readings on three beams. It can be seen that the shrinkage deformations in the air-dried specimens were more than twice those in the epoxy-coated specimens.

Autogenous shrinkage or shrinkage in sealed concrete may be assumed to be approximately one-fifth of the shrinkage produced by drying.[46] Thus, for the specimens described above, the autogenous shrinkage deformation would be about 0.5×10^{-3} in. over a 10-in. gage length. The shrinkage deformations in the epoxy-coated specimens were significantly larger than this, so it is evident that the epoxy layer did not prevent all moisture loss.

The concrete in the air-dried and epoxy-coated specimens had comparable properties. The average compressive strengths were 5800 and 5600 psi, the average splitting strengths were 385 and 390 psi, and the average moduli of rupture were 480 and 730 psi for the air-dried and epoxy-coated specimens, respectively. The slope of the stress-strain curve in compression was the same for the two types of specimens. The effects of differential shrinkage were most notable in the modulus of rupture tests.

The specimens were tested 18 days after casting. Crack profiles for the six beams are given in Figures A21 to A26 and A28 to A33. The spalling cracks could be seen with the aid of a magnifying glass at loads larger than 15 kips in the three air-dried specimens, and at loads larger than 25 kips in the three epoxy-coated beams. Crack propagation in these specimens was similar to that in specimens R19 and R22 as previously described.

Figure 20 shows the relationships between load and transverse deformation measured at the beam end for both the air-dried and epoxy-coated specimens. The curves in Figure 20 are the average of six tests on each type of specimen. Curves for the individual tests are given in Figures A27 and A34. The transverse deformations at the beam end were significantly smaller in the epoxy-coated beams at low loads. At loads close to 40 kips there was little difference in the magnitude of the deformations in the epoxy-coated and air-dried beams.

The two load-deformation curves in Figure 20 refer to specimens in which the concrete properties were comparable and yet the initial slopes differed measurably. The observed difference can be ascribed to differential shrinkage as follows. At an early stage of loading, the applied transverse stresses in the two types of specimens may be assumed to be about the same. However, in the air-dried specimens the applied stress is superimposed on an existing tensile shrinkage stress, while in the epoxy-coated specimens the total stress is not much greater than that applied. Thus, for a given load, the total transverse stresses in the air-dried specimens are considerably higher. If it is accepted that the apparent load-deformation curve for concrete in flexural tension is nonlinear with a decreasing slope, it follows that the incremental deformation in the case of the air-dried specimens should be larger than that for the epoxy-coated specimens. This phenomenon is discussed quantitatively in Section 5.2.2.

The cracking strain of the concrete in the specimens was estimated from longitudinal strain readings made in the middle of the specimen. Typical relationships between the load and longitudinal strain are given in Figure 21 for both an air-dried and an epoxy-coated specimen. The sharp break in the curve for the epoxy-coated specimen indicated the formation of a transverse crack between the gage points at a strain of approximately 150×10^{-6}. The first transverse crack in the air-dried specimen could be seen with a magnifying glass at a load of 20 kips. The strain reading at this load may be taken as an upper limit to the cracking strain. The cracking strain in the air-dried specimen, therefore, was approximately 100×10^{-6}. It should be pointed out that the strains plotted in Figure 21 were determined from deformation measured over a 10-in. gage length. Localized strains at the initiation of cracking could be somewhat larger than those values shown.

It is assumed in Chapter V that the cracking strain in the spalling zone is equal to cracking strain measured in the middle of the specimen. The above assumption leads to the conclusion that the transverse deformations measured over a 2-in. gage length on the beam end were 0.20×10^{-3} in. and 0.30×10^{-3} in. at the initiation of cracking in the spalling zones of the air-dried and epoxy-coated specimens, respectively. Figure 20 shows that a deformation of 0.20×10^{-3} in. occurred at a load of about 7.5 kips in the air-dried specimens and that a deformation of 0.30×10^{-3} in. occurred at a load of approximately 18 kips in the epoxy-coated specimens.

3.3 SHORT-TIME TESTS ON SPECIMENS WITH TRANSVERSE REINFORCEMENT

3.3.1 Stirrup Strains in Precracked Specimens

A longitudinal crack was preformed in 14 rectangular and 11 I-specimens. A thin plastic sheet placed along the expected trajectory of the spalling crack eliminated the transverse tensile

force in the concrete. The total of 25 specimens can be divided into three groups according to the information obtained. The two specimens in the first group (R4,I8) did not have longitudinal reinforcement to resist bending. These specimens failed at early loads. The specimens in the second group either did not have sufficient instrumentation to obtain enough numerical data or were single exploratory specimens (R5-R10, I9-I12). The third group of 13 specimens (R11-R17, I13-I18) provided most of the data in this discussion. These specimens were instrumented with strain gages on the transverse reinforcement and dial gages across the preformed crack. The specimens were reinforced with one stirrup at 0.5 in. or two stirrups at 0.5 and 2.0 in. from the end face. The stirrups were No. 2 deformed bars (A = 0.05 in.^{2}) or No. 7 USSWG wires (A = 0.025 in.^{2}).

The variation of strain in stirrups placed at 0.5 in. from the end faces of specimens R11, R12, R14, and R17 is given in Figure 22. The strains measured in the wires before yielding were slightly larger than the strains in the No. 2 bars. However, at a given load, the forces in the No. 2 bars were larger than those in the wires. The spalling cracks observed at a given load in specimens reinforced with No. 7 USSWG wire stirrups were wider and longer than those observed at the same load in specimens reinforced with No. 2 bar stirrups. This difference in behavior can be explained as follows.

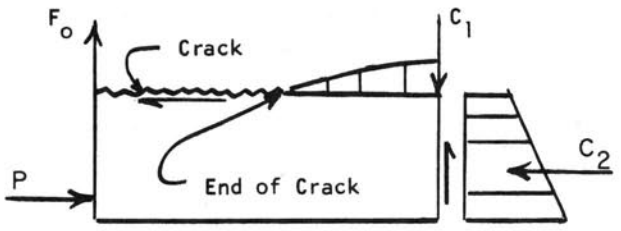

The forces acting on a free body of the portion of the beam below the spalling crack in a precracked specimen are shown in the sketch. The applied force P produces a linear stress distribution with the resultant force C_2. To maintain the equilibrium of the free body, a moment must be supplied by the stirrup force F_o and the transverse compression C_1 in the concrete. This resisting moment is dependent on the magnitude of the stirrup force and on the length of the spalling crack, since the lever arm between F_o and C_1 varies directly with the crack length. For a given load the value of the resisting moment is a constant. The spalling crack length, therefore, must be inversely proportional to the stirrup force. Thus, for the specimens described in the preceding paragraph, longer spalling cracks would be expected in the specimens reinforced with wire stirrups, since the stirrup forces measured in these specimens were less than those measured in specimens reinforced with No. 2 bars. This was confirmed by the test results as previously mentioned.

Figure A11 shows the relationships between stirrup force and crack width

(assumed to be twice the slip measured in a pull-out test) for the No. 2 bars and No. 7 USSWG wires. It can be seen from this figure that as long as the force in the wire is more than half the force in the bar, the crack width in a specimen reinforced with a No. 2 bar. The wire force will be more than half the force in the No. 2 bar whenever the strain in the wire is larger than that in the bar.

For specimens R11, R12, R14, and R17 described above, the strain in the wires was always larger than the strain in the No. 2 bars. Thus, wider cracks would be expected to occur in the specimens reinforced with wire stirrups, since the stirrup force in these specimens was always more than half that measured in the specimens reinforced with No. 2 bars. This was also confirmed by the test results.

The variation of strains in stirrups placed at 0.5 in. and 2.0 in. from the end faces of specimens R8 and R15 is presented in Figure 23. The stirrup strains measured in specimen R13 (reinforced the same as R8) were nearly equal to those measured in specimen R8 and therefore have been omitted from Figure 23. It can be seen in Figure 23 that the strains in the sturrups 0.5 in. from the end were slightly larger than those in the stirrups 2.0 in. from the end. The strains measured in the wires before yielding were approximately equal to those in the No. 2 bars. The spalling cracks were longer and wider in specimen R15 as would be expected.

Comparing Figure 22 with Figure 23 shows that the stirrup strains measured in the specimens reinforced with two stirrups were more than half those measured in specimens reinforced with only one stirrup. Thus, for a given stirrup size, the total stirrup force for the two stirrups was larger than the force for the single stirrup. As would be expected, the crack widths and lengths measured in the specimens with two stirrups were smaller than those measured in the specimens with one stirrup.

The relationships between applied load and stirrup strain for I-specimens reinforced with one stirrup 0.5 in. from the end face is presented in Figure 24. Although the strains in the No. 2 bars were smaller than those in the No. 7 USSWG wires, the stirrup forces in the bars were larger as would be expected.

3.3.2 Crack Propagation in Initially Uncracked Specimens

The widths and lengths of the spalling cracks in 15 rectangular specimens were determined from deformation measurements taken across the cracks. The specimens were reinforced with one stirrup 3/4 in. from the end face. In eight specimens the stirrups were 1/4-in. diameter plain bars while in seven specimens, 1/8-in. diameter plain bars were used. The development of the spalling cracks in these beams was similar to the development of the spalling cracks in the plain specimens as described in Section 3.2.4.

The eight specimens reinforced with 1/4-in. diameter bars can be divided into three groups according to their age at the time of testing.

Specimens R23, R24, and R25 were tested at seven days, specimens R29a, R29b, and R30 at 15 days, and specimens R33 and R35 at 240 days. Crack profiles for the specimens are given in Figures A35, A36, A37, and A38. Figure 25 shows the measured relationships between load and transverse deformation at the beam end. The curves in Figure 25 are the average of eight tests on specimens seven and 15 days old and four tests on specimens 240 days old. Curves for the tests on individual specimens are given in Figures A39, A40, and A41. The results for the beams seven and 15 days old were so nearly equal that one curve was used to represent all the data from these tests. The spalling cracks in specimens tested at 240 days were significantly smaller than those in the specimens tested at 15 days.

Of the specimens reinforced with 1/8-in. diameter bars, three were tested at seven days (R26, R27, and R28), two were tested at 15 days (R36 and R37), and two were tested at 430 days (R39 and R41). Crack profiles for the seven beams are given in Figures A43, A44, and A45. Figure 25 shows the relationship between load and transverse deformation at the beam end. The curves in Figure 25 are the average of seven tests on beams seven and 15 days old and four tests on beams 240 days old. Curves for individual tests are given in Figures A46, A47, and A48. The test results for the specimens tested at seven and 15 days were so close that they are represented by one curve in Figure 25. The spalling cracks were significantly smaller in the 430-day old specimens than in those 15 days old.

Two more observations can be made from Figure 25. First, as would be expected, the 1/4-in. diameter bars were more effective in restraining the crack than the 1/8-in. bars in specimens of the same age. Second, the initial slopes of the curves increased as the age of the concrete increased. This phenomenon may be attributed to shrinkage as previously discussed in Section 3.2.4.

Longitudinal deformations were measured at the center of specimens R33, R35, R39, and R41. A Whittemore gage with a 10-in. gage length was used. The distribution of deformation was nearly linear and was close to that calculated from $\sigma = P/A \pm Mc/I$. The measured deformations are given in Figures A42 and A49.

3.4 SUSTAINED-LOAD TESTS ON SPECIMENS WITH TRANSVERSE REINFORCEMENT

Six specimens were subjected to sustained loads for periods of time ranging from eight to fourteen months. A description of the specimens and the testing procedure is given in Sections A.2 and A.4. The magnitude of the sustained load was 30 kips in all specimens.

Three of the six specimens (R31, R32, and R34) were reinforced with 1/4-in. diameter plain bar stirrups at 3/4 in. from the end faces. Crack profiles for these beams are given in Figures A50 and A51. The crack profiles for beam R34 which are shown in Figure 26 are typical for the sustained-load tests. The crack profiles show that

the spalling cracks increased in length and width with time. The crack growth was fastest during the first few days of the test. More than one-half of the total growth over eight months occurred during the first week. The relationship between crack width measured at the beam end and crack length is presented in Figure 27 for both the sustained-load and short-time tests on specimens reinforced with 1/4-in. diameter bars. It can be seen in Figure 27 that the width to length ratio increased more rapidly in the sustained-load tests. This phenomenon and some of the factors affecting it are discussed in more detail in Section 5.4.

Longitudinal deformations were measured over 10-in. gage lengths at the center of the specimens as shown in Figure A7. The variation in the distribution of these deformations with time are shown in Figure A52. The distribution remained almost linear and rotated about one point as the concrete crept.

Figures 28, 29, and 30 show the time-dependent variation in crack width measured at the beam end and in the longitudinal deformation measured at "End D." End D is defined in Figure A8. These curves show in another form the phenomenon of crack growth and longitudinal creep.

Specimens R38, R40, and R42 were reinforced with 1/8-in. diameter plain bar stirrups at 3/4 in. from the end faces. Crack profiles for these beams are given in Figures A53 and A54. Longitudinal deformations measured over 10-in. gage lengths in the center of these specimens are shown in Figure A55. The relationship between crack width and crack length is presented in Figure 31 and the time-dependent variation in crack width measured at the beam end and in the longitudinal deformation measured at end D are shown in Figures 32, 33, and 34.

The development and growth of the spalling cracks in specimens reinforced with 1/8-in. diameter stirrups parallels that for specimens reinforced with 1/4-in. diameter stirrups as described in the preceding paragraphs. It was noticed, however, that the spalling cracks in specimens reinforced with 1/8-in. stirrups were wider, longer, and grew faster than the cracks in specimens with 1/4-in. stirrups.

IV. TESTS AT OTHER LABORATORIES

4.1 INTRODUCTORY REMARKS

The test results from four experimental programs designed to investigate anchorage-zone stresses are presented in this chapter. The experimental programs included are: (1) the tests on pretensioned girders by Marshall and Mattock,[28] (2) the tests to determine the bearing strength of concrete column heads by Kriz and Raths,[23] (3) the tests on pretensioned girders by Arthur and Ganguli,[1] and (4) the tests on concrete end blocks by Zielinski and Rowe.[48] Details pertaining to the test specimens and the testing procedure used in the investigations are given in Appendix B.

4.2 TESTS AT THE PORTLAND CEMENT ASSOCIATION RESEARCH AND DEVELOPMENT LABORATORIES (SKOKIE)

4.2.1 Pretensioned Girders by Marshall and Mattock[28]

Marshall and Mattock tested 35 pretensioned I-girders. The variables in the test series were: (1) amount of transverse reinforcement, (2) size and shape of cross section, (3) prestressing strand diameter, and (4) the distribution of the prestress force. Data on the properties of the specimens are given in Table 11. The dimensions of the specimens are shown in Figures B1 and B2.

Ten girders without transverse reinforcement were tested. In each test, the pretensioned strands were released by severing groups of strands in succession. The web thickness and the arrangement of the strand were the controlled variables. The distribution of transverse strains in the ends of the girders was similar for all specimens. The maximum spalling strain occurred near mid-depth of the web on the end face. The strain decreased rapidly toward the center of the girder in a manner typical of spalling strains. In all cases in which the girder did not crack, the point of zero spalling strain occurred within one-third the depth of the specimen from the end face.

Twenty-five girders reinforced with vertical stirrups in the anchorage zone were tested. The variables in these tests were: (1) the size of the stirrups, (2) size and shape of cross section, and (3) the diameter and location of the strands. Table 1 presents data from the tests. Eighteen of the 25 girders cracked on transfer. In 14 of the cracked girders, the cracks occurred in the lower part of the web near the strain gages which

were located at the centroidal axis of the section. A typical distribution representing the stirrup strains measured in these 14 girders is given in Figure 35. The stirrup strain distribution in Figure 35 resembles the spalling strain distribution measured in an uncracked plain concrete specimen. In the other four girders which cracked, the crack occurred in the upper part of the web far away from the gages on the stirrups. The distribution of stirrup strains near the cracks in these specimens is therefore not known.

The maximum stirrup stress and the total stirrup force are given in Table 1 for those beams that cracked near the centroidal axis. It is pertinent to note that in comparable pairs of specimens, such as B3 vs. B4, B9 vs. B10, and B12 vs. B13, the larger the size of the stirrup, the larger is the stirrup force, a phenomenon described in Section 3.3.7 with respect to the University of Illinois tests.

The spalling crack lengths given in Table 1 were determined from a graph of the stirrup strain distribution similar to the distribution for girder B10 given in Figure 35. The tensile cracking strain of the concrete was assumed to be 125×10^{-6}. Thus, the point at which the vertical tensile strain in Figure 35 became equal to 125×10^{-6} was taken to be the point to which the crack extended. The spalling cracks in girders reinforced with No. 2 stirrups were longer than those in specimens reinforced with No. 3 stirrups. This is consistent with the fact that the forces in the No. 3 bars were larger than those in the No. 2 bars (See Section 3.3.1).

4.2.2 Tests to Determine the Bearing Strength of Concrete Column Heads by Kriz and Raths[23]

Kriz and Raths investigated the bearing strength of concrete column heads. The bearing failure of a column head and the failure of the anchorage zone in a prestressed girder are closely related. They are both produced by concentrated loads applied to a concrete cross section. Tests were made on 38 plain concrete and 185 reinforced column heads. Data pertaining to the plain concrete specimens are given in Table 12 and Figure B4. No data are given herein for the reinforced columns.

The variables investigated in the tests on the plain concrete specimens were: (1) concrete compressive strength, (2) eccentricity of load, (3) width of bearing plate, and (4) size of specimen. The specimens had a rectangular cross section and were loaded symmetrically about their centroidal axis as shown in Figure B4.

The failure load for each of the plain concrete specimens is given in Table 12. The failure was sudden and violent in all specimens. Cracking occurred prior to failure only in those specimens with the bearing plates at or near the edge of the column. The cracks in these specimens started at some point in the spalling zone between the two loads and propagated downward along the center line of the column. Cracks were not observed before failure

in specimens with bearing plates located more than one inch from the edge. The bearing strength depended on the width of the bearing plates and on their eccentricity from the center of the specimen. The bearing strength increased as the eccentricity of the load was decreased and as the width of the bearing plate was increased.

4.3 TESTS AT THE UNIVERSITY OF GLASGOW[1]

Nineteen pretensioned I-beams were tested by Arthur and Ganguli. The variables investigated in the test program were the web width and the distribution of the prestressing wires. The prestressing force was transferred to the beam in increments by releasing all the wires simultaneously. The test specimens are shown in Figure B5 and data pertaining to them given in Table 13.

The transfer length for the prestressing wire was determined from longitudinal deformation readings made on the surface of the specimen along the length of the wires. A typical build-up of the longitudinal strain in this region is shown in Figure 36. The distance from the beam end to the point at which the longitudinal strain first reaches a constant value can be taken as the transfer length. In Figure 36, the region of constant longitudinal strain is well defined, although the point at which this region begins is not perfectly clear. Thus, personal judgment may have some influence on the transfer length obtained from a plot such as that shown. It is fortunate, therefore, that the transverse stresses in pretensioned beams appear to be fairly insensitive to small variations in the transfer length. This is shown in the analysis for pretensioned beams described in Section 2.4. It is also shown in Section 2.4 that an underestimate of the transfer length is on the safe side for the calculation of anchorage-zone stresses. Therefore, it seems sufficiently accurate under these conditions to determine the transfer length from two straight lines fitted to the data as is shown in Figure 36. The transfer length for the 0.2-in. diameter wires used in this test series has been taken as 10 in.

Table 2 summarizes the main test results. Longitudinal cracks were observed in 13 of the 19 test specimens. In five specimens cracks occurred at both ends. Eight specimens cracked at one end only.

In nine cases the cracks occurred near the centroidal axis of the specimen, while in seven instances they occurred at the junction of the web and the top flange. In only two cases was cracking observed at the junction of the web and bottom flange.

In most of the specimens, cracking occurred after 30 to 55 per cent of the prestress force had been transferred. The transverse strain measured on the beam end with a Demec gage that had a 2-in. gage length ranged from 300×10^{-6} to 470×10^{-6} at the initiation of visible cracking.

Transverse deformations were measured in three specimens at 24 and 48 hours after transfer. It was found in the uncracked specimens that the

maximum strain decreased by about 20×10^{-6} in 24 hours and by 100×10^{-6} in 48 hours. Although the decrease appears to reflect the expected time-dependent loss in the prestressing force, the observed rate seems unusual. The distribution of strain remained unchanged. In the cracked specimens, the transverse deformations measured across the cracks increased with time.

4.4 TESTS AT THE CEMENT AND CONCRETE ASSOCIATION LABORATORIES[48]

Zielinski and Rowe investigated the transverse and longitudinal strain distributions in three rectangular and four I-section end blocks. Nine tests were carried out on the rectangular end blocks while eleven tests were performed on the I-section specimens. The variables investigated were: (1) location of the applied load, (2) cross section (I or rectangular), and (3) size of loading plate. Figure B6 shows the test specimen and the loading positions. Table 14 gives the data pertaining to the tests and the properties of the control specimens.

Longitudinal and transverse strain distributions were measured in all specimens. The strain distribution for the specimens in tests 1, 19, 17, and 16 are given in Figures 37, 38, 39, and 40. Tests 1 and 19 were made on the I-shaped end blocks, while tests 16 and 17 were made on the rectangular end blocks.

The specimen in test 1 was loaded with a single concentrated load at the center of the web. Figure 37 shows the variation of transverse strain along the load line and along a longitudinal line 2.25 in. from the load line. The strain distribution along these lines was typical of bursting strains.

Figure 38 shows the transverse strain distribution measured in the web, flange, and across the bottom of the flange for test 19. The specimen in this test was loaded with two concentrated loads in the web and three concentrated loads in the flange. The resultant load was eccentric with respect to the centroidal axis of the specimen. All the strain distributions are typical of bursting strains.

The transverse strain distributions measured in test 17 are given in Figure 39. The specimen in this test was loaded with one eccentric load applied through a large loading plate. There were two areas in the specimen in which large transverse strains were measured. The first area was located on the axis of the applied load at a short distance from the beam end. This was the bursting zone. The second area of high transverse strain was at the junction of the rectangular end block and the I-section. The transverse strain distribution in this area was similar to a spalling strain distribution.

Figure 40 shows the transverse strain distributions measured in test 16. Three concentrated loads were applied to the specimen in this test. Two of the loads were applied near the bottom of the specimen, while the remaining load was applied above the center line. Bursting strains were measured across the axis of each load. High spalling strains were measured on the side of the specimen midway between

the applied loads. Spalling strains were also measured on the bottom of the beam at a section between the two loads.

Seven tests were continued until the specimens failed. The cracking and failure loads for these tests are given in Table 3. Failure occurred in a bursting zone in all the specimens. Failure in test 1 occurred when a crack formed in the web under the single applied load. The first crack in test 9 appeared at about 27 kips. It was visible on the bottom flange in the spalling zone between the two loads. Subsequent cracking occurred on the bottom flange in the bursting zones below the loads at about 67 kips. Failure finally occurred in the bursting zone. Failure in test 18 was produced by the formation of a crack at the junction of the web and flange with subsequent crushing of the concrete under the load on the web. In test 19 a longitudinal crack under the load at the centroid of the specimen produced failure. The first crack in test 16 developed at about 55 kips. It could be seen on the bottom of the specimen in the spalling zone between the two loads. At this load, further cracking developed in the bursting zones beneath the two loads applied near the edge of the section. These cracks were visible on both the side and bottom of the end block. The ultimate load for this test was 66.3 kips. In test 17 the initial crack appeared in the region of high transverse strain at the junction of the end block and the I-section. This crack led to failure at a load of 121 kips. Initial cracking occurred in the bursting zone near the edge of the specimen in test 20. No failure load was recorded for this test.

V. ANALYSIS OF TEST RESULTS

In this chapter, a modified version of Lenschow's analysis will be used to examine the behavior of the specimens described in Chapters III and IV. Specifically, the transverse strains before cracking, the cracking load, and the crack propagation will be studied for the plain concrete specimens. For the specimens with transverse reinforcement, crack propagation and time-dependent behavior will be investigated.

5.1 TRANSVERSE AND LONGITUDINAL STRAINS BEFORE CRACKING

The transverse strain distribution before cracking is dependent on the transverse stress, the longitudinal stress, Poisson's ratio, and the modulus of elasticity of the concrete. Although the transverse stresses can be calculated without difficulty from Lenschow's analysis, the longitudinal stress cannot be found without a major modification of the physical analog. Consequently, Gergely's elastic solution[12] which gives both the transverse and longitudinal stresses will be used. It has been shown in Section 2.6 and Figure 9 that Gergely's and Lenshow's solutions give comparable transverse-stress distributions.

In a linear elastic material, the transverse strain is given as

$$\varepsilon_y = \frac{1}{E} (\sigma_y - \mu\sigma_x) , \qquad (33)$$

where E is the modulus of elasticity, μ is Poisson's ratio, and σ_y and σ_x the transverse and longitudinal stresses.

The transverse-strain distributions along the line of the applied load in specimens R2 and R3 are compared with the results of Gergely's solution in Figure 41. The four curves for Gergely's solution represent the strains calculated for two values of both the modulus of elasticity and Poisson's ratio. The calculated strains are increased by about 30 per cent if Poisson's ratio is increased from 0.1 to 0.2. Since the value of Poisson's ratio for concrete is between 0.1 and 0.2, the variation of this parameter may cause a change in the strains of about 15 per cent.

The modulus of elasticity in compression for the concrete in specimens R2 and R3 was approximately 3.9×10^6 psi. Two curves in Figure 41 have been computed with this value. Both curves underestimate the measured strains. In tension, however, the modulus of elasticity decreases as the tensile stress increases. The bursting stress at a load of 15 kips is about 170 psi. At this stress, the modulus of

elasticity could be reduced by as much as 50 per cent if creep is also taken into consideration. Thus, two curves are plotted in Figure 41 for a lower limit of the modulus of elasticity of 1.95×10^6 psi. The combined effects of a variation in Poisson's ratio and modulus of elasticity may change the calculated maximum strain from 70×10^{-6} to 190×10^{-6}. The measured strains fall within this range which represents the probable extremes of the concrete properties.

A comparison of the spalling strains along the center line of specimens R2 and R3 with the results of Gergely's solution is given in Figure 42. In computing the curves in this figure, Poisson's ratio was assumed to be 0.1 and the modulus of elasticity was taken as 3.9×10^6 psi or 1.95×10^6 psi. Since the longitudinal stresses are small in the spalling zone, the effect of Poisson's ratio on the spalling strains is negligible. The measured transverse-strain distributions follow the computed ones and lie between the curves for $E_c = 3.9 \times 10^6$ psi and $E_c = 1.95 \times 10^6$ psi. One factor that may reduce the effective modulus of elasticity in the spalling zone is the shrinkage stress. Tensile stresses exist at the beam end prior to loading because of differential shrinkage. The total transverse tensile stress after application of the load is the sum of the shrinkage stress and the tensile stress produced by the load. The total stress may be quite high and the apparent modulus quite low if a large amount of differential shrinkage has occurred. It is interesting to note that the initial slopes of the load-strain curves shown in Figure 14 for the strain gages nearest the beam end correspond to an initial effective modulus of elasticity of between 1.7×10^6 and 3.0×10^6 psi. Since the initial tangent modulus of elasticity in tension can be assumed to be equal to that in compression (which was about 3.9×10^6 psi for these beams), it appears as if the shrinkage stresses did reduce the effective modulus of deformation.

5.2 CRACKING LOAD AND CRACK PROPAGATION IN PLAIN CONCRETE SPECIMENS

5.2.1. Effect of Transverse Shrinkage Stresses

The maximum spalling stress on a specific reference plane as determined by Lenschow's analysis is given in Equation (12). If a maximum tensile stress criterion is accepted as the failure criterion for concrete, Equation (12) can be used to calculate the value of the prestressing force which will initiate a spalling crack. If the tensile strength of the concrete is f_{te}, then the moment at cracking is:

$$M_{cr} = b f_{te} \sqrt{E_c I_b / k} \quad . \qquad (34)$$

The position of the crack in the anchorage zone must be found by trial. It corresponds to the position of the reference plane that gives the minimum value of the moment in Equation (34). Once the moment at cracking is known, the applied load at cracking can be found from Equation (7).

Two questions must be solved before Equation (34) is applied to a specific example. These are: (1) what is the tensile strength of the concrete in the anchorage zone and (2) what control test is most suitable for estimating this strength? The tensile strength of the concrete in the anchorage zone depends not only on the concrete quality but also on the tensile stresses produced by differential shrinkage. Differential shrinkage produces stresses in the anchorage zone in the following way. The surfaces and end face of the anchorage zone dry faster and therefore shrink more than the interior of the beam. Since the interior shrinks less, it restrains the shrinkage of the end and surfaces thereby producing tensile stresses in these regions. The tensile shrinkage stresses decrease with increasing distance from the beam end. Thus, the available tensile strength in the anchorage zone may increase with increasing distance from the end face as is shown in Figure 3b.

There are three common tests for the determination of concrete tensile strength: (1) the direct tension test, (2) the splitting test, and (3) the modulus of rupture test. The apparent strengths measured for one concrete mix will vary widely depending on the type of test. The modulus of rupture may be twice the strength indicated by the direct tension test. The splitting test may give an intermediate value. Because the spalling strain distribution has somewhat the same shape as the longitudinal strain distribution in the modulus of rupture test, the modulus of rupture may be the most significant measure of the tensile strength of the concrete in the anchorage zone. Reasonable values of the effective tensile strength for the test specimens is discussed in the following sections. Recommendations for the tensile strength to be used in design are given in Chapter VI.

5.2.2 Tests at the University of Illinois

In order to study the variation in apparent tensile strength of the concrete along the length of the beam, a series of six specimens was tested. The specimens were divided into two groups representing two extreme curing conditions. The first group of specimens (R43, R45, and R47) were allowed to dry in the laboratory from the time of form removal until the time of testing. The specimens of the second group (R44, R46, and R48) were coated with an epoxy resin at the time they were removed from their forms. The epoxy resin retarded moisture loss from the specimens. Curves which show the relationships between the transverse deformations measured over a 2-in. gage length on the beam ends of these six specimens are given in Figures A27 and A34. Average relationships for these curves are shown in Figure 20.

Consider first the value of the effective tensile strength at the beam end at the initiation of cracking. Inspection of the concrete surface with a magnifying glass during the test permitted visual observation of the cracks. These observations, however, could not detect the cracking load,

since they were made only at loads corresponding to the load increments. Consequently, the load-deformation curves shown in Figure A27 and A34 were used to determine the cracking load.

In order to determine the cracking load from Figures A27 and A34, the strain at cracking must be known. To investigate the cracking strain, a study was made of the load-strain measurements for the longitudinal tensile zone in the center of the specimens. From these measurements (an example is shown in Figure 21) it appears that the average tensile cracking strain was 0.0001 for the air-dried specimens and 0.00015 for those which were coated with epoxy. These values do not appear to be untenable.

The load at the initiation of cracking in the spalling zone can be found from Figures A27 and A34, if it is assumed that the cracking strain in the spalling zone is equal to the cracking strain in the middle of the beam. With this assumption, it was found that the load at the initiation of cracking was 8, 7.5, and 7 kips for end C and 7, 7, and 9 kips for end D of specimens R43, R45, and R47. Thus, the average cracking load for the air-dried specimens was about 7.5 kips. For the specimens coated with epoxy (R44, R46, and R48) the cracking load was 16, 19, and 18.5 kips for end C and 17, 16.5, and 20 kips for end D. The average cracking load for these specimens was about 18 kips.

The effective tensile strengths at the initiation of cracking were calculated from Equation (34) using the values given above for the applied load at cracking. For the air-dried specimens the effective tensile strength ranged from 150 to 190 psi with an average of 160 psi. The effective tensile strength for the epoxy-coated specimens ranged from 335 to 420 psi and averaged about 380 psi.

Two observations can be made about these values of the effective tensile strength. The first observation that can be made is that neither of the average values of effective tensile strength was as high as the modulus of rupture. The average modulus of rupture was 480 psi for the air-dried beams and 730 psi for the epoxy-coated beams. There are two reasons why the effective tensile strength may be less than the modulus of rupture. First, it is known that cracking occurs in a modulus of rupture specimen at loads below the ultimate. Thus, the modulus of rupture overestimates the stress at first cracking. Second, tensile stresses produced by differential shrinkage reduce the effective tensile strength. Shrinkage stresses caused the modulus of rupture for the air-dried specimens to be less than that for the epoxy-coated specimens. The shrinkage stresses should be larger and have more effect on the beams than on the modulus of rupture specimens for the following reason. The cross section of a beam is larger than that of a modulus of rupture specimen. Since there is a larger area in the center of the beam in which the shrinkage strains are small, the shrinkage in the beam is restrained more than that in the modulus of rupture specimen. Therefore, the shrinkage stresses in the beam should be larger than those in the middle of

SUPPORTING DATA

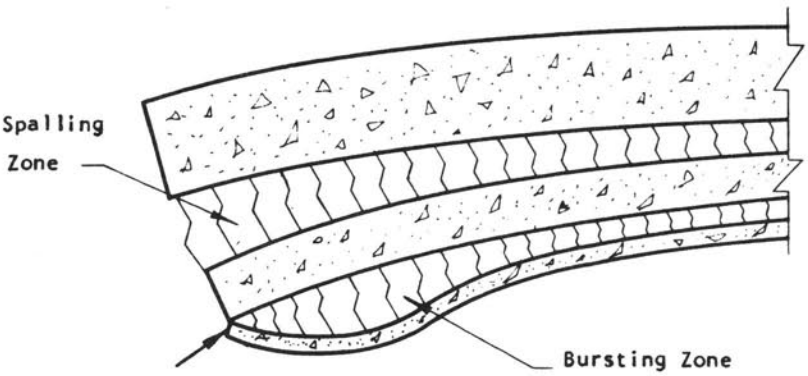

FIGURE 1. EXAGGERATED DEFORMATIONS IN THE ANCHORAGE ZONE

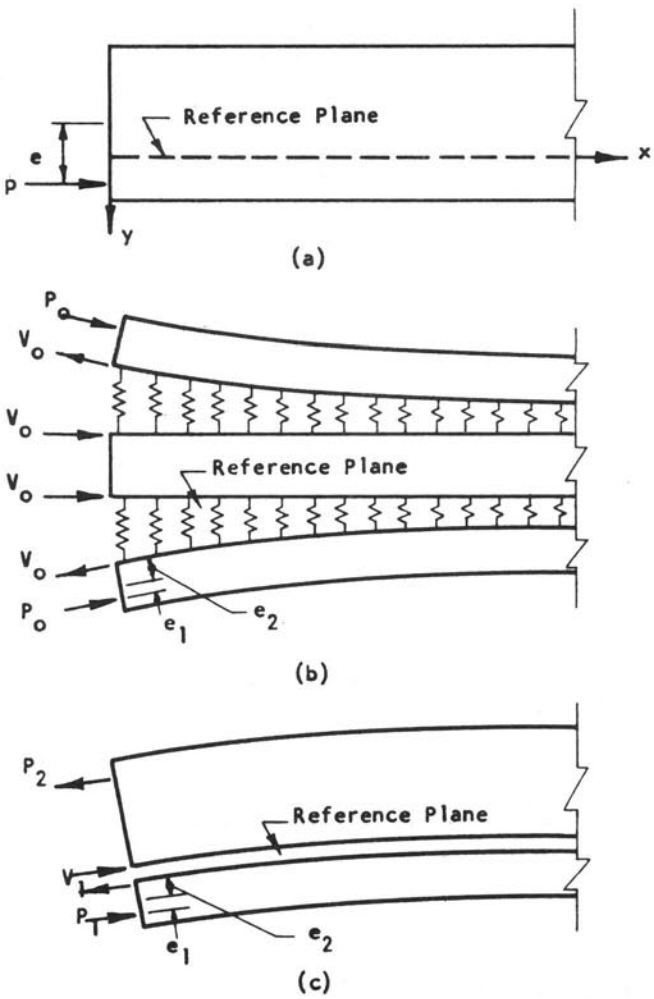

FIGURE 2. THE PHYSICAL ANALOG FOR POST-TENSIONED BEAMS

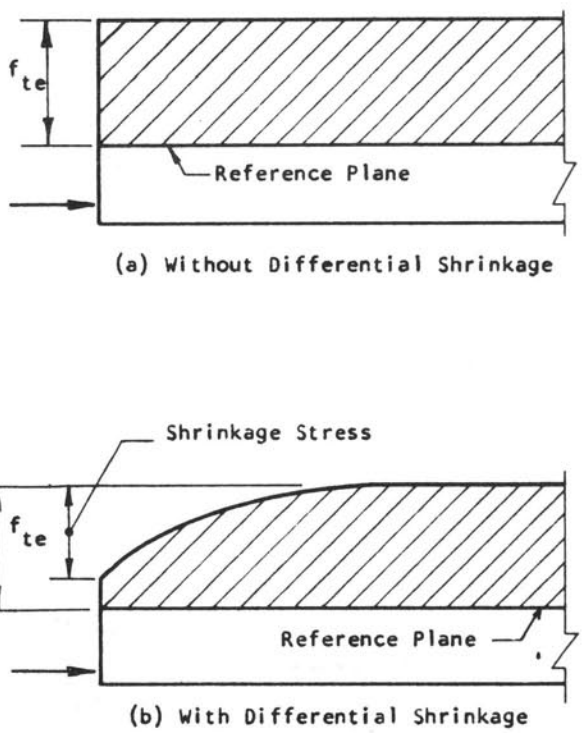

FIGURE 3. THE EFFECTIVE STRENGTH ENVELOPE

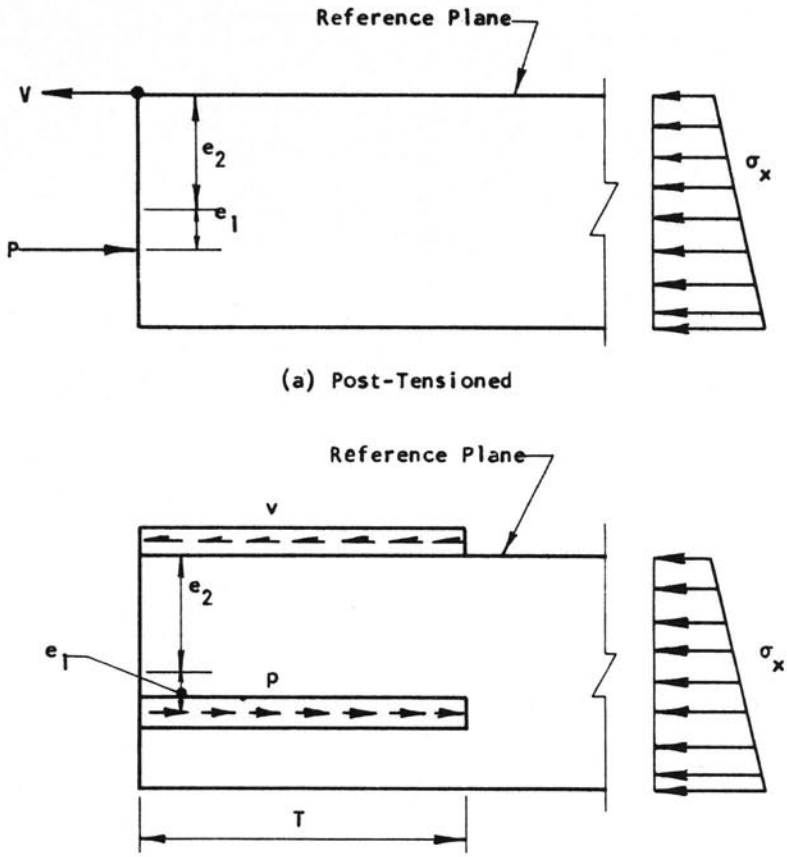

FIGURE 4. DISTRIBUTION OF SHEAR AND APPLIED PRESTRESS FORCE

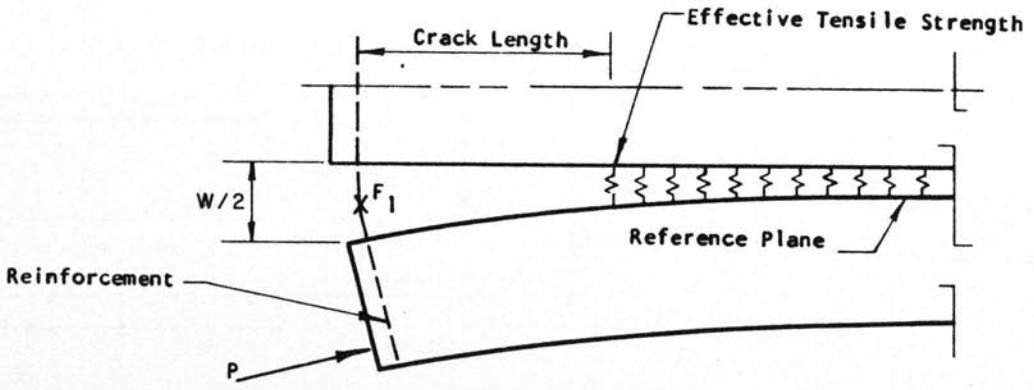

FIGURE 5. THE ANALOG FOR THE CRACKED BEAM

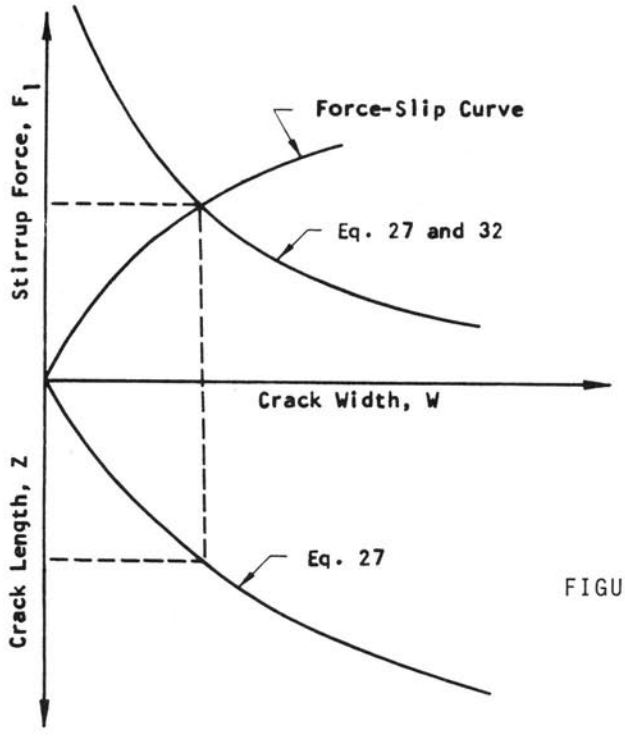

FIGURE 6. RELATIONSHIPS BETWEEN CRACK LENGTH, CRACK WIDTH, AND STIRRUP FORCE

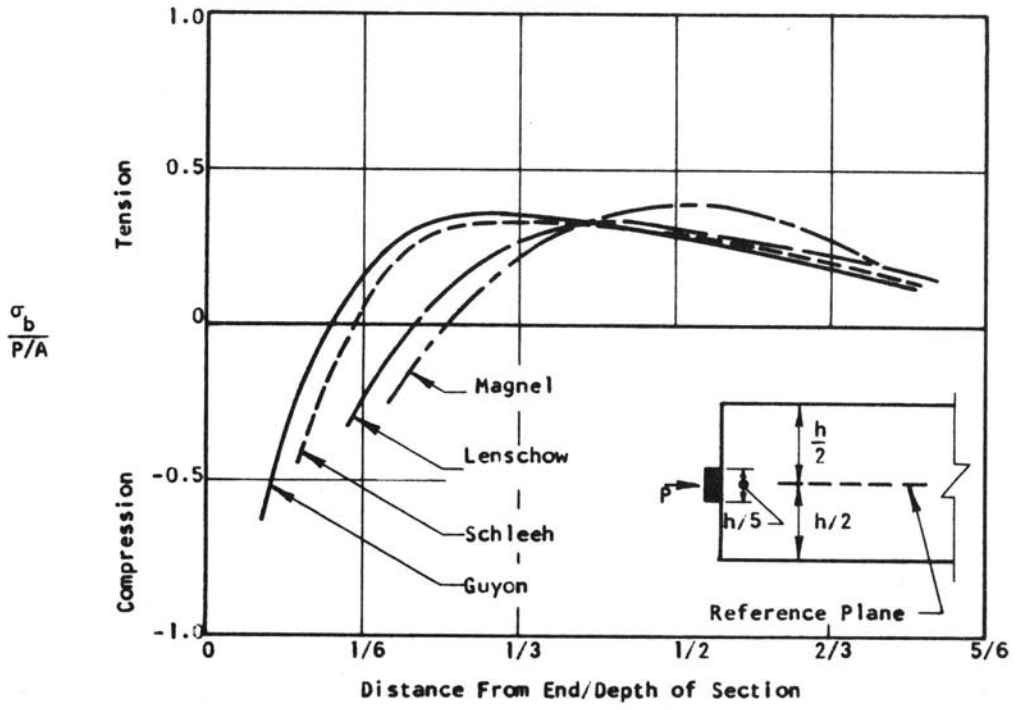

FIGURE 7. COMPARISON OF BURSTING STRESSES UNDER A CONCENTRIC LOAD

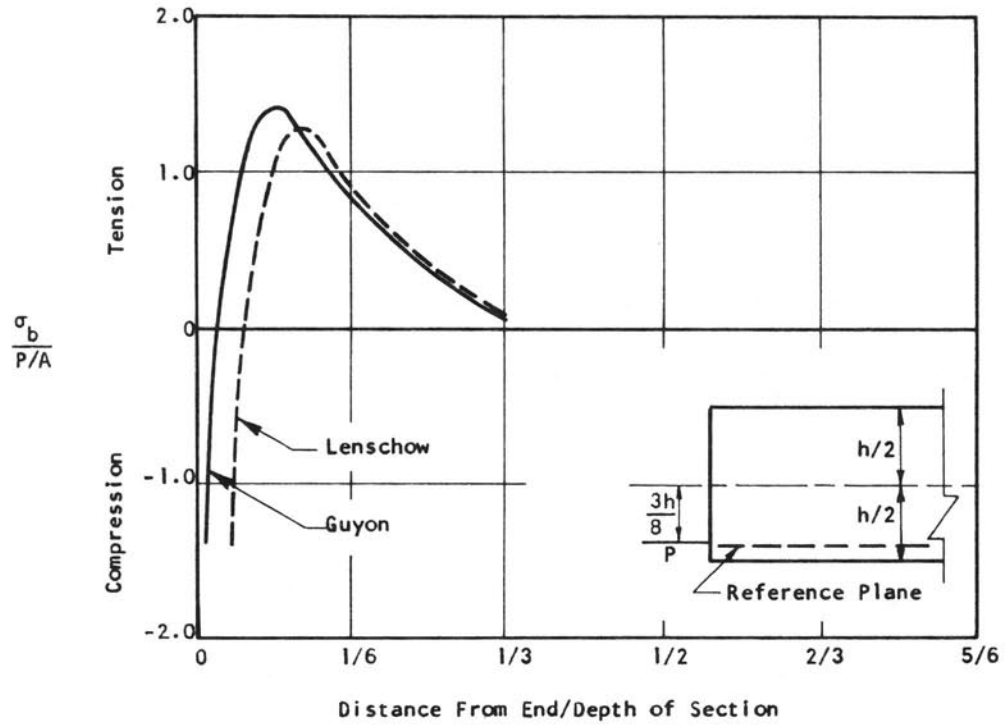

FIGURE 8. COMPARISON OF BURSTING STRESSES UNDER AN ECCENTRIC LOAD

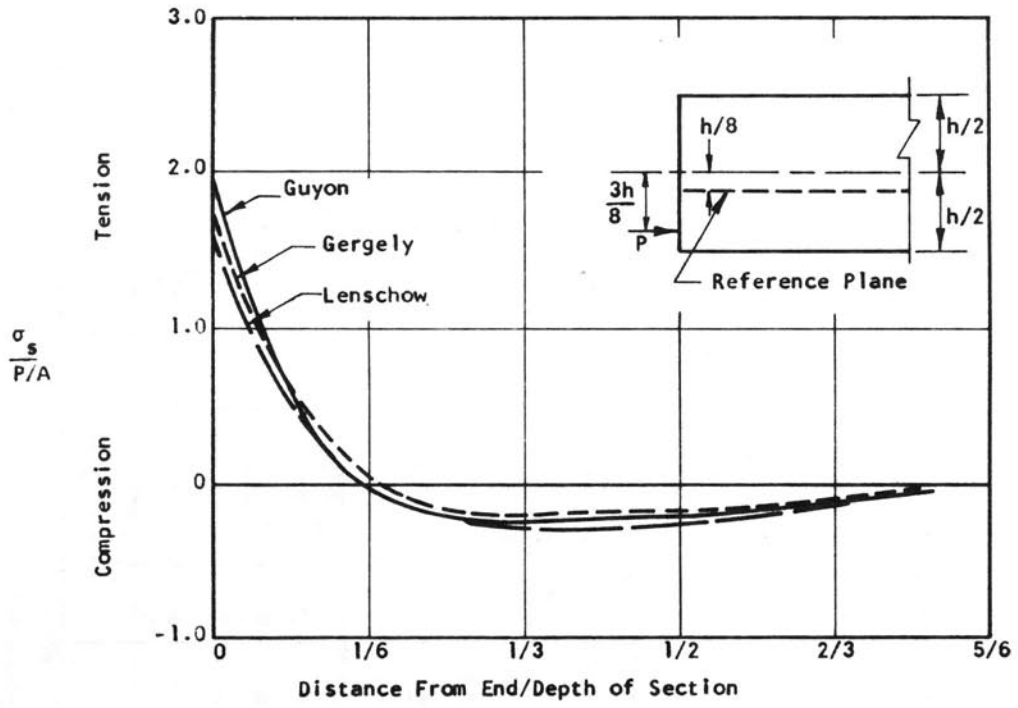

FIGURE 9. COMPARISON OF SPALLING STRESSES

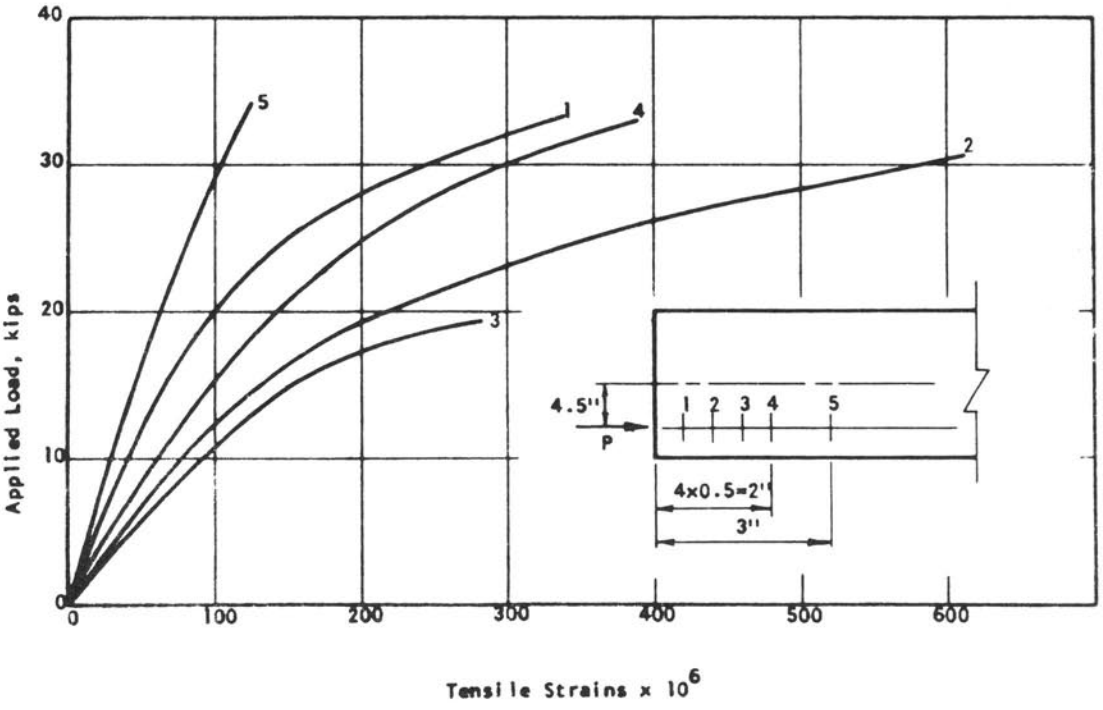

FIGURE 10. MEASURED RELATIONSHIPS BETWEEN LOAD AND TRANSVERSE CONCRETE STRAIN FOR SPECIMEN R1

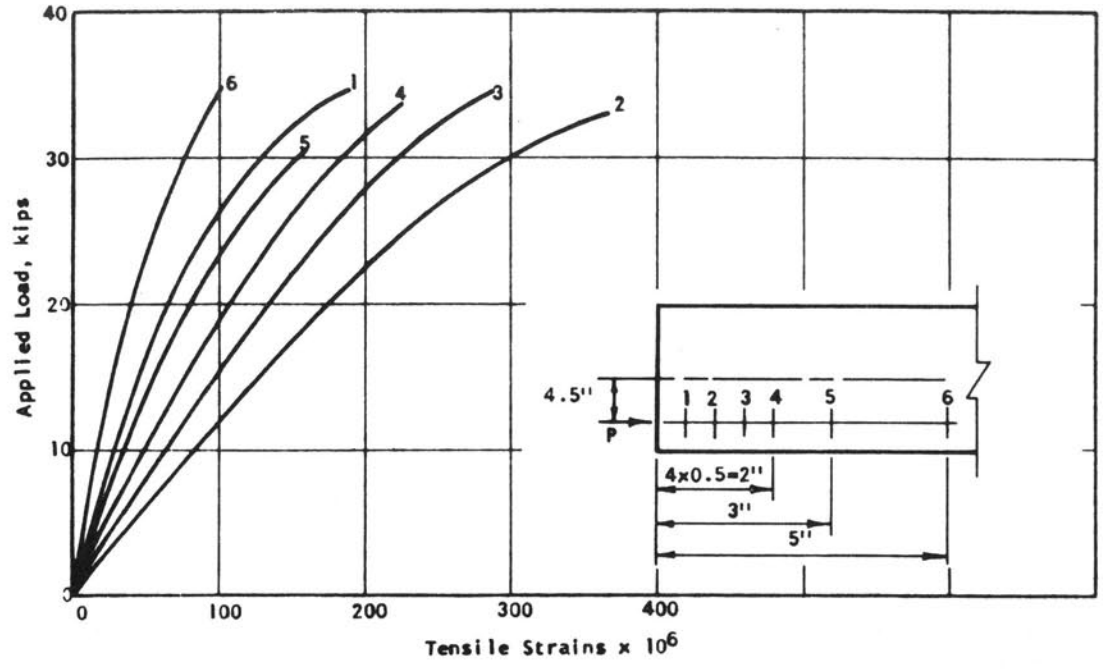

FIGURE 11. MEASURED RELATIONSHIPS BETWEEN LOAD AND TRANSVERSE CONCRETE STRAIN FOR SPECIMEN R2

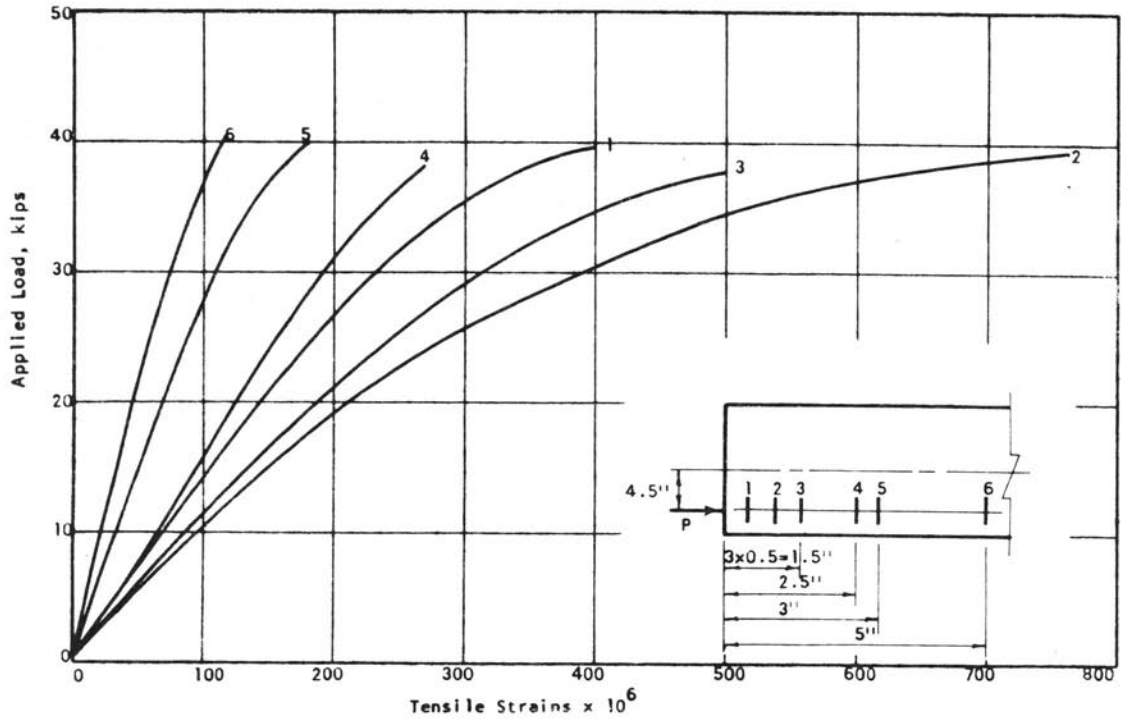

FIGURE 12. MEASURED RELATIONSHIPS BETWEEN LOAD AND TRANSVERSE CONCRETE STRAIN FOR SPECIMEN R3

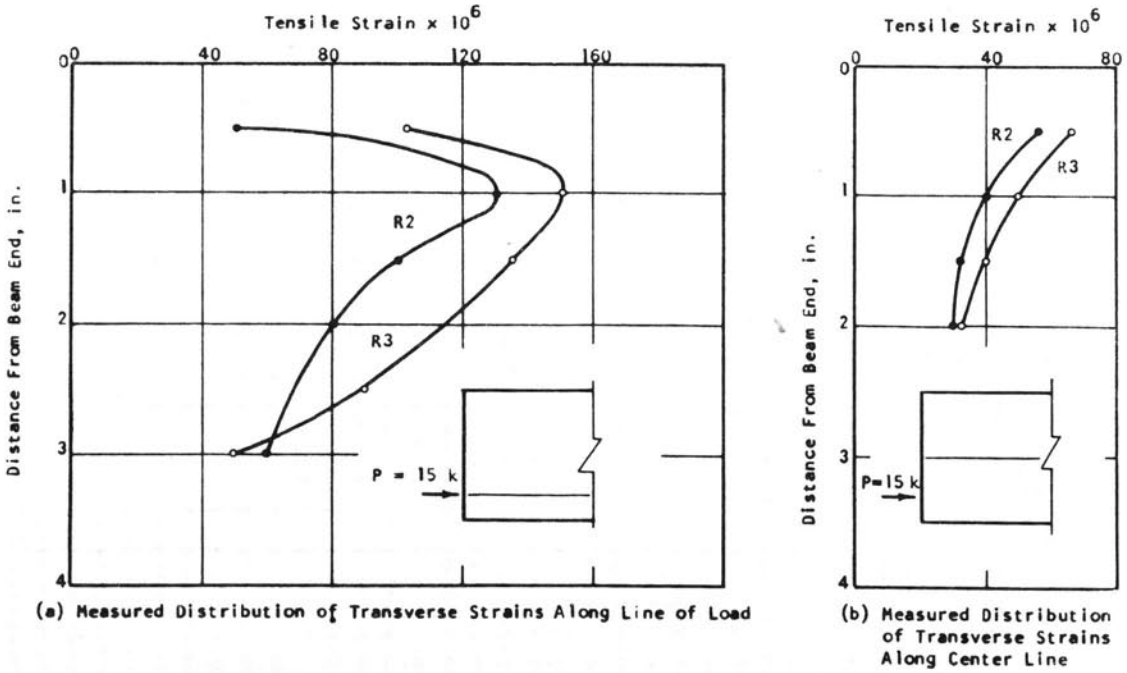

FIGURE 13. DISTRIBUTION OF TRANSVERSE CONCRETE STRAINS ALONG THE BEAM

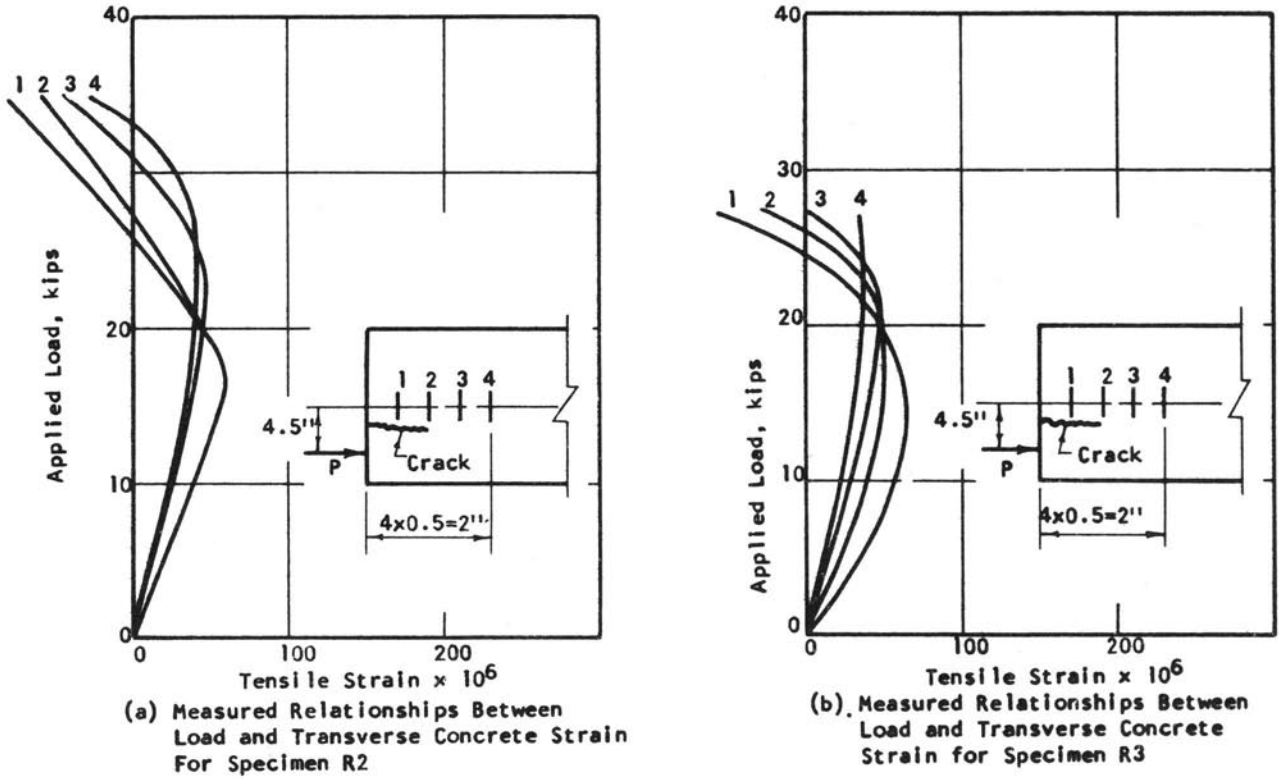

FIGURE 14. SPALLING STRAINS FOR SPECIMENS R2 AND R3

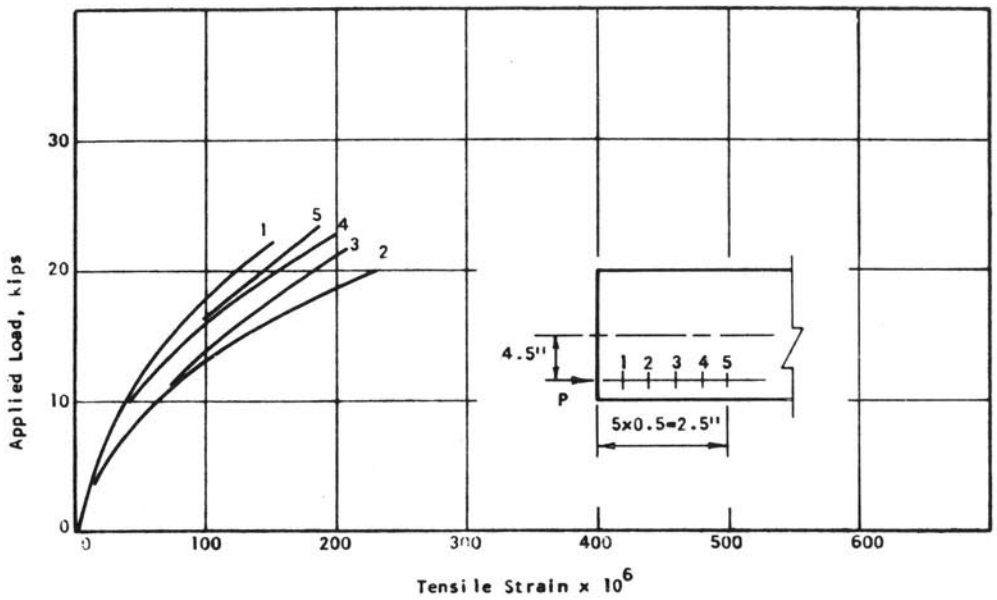

FIGURE 15. MEASURED RELATIONSHIPS BETWEEN LOAD AND TRANSVERSE STRAIN FOR SPECIMEN I3

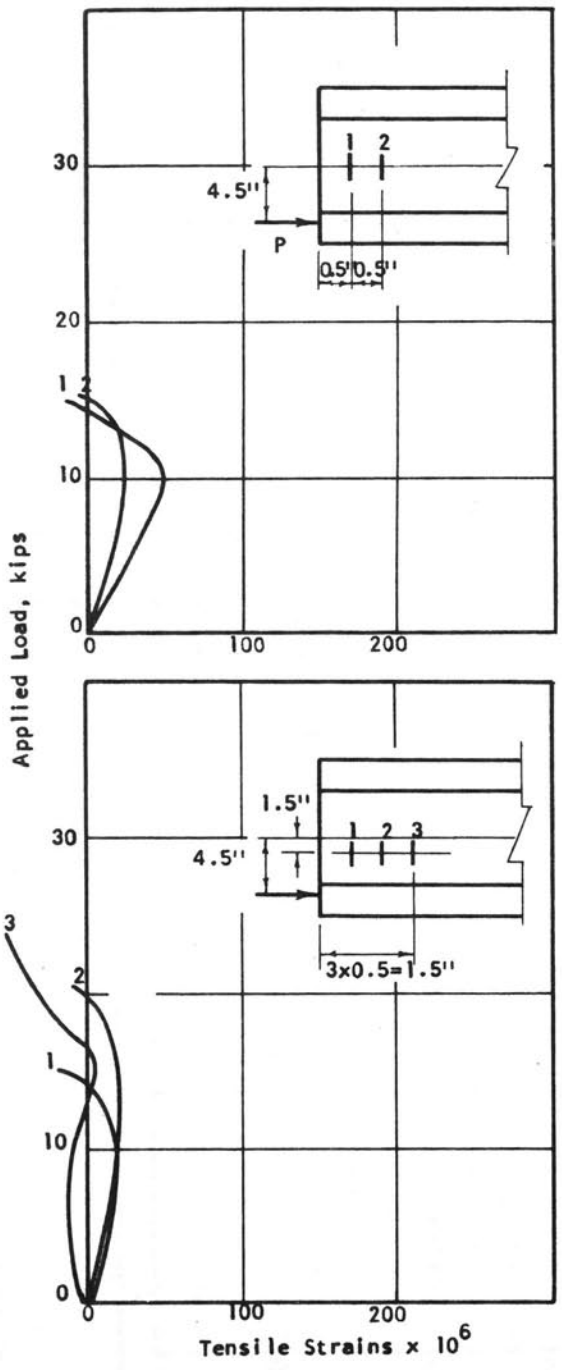

FIGURE 16. MEASURED RELATIONSHIPS BETWEEN LOAD AND TRANSVERSE CONCRETE STRAIN FOR SPECIMEN I3

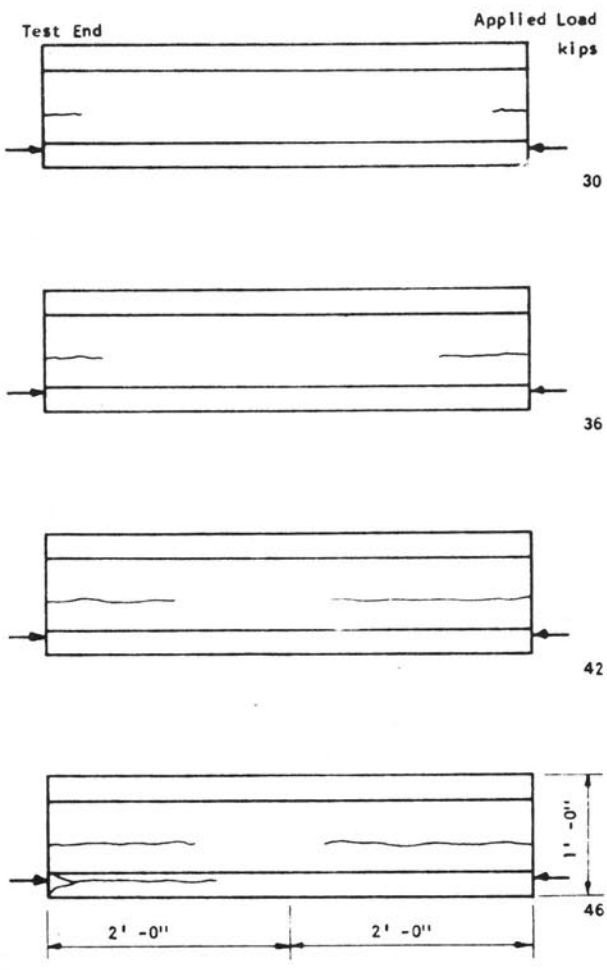

FIGURE 17. DEVELOPMENT OF CRACKS IN I-BEAMS

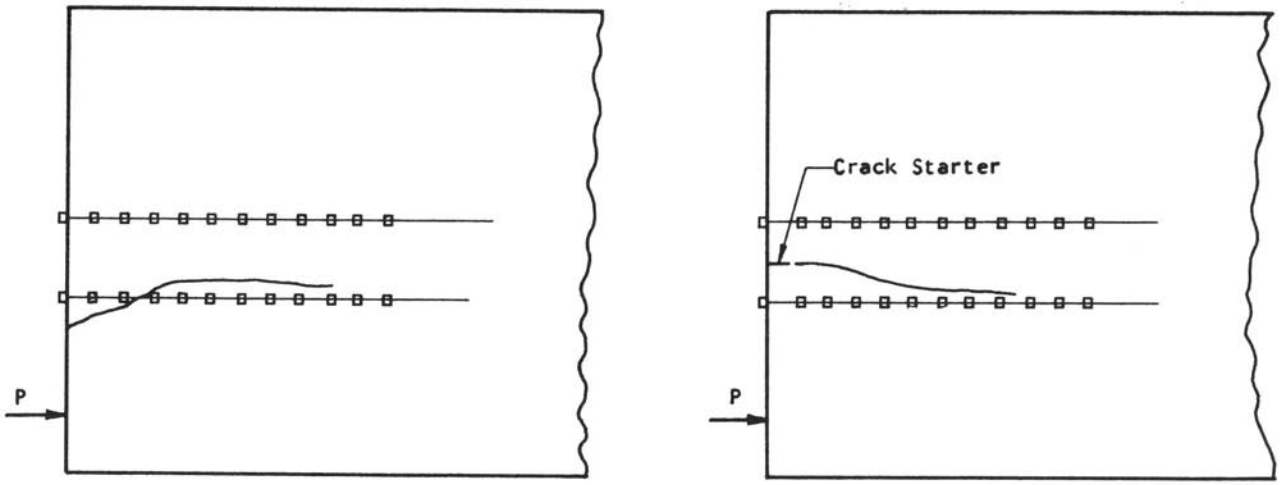

FIGURE 18. CRACK LOCATIONS FOR SPECIMENS WITH AND WITHOUT A CRACK STARTER

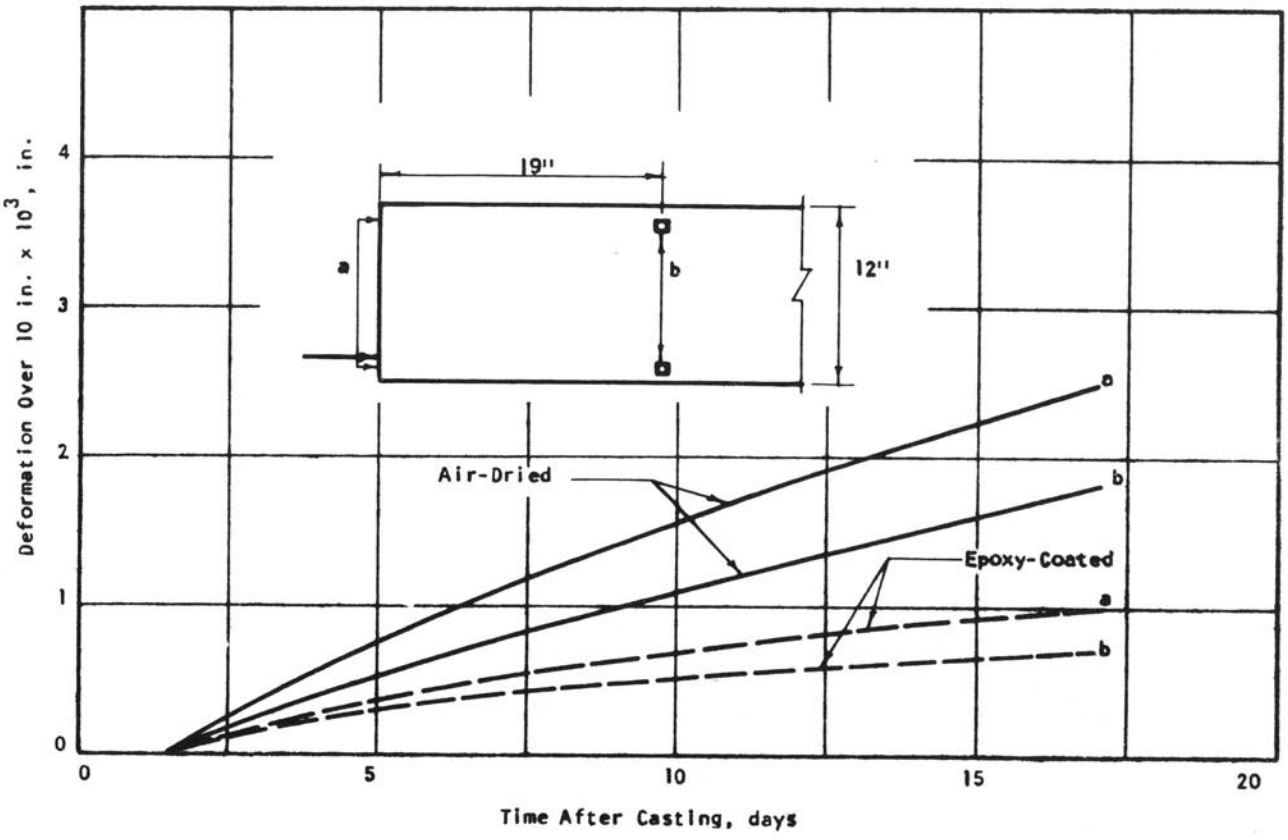

FIGURE 19. DEVELOPMENT OF SHRINKAGE DEFORMATIONS

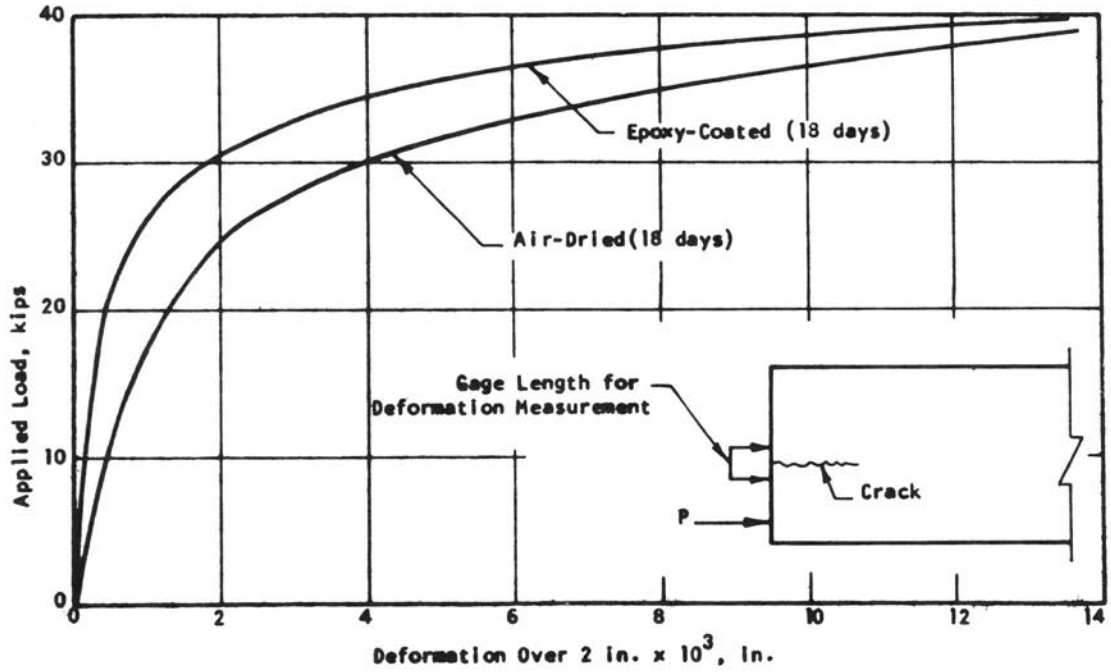

FIGURE 20. MEASURED RELATIONSHIPS BETWEEN LOAD AND TRANSVERSE DEFORMATION AT BEAM END FOR PLAIN CONCRETE SPECIMENS

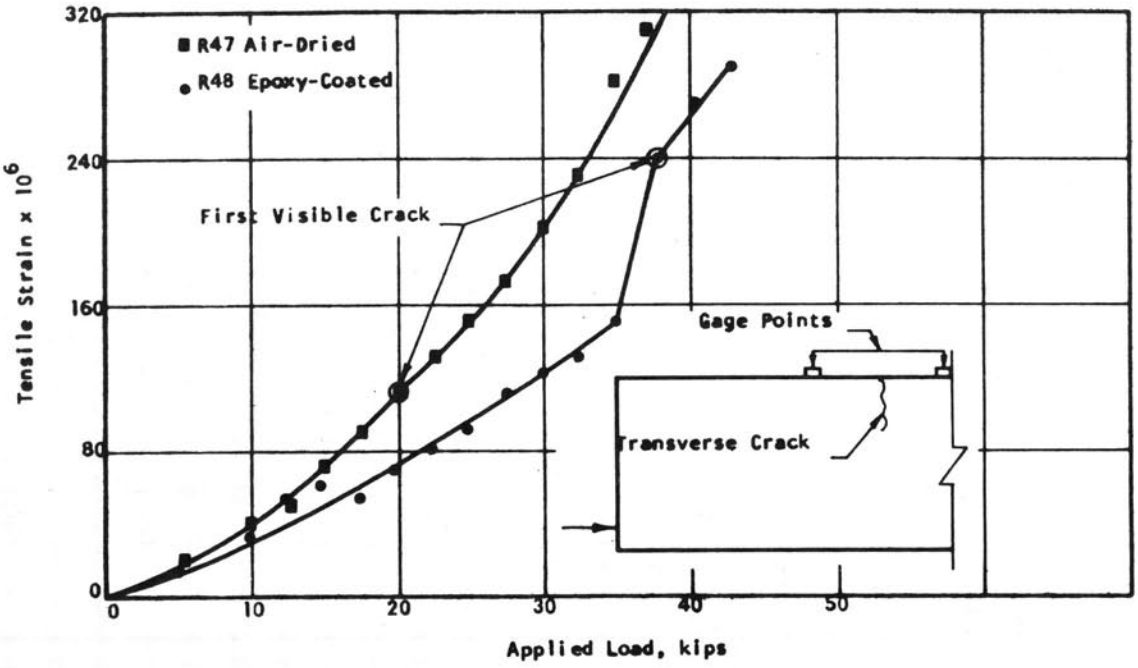

FIGURE 21. MEASURED RELATIONSHIPS BETWEEN LOAD AND LONGITUDINAL STRAIN IN MIDDLE OF SPECIMEN

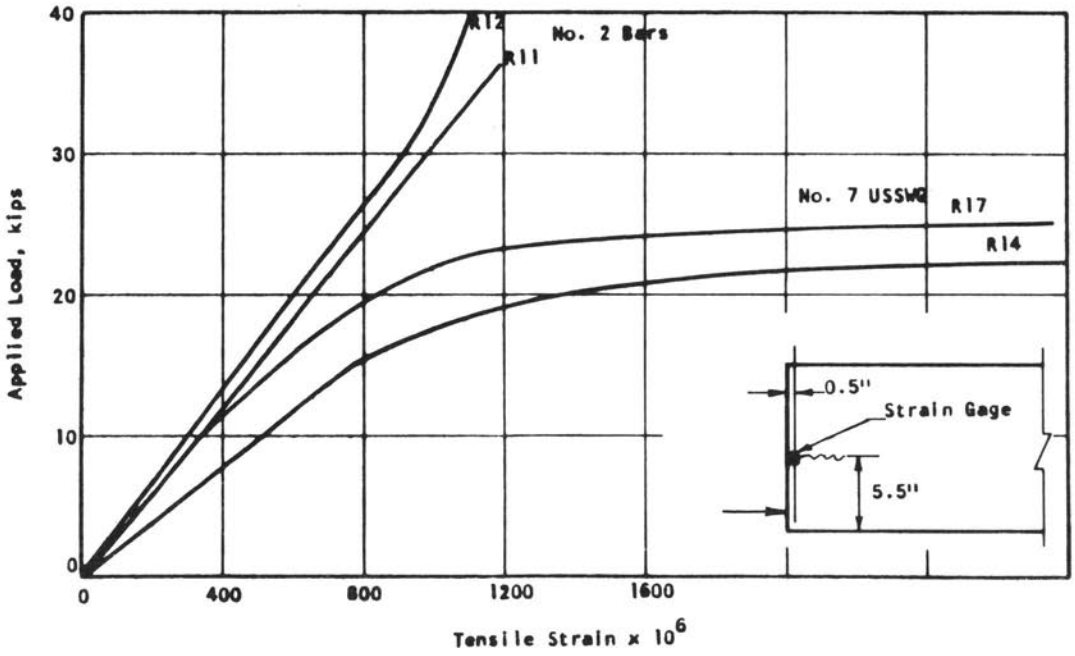

FIGURE 22. MEASURED RELATIONSHIPS BETWEEN APPLIED LOAD AND STIRRUP STRAIN FOR SPECIMENS R11, R12, R14, AND R17

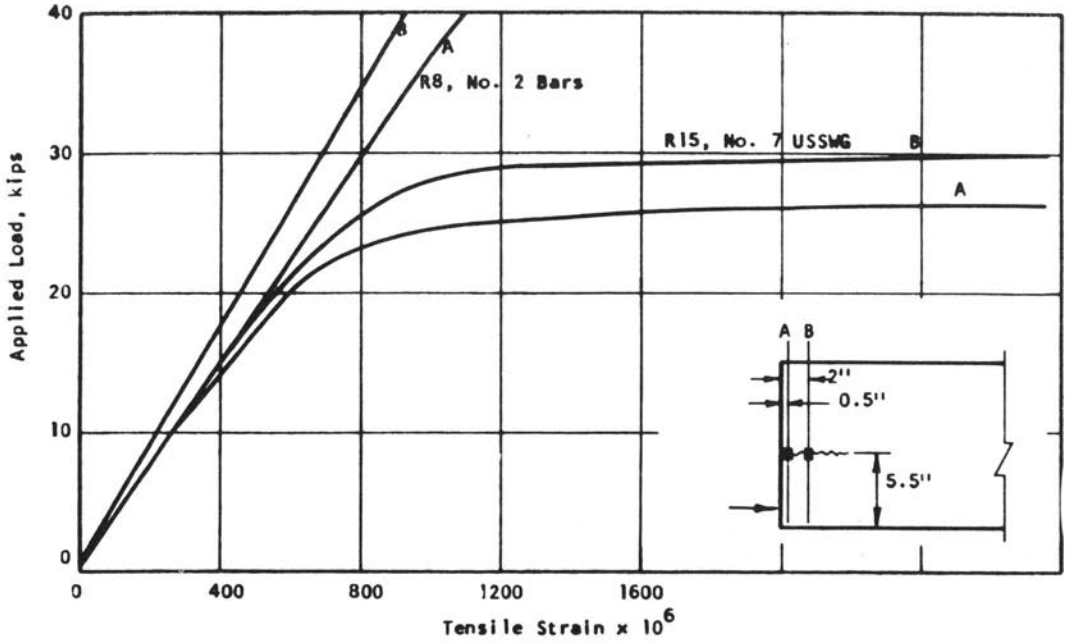

FIGURE 23. MEASURED RELATIONSHIPS BETWEEN APPLIED LOAD AND STIRRUP STRAIN FOR SPECIMENS R8 AND R15

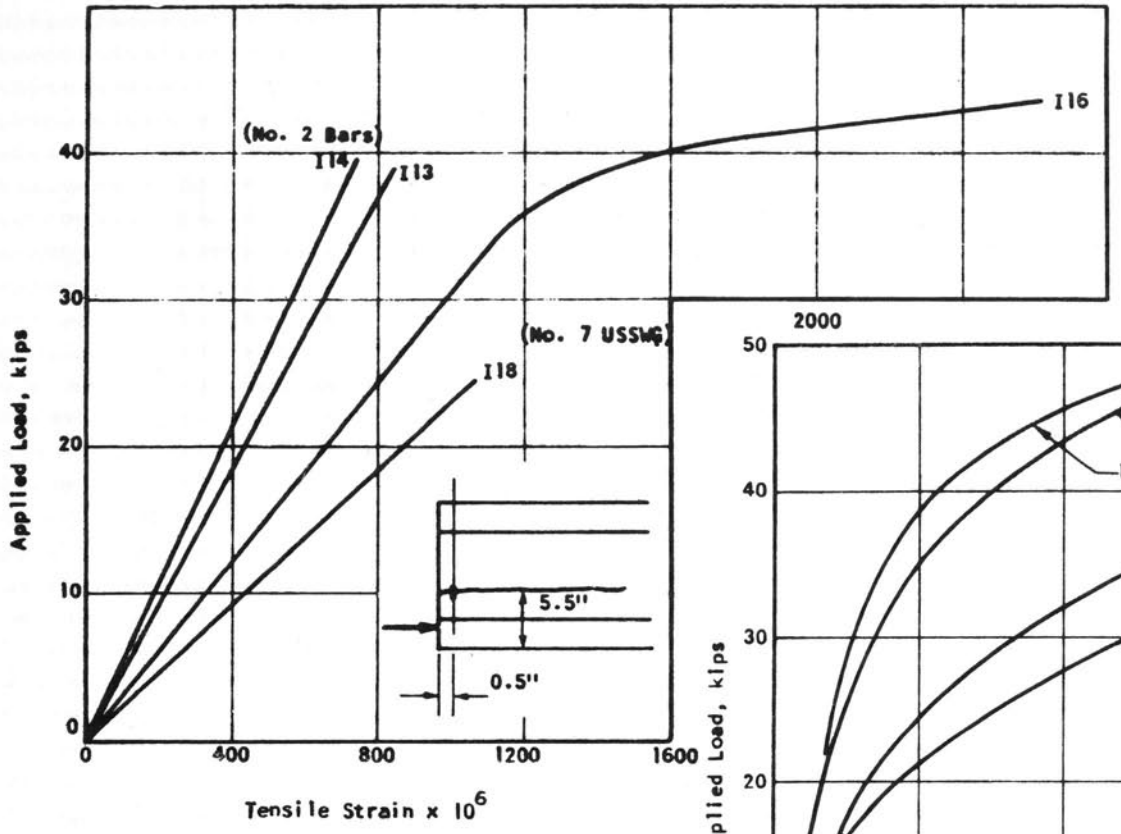

FIGURE 24. MEASURED RELATIONSHIPS BETWEEN APPLIED LOAD AND STIRRUP STRAIN FOR SPECIMENS I13, I14, I16, AND I18

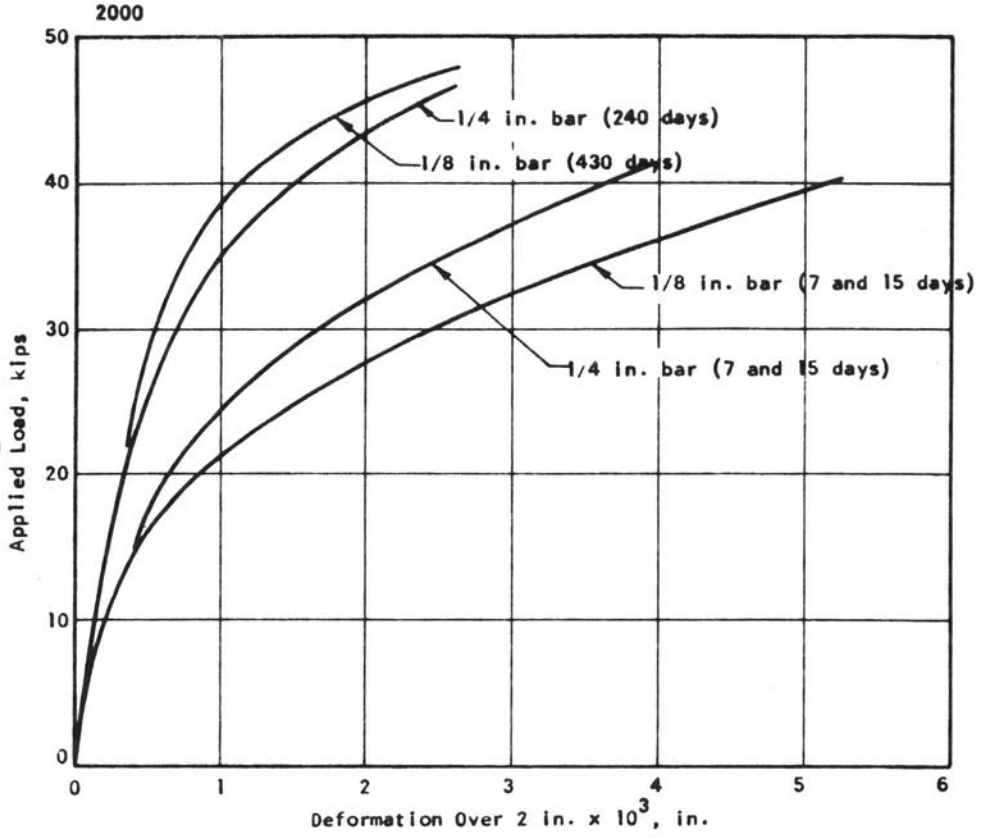

FIGURE 25. MEASURED RELATIONSHIPS BETWEEN LOAD AND TRANSVERSE DEFORMATION AT BEAM END FOR REINFORCED SPECIMENS

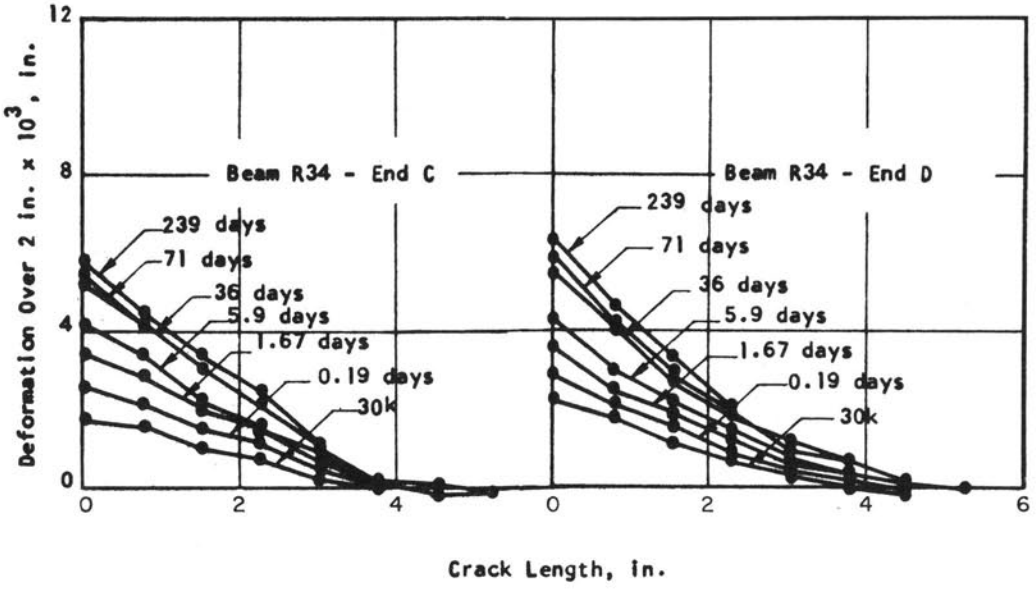

FIGURE 26. CRACK PROFILES FOR R34, 1/4-IN. DIAMETER STIRRUPS

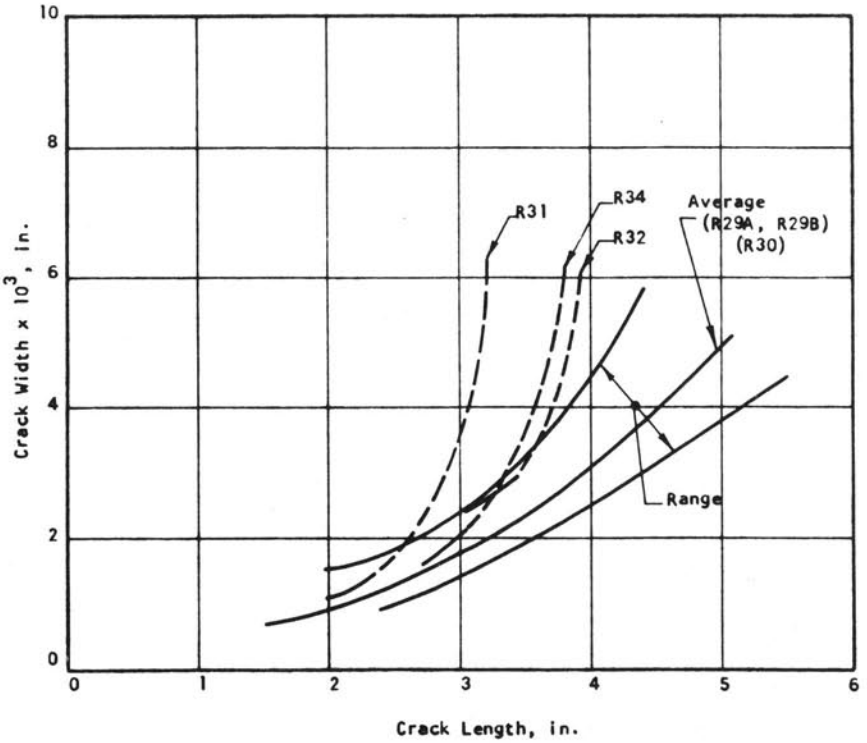

FIGURE 27. CRACK WIDTH VERSUS CRACK LENGTH FOR SPECIMENS WITH 1/4-IN. DIAMETER STIRRUPS

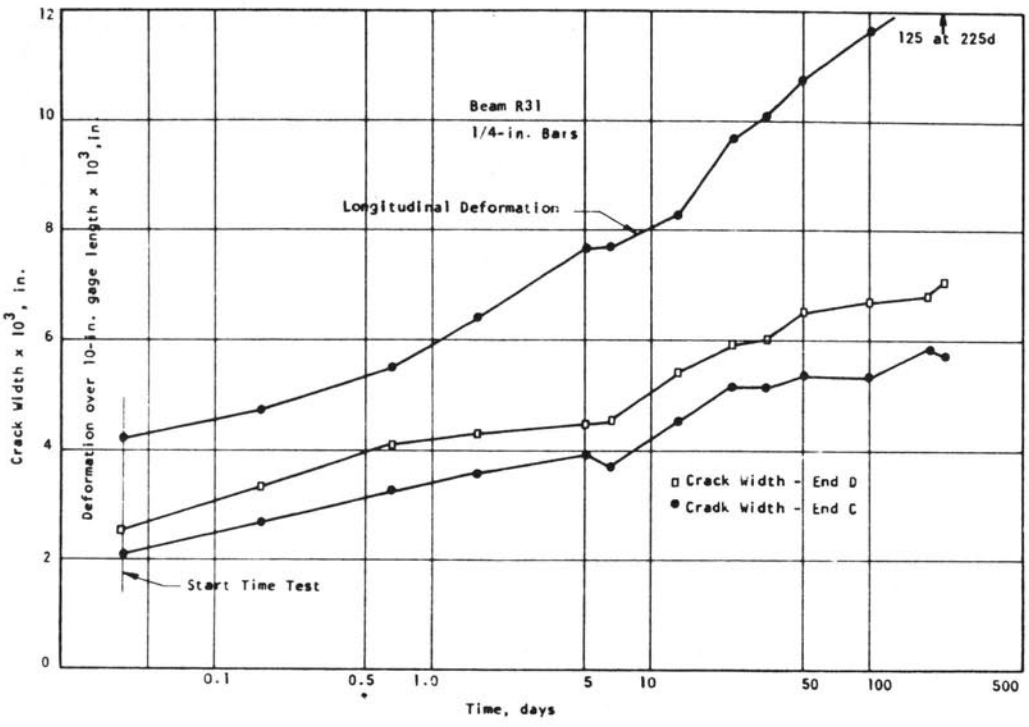

FIGURE 28. CRACK WIDTH AND LONGITUDINAL DEFORMATION VERSUS TIME FOR R31

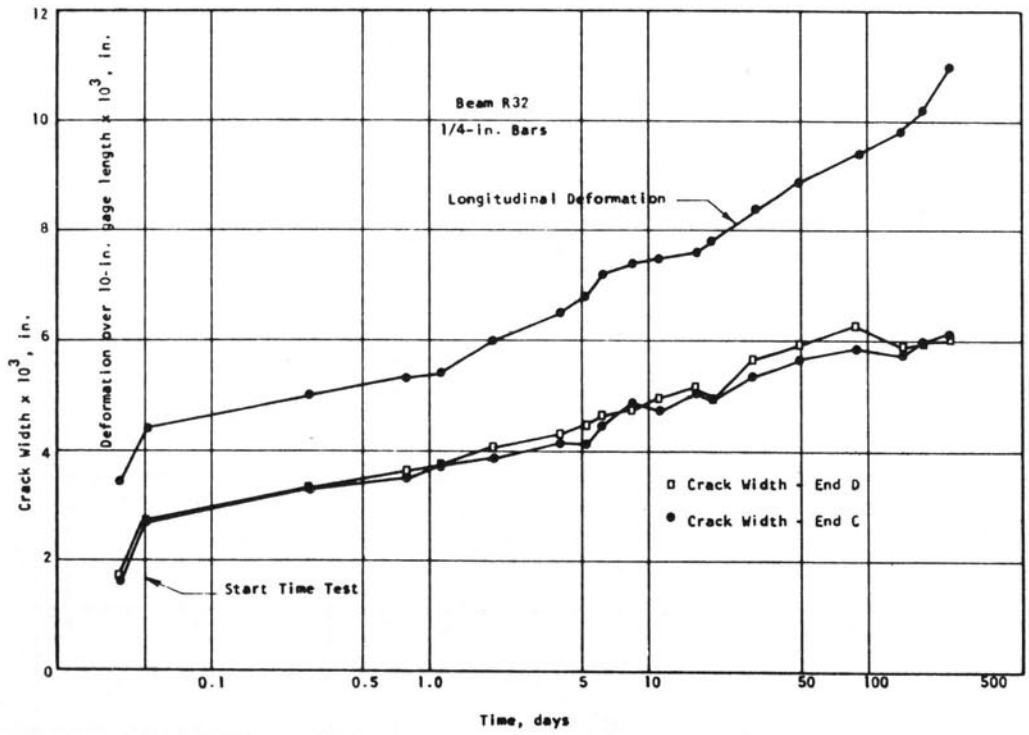

FIGURE 29. CRACK WIDTH AND LONGITUDINAL DEFORMATION VERSUS TIME FOR R32

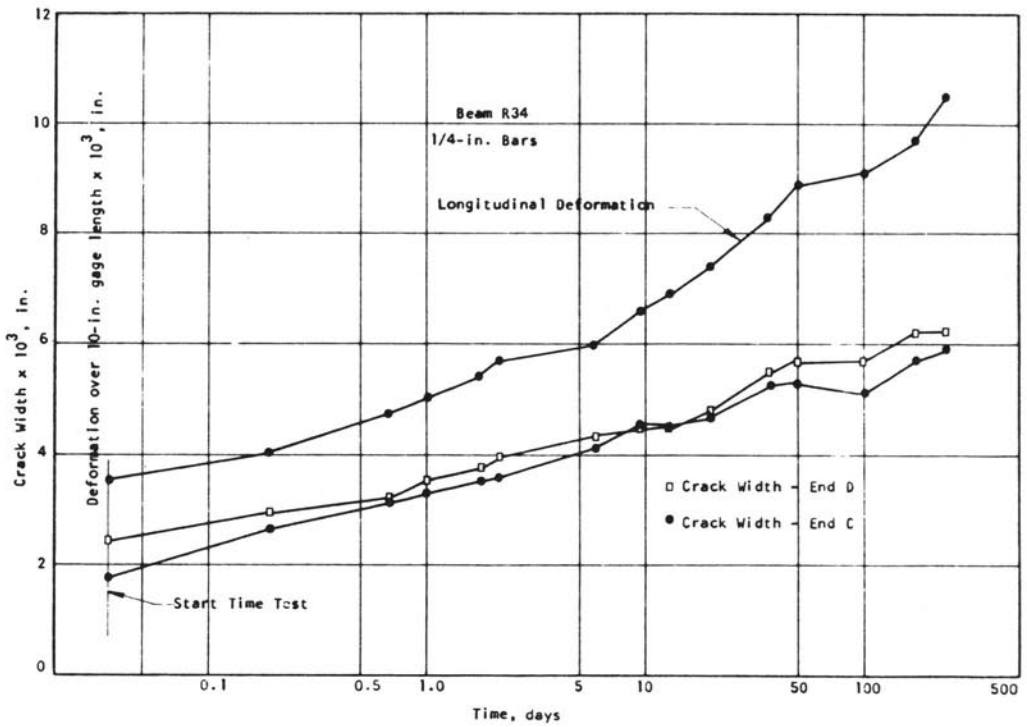

FIGURE 30. CRACK WIDTH AND LONGITUDINAL DEFORMATION VERSUS TIME FOR R34

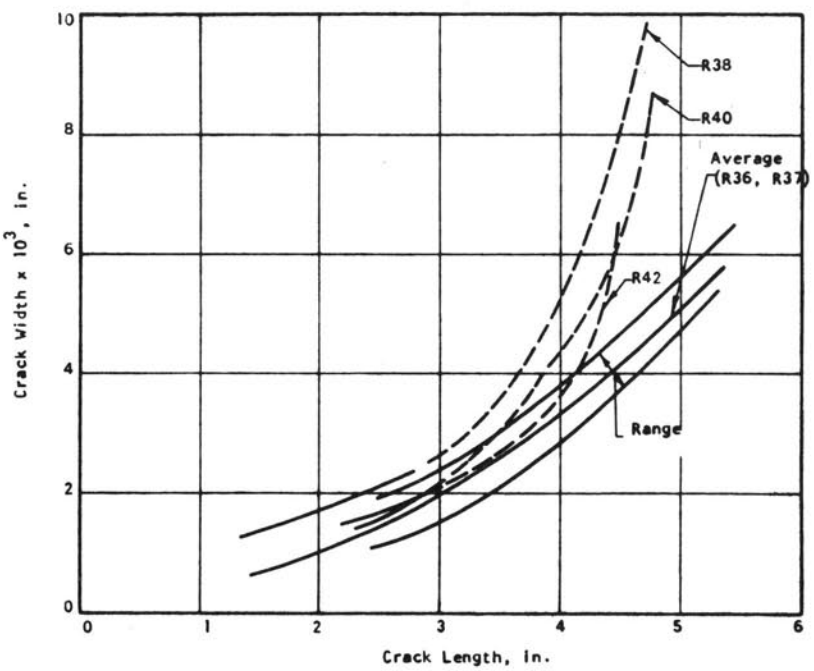

FIGURE 31. CRACK WIDTH VERSUS CRACK LENGTH FOR SPECIMENS WITH 1/8-IN. DIAMETER STIRRUPS

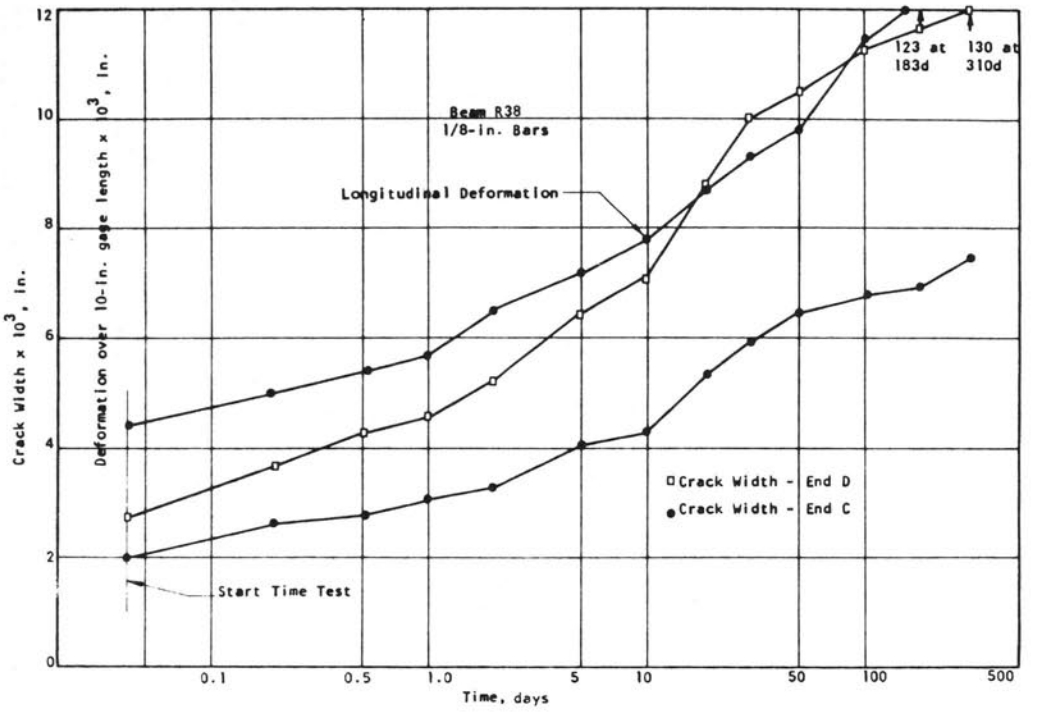

FIGURE 32. CRACK WIDTH AND LONGITUDINAL DEFORMATION VERSUS TIME FOR R38

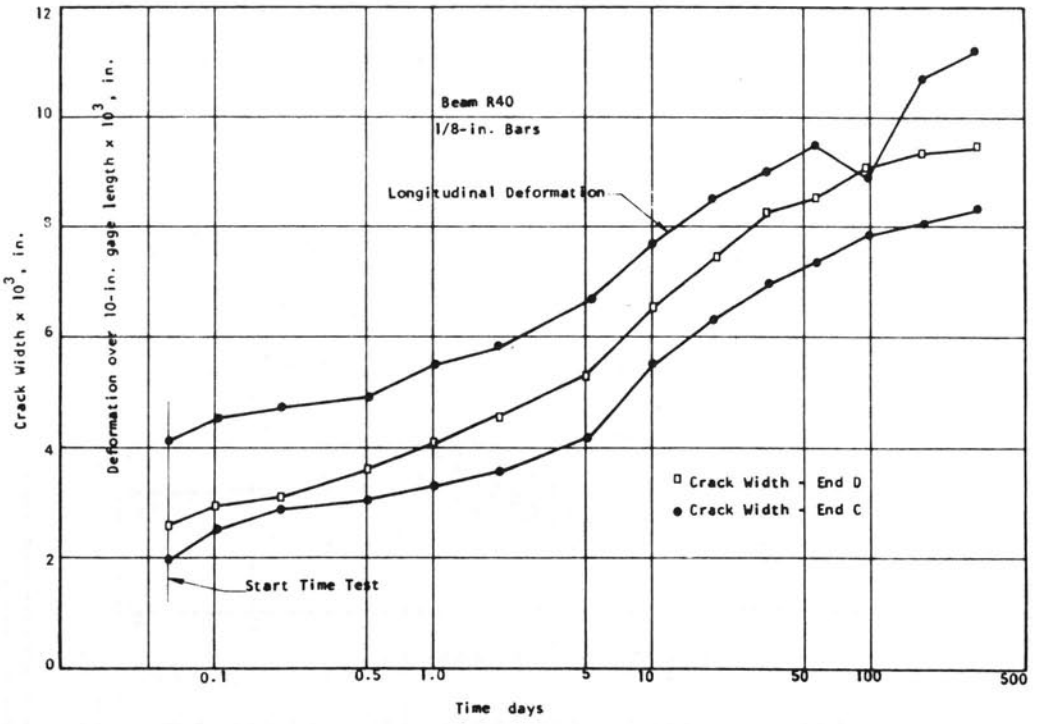

FIGURE 33. CRACK WIDTH AND LONGITUDINAL DEFORMATION VERSUS TIME FOR R40

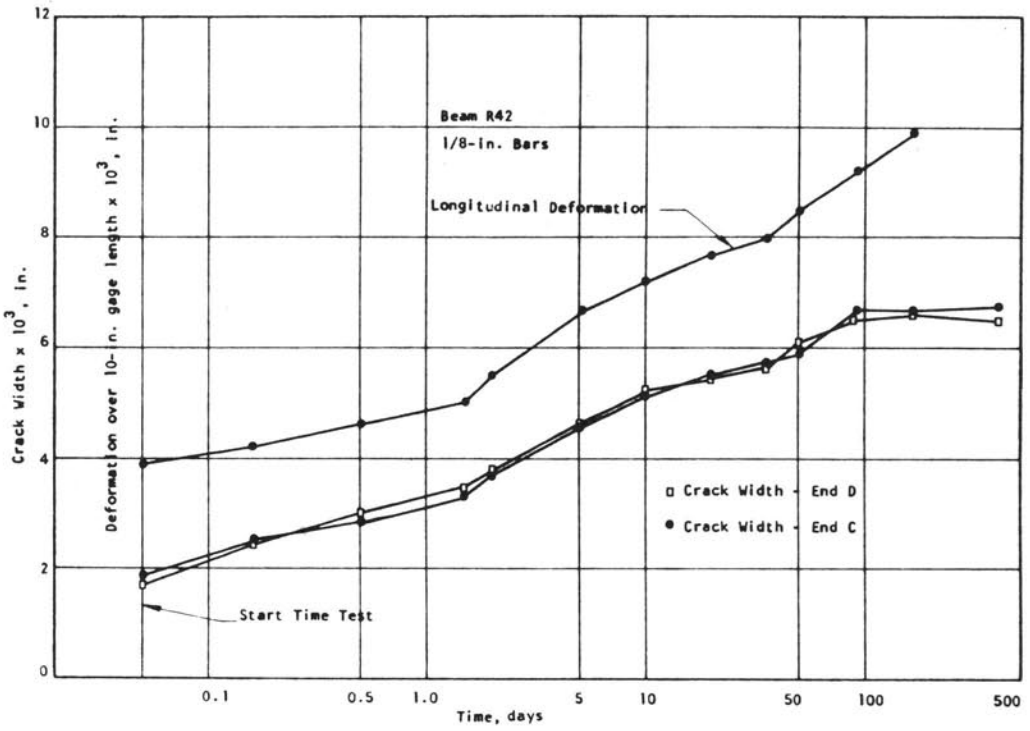

FIGURE 34. CRACK WIDTH AND LONGITUDINAL DEFORMATION VERSUS TIME FOR R42

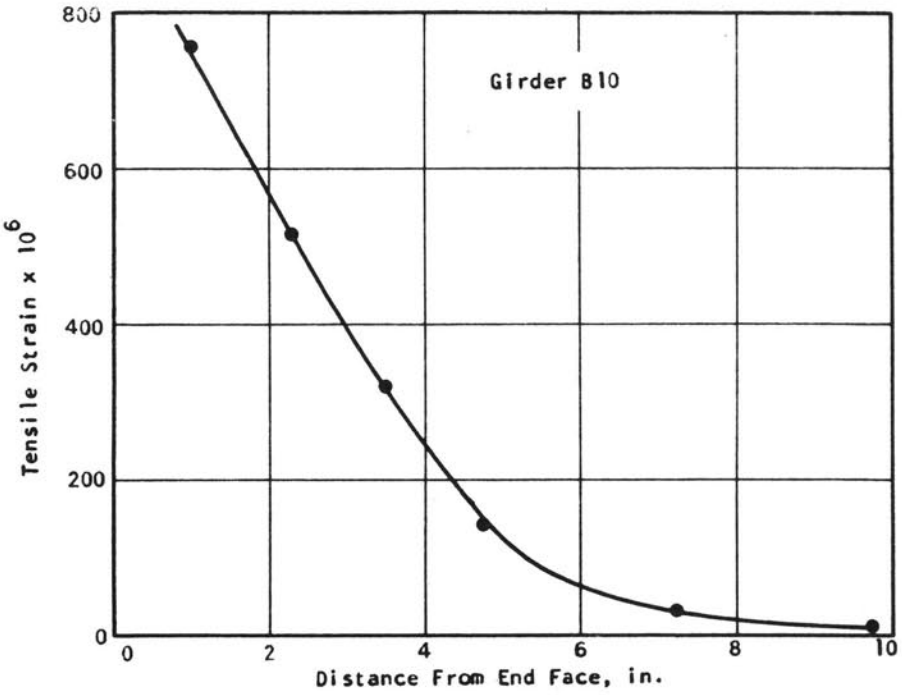

FIGURE 35. TYPICAL VARIATION IN STIRRUP STRAIN WITH DISTANCE FROM END OF GIRDER

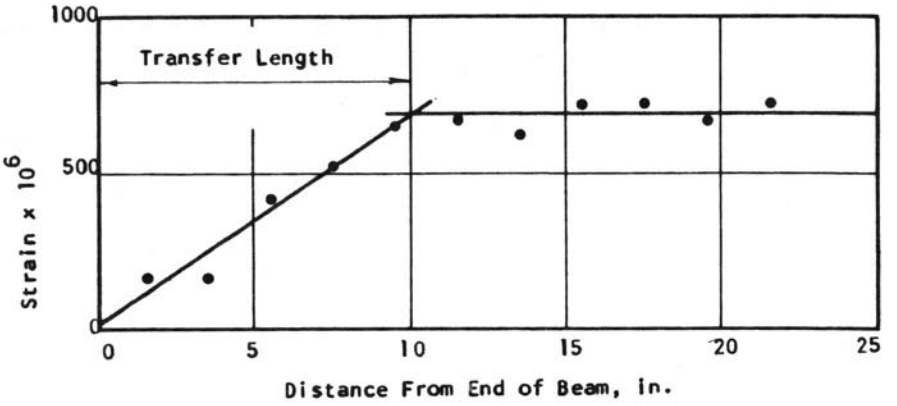

FIGURE 36. TYPICAL BUILD-UP OF LONGITUDINAL STRAIN IN SERIES A GIRDERS [BEAM A2(2), SECTION ONE IN. ABOVE BOTTOM]

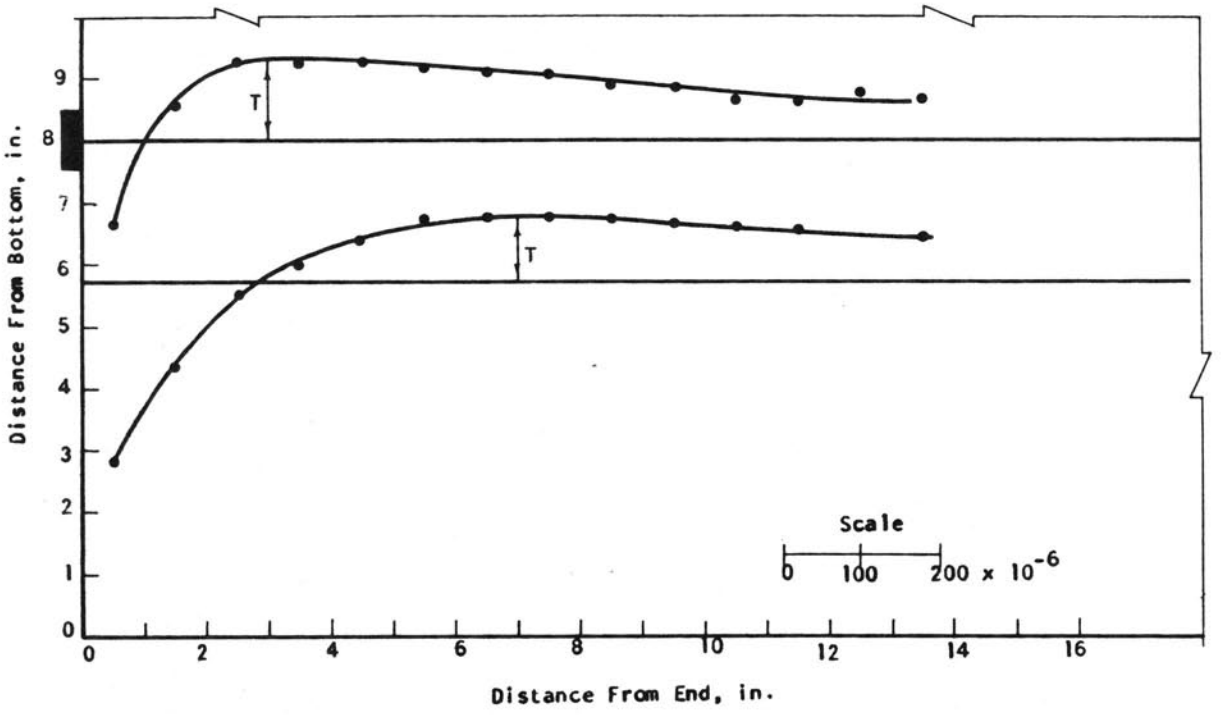

FIGURE 37. TRANSVERSE-STRAIN DISTRIBUTION FOR TEST 1 AT 15 KIPS

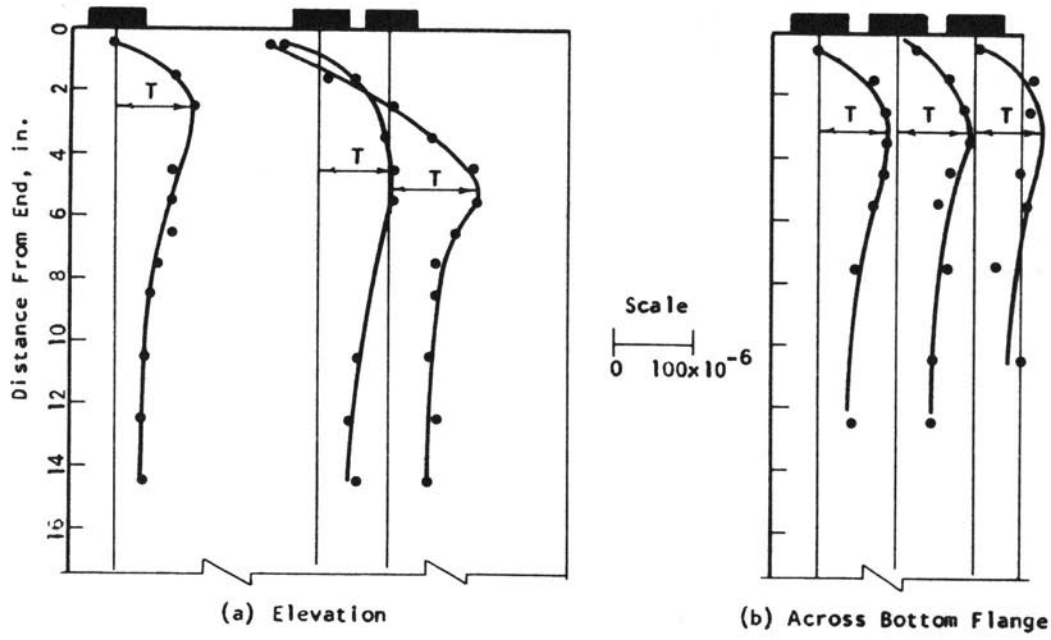

FIGURE 38. TRANSVERSE-STRAIN DISTRIBUTION FOR TEST 19 AT 67.2 KIPS

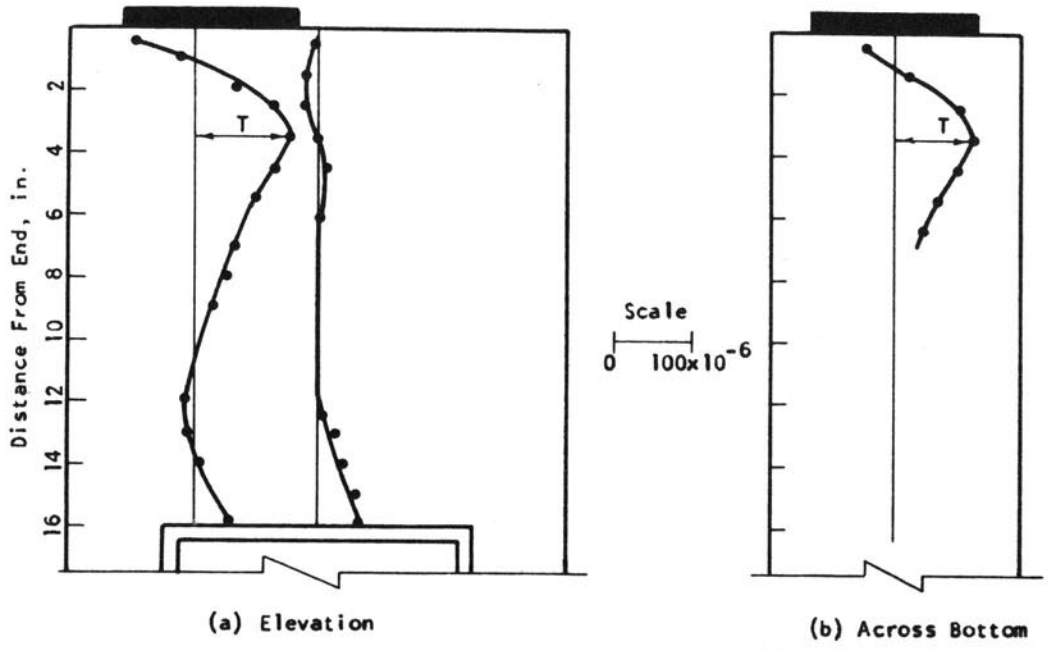

FIGURE 39. TRANSVERSE-STRAIN DISTRIBUTION FOR TEST 17 AT 67.2 KIPS

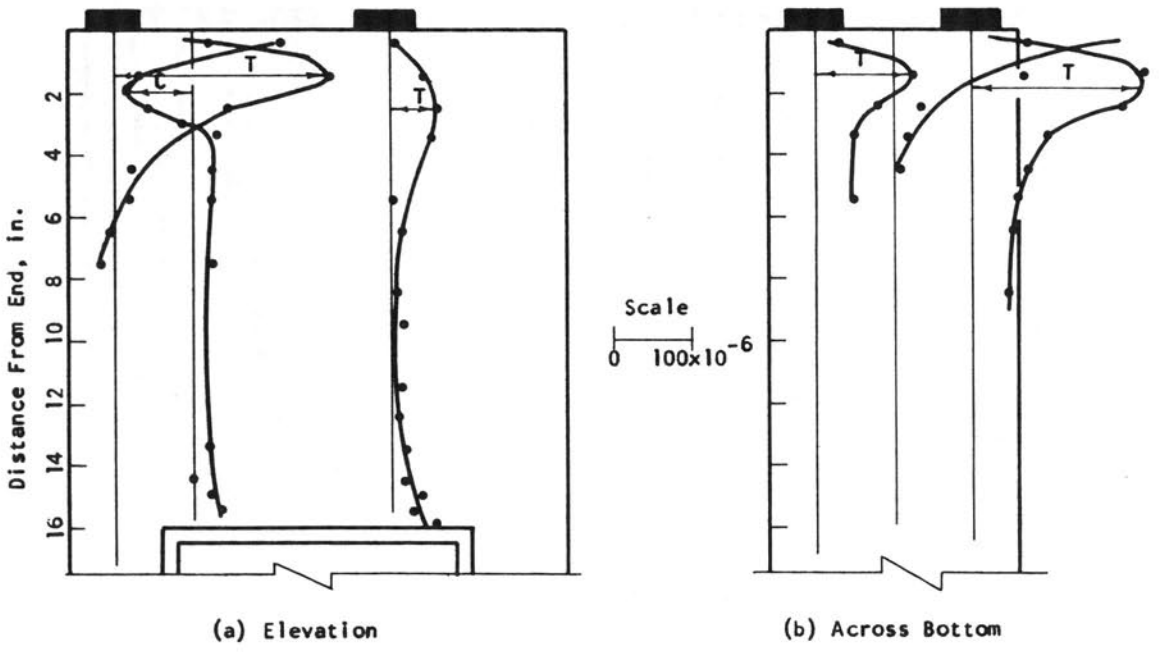

FIGURE 40. TRANSVERSE-STRAIN DISTRIBUTION FOR TEST 16 AT 44.8 KIPS

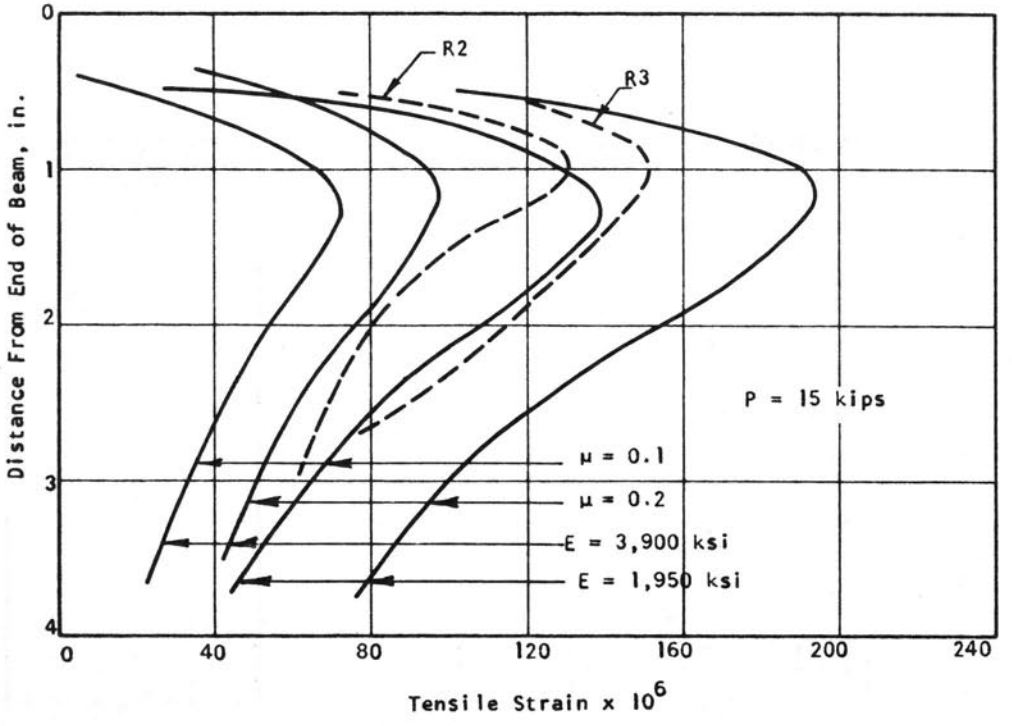

FIGURE 41. COMPARISON OF MEASURED TRANSVERSE STRAINS ALONG THE LINE OF APPLIED LOAD WITH GERGELY'S FINITE DIFFERENCE SOLUTION

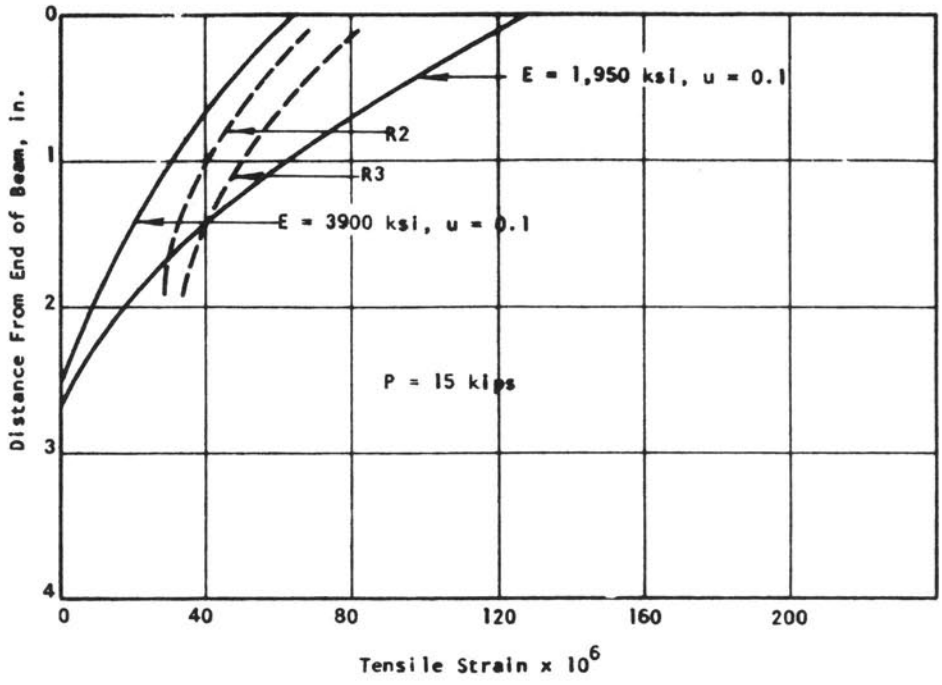

FIGURE 42. COMPARISON OF MEASURED TRANSVERSE STRAINS ALONG CENTER LINE WITH GERGELY'S FINITE DIFFERENCE SOLUTION

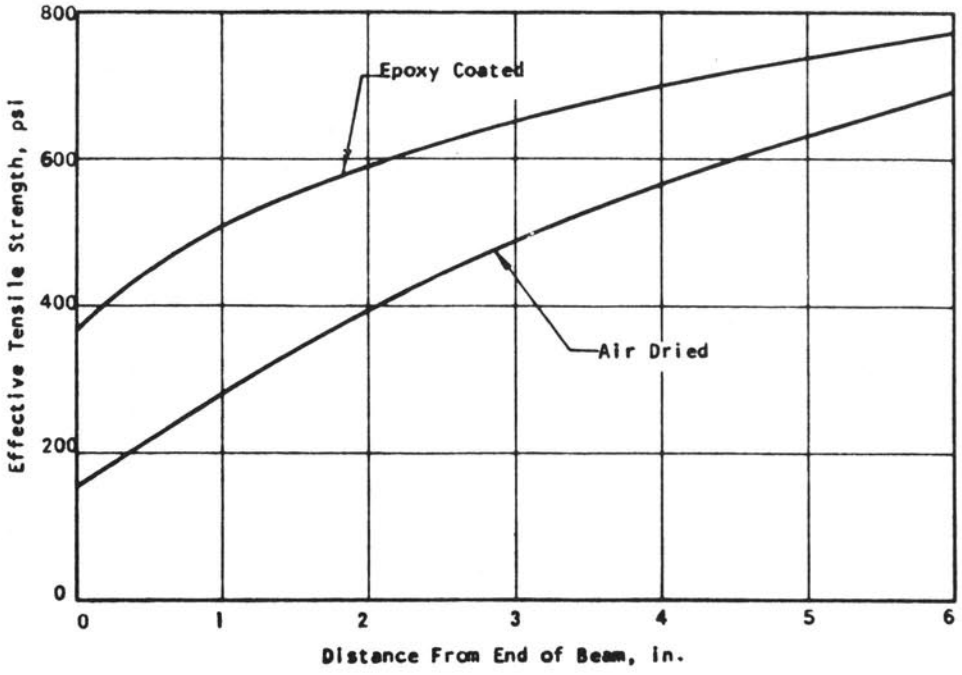

FIGURE 43. EFFECTIVE TENSILE STRENGTH ENVELOPES FOR AIR-DRIED AND EPOXY-COATED PLAIN CONCRETE SPECIMENS

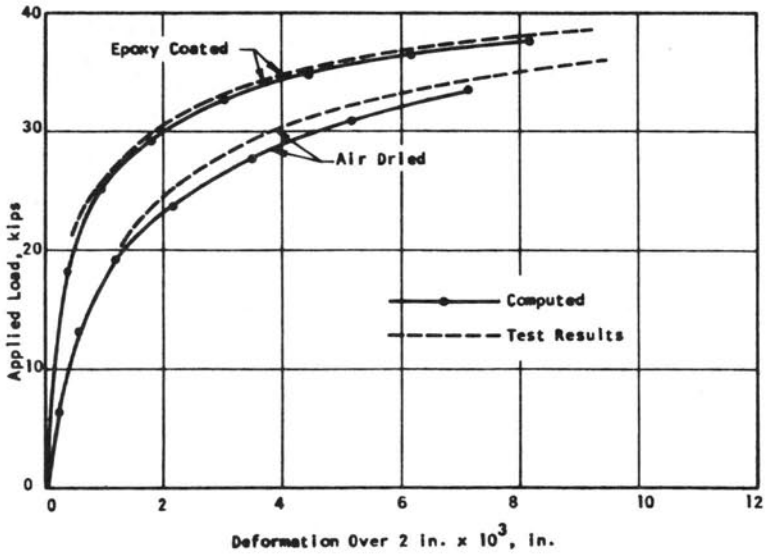

FIGURE 44. COMPARISON OF COMPUTED CRACK WIDTH AT BEAM END WITH TEST RESULTS FOR PLAIN CONCRETE SPECIMENS

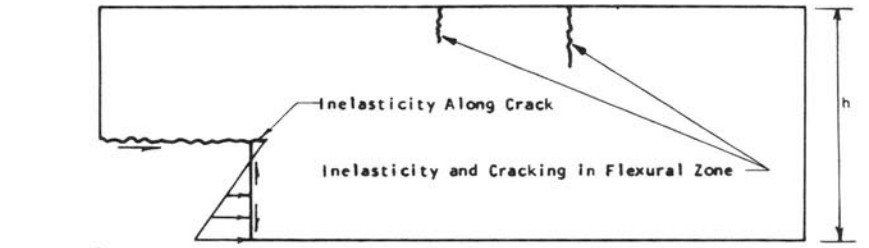

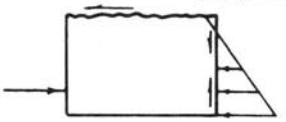

FIGURE 45. FREE BODY OF CRACKED ANCHORAGE ZONE

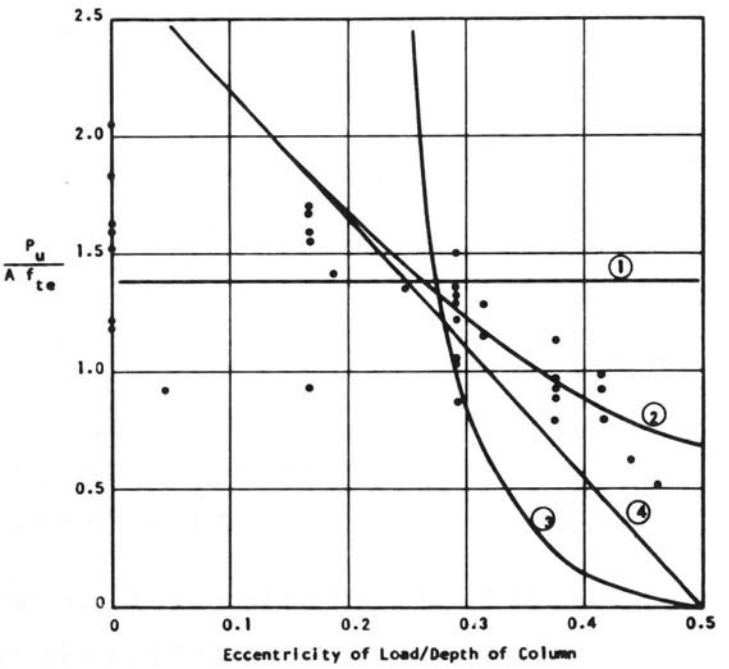

FIGURE 46. COMPARISON OF TEST RESULTS FROM KRIZ AND RATHS WITH THEORETICAL CALCULATIONS

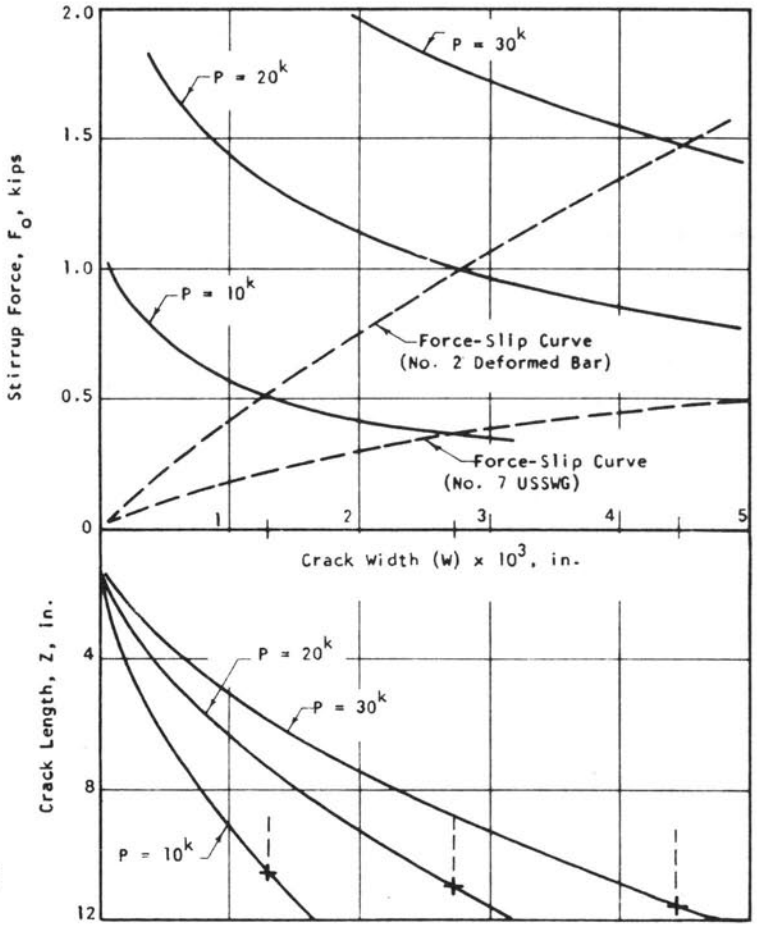

FIGURE 47. RELATIONSHIPS BETWEEN STIRRUP FORCE, CRACK WIDTH, AND CRACK LENGTH FOR RECTANGULAR SECTIONS

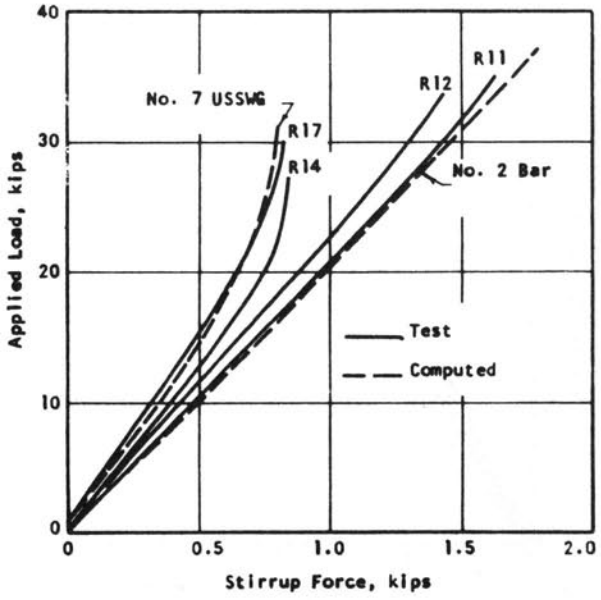

FIGURE 48. COMPARISON OF TEST RESULTS WITH CALCULATED VALUES FOR RECTANGULAR SPECIMENS WITH A PREFORMED CRACK

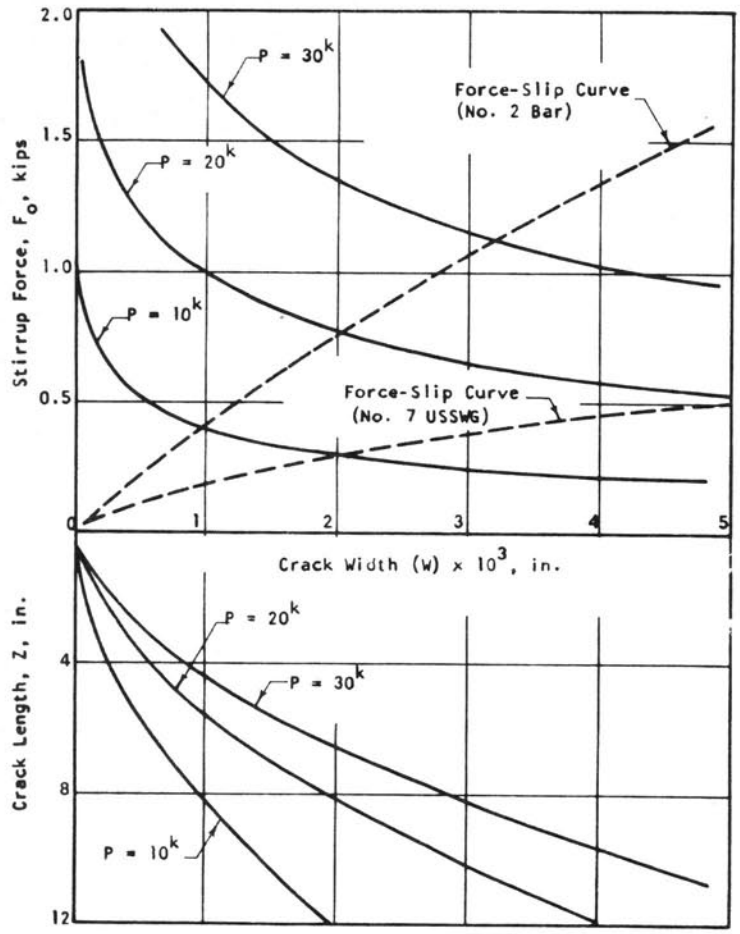

FIGURE 49. RELATIONSHIPS BETWEEN STIRRUP FORCE, CRACK WIDTH, AND CRACK LENGTH FOR I-SPECIMENS

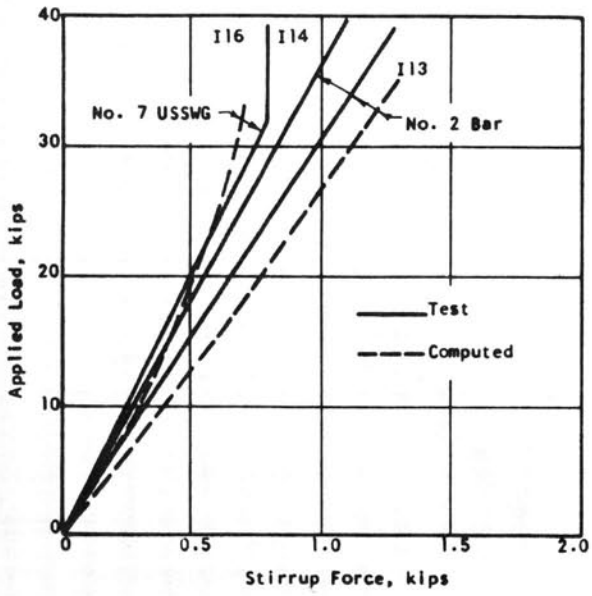

FIGURE 50. COMPARISON OF TEST RESULTS WITH CALCULATED VALUES FOR I-SPECIMENS WITH A PREFORMED CRACK

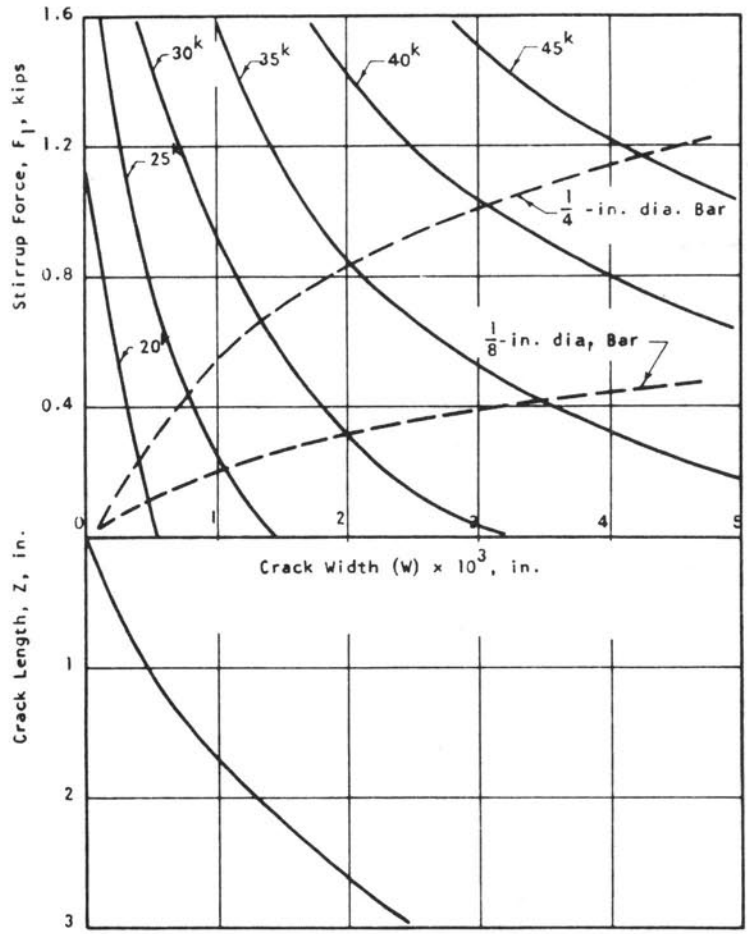

FIGURE 51. RELATIONSHIPS BETWEEN STIRRUP FORCE, CRACK WIDTH, AND CRACK LENGTH FOR INITIALLY UNCRACKED SPECIMENS

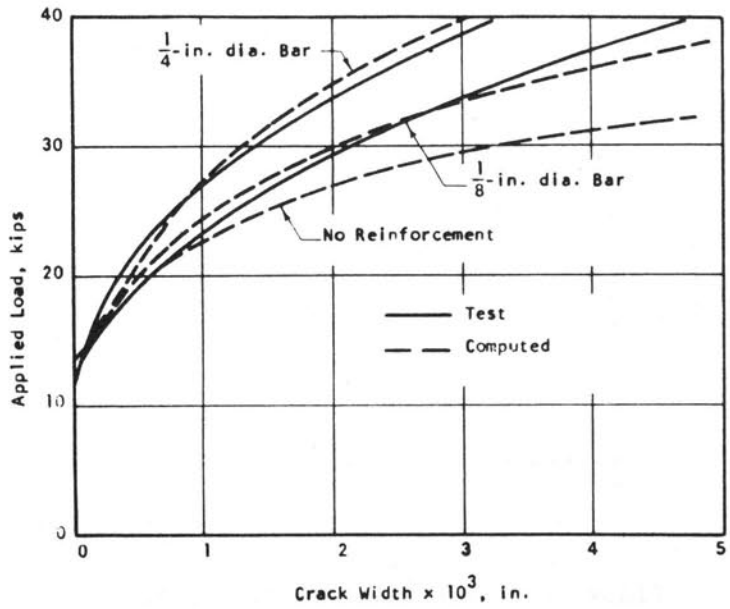

FIGURE 52. COMPARISON OF TEST RESULTS WITH CALCULATED VALUES FOR INITIALLY UNCRACKED SPECIMENS

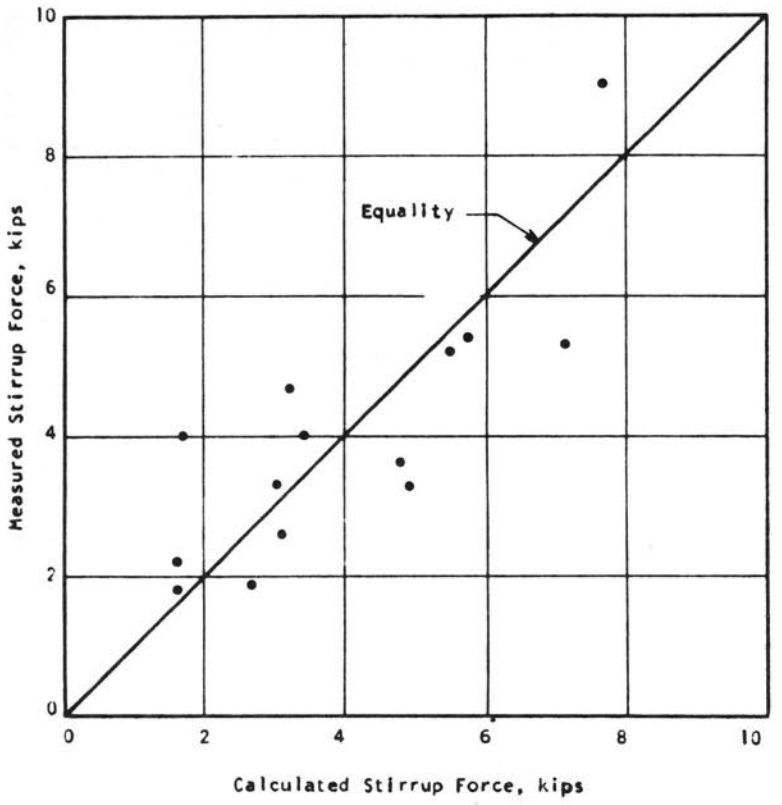

FIGURE 53. CALCULATED VERSUS MEASURED STIRRUP FORCES FOR TESTS BY MARSHALL AND MATTOCK

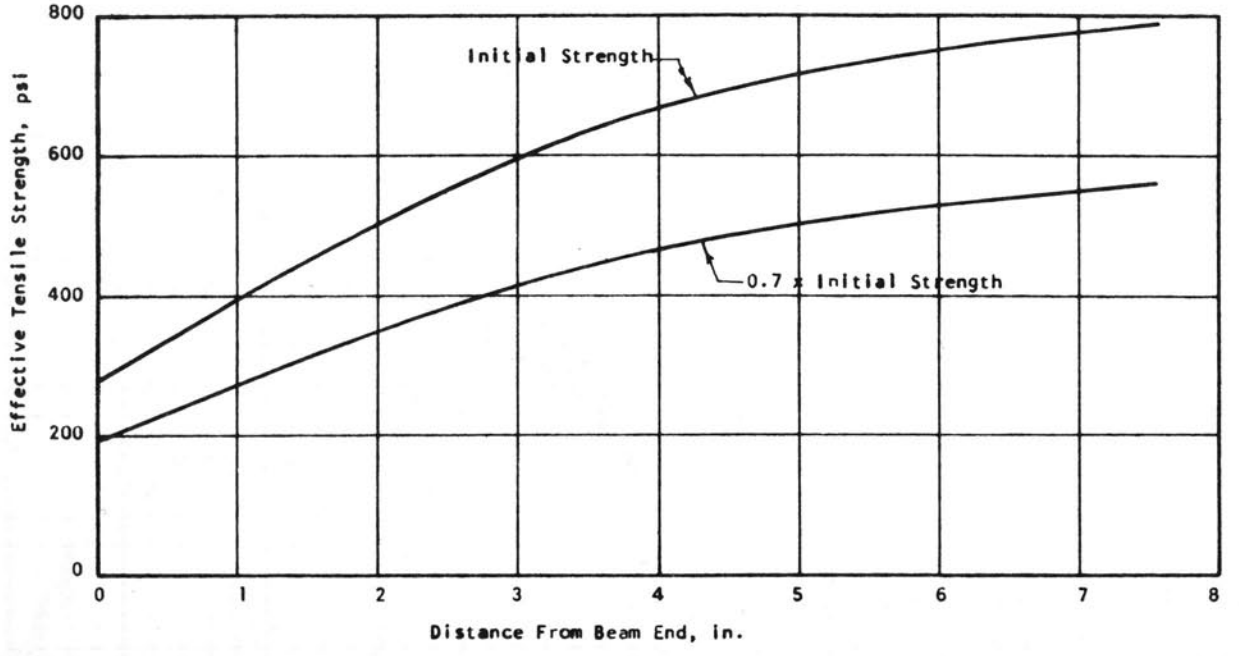

FIGURE 54. EFFECTIVE TENSILE STRENGTH ENVELOPES FOR SUSTAINED-LOAD TESTS

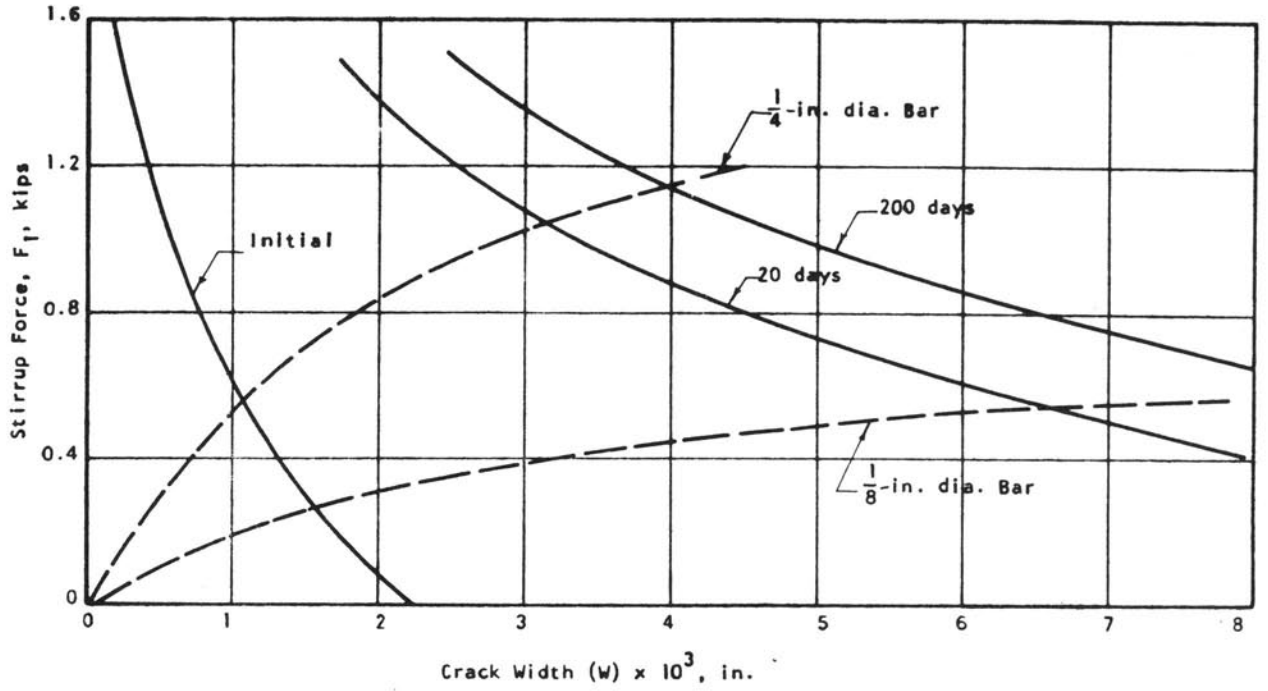

FIGURE 55. RELATIONSHIP BETWEEN CRACK WIDTH AND STIRRUP FORCE FOR SUSTAINED-LOAD TESTS

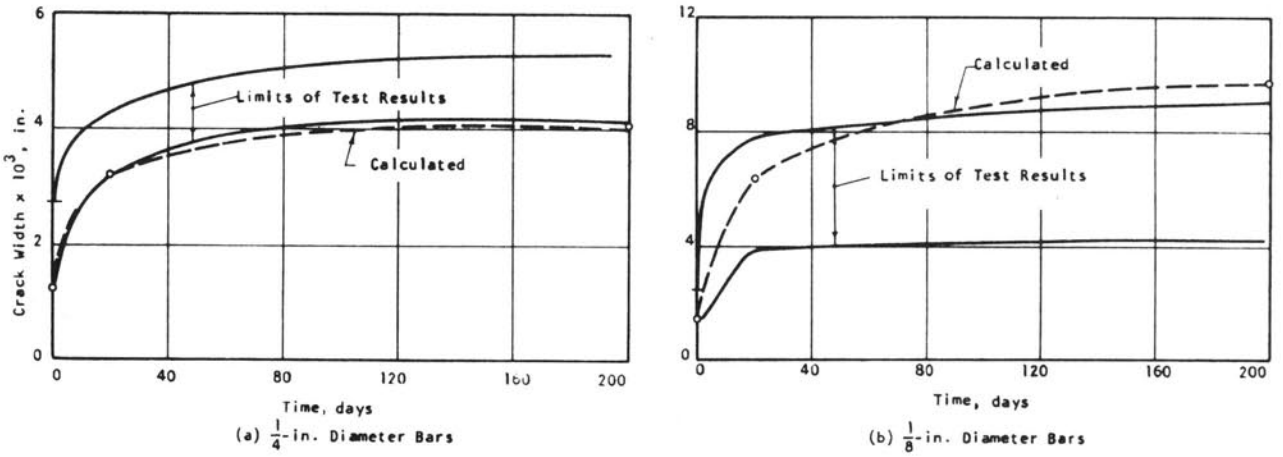

FIGURE 56. COMPARISON OF MEASURED AND COMPUTED CRACK WIDTHS FOR SUSTAINED-LOAD TESTS

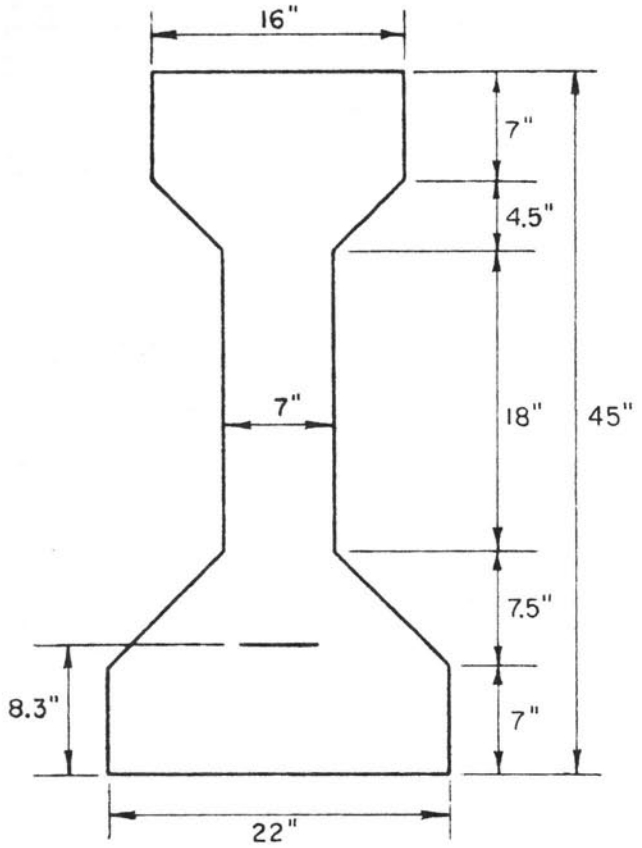

FIGURE 57. AASHO TYPE III GIRDER

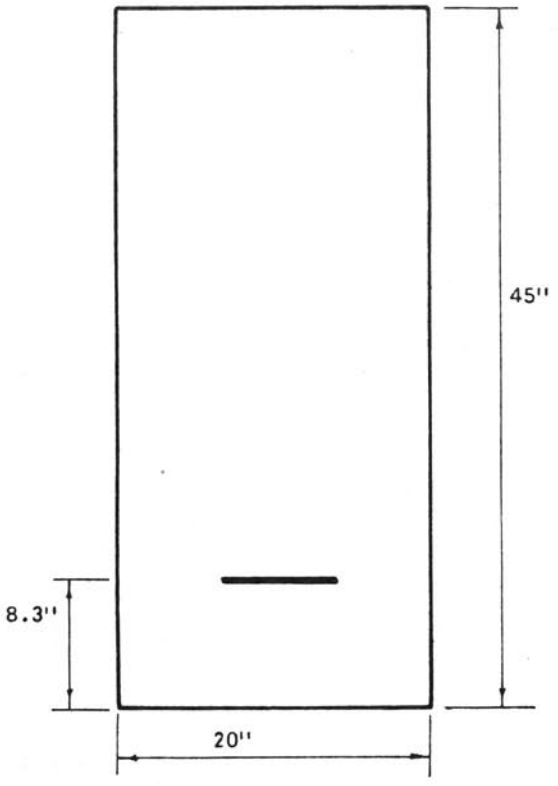

FIGURE 58. RECTANGULAR END BLOCK

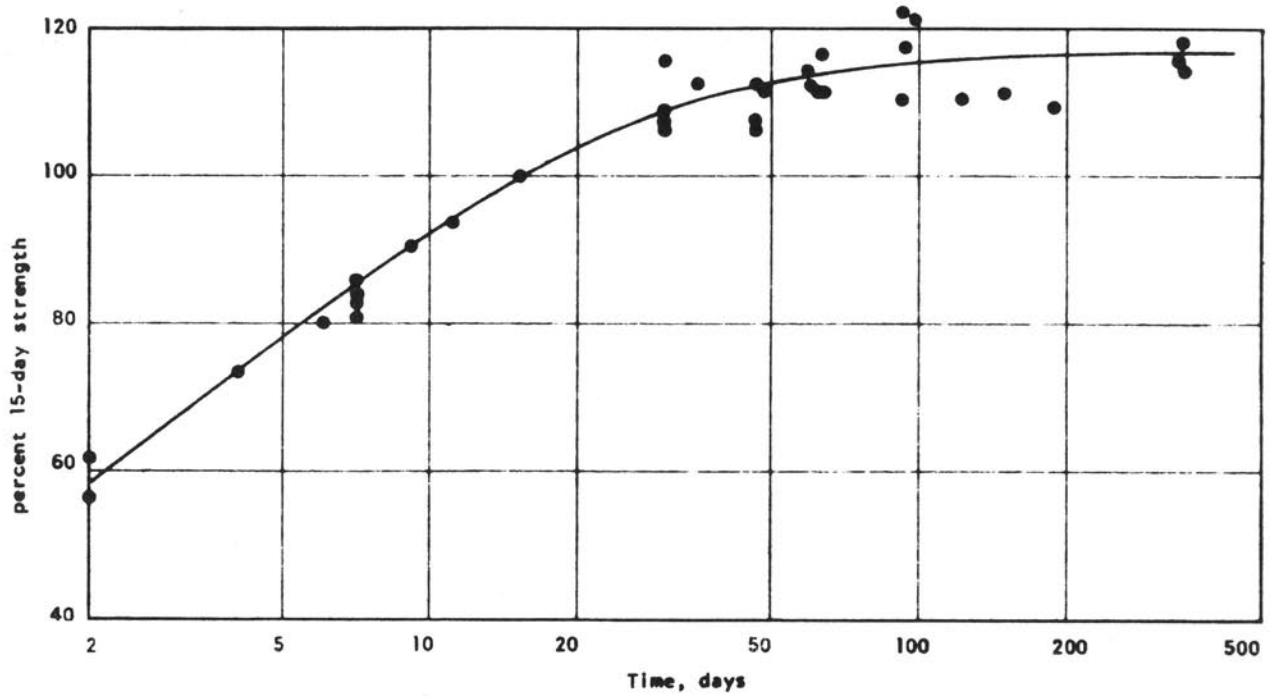

FIGURE A1. COMPRESSIVE STRENGTH OF 6-BY 12-IN. CONTROL CYLINDERS

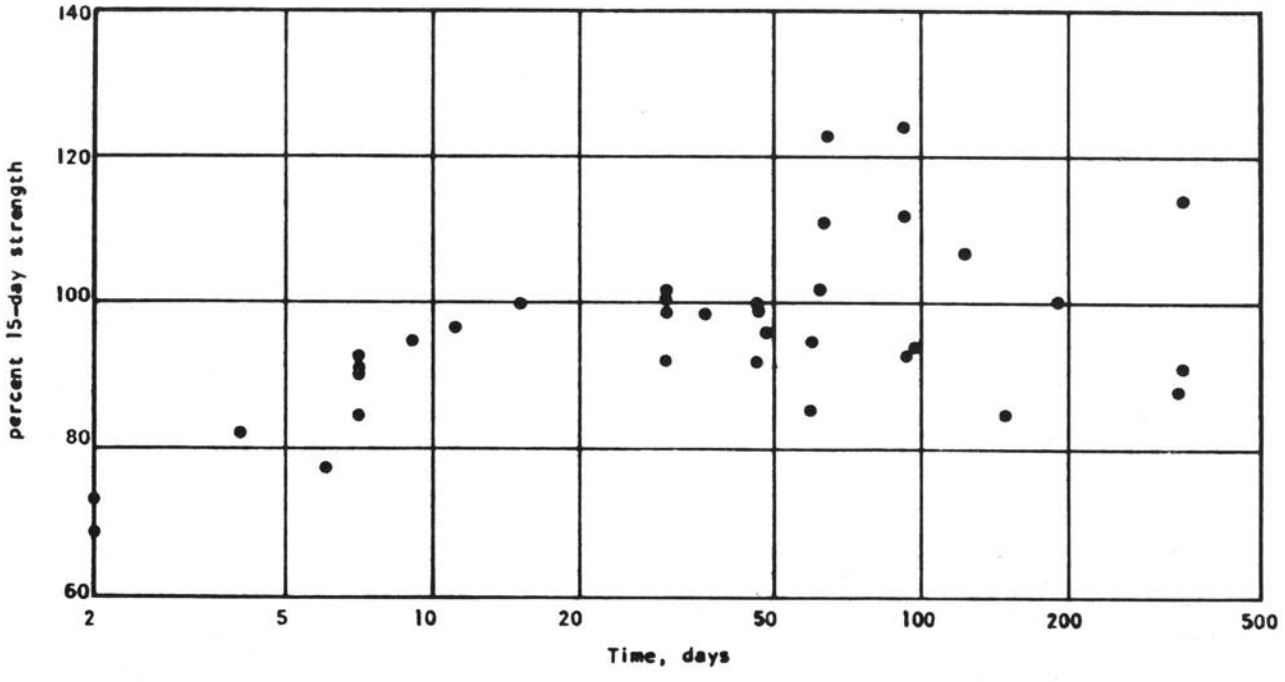

FIGURE A2. SPLITTING STRENGTH OF 6-BY 6-IN. CONTROL CYLINDERS

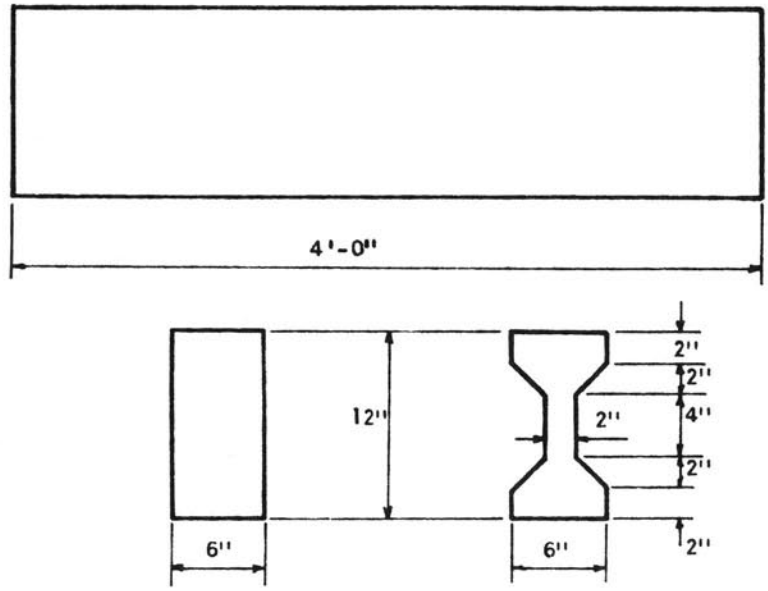

FIGURE A3. NOMINAL DIMENSIONS OF TEST SPECIMENS

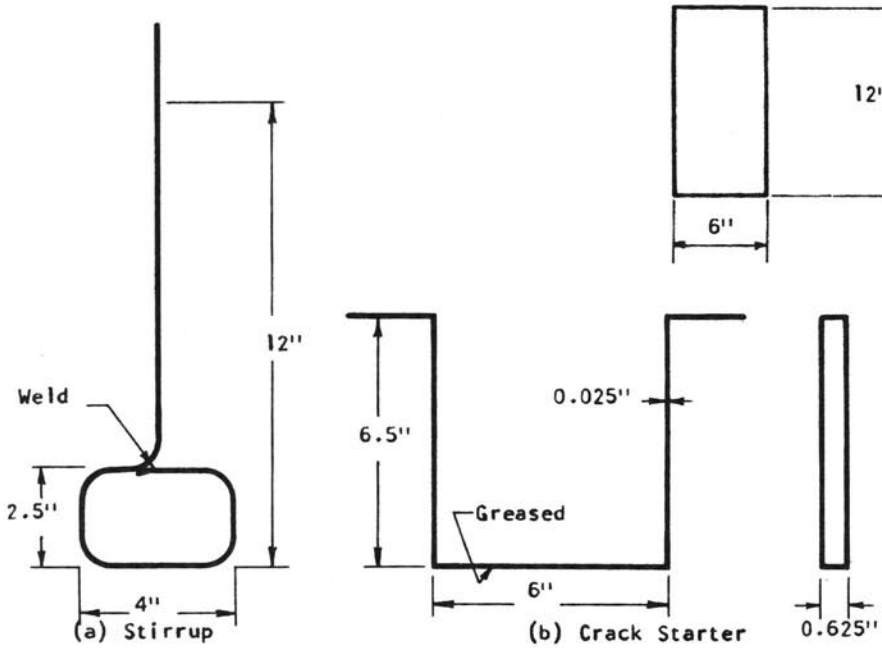

FIGURE A4. STIRRUP AND CRACK STARTER

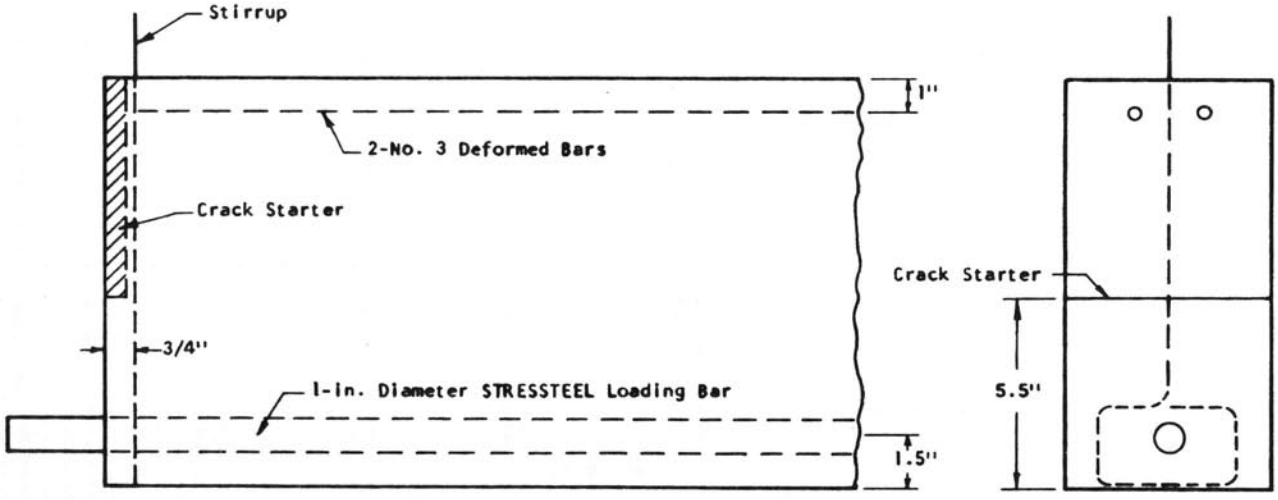

FIGURE A5. DETAILS OF THE REINFORCEMENT IN A BEAM

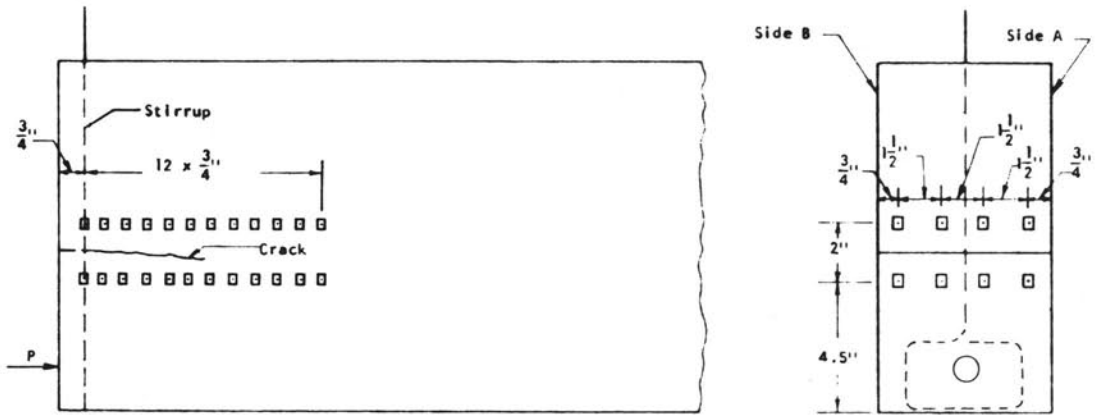

FIGURE A6. TYPICAL GAGE POINT ARRANGEMENT FOR THE MEASUREMENT OF CRACK WIDTH WITH 2-IN. BERRY GAGE

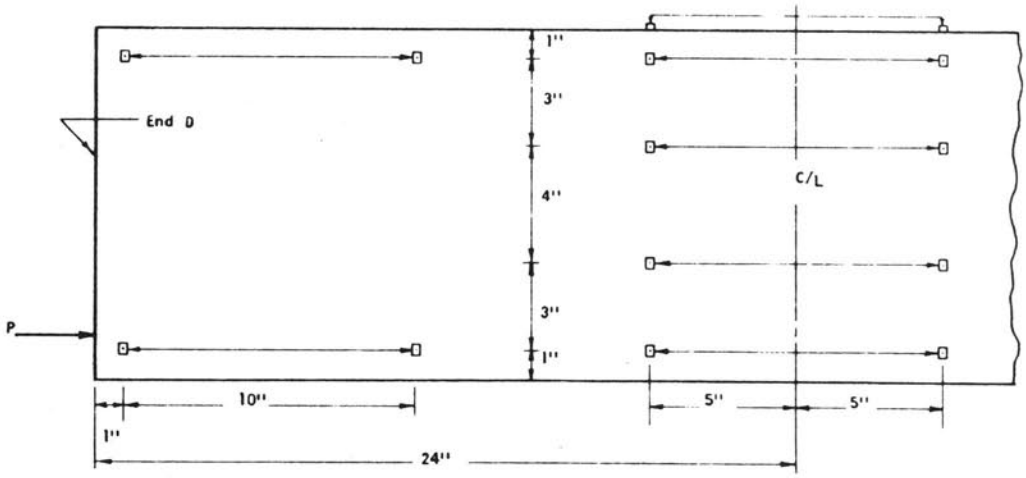

FIGURE A7. GAGE POINT ARRANGEMENT FOR THE MEASUREMENT OF LONGITUDINAL DEFORMATIONS WITH 10-IN. WHITTEMORE GAGE

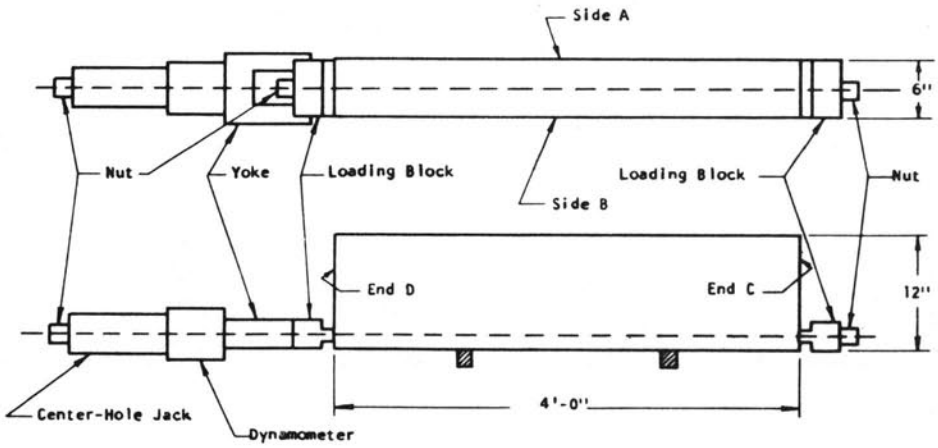

FIGURE A8. TEST SETUP FOR LOADING BOTH ENDS OF THE BEAM

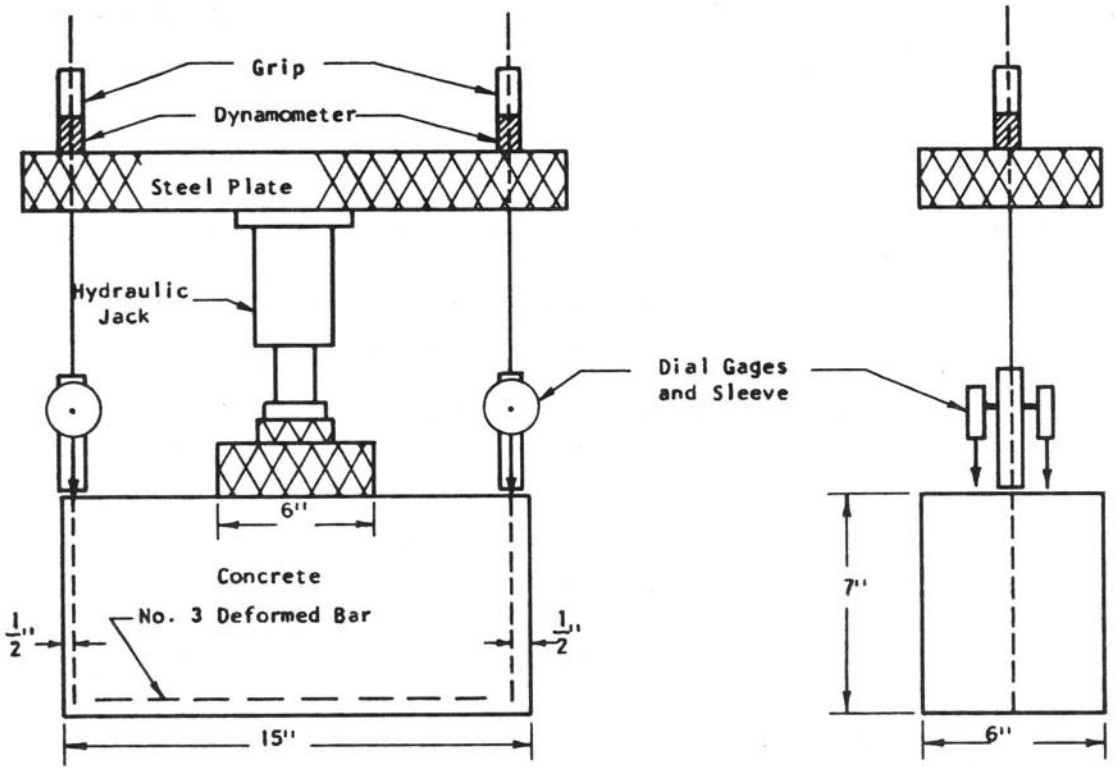

FIGURE A9. TWIN PULL-OUT SPECIMEN

(a)

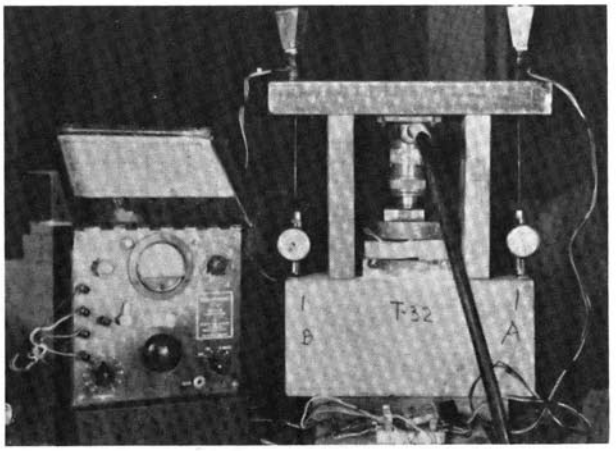

(b)

FIGURE A10. PHOTOGRAPHS OF BEAM AND TWIN PULL-OUT SPECIMENS

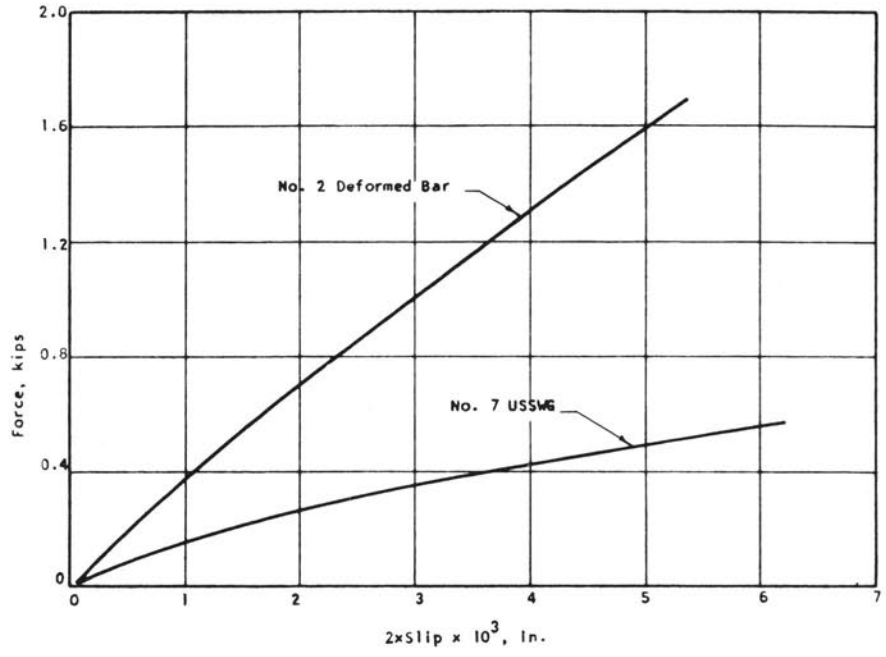

FIGURE A11. AVERAGE RELATIONSHIPS BETWEEN BAR FORCE AND SLIP FROM BOND TESTS ON NO. 2 BARS AND NO. 7 USSWG WIRES

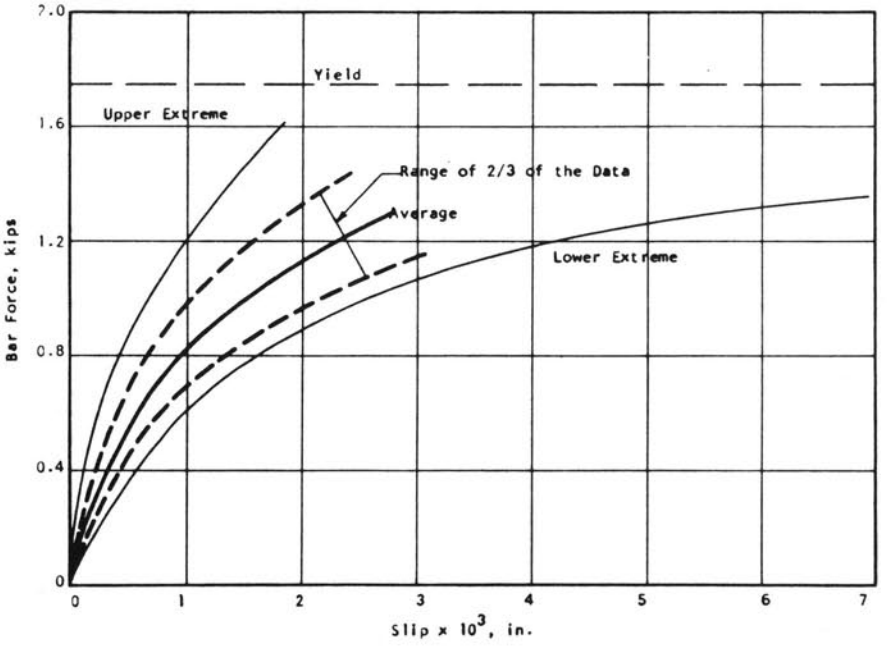

FIGURE A12. LOAD-SLIP ENVELOPE AND AVERAGE CURVE FOR 1/4-IN. DIAMETER PLAIN BARS

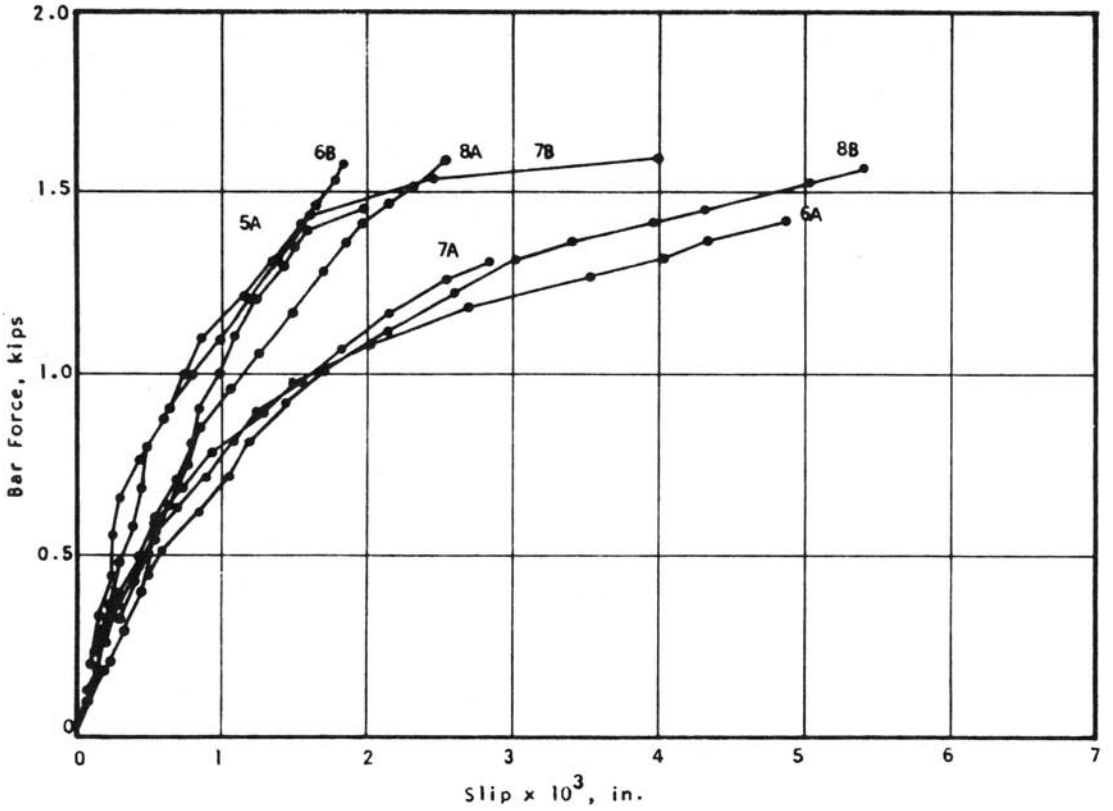

FIGURE A13. BOND TESTS ON 1/4-IN. DIAMETER ANNEALED WIRE, LOT NO. 1

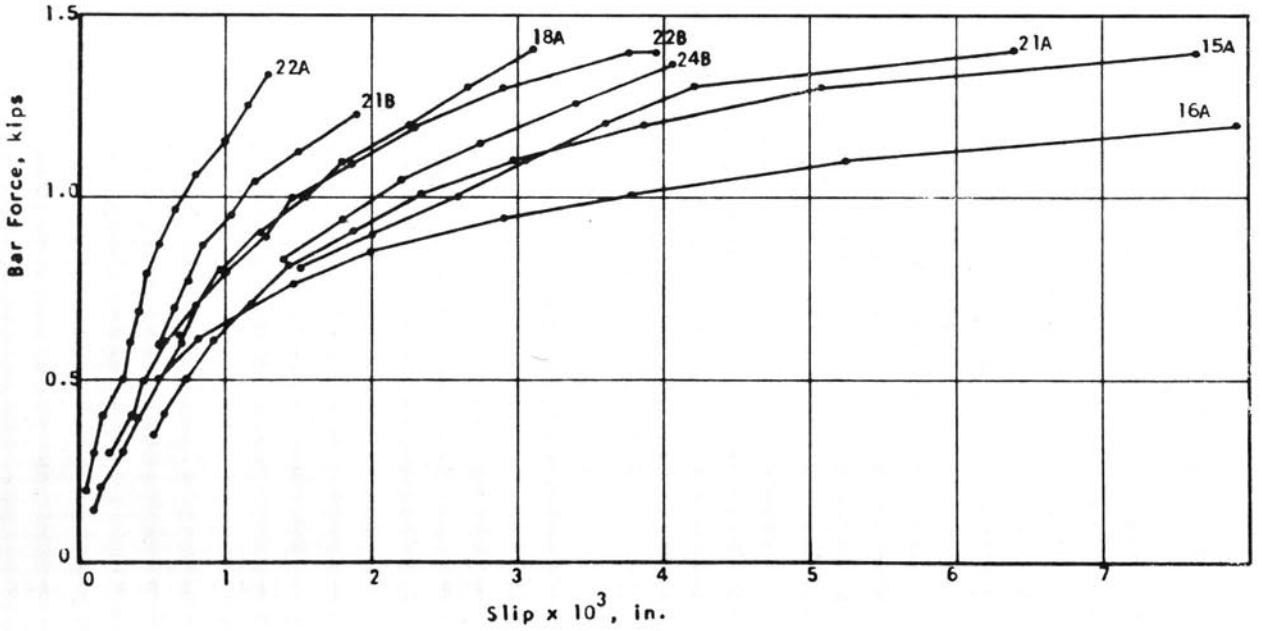

FIGURE A14. BOND TESTS ON 1/4-IN. DIAMETER ANNEALED WIRE, LOT NO. 2

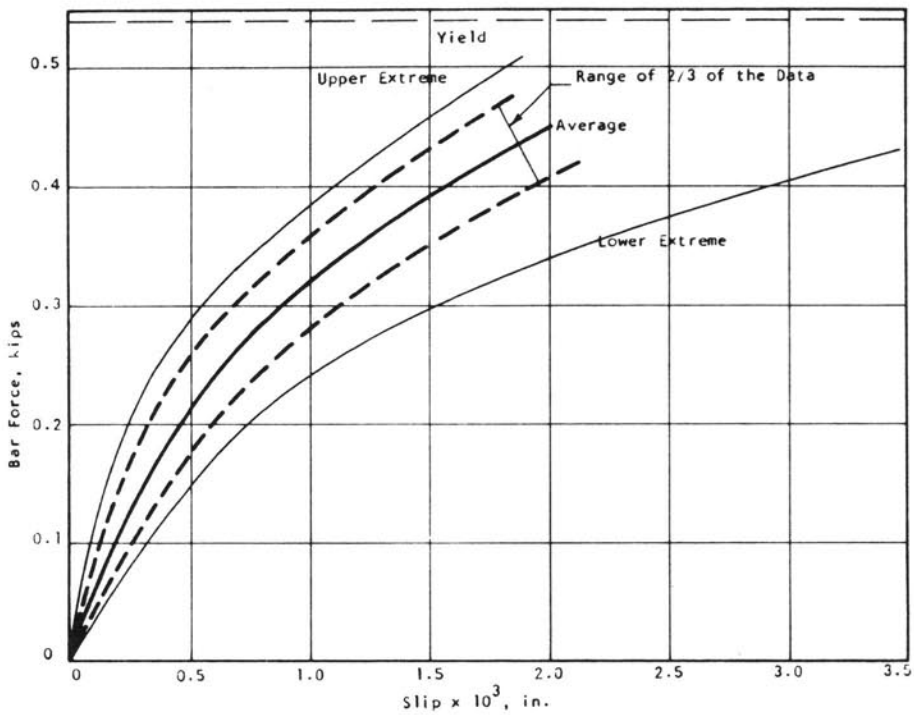

FIGURE A15. LOAD-SLIP ENVELOPE AND AVERAGE CURVE FOR 1/8-IN. DIAMETER PLAIN BARS

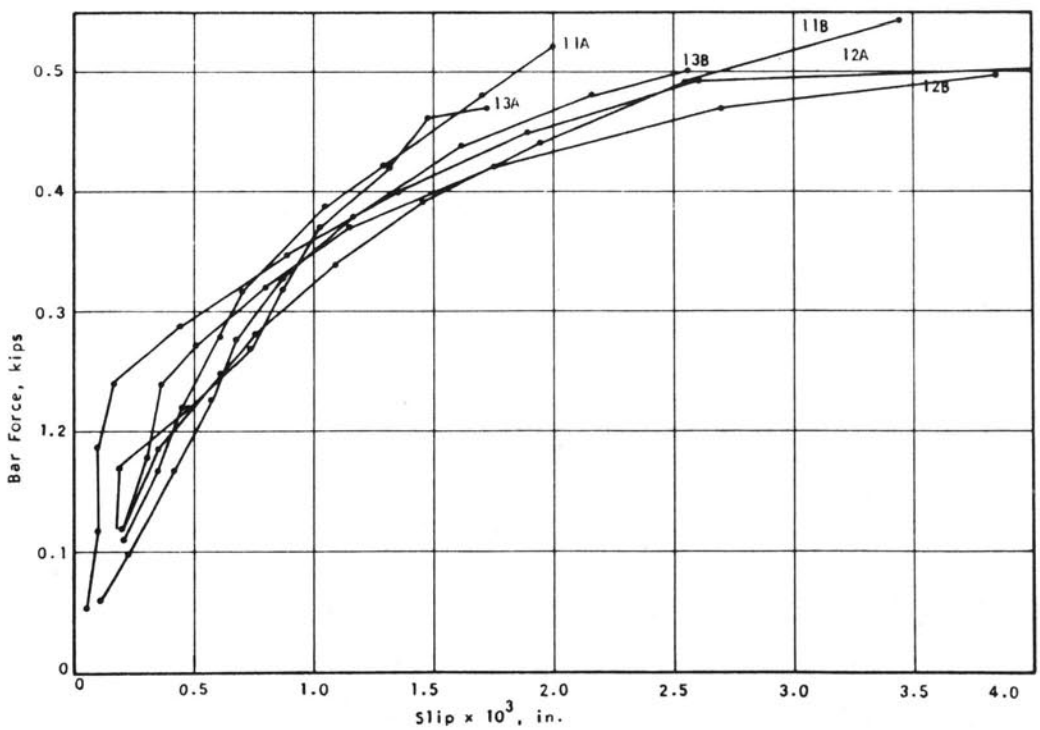

FIGURE A16. BOND TESTS ON 1/8-IN. DIAMETER ANNEALED WIRE, LOT NO. 1

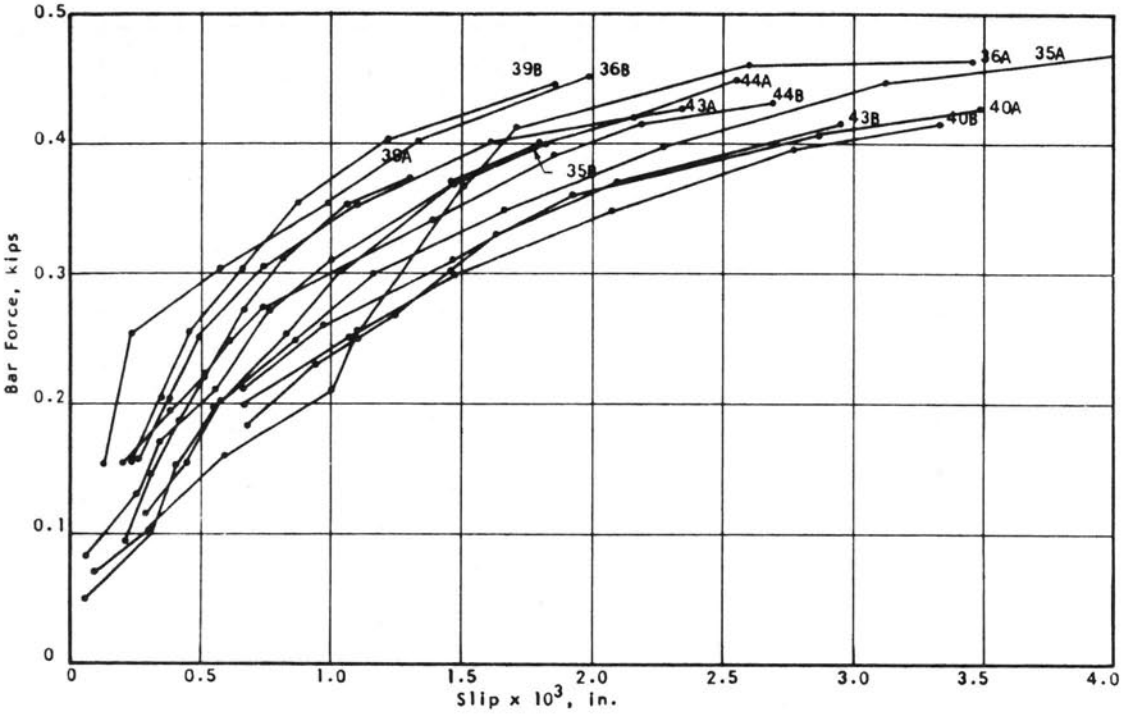

FIGURE A17. BOND TESTS ON 1/8-IN. DIAMETER ANNEALED WIRE, LOT NO. 2

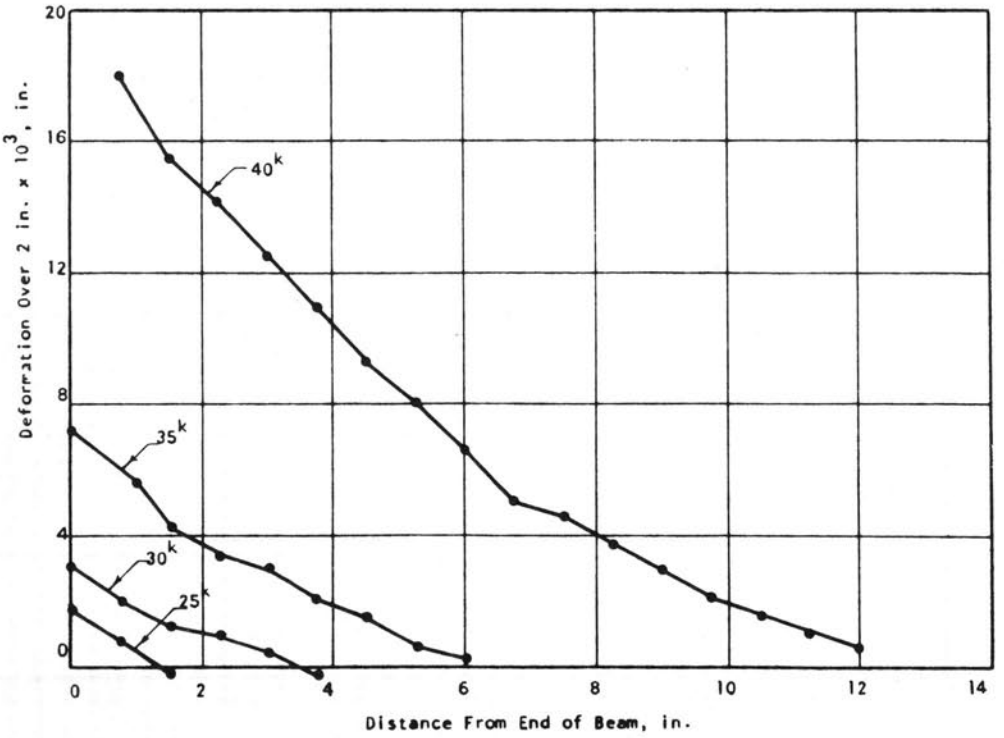

FIGURE A18. CRACK PROFILES FOR R19, PLAIN CONCRETE

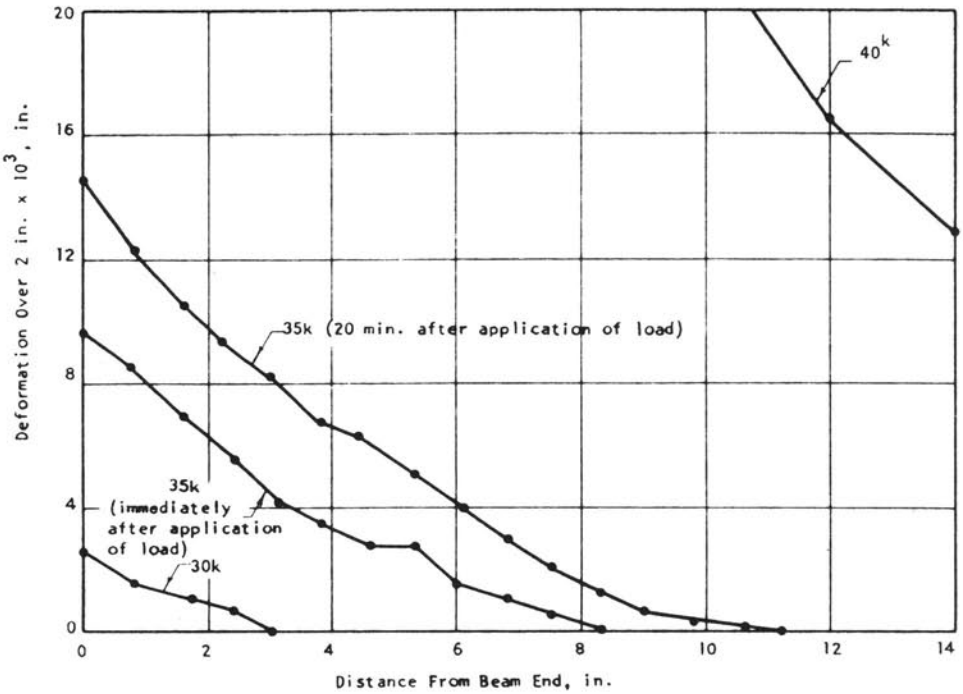

FIGURE A19. CRACK PROFILES FOR R22, PLAIN CONCRETE

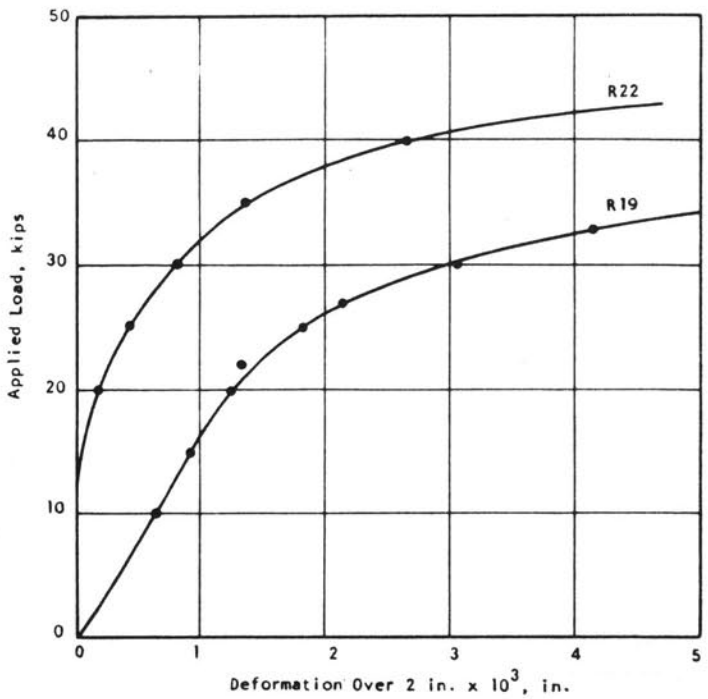

FIGURE A20. MEASURED RELATIONSHIPS BETWEEN LOAD AND TRANSVERSE DEFORMATION AT BEAM END FOR SPECIMENS R19 AND R22

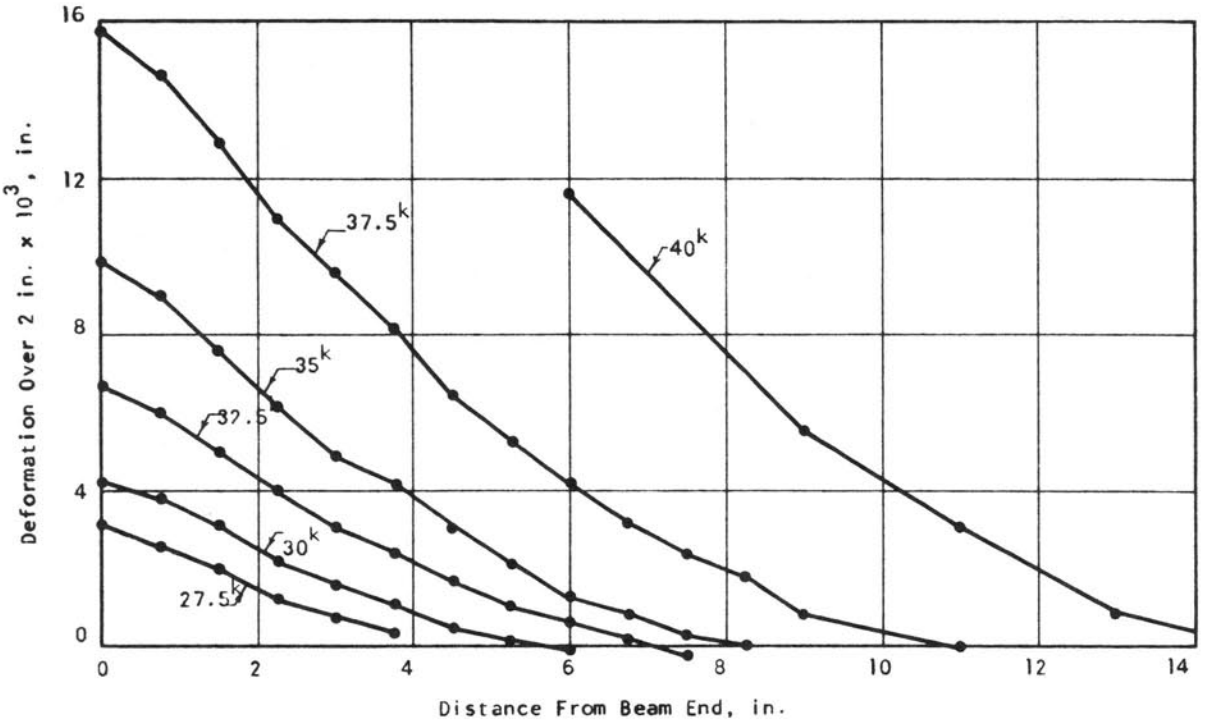

FIGURE A21. CRACK PROFILES FOR R43 - END C

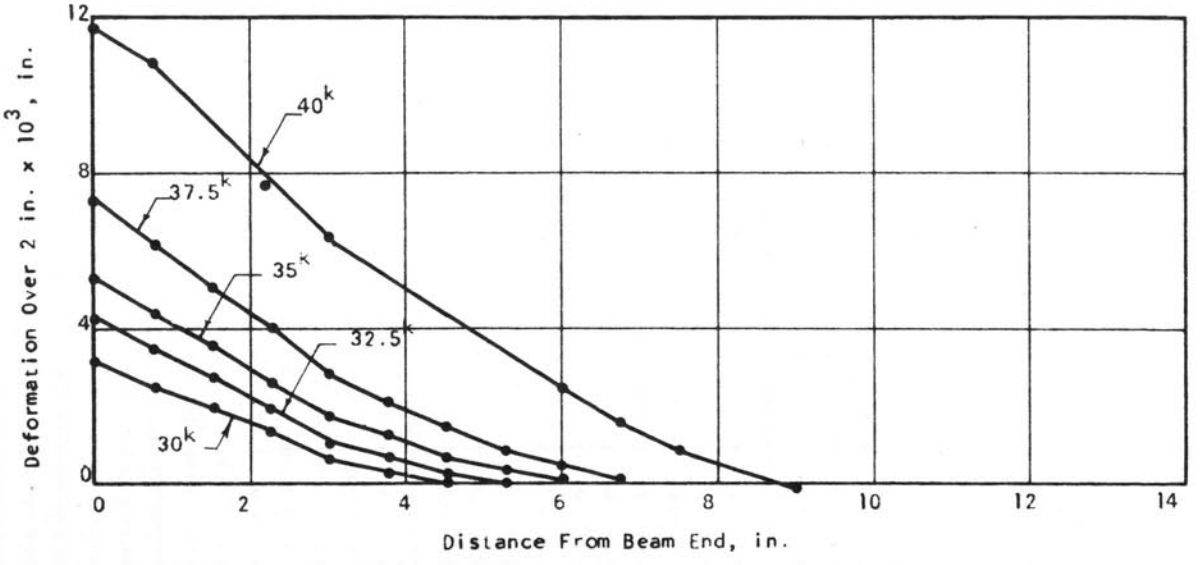

FIGURE A22. CRACK PROFILES FOR R43 - END D

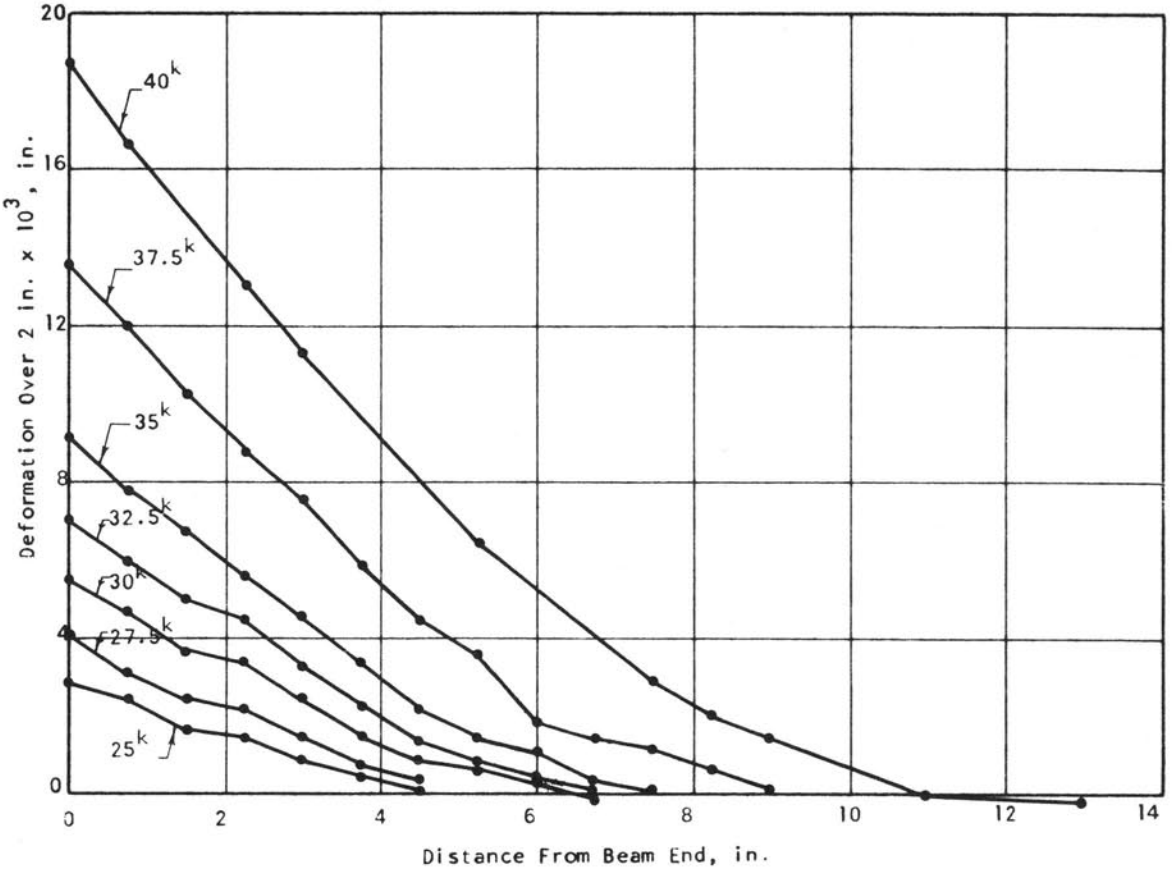

FIGURE A23. CRACK PROFILES FOR R45 - END C

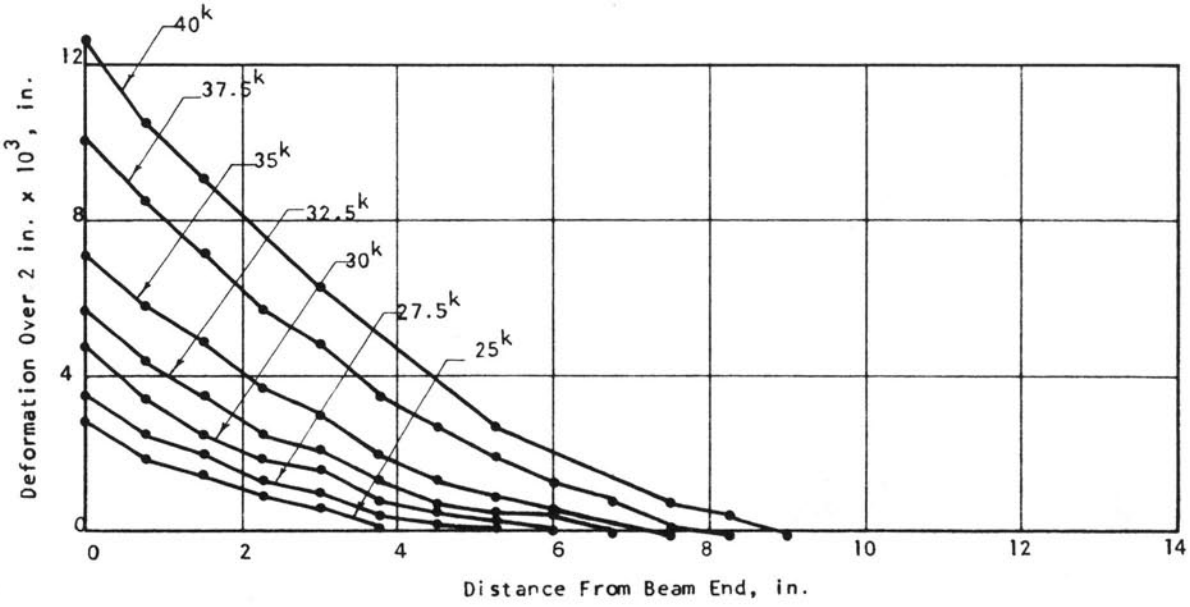

FIGURE A24. CRACK PROFILES FOR R45 - END D

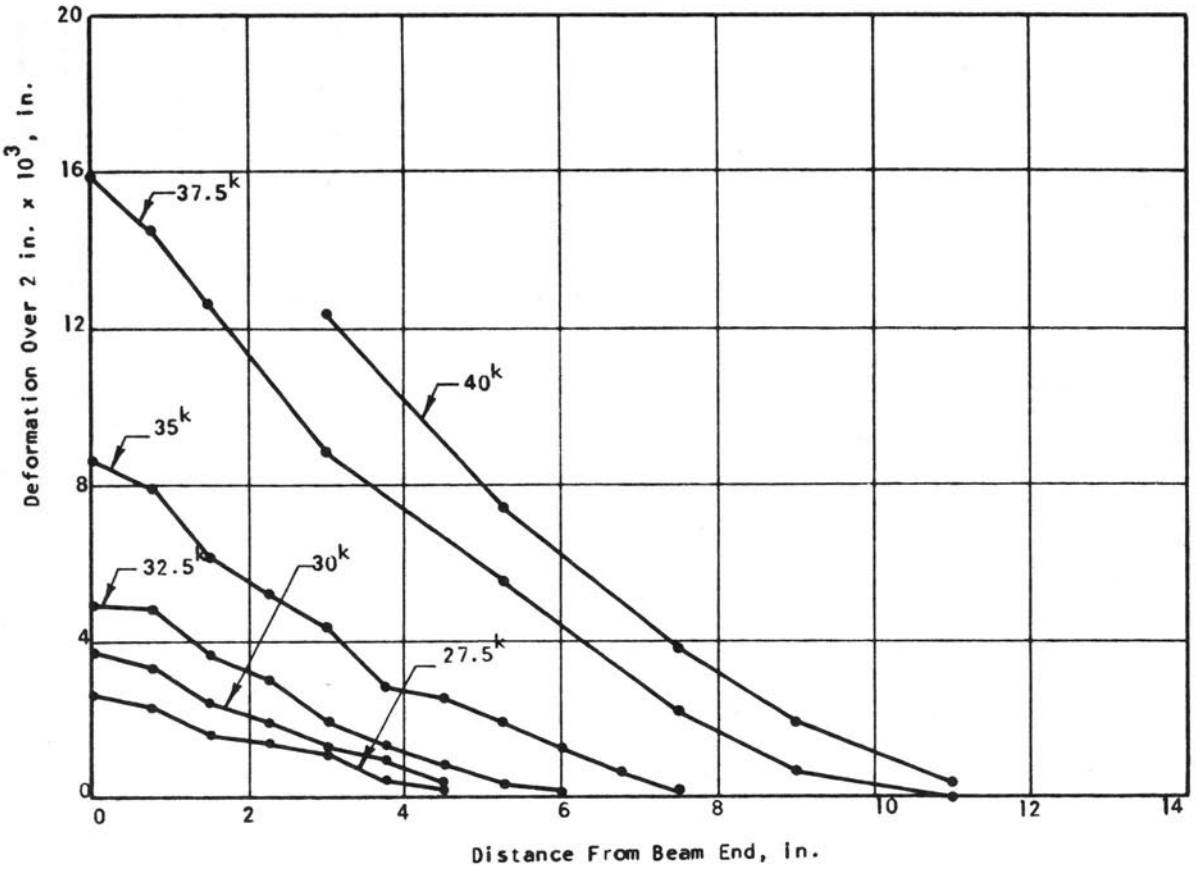

FIGURE A25. CRACK PROFILES FOR R47 - END C

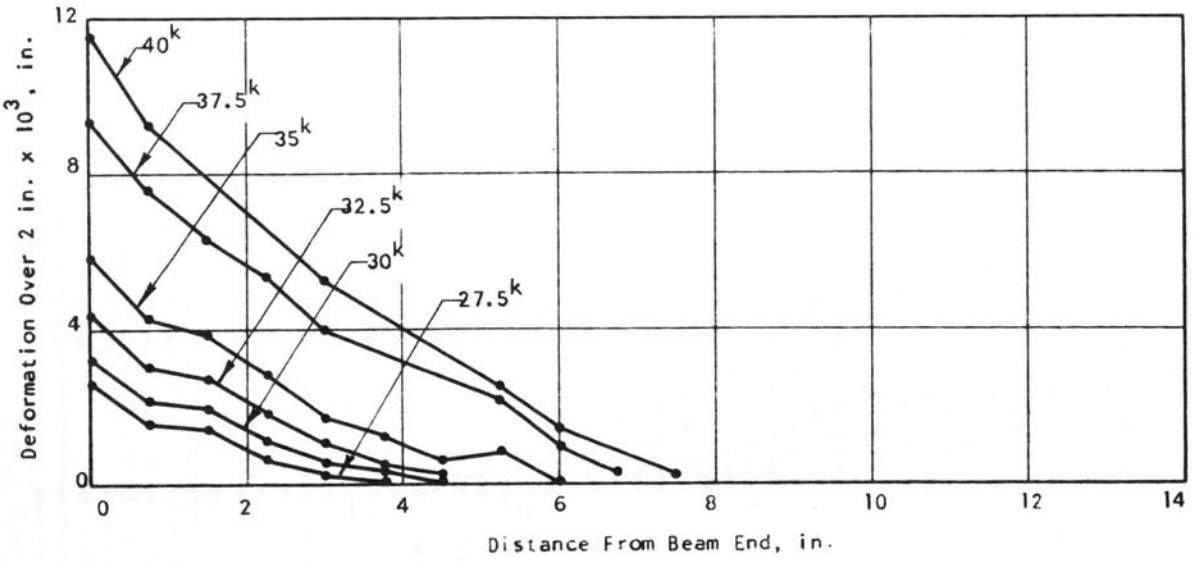

FIGURE A26. CRACK PROFILES FOR R47 - END D

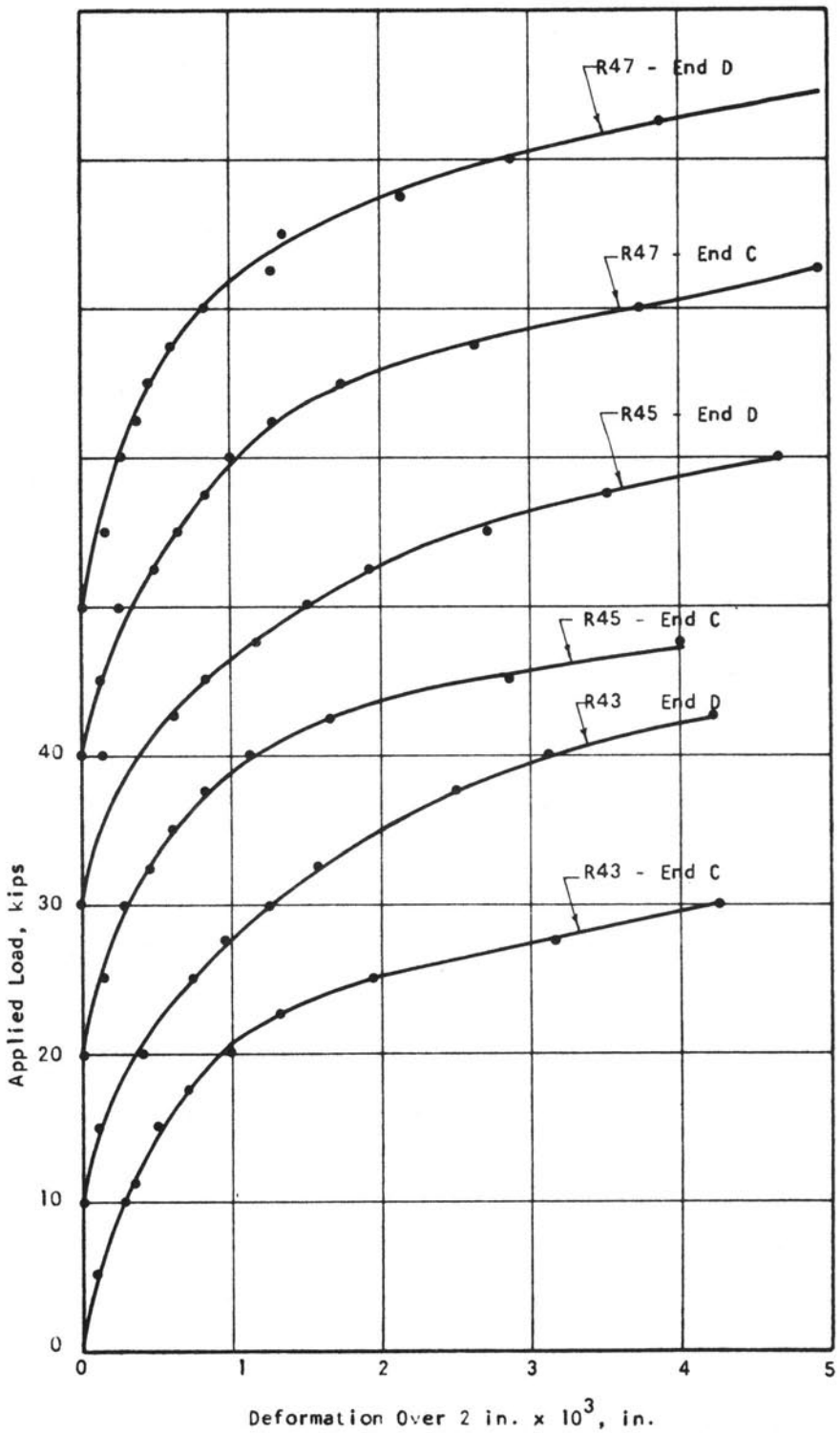

FIGURE A27. MEASURED RELATIONSHIPS BETWEEN LOAD AND TRANSVERSE DEFORMATION AT BEAM END FOR SPECIMENS R43, R45, AND R47

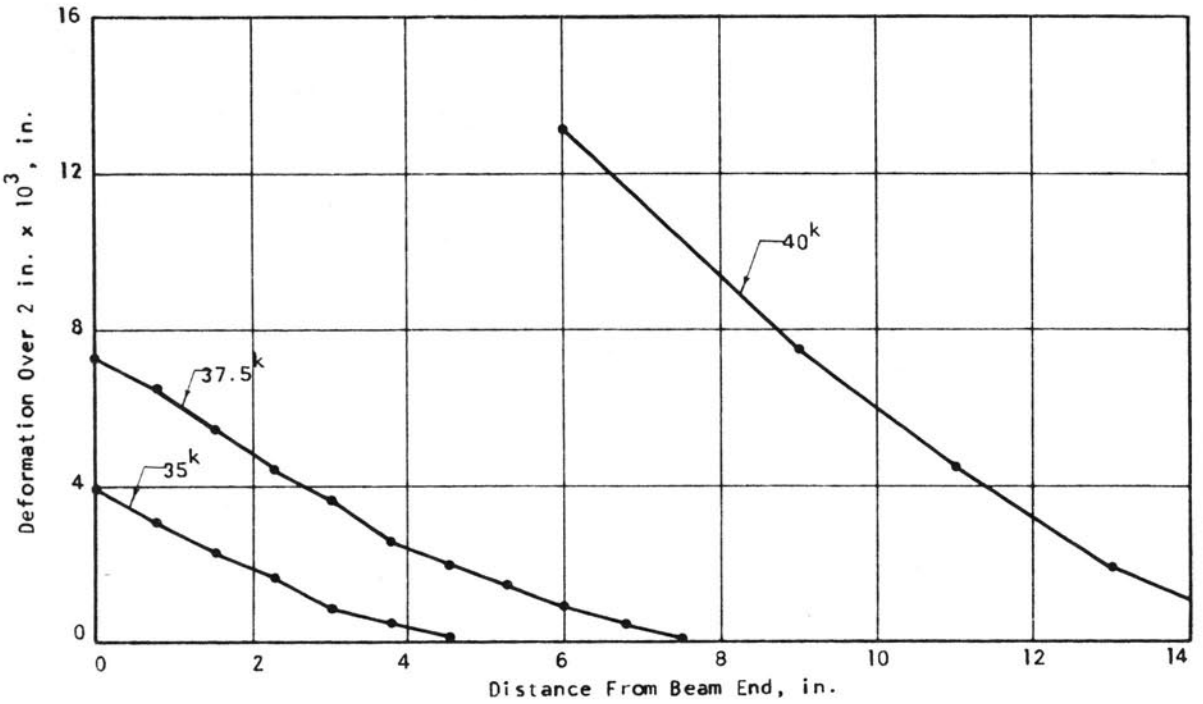

FIGURE A28. CRACK PROFILES FOR R44 - END C

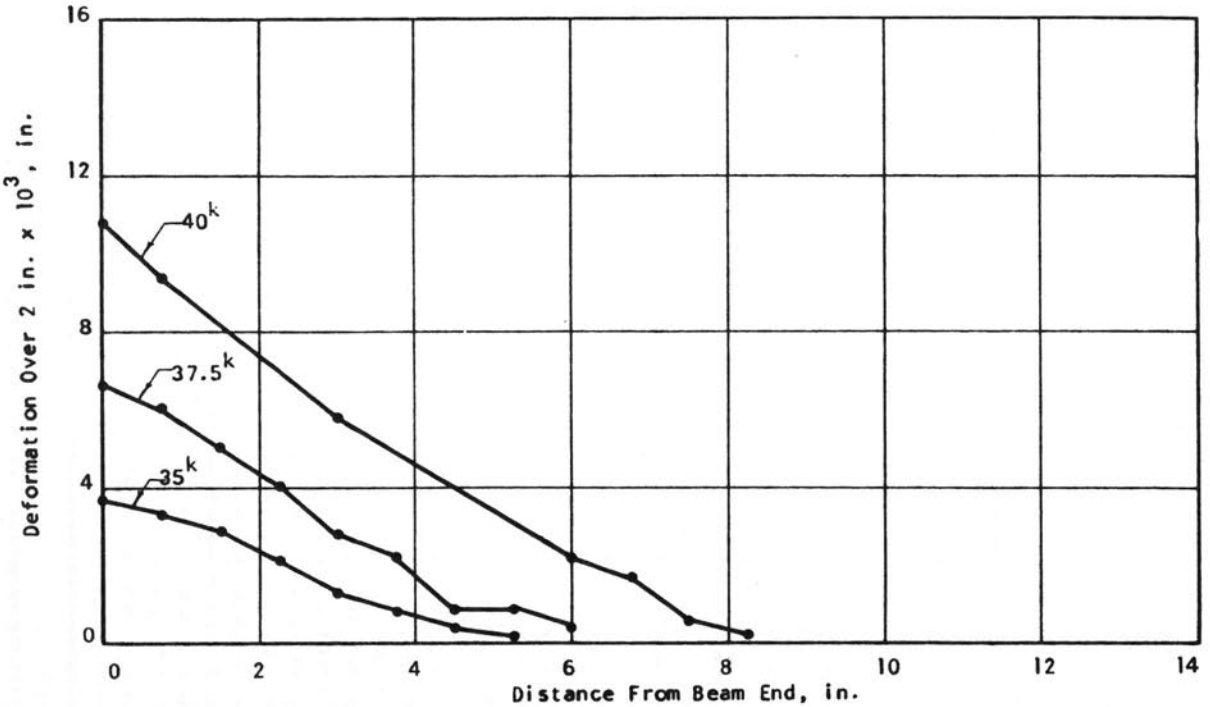

FIGURE A29. CRACK PROFILES FOR R44 - END D

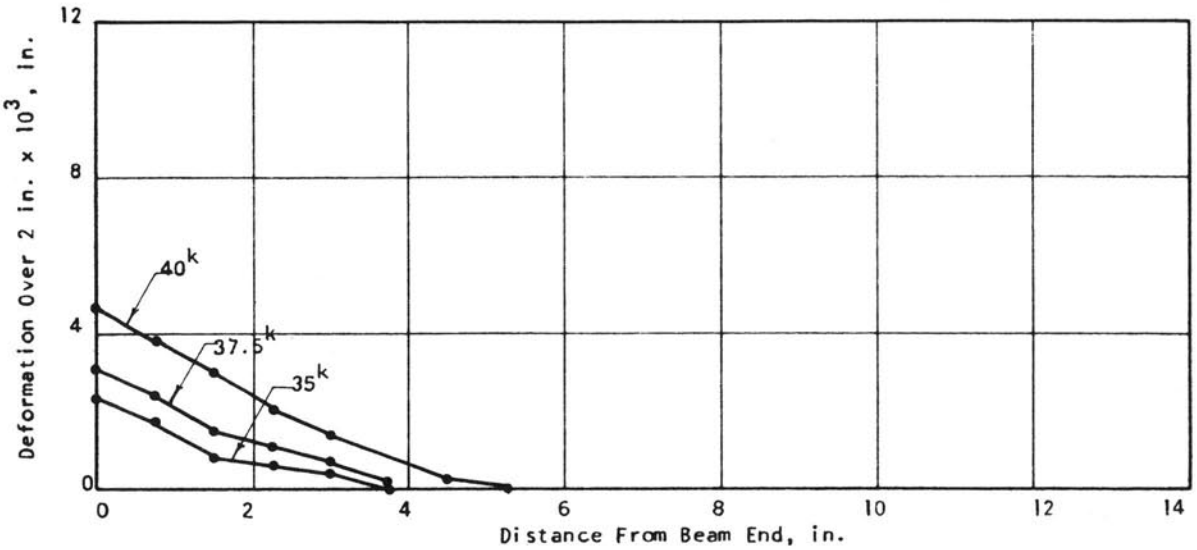

FIGURE A30. CRACK PROFILES FOR R46 - END C

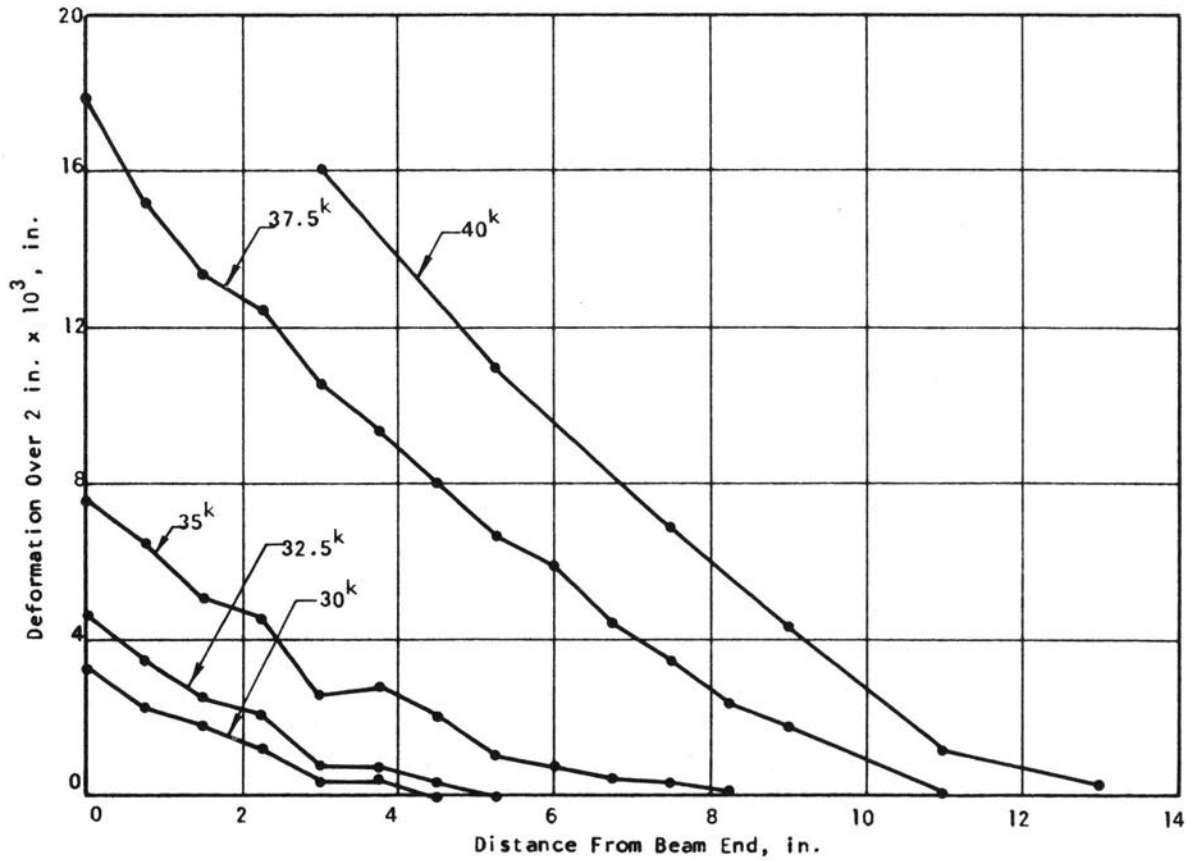

FIGURE A31. CRACK PROFILES FOR R46 - END D

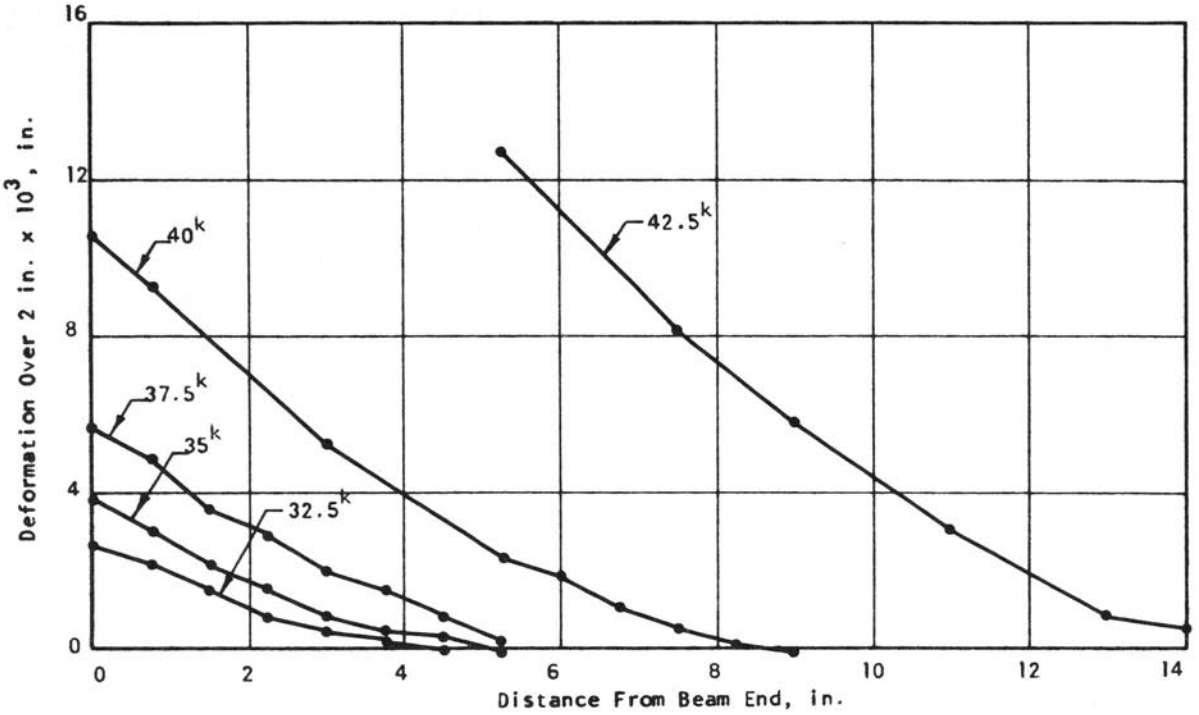

FIGURE A32. CRACK PROFILES FOR R48 - END C

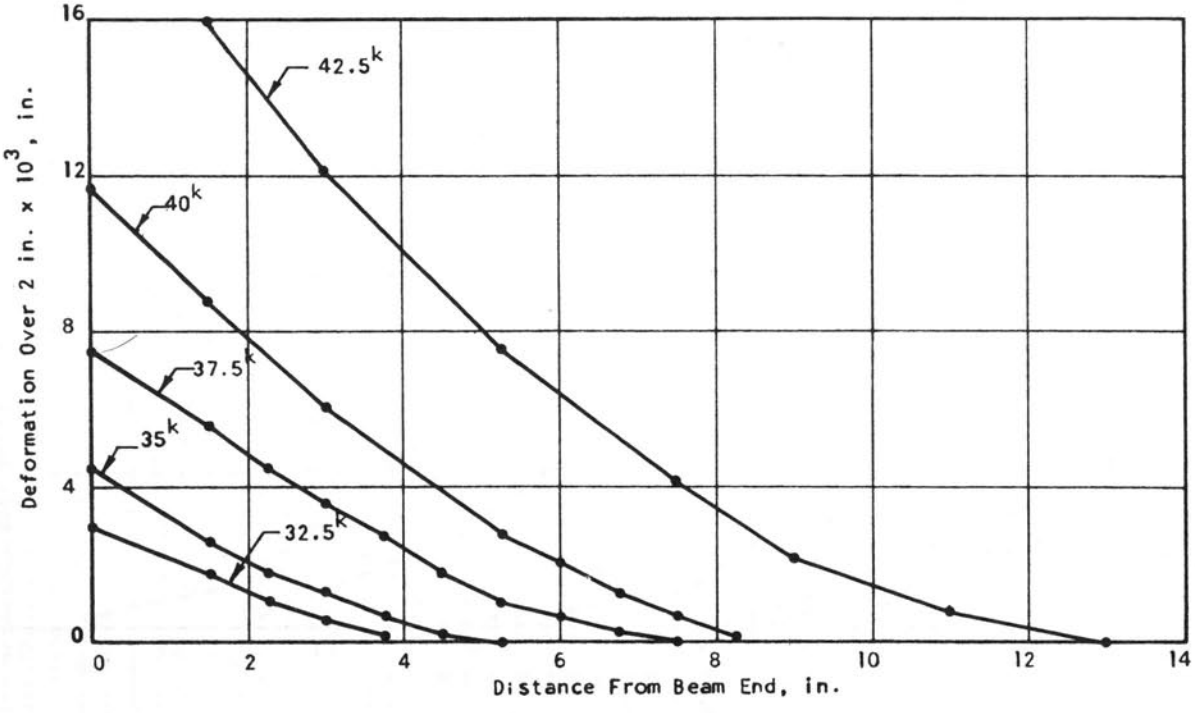

FIGURE A33. CRACK PROFILES FOR R48 - END D

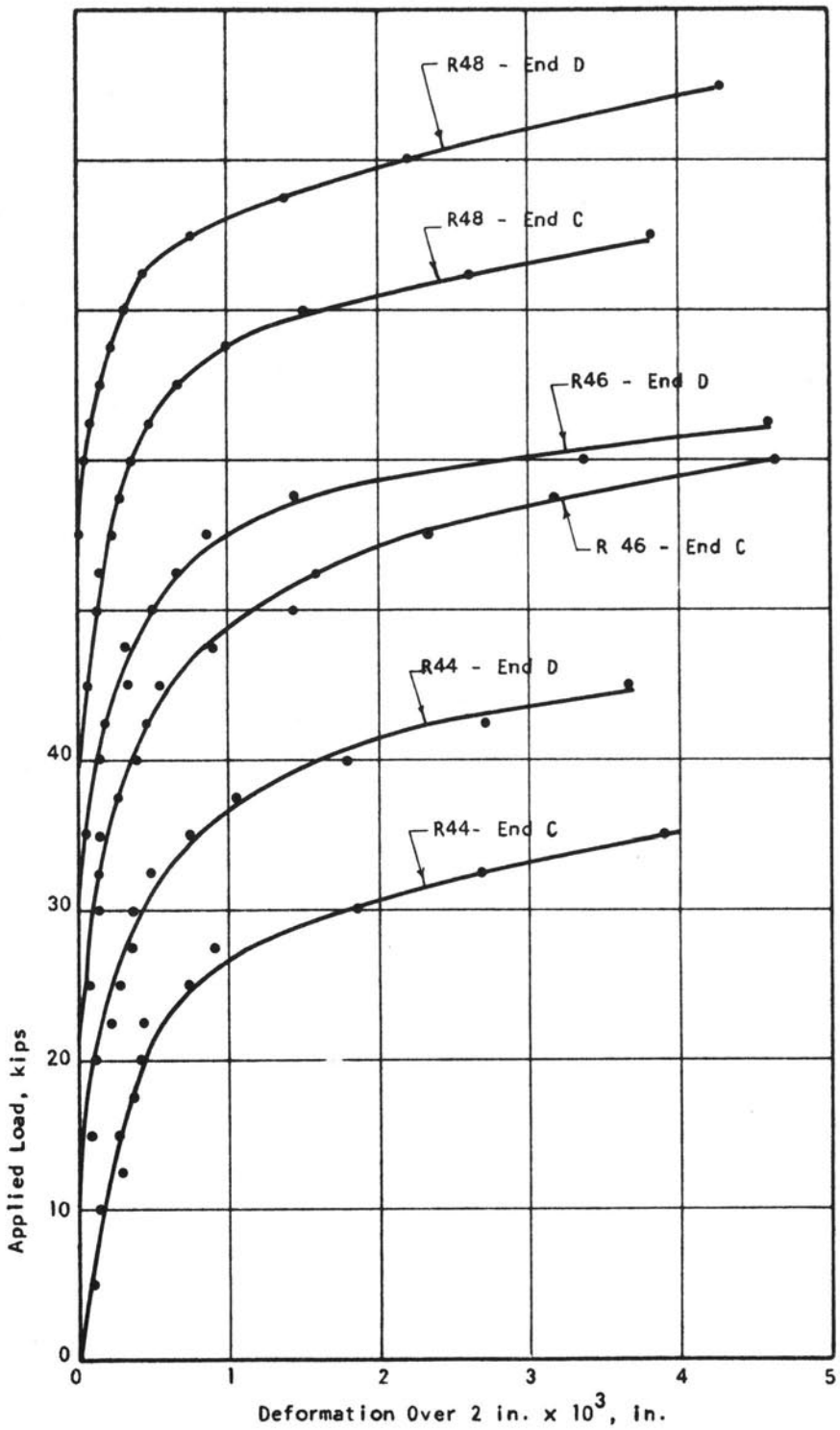

FIGURE A34. MEASURED RELATIONSHIPS BETWEEN LOAD AND TRANSVERSE DEFORMATION AT BEAM END FOR SPECIMENS R44, R46, AND R48

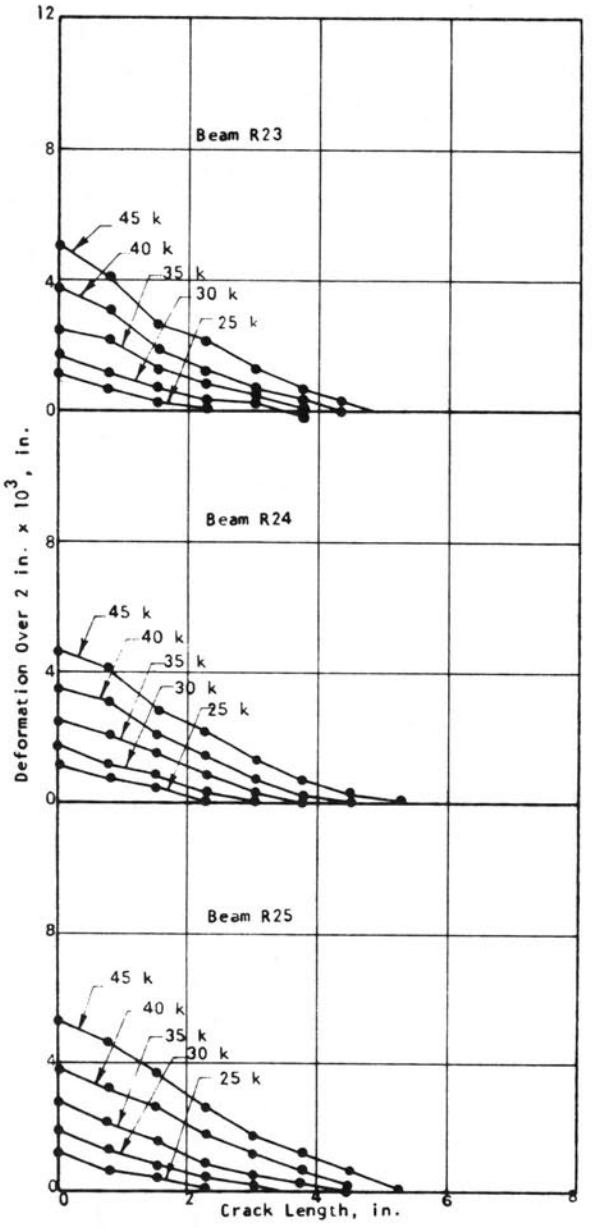

FIGURE A35. CRACK PROFILES FOR R23, R24, AND R25, 1/4-IN. DIAMETER STIRRUPS

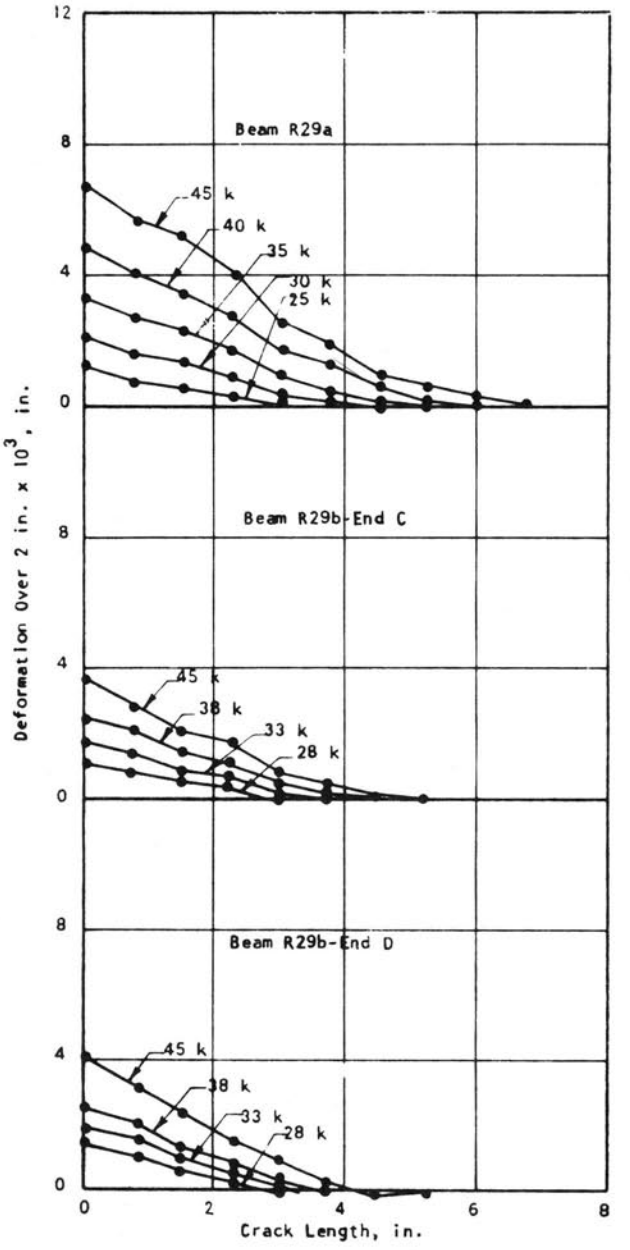

FIGURE A36. CRACK PROFILES FOR R29a AND R29b, 1/4-IN. DIAMETER STIRRUPS

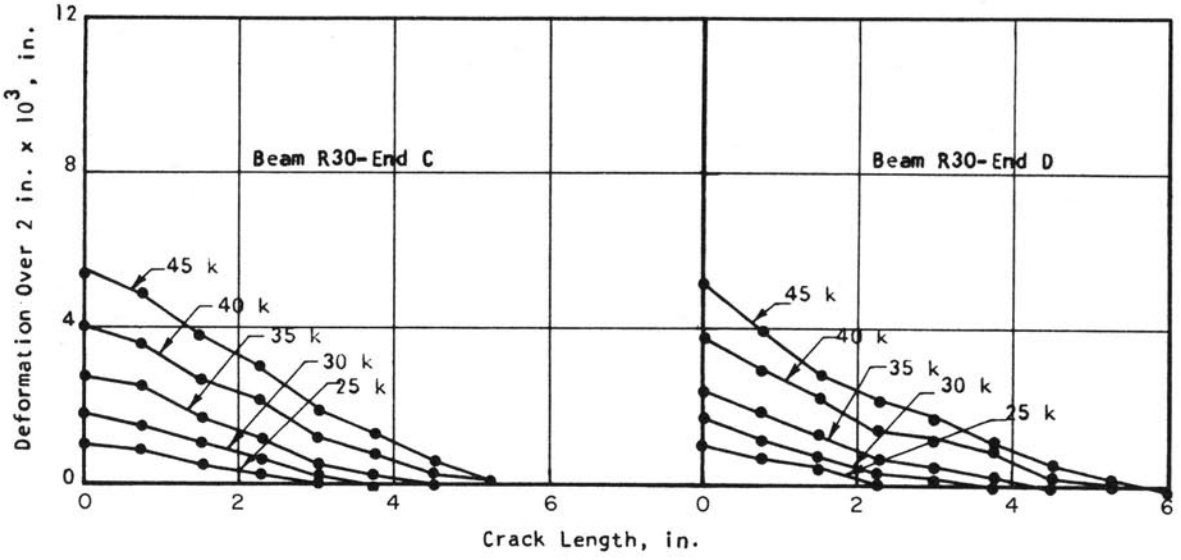

FIGURE A37. CRACK PROFILES FOR R30, 1/4-IN. DIAMETER STIRRUPS

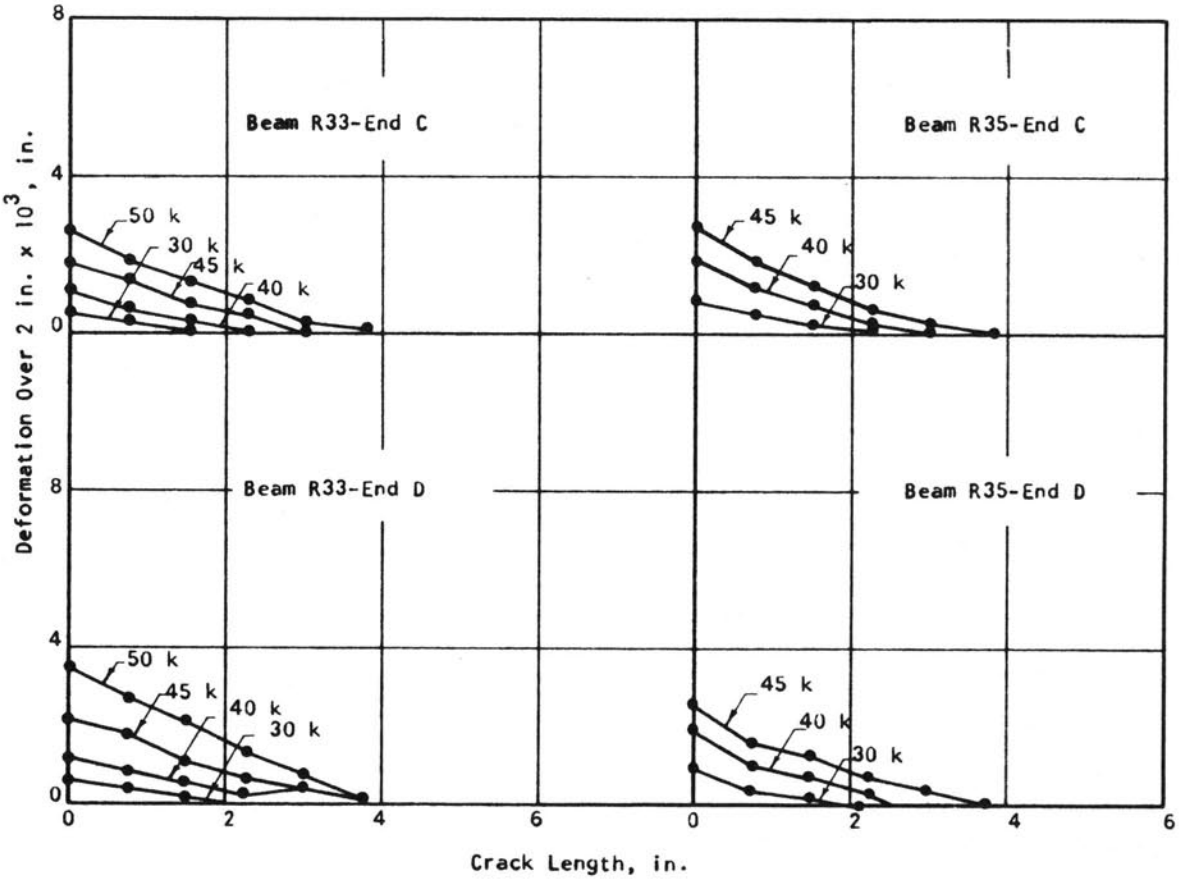

FIGURE A38. CRACK PROFILES FOR R33 AND R35, 1/4-IN. DIAMETER STIRRUPS

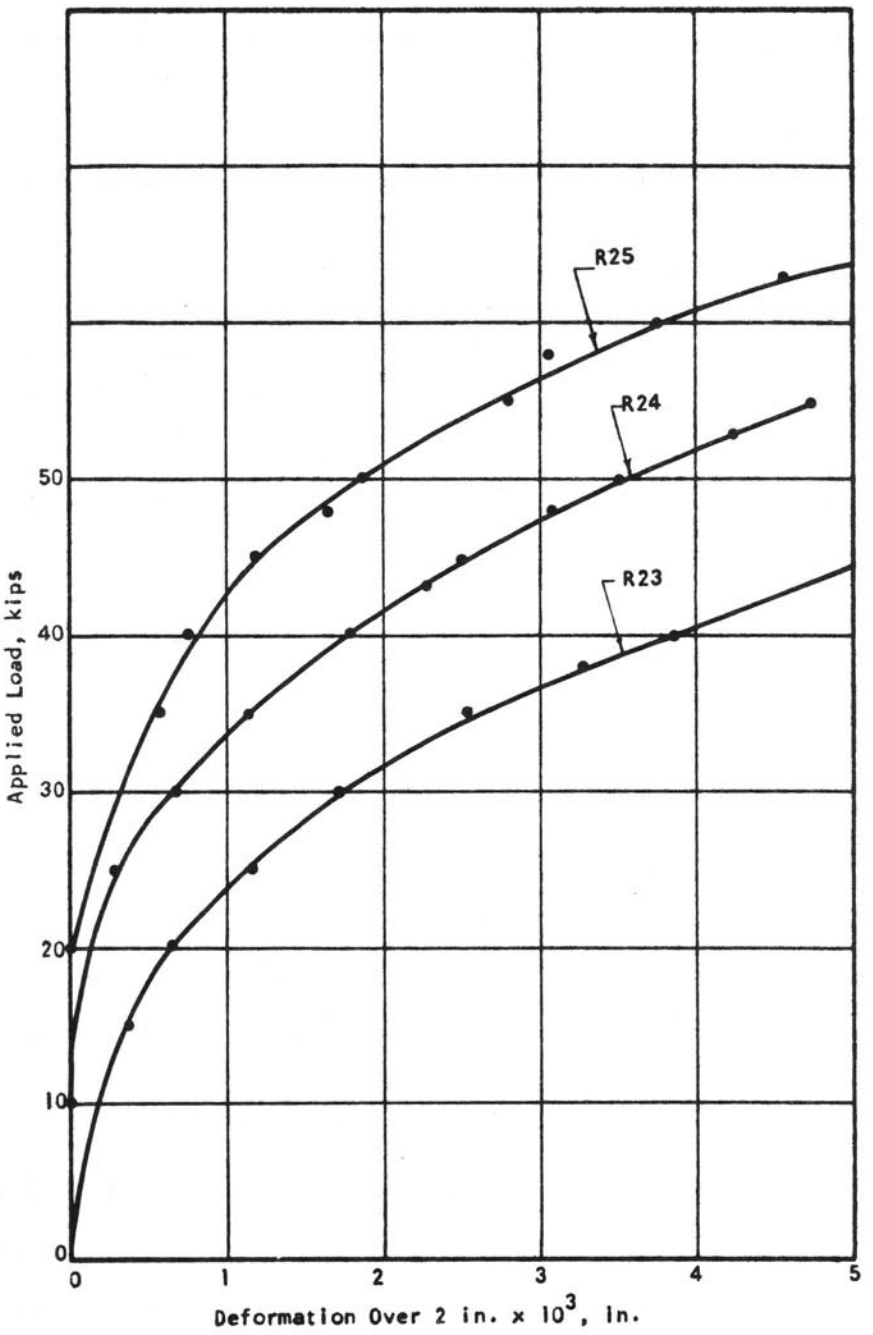

FIGURE A39. MEASURED RELATIONSHIPS BETWEEN LOAD AND TRANSVERSE DEFORMATION AT BEAM END FOR SPECIMENS R23, R24, AND R25

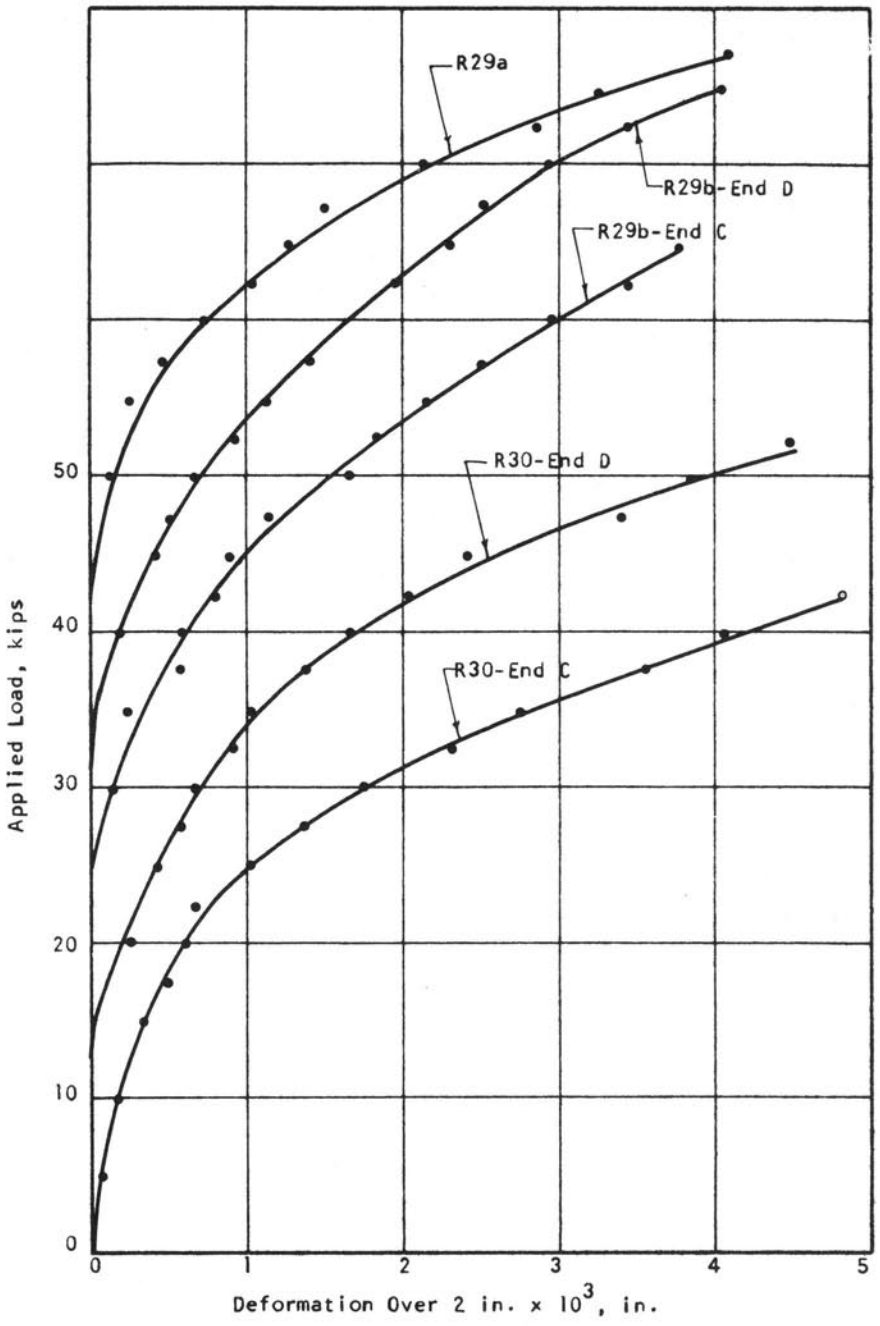

FIGURE A40. MEASURED RELATIONSHIPS BETWEEN LOAD AND TRANSVERSE DEFORMATION AT BEAM END FOR SPECIMENS R29a, R29b, AND R30

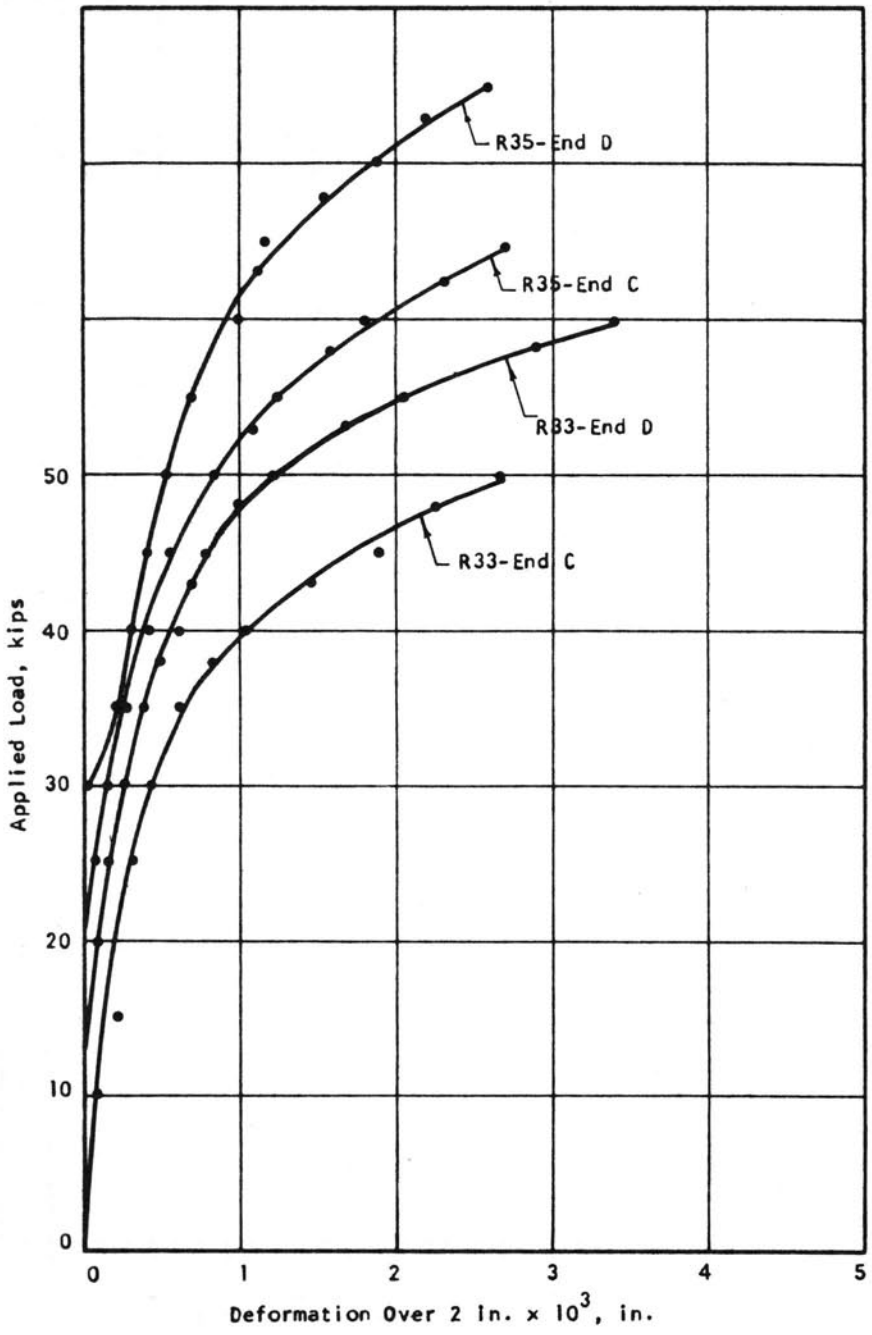

FIGURE A41. MEASURED RELATIONSHIPS BETWEEN LOAD AND TRANSVERSE DEFORMATION AT BEAM END FOR SPECIMENS R33 AND R35

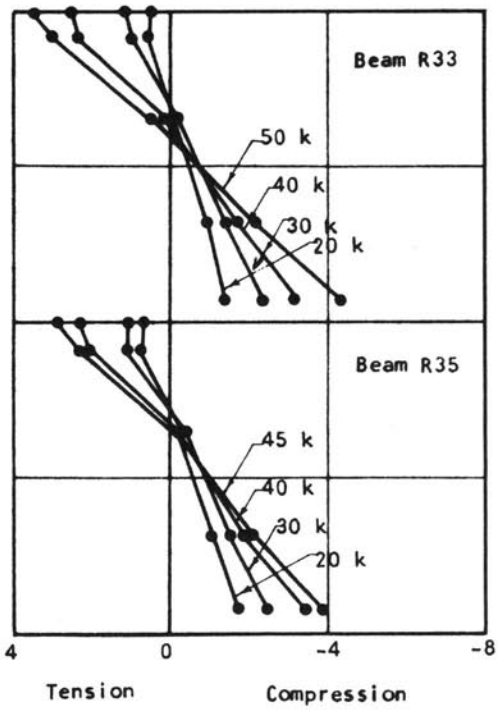

FIGURE A42. LONGITUDINAL DEFORMATION AT CENTER OF BEAM FOR R33 AND R35

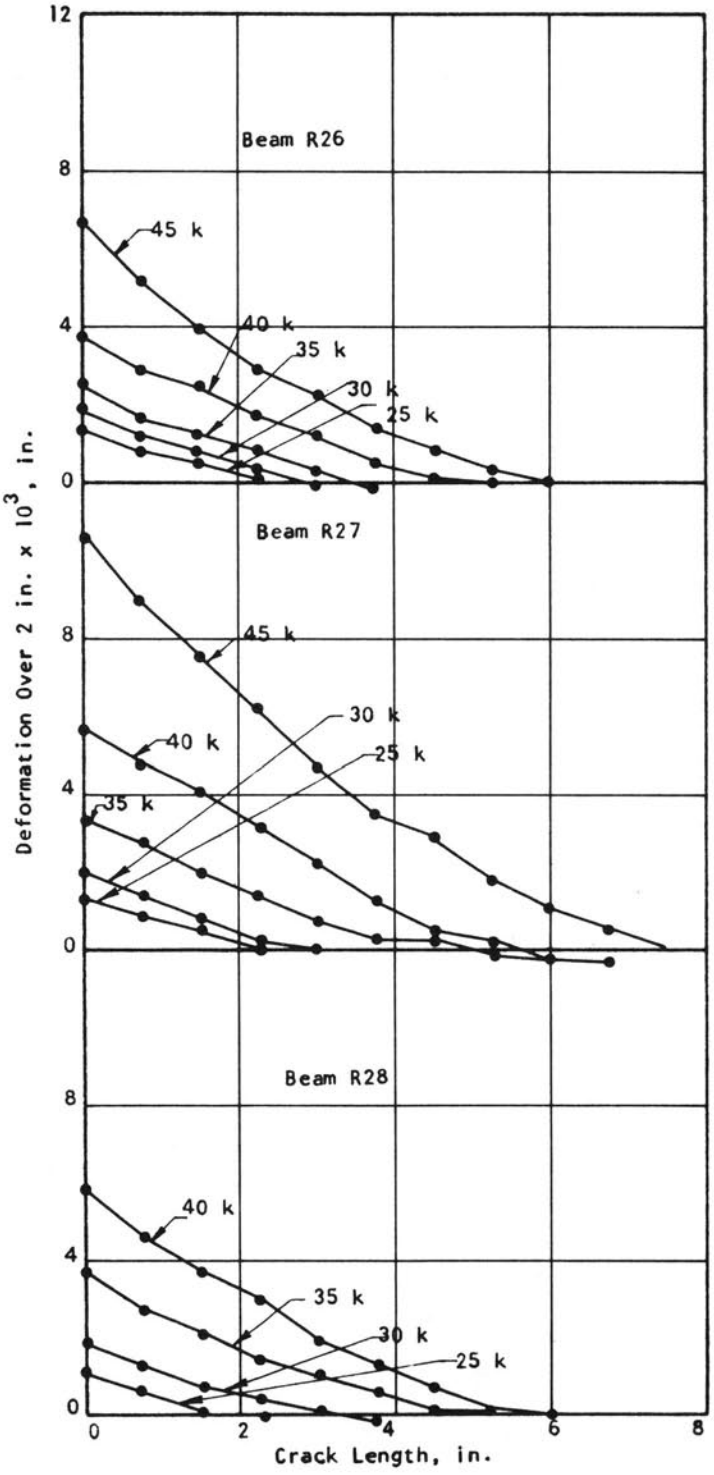

FIGURE A43. CRACK PROFILES FOR R26, R27, AND R28, 1/8-IN. DIAMETER STIRRUPS

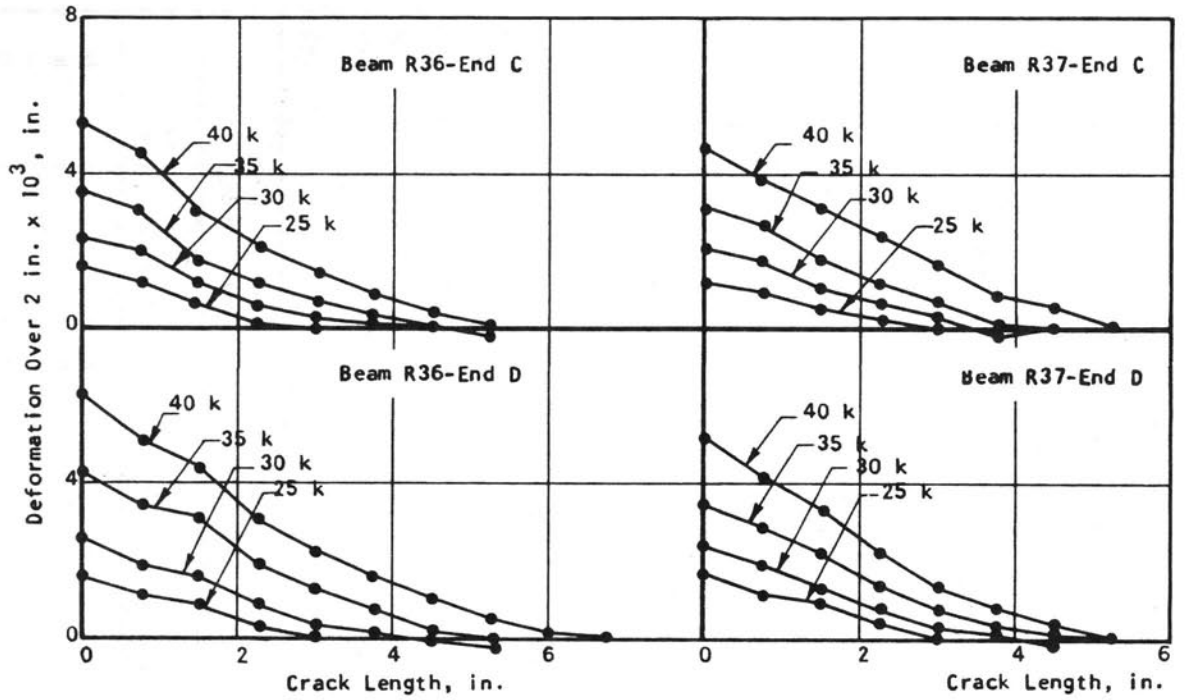

FIGURE A44. CRACK PROFILES FOR R36 AND R37, 1/8-IN. DIAMETER STIRRUPS

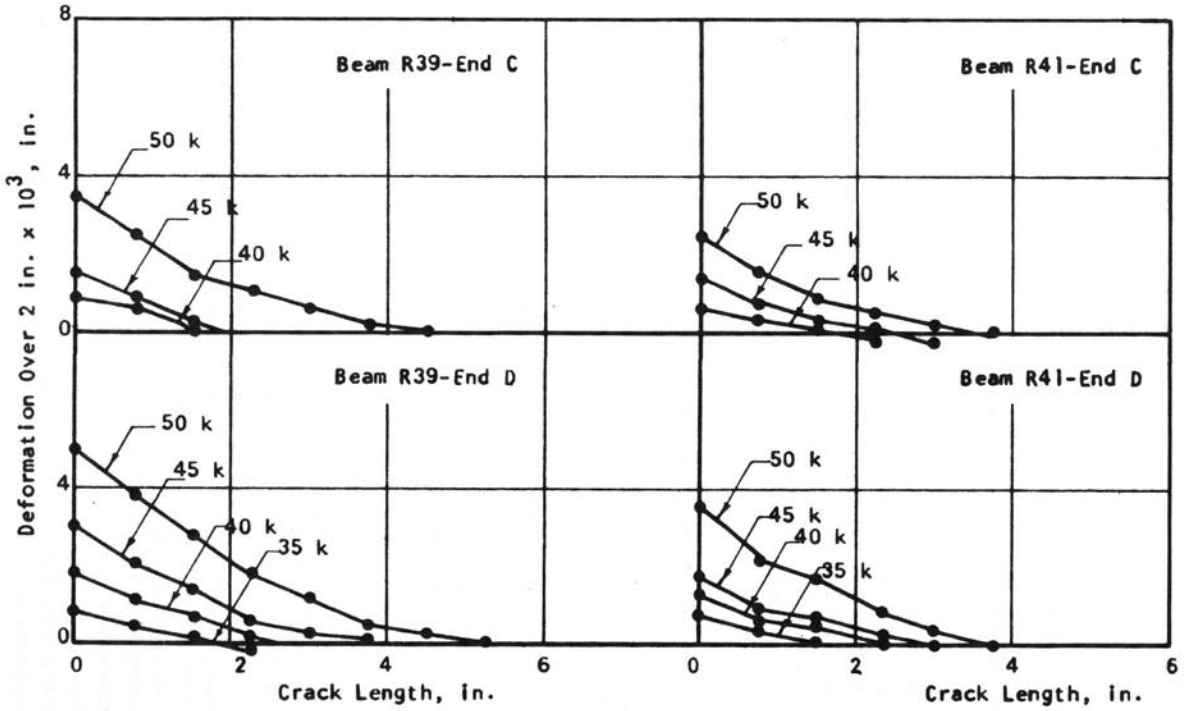

FIGURE A45. CRACK PROFILES FOR R39 AND R41, 1/8-IN. DIAMETER STIRRUPS

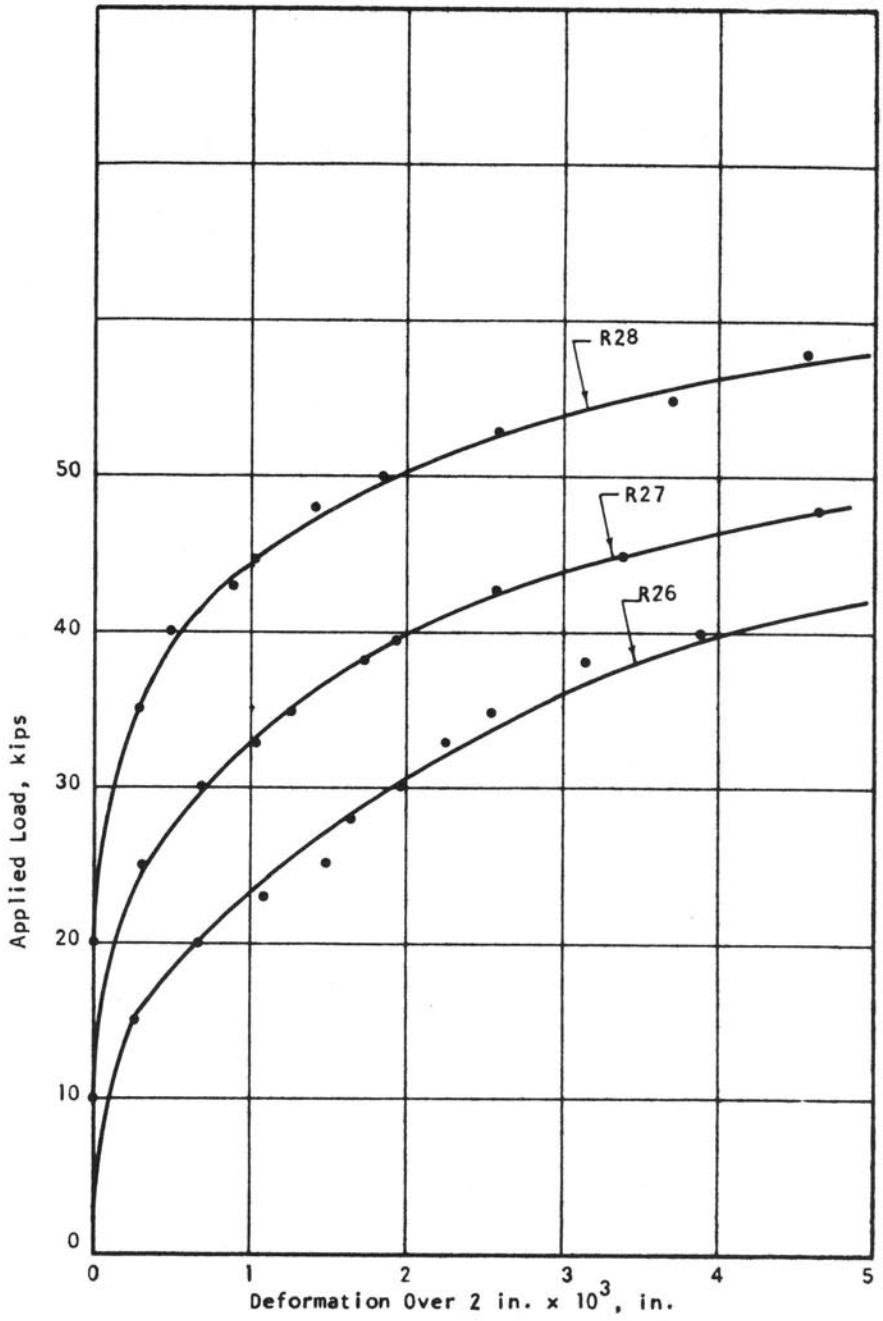

FIGURE A46. MEASURED RELATIONSHIPS BETWEEN LOAD AND TRANSVERSE DEFORMATION AT BEAM END FOR SPECIMENS R26, R27, AND R28

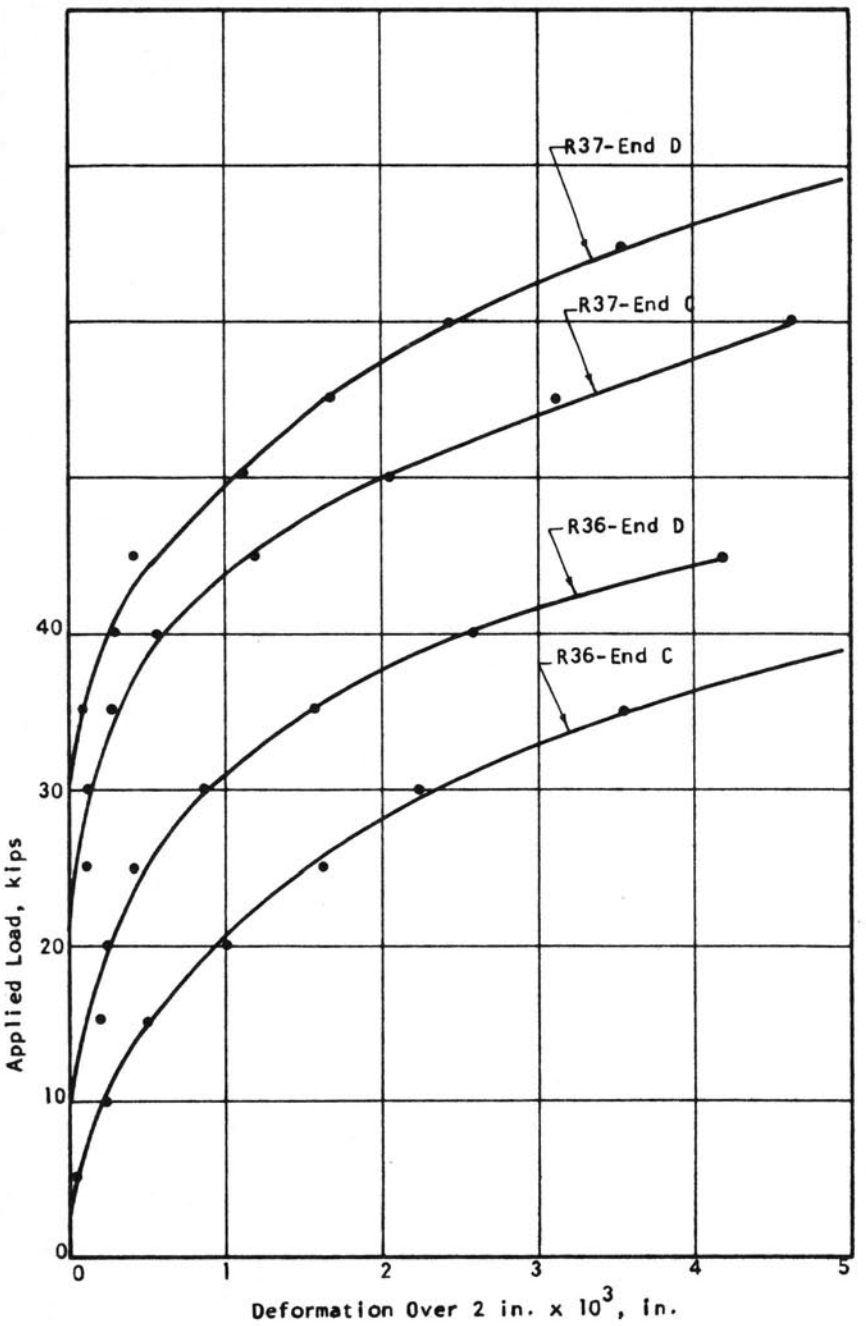

FIGURE A47. MEASURED RELATIONSHIPS BETWEEN LOAD AND TRANSVERSE DEFORMATION AT BEAM END FOR SPECIMENS R36 AND R37

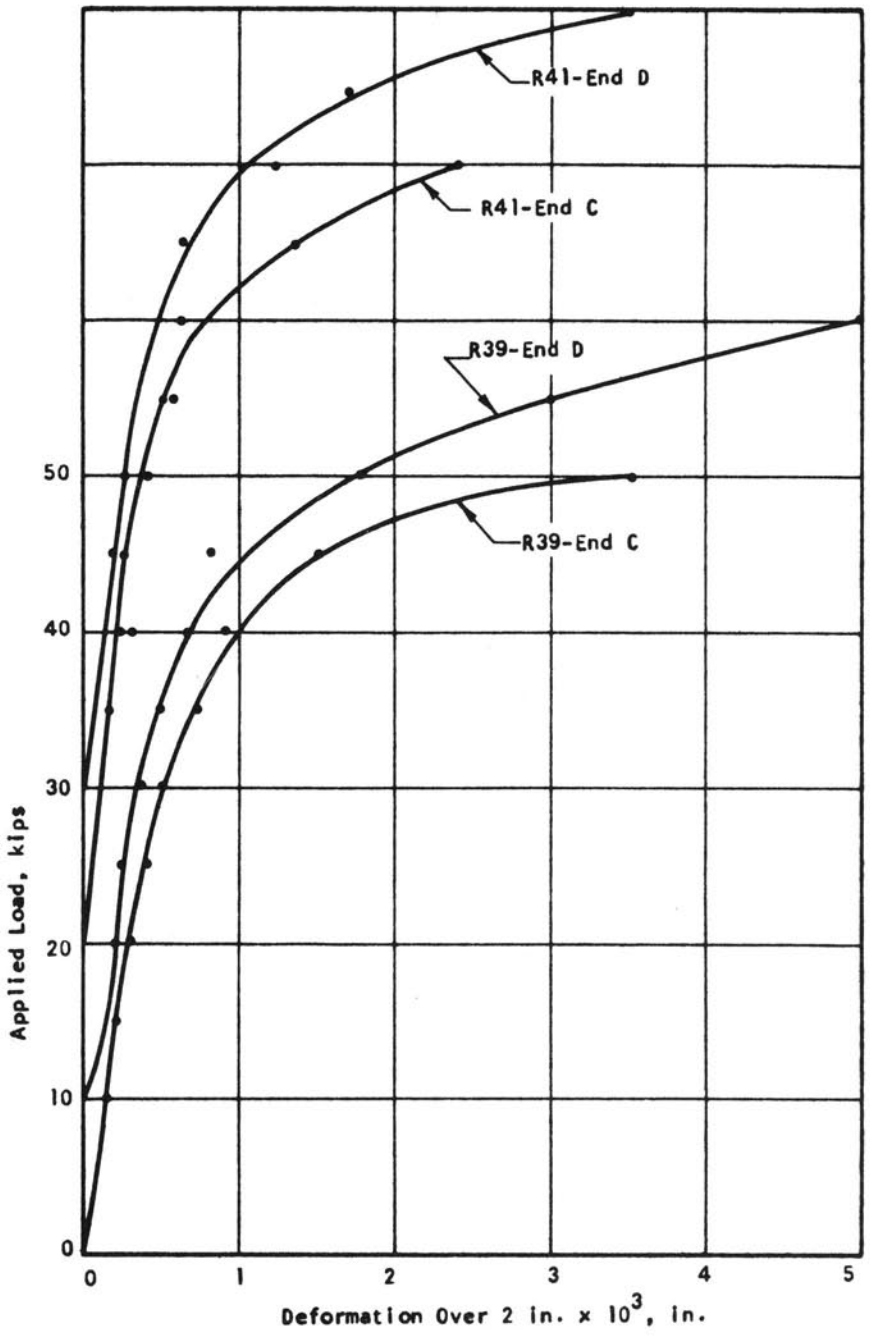

FIGURE A48. MEASURED RELATIONSHIPS BETWEEN LOAD AND TRANSVERSE DEFORMATION AT BEAM END FOR SPECIMENS R39 AND R41

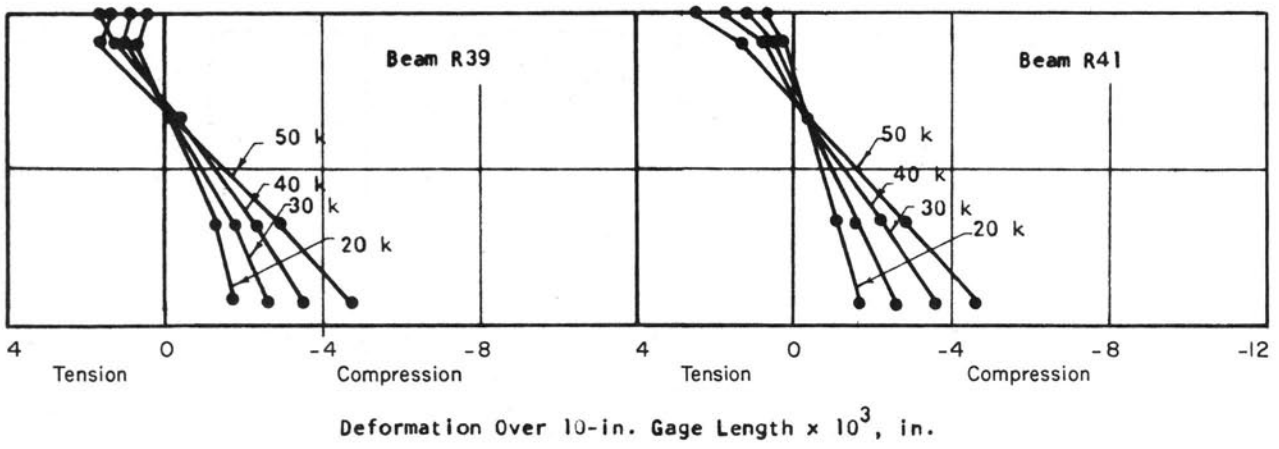

FIGURE A49. LONGITUDINAL DEFORMATION AT CENTER OF BEAM FOR R39 AND R41

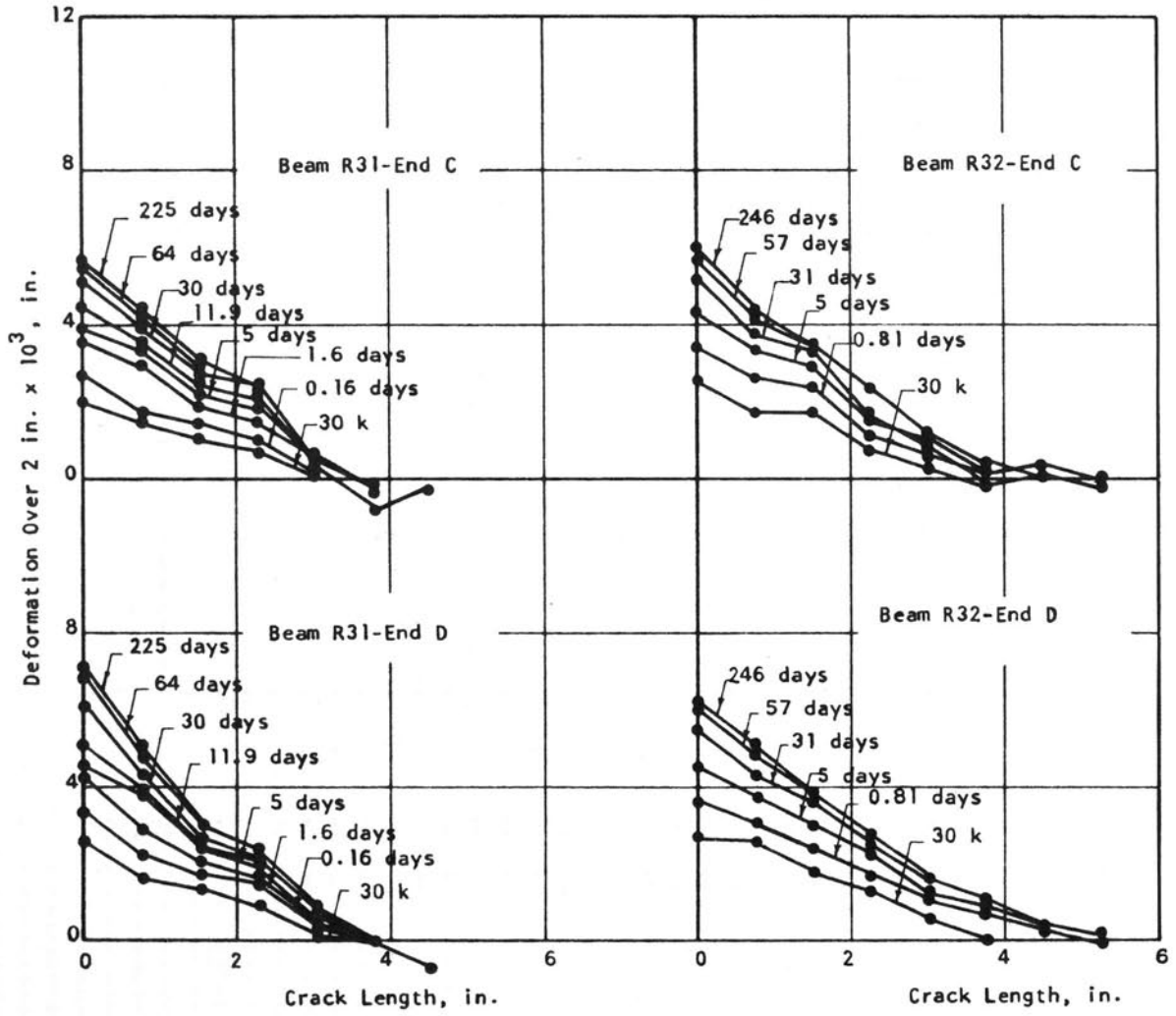

FIGURE A50. CRACK PROFILES FOR R31 AND R32, 1/4-IN. DIAMETER STIRRUPS

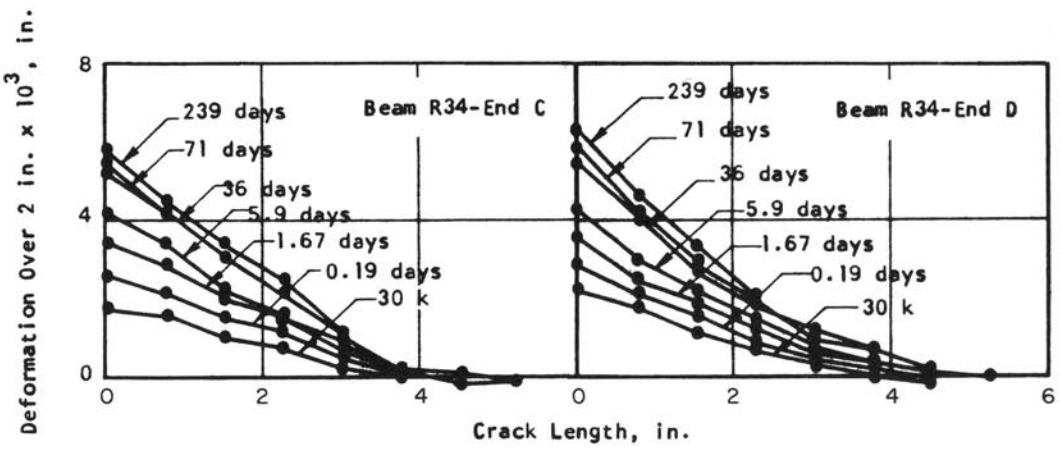

FIGURE A51. CRACK PROFILES FOR R34, 1/4-IN. DIAMETER STIRRUPS

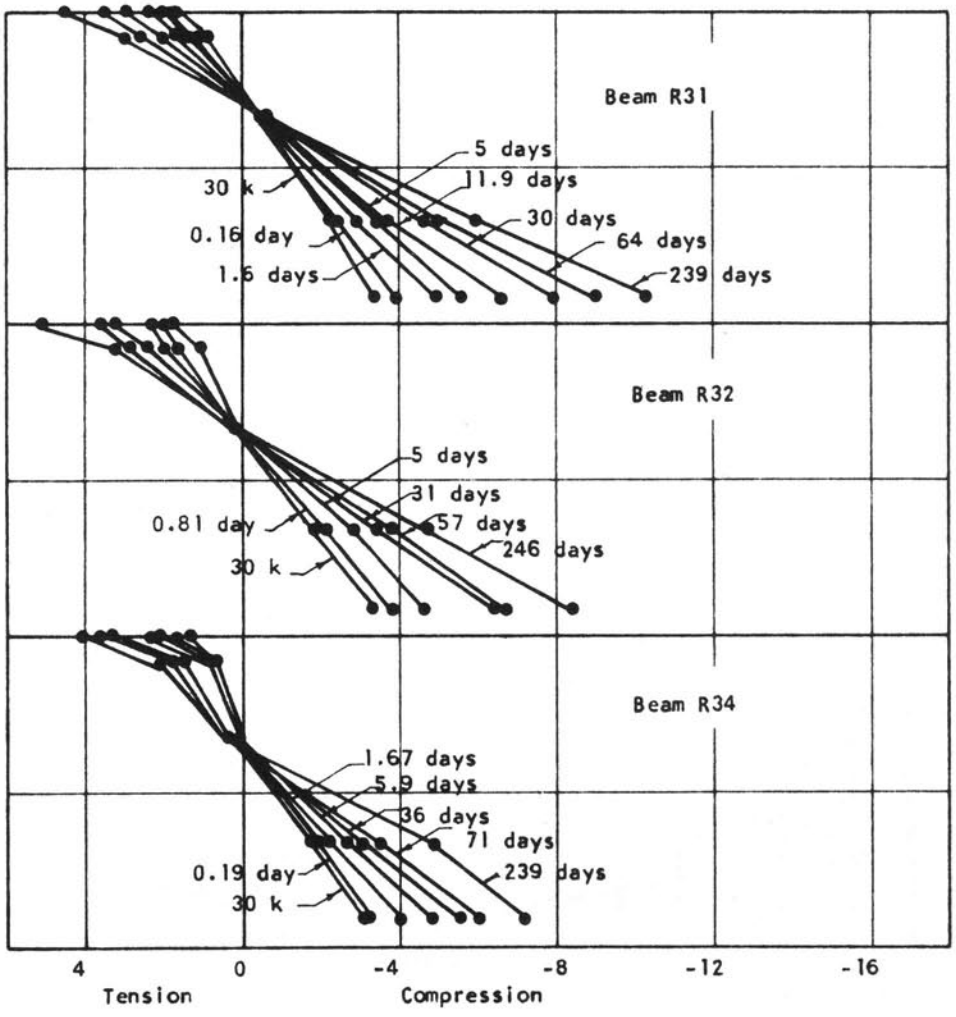

FIGURE A52. LONGITUDINAL DEFORMATIONS AT CENTER OF BEAM FOR R31, R32, AND R34

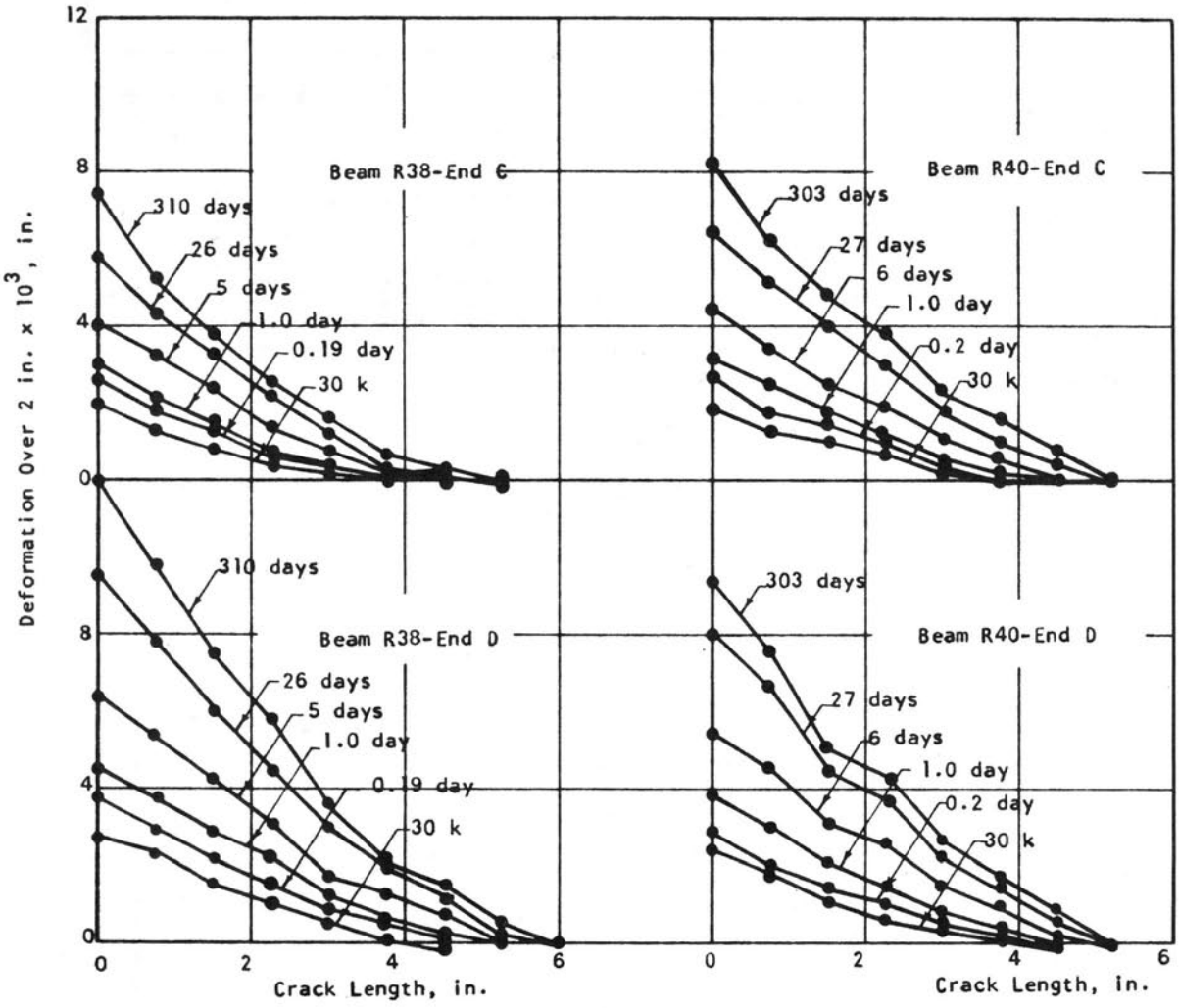

FIGURE A53. CRACK PROFILES FOR R38 AND R40, 1/8-IN. DIAMETER STIRRUPS

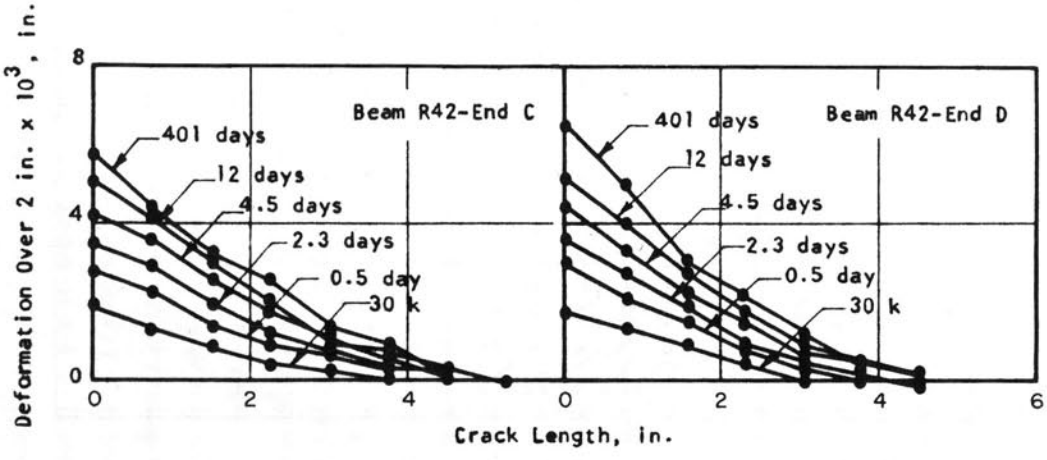

FIGURE A54. CRACK PROFILES FOR R42, 1/8-IN. DIAMETER STIRRUPS

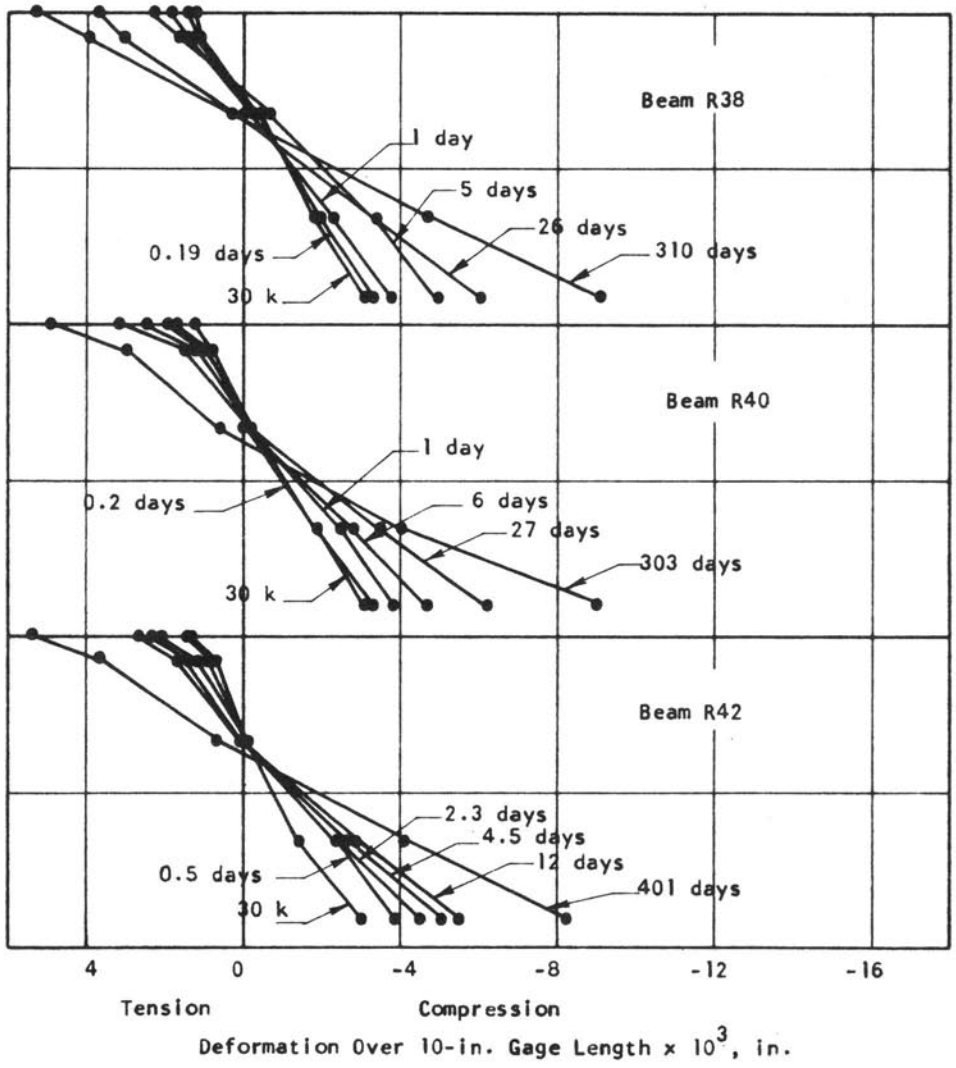

FIGURE A55. LONGITUDINAL DEFORMATION AT CENTER OF BEAM FOR R38, R40, AND R42

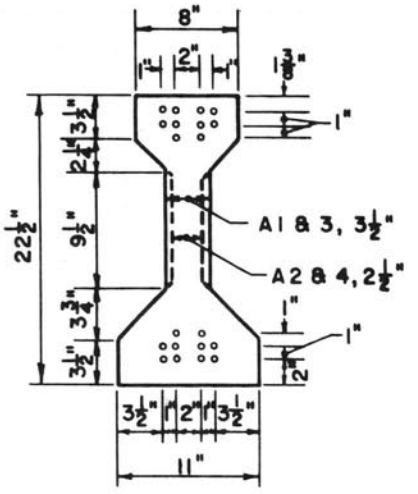

A1,2,3,&4 ($\frac{1}{4}$ in. Strand)

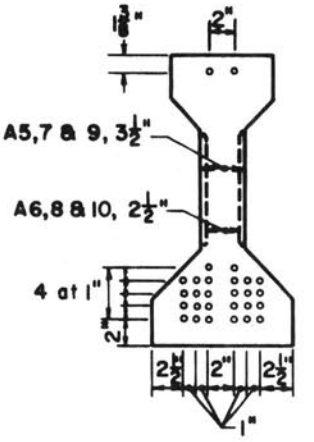

A5,6,7,8,9,&10 ($\frac{1}{4}$ in. Strand)

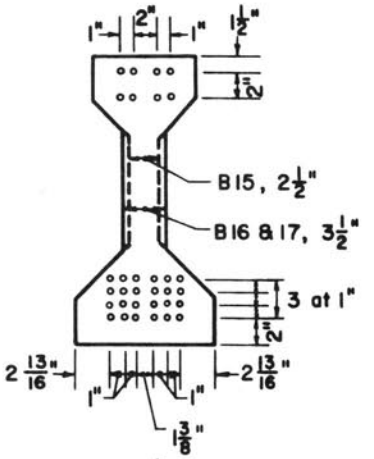

B15,16&17 ($\frac{1}{4}$ in. Strand)

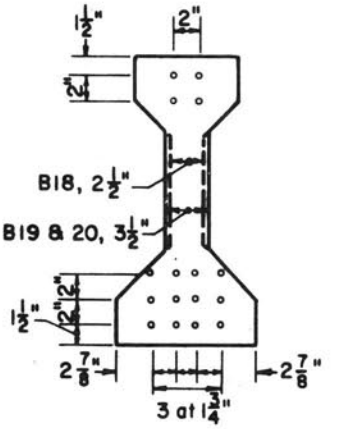

B18,19&20 ($\frac{3}{8}$ in. Strand)

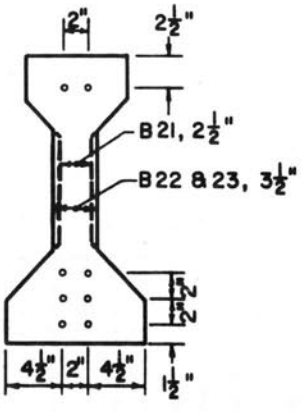

B21,22&23 ($\frac{1}{2}$ in. Strand)

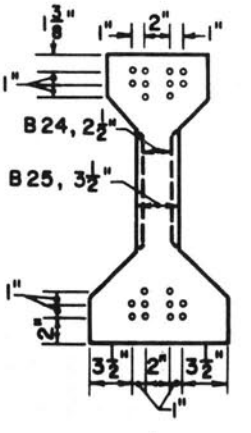

B24&25 ($\frac{1}{4}$ in. Strand)

FIGURE B1. NOMINAL DIMENSIONS OF GIRDERS A1 TO A10 AND B15 TO B25

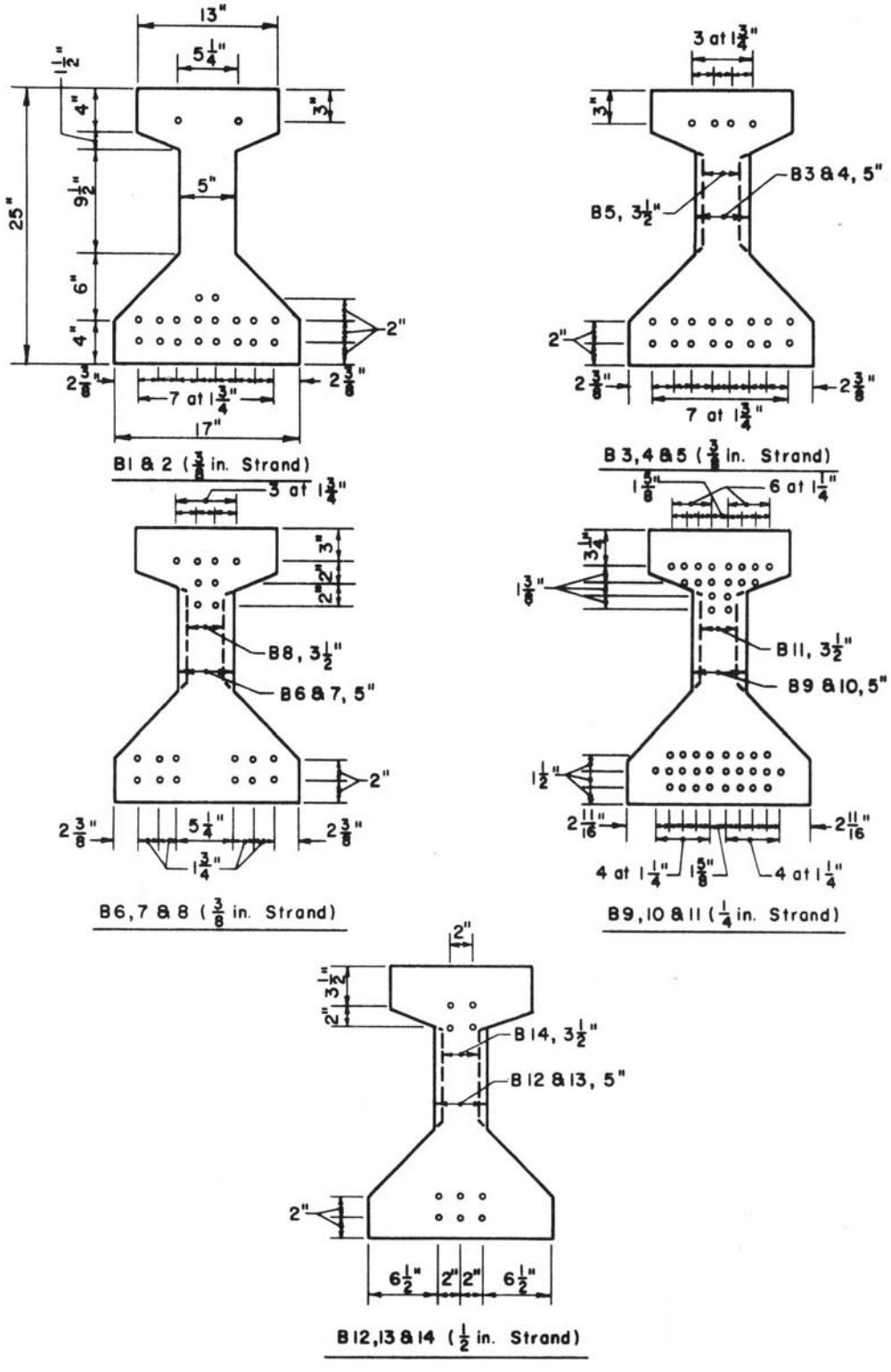

FIGURE B2. NOMINAL DIMENSIONS OF GIRDERS B1 TO B14

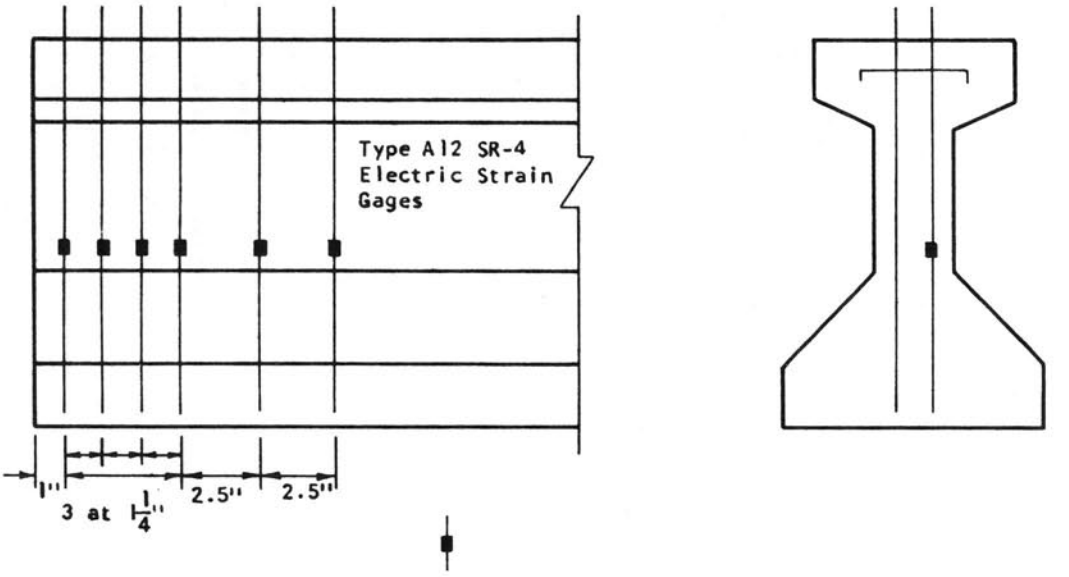

FIGURE B3. SPACING OF VERTICAL STIRRUPS IN ENDS OF SERIES B GIRDERS

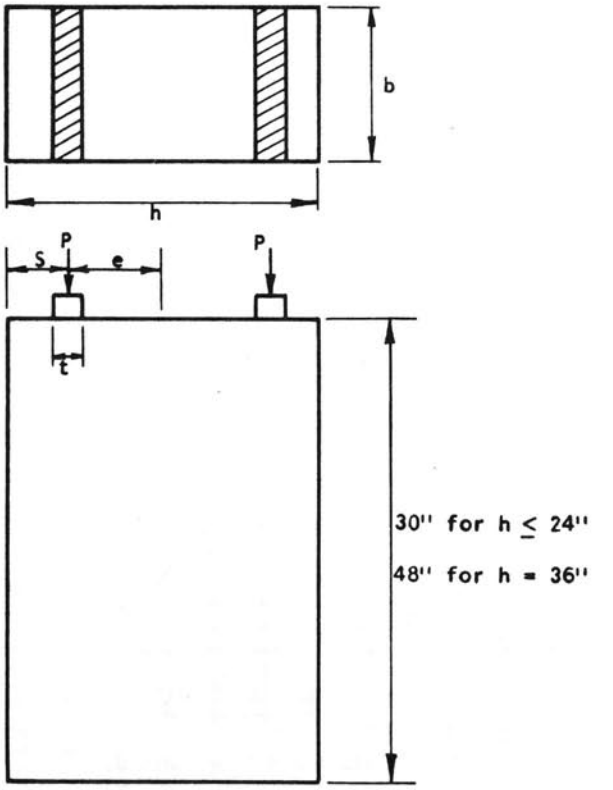

FIGURE B4. CROSS-SECTIONAL DIMENSIONS FOR CONCRETE COLUMN HEADS

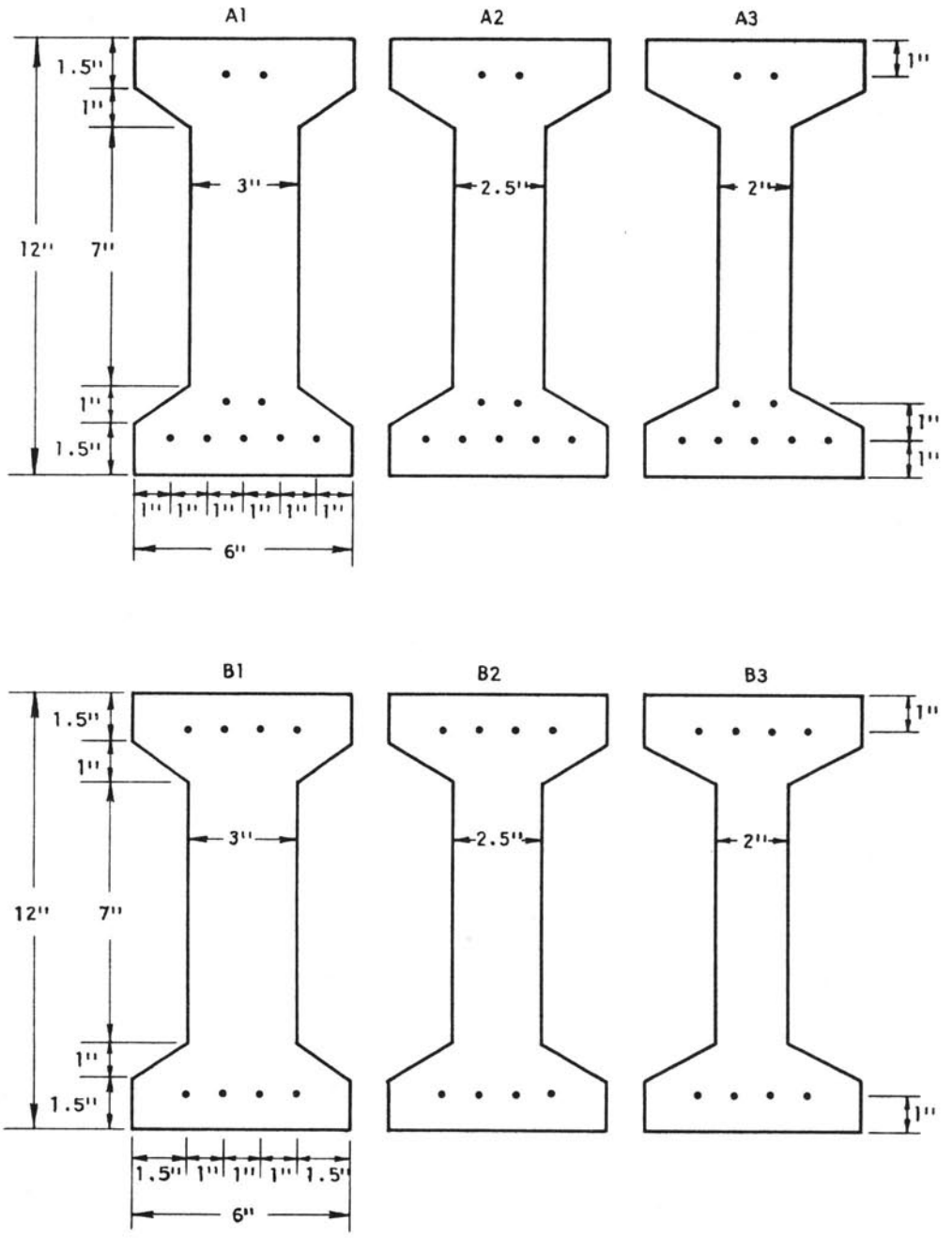

FIGURE B5. ARTHUR AND GANGULI, BEAM CROSS SECTIONS

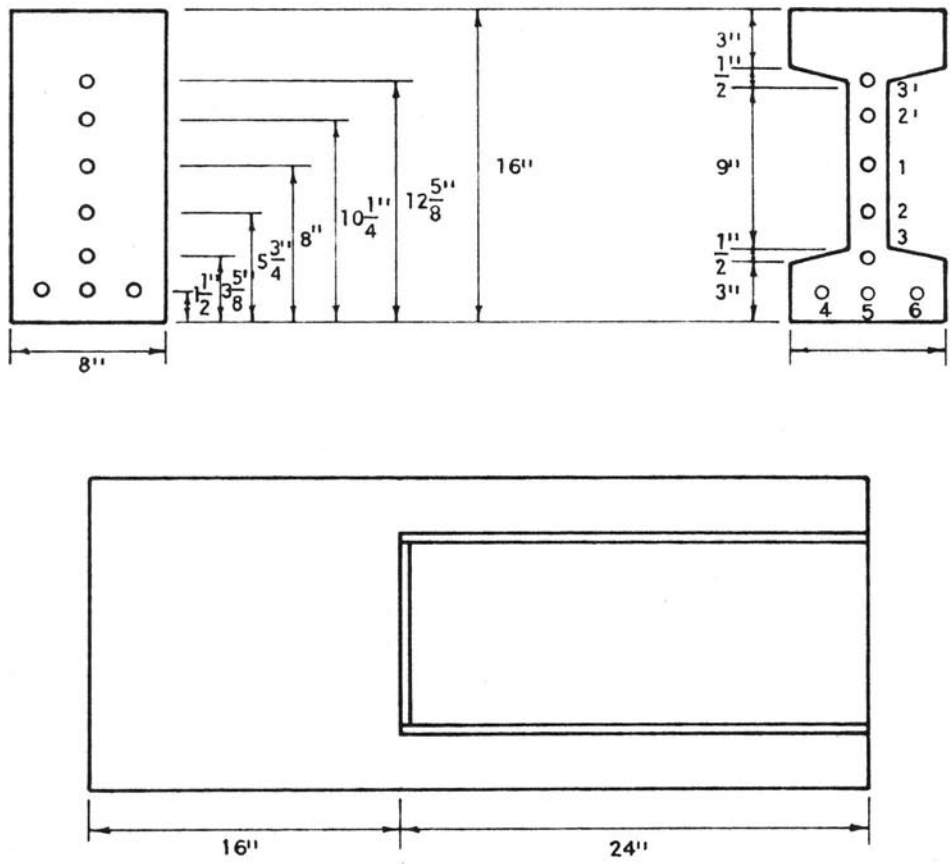

FIGURE B6. SPECIMENS OF ZIELINSKI AND ROWE

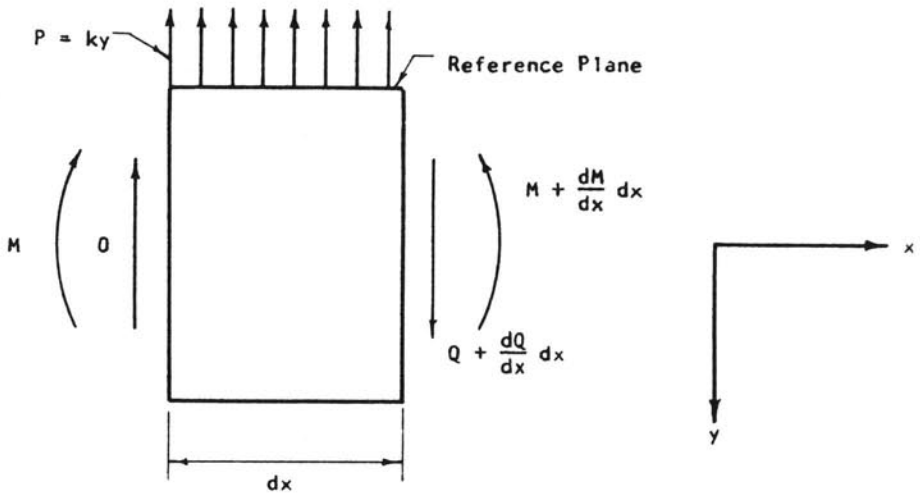

FIGURE C1. SIGN CONVENTION FOR PORTION OF BEAM BELOW REFERENCE PLANE

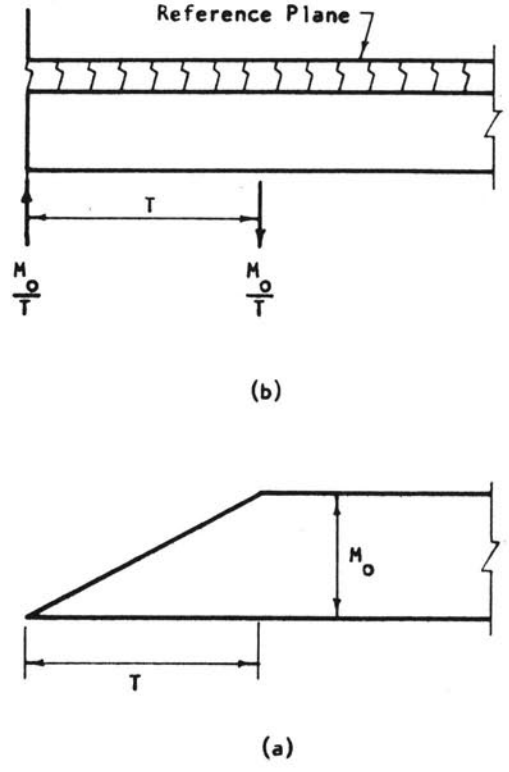

FIGURE C2. MOMENT AND EQUIVALENT COUPLE FOR PRETENSIONED BEAMS

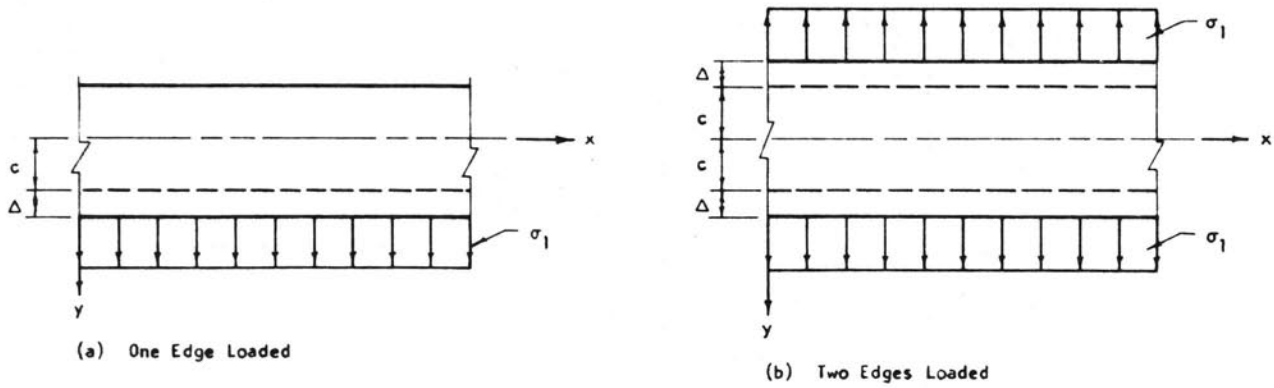

FIGURE C3. UNIFORM EDGE LOAD

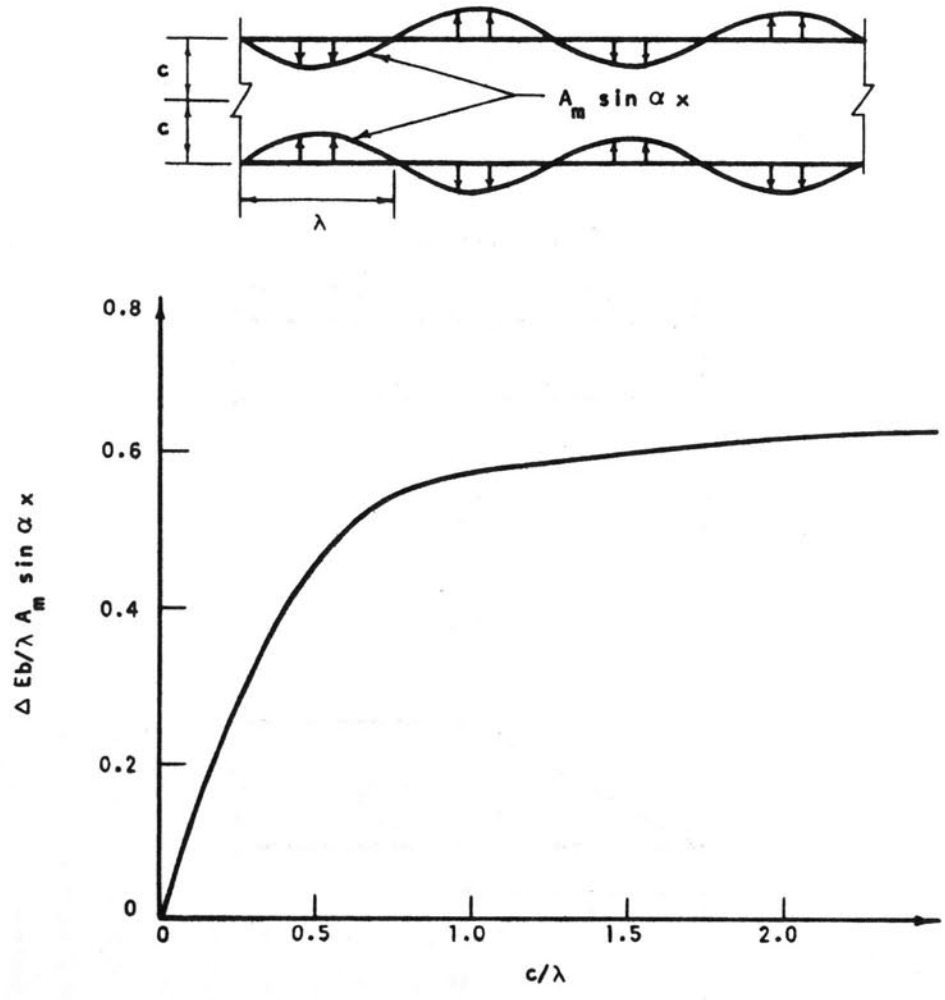

FIGURE C4. VARIATION OF Δ WITH c/λ FOR A SINUSOIDAL LOAD

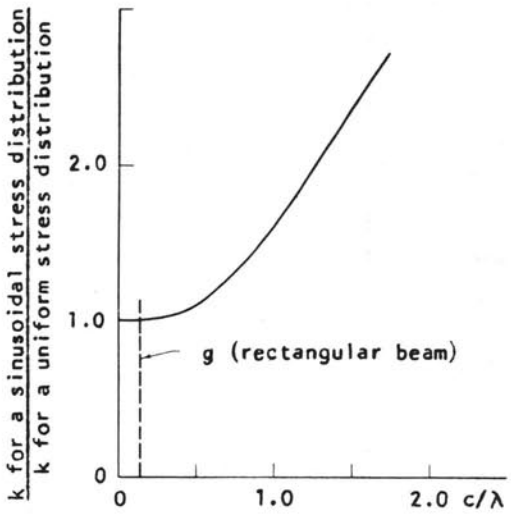

FIGURE C5. SPRING CONSTANT FOR A SINUSOIDAL STRESS DISTRIBUTION

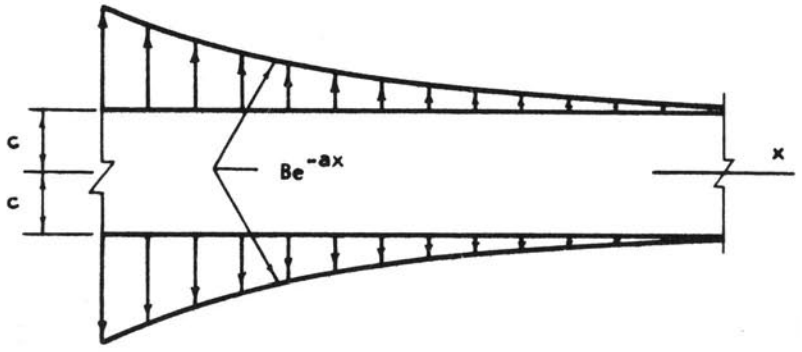

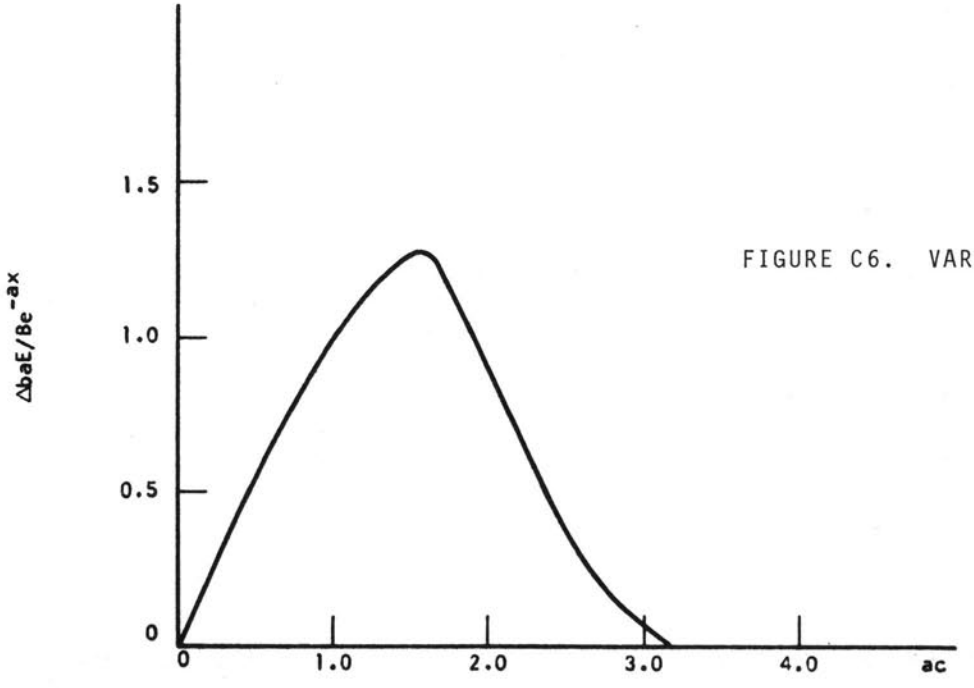

FIGURE C6. VARIATION OF Δ WITH ac

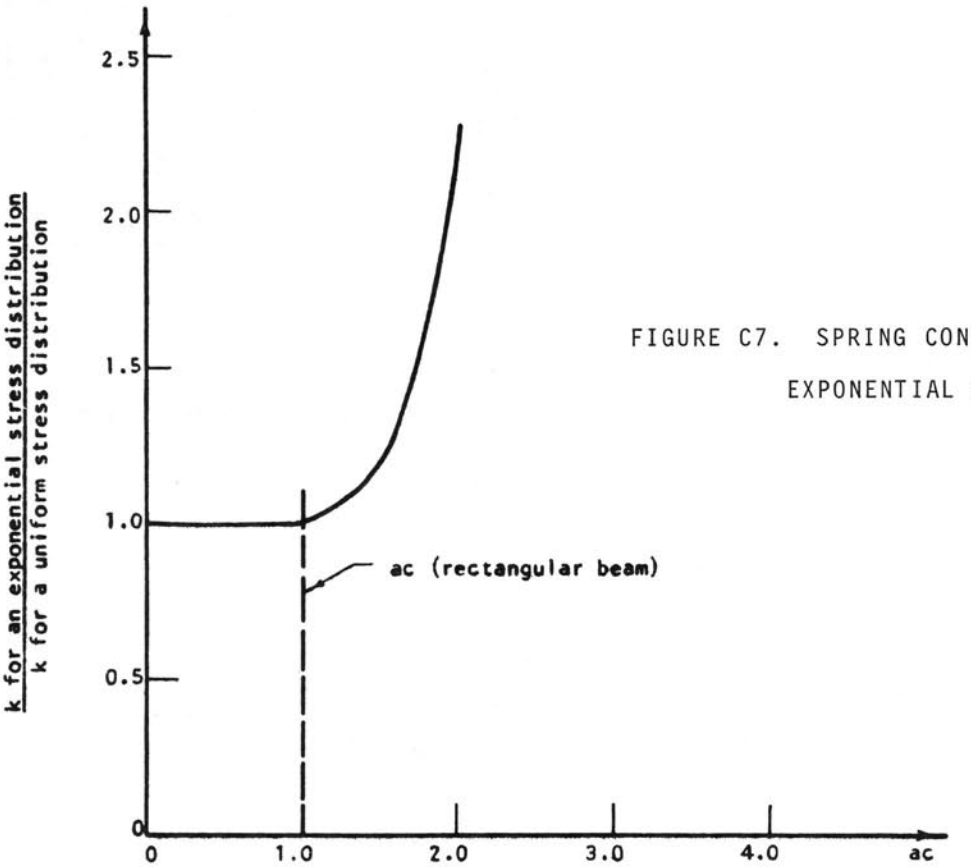

FIGURE C7. SPRING CONSTANT FOR AN EXPONENTIAL STRESS DISTRIBUTION

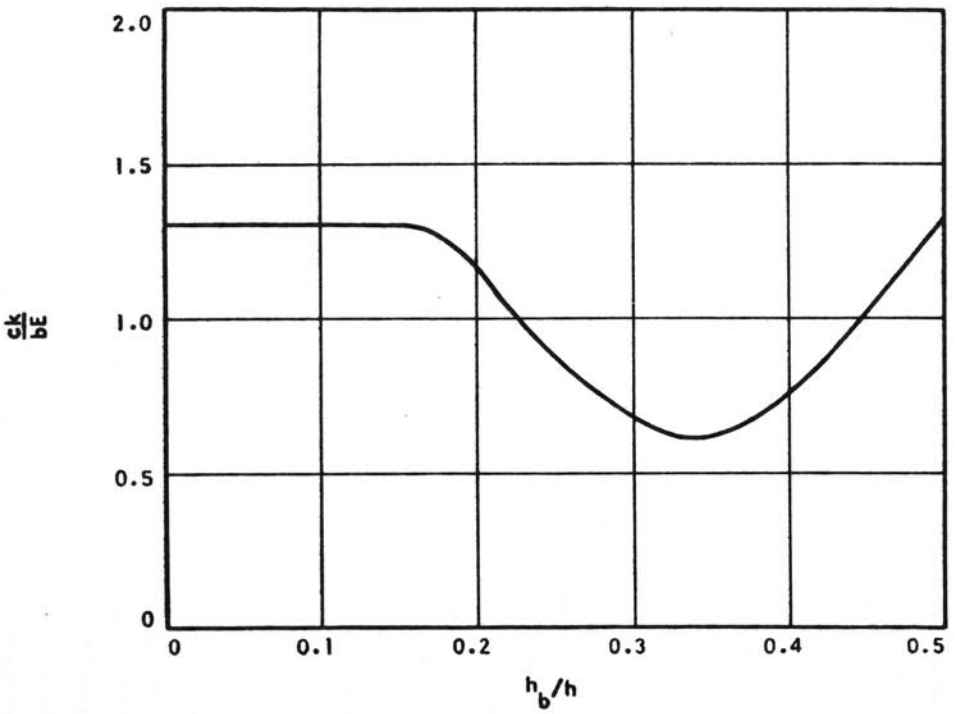

FIGURE C8. VARIATION OF SPRING CONSTANT WITH POSITION OF THE REFERENCE PLANE

TABLE 1

EFFECTIVE PRESTRESS FORCE AND TOTAL STIRRUP FORCE AT TRANSFER IN THE TESTS BY MARSHALL AND MATTOCK

Girder No.	Effective Prestress Force kip	Stirrup Size	Total Stirrup Force kip	Maximum Stirrup Stress ksi	Crack Length in.	Comments
B1	246	3				No Crack
B2	246	2				No Crack
B3	246	3	5.17	11.32	3.6	
B4	246	2	3.57	13.12	5.0	
B5	246	2	3.28	12.80	4.5	
B6	246	3				Remote Crack
B7	246	2	3.99	13.90	5.4	
B8	246	2	3.28	12.30	4.2	
B9	261	3	9.00	18.27	4.3	
B10	261	2	5.26	22.50	4.9	
B11	261	2	5.36	23.20	4.9	
B12	214	3	4.04	9.00	2.6	
B13	214	2	2.20	10.80	3.2	
B14	214	2	1.82	9.00	2.7	
B15	186	2				No Crack
B16	186	3	4.71	11.30	2.9	
B17	186	2	2.61	13.50	3.2	
B18	196	2				Remote Crack
B19	196	3				Remote Crack
B20	196	2				No Crack
B21	163	2				No Crack
B22	163	3				No Crack
B23	163	2				No Crack
B24	116	2	1.86	8.10	3.3	
B25	116	2				Remote Crack

TABLE 2

PRETENSIONED BEAMS BY ARTHUR AND GANGULI

Mark*	Number of Ends Cracked	Distance of Crack from Top Face, in.	Vertical Strain at Cracking x 10^5	Max. Vert. Strain at Transfer if Not Cracked x 10^5	Per Cent Prestress at Cracking	Length of Crack in.
A1(1)	1	5.5	32	58	38	1
A1(2)	1	5.5	35	65	44	16
A1(3)	1	5.5	38	--	38	12
A2(1)	0			20,26		
A2(2)	0			40,25		
A2(3)	1	6.5	34	30	44	negligible
A3(5)	2	2.5	45		31	severe
		2.5	35		44	severe
A3(6)	1	4.0	35	90	31	18
A3(7)	2	8.0	35		31	24
		6.0	35		31	0
B1(1)	1	5.0	42	32	56	0
B1(2)	0			40,15		
B1(3)	2	2.5	32		31	0
		9.5	30		69	0
B2(1)	0			17,25		
B2(2)	0			40,40		
B2(3)	1	9	35	40	44	18
B3(1)	2	2.5	44		56	4
		2.5	47		31	26
B3(2)	2	2.5	74		100	1
		7	44		56	3
B3(3)	0			37,27		
B3(4)	1	2.5	44	32	38	negligible

*Refer to Figure B5.

TABLE 3

END BLOCKS TESTED BY ZIELINSKI AND ROWE

Test No.	Cracking Load kips	Ultimate Load kips
1	31.8	31.8
9	66.3	77.0
16	55.2	66.3
17	110.0	121.0
18	66.3	77.0
19	165.5	165.5
20	101.5	-----

TABLE 4

CALCULATED ULTIMATE LOADS FOR THE TESTS BY ZIELINSKI AND ROWE

Test No.	Measured Cracking Load kips	Measured Ultimate Load kips	Predicted Ultimate Load kips	P_{test}/P_{calc}	Section Shape
1	31.8	31.8	27	1.18	I
9	66.3	77.0	47	1.64(1.41)	I
16	55.2	66.3	69	0.96(0.80)	R
17	110.0	121.0	118	1.03	R
18	66.3	77.0	50	1.54	I
19	165.5	165.5	172	0.96	I
20	101.5	-----	94.5		R

Avg = 1.22(1.15)

TABLE 5

CALCULATED AND OBSERVED BEHAVIOR IN THE TESTS
BY MARSHALL AND MATTOCK

Girder Number	Predicted Cracking Load kips	Effective Prestress Force kips	Observed Behavior*	Predicted Behavior Observed
A1	22	116	C	Yes
A2	18	116	C	Yes
A3	22	116	C	Yes
A4	18	116	C	Yes
B1	77	246	N	No
B2	77	246	N	No
B3	70	246	C	Yes
B4	70	246	C	Yes
B5	67	246	C	YEs
B6	79	246	C	Yes
B7	79	246	C	Yes
B8	79	246	C	Yes
B9	52	261	C	Yes
B10	52	261	C	Yes
B11	53	261	C	Yes
B12	103	214	C	Yes
B13	103	214	C	Yes
B14	96	214	C	Yes
B15	55	186	N	No
B16	49	186	C	Yes
B17	49	186	C	Yes
B18	83	196	C	Yes
B19	82	196	C	Yes
B20	82	196	N	No
B21	107	163	N	No
B22	109	163	N	No
B23	109	163	N	No
B24	18	116	C	Yes
B25	22	116	C	Yes

*C = cracking, N = no cracking.

TABLE 6

CALCULATED AND OBSERVED BEHAVIOR IN THE TESTS BY ARTHUR AND GANGULI

Girder No.	Per Cent Prestress at Cracking	
	Measured	Computed
A1(1)	38	34
A1(2)	44	38
A1(3)	38	39
A3(5)	31-44	39
A3(6)	31	39
A3(7)	31	25
B1(1)	56	37
B1(2)	no crack	35
B1(3)	31-69	31
B3(1)	31-56	30
B3(2)	56	29
B3(3)	no crack	29
B3(4)	38	24

TABLE 7

SPALLING STRESS ANALYSIS FOR AASHO TYPE III GIRDER

Trial	y in.	c in.	b_{eq} in.	I_b in.^{4}	A_b in.^{2}	V kip	M_o in.-kip	σ_s psi
1	11.5	6.3	12.8	1590	164	-8.8	154	375
2	13	7.4	11.4	2080	174	-4.9	167	345

TABLE 8

POST-TENSIONED BEAMS, GERGELY

Mark	Concrete		Reinforcement				Precrack	Age at Loading
	Compressive Strength psi	Splitting Strength psi	Diameter in.	Yield Force kips	Distance from End in.	No. of Bars		Days
I1	5500	350	----	--	--	0	No	--
I2	5500	350	----	--	--	0	No	--
I3	4400	390	----	--	--	0	No	--
I4	5500	410	----	--	--	0	No	--
I5	5200	320	----	--	--	0	No	--
I6	5100	400	----	--	--	0	No	--
I7	4600	350	----	--	--	0	No	--
I8	5100	390	#2 bar	2.5	1/2	1	Yes	8
I9	5200	310	#2 bar	2.5	1/2	1	Yes	8
I10	5400	460	#2 bar	2.5	1	1	Yes	7
I11	5350	390	#2 bar	2.5	1/2,2	2	Yes	8
I12	5200	420	#2 bar	2.5	1	1	Yes	8
I13	4650	400	#2 bar	2.5	1/2	1	Yes	8
I14	4500	400	#2 bar	2.5	1/2	1	Yes	7
I15	4700	370	#2 bar	2.5	1/2,2	2	Yes	--
I16	5600	450	#7USSWG	0.8	1/2	1	Yes	--
I17	5200	360	#7USSWG	0.8	1/2	1	Yes	6
I18	5000	370	#7USSWG	0.8	1/2	1	Yes	6
R1	5630	460	----	--	--	0	No	--
R2	6130	450	----	--	--	0	No	--
R3	5200	360	----	--	--	0	No	--
R4	4500	380	#2 bar	2.5	1/2	1	Yes	9
R5	5500	390	#2 bar	2.5	1/2	1	Yes	10
R6	5300	400	#2 bar	2.5	1	1	Yes	9
R7	5800	410	#2 bar	2.5	1	1	Yes	8
R8	5900	380	#2 bar	2.5	1/2,2	2	Yes	8
R9	5500	420	#2 bar	2.5	1/2,3	2	Yes	7
R10	5300	420	#2 bar	2.5	1/2,2 1/2	2	Yes	7
R11	5200	430	#2 bar	2.5	1/2	1	Yes	8
R12	5450	390	#2 bar	2.5	1/2	1	Yes	8
R13	4900	380	#2 bar	2.5	1/2,2	2	Yes	7
R14	4900	380	#7USSWG	0.8	1/2	1	Yes	--
R15	5700	430	#7USSWG	0.8	1/2,2	2	Yes	--
R16	6000	415	#7USSWG	0.8	1/2	1	No	--
R17	5800	440	#7USSWG	0.8	1/2	1	Yes	8

TABLE 9

POST-TENSIONED RECTANGULAR BEAMS, WELSH

Mark	Concrete		Reinforcement				Related Bond Tests	Duration of Loading Days	Age at Loading Days
	Compressive Strength psi	Splitting Strength psi	Diameter in.	Yield Force kip	Distance to Beam End in.	Lot			
R19	5700	435	None	----	---	-	---	1	7
R20	5200	415	None	----	---	-	---	1	7
R21	5650	400	None	----	---	-	---	1	7
R22	5400	410	None	----	---	-	---	1	7
R23	5200	420	1/4	1.75	3/4	1	T1,T2	1	7
R24	5900	445	1/4	1.75	3/4	1	T3,T4	1	7
R25	5650	420	1/4	1.75	3/4	1	T5,T6	1	7
R26	5350	420	1/8	0.53	3/4	1	T9,T10	1	7
R27	5550	430	1/8	0.53	3/4	1	T11,T12	1	7
R28	6050	485	1/8	0.53	3/4	1	T13,T14	1	7
R29a	5510	445	1/4	1.72	3/4	2	T15,T16	1	15
R29b	6760	511	1/4	1.70	3/4	2	T17,T18	1	15
R30	6090	482	1/4	1.71	3/4	2	T19,T20	1	15
R31	6115	507	1/4	1.65	3/4	2	T21,T22	225	15
R32	6240	460	1/4	1.72	3/4	2	T23,T24	246	15
R33	7430	495	1/4	1.68	3/4	2	T25,T26	1	236
R34	6370	510	1/4	1.68	3/4	2	T27,T28	239	15
R35	6780	440	1/4	1.65	3/4	2	T29,T30	1	238
R36	5940	470	1/8	0.50	3/4	2	T31,T32	1	15
R37	6325	445	1/8	0.54	3/4	2	T33,T34	1	15
R38	6210	521	1/8	0.50	3/4	2	T35,T36	310	15
R39	6900	480	1/8	0.47	3/4	2	T37,T38	1	430
R40	6055	521	1/8	0.54	3/4	2	T39,T40	303	15
R41	7175	510	1/8	0.47	3/4	2	T31,T42	1	430
R42	6270	475	1/8	0.50	3/4	2	T43,T44	401	15
	4900	410	1/4	1.75	---	1	T7,T8	1	7
R43	5900	399	None	----	---	-	---	1	18
R44	5630	366	None	----	---	-	---	1	18
R45	5800	390	None	----	---	-	---	1	18
R46	5470	370	None	----	---	-	---	1	18
R47	5730	370	None	----	---	-	---	1	18
R48	5680	437	None	----	---	-	---	1	21

TABLE 10

TEST RESULTS AND CORRESPONDING FIGURES

Mark	Crack Profile	Transverse Deformation at Beam End	Longitudinal Deformation at Beam Center
R19	A.18	A.20	----
R22	A.19	A.20	----
R23	A.35	A.39	----
R24	A.35	A.39	----
R25	A.35	A.39	----
R26	A.43	A.46	----
R27	A.43	A.46	----
R28	A.43	A.46	----
R29a	A.36	A.40	----
R29b	A.36	A.40	----
R30	A.37	A.40	----
R31	A.50	----	A.52
R32	A.50	----	A.52
R33	A.38	A.41	A.42
R34	A.51	----	A.52
R35	A.38	A.41	A.42
R36	A.44	A.47	----
R37	A.44	A.47	----
R38	A.53	----	A.55
R39	A.45	A.48	A.49
R40	A.53	----	A.55
R41	A.45	A.48	A.49
R42	A.54	----	A.55
R43	A.21,A.22	A.27	----
R44	A.28,A.29	A.34	----
R45	A.23,A.24	A.27	----
R46	A.30,A.31	A.34	----
R47	A.25,A.26	A.27	----
R48	A.32,A.33	A.34	----

TABLE 11

PRETENSIONED BEAMS, MARSHALL AND MATTOCK

Mark	Per Cent Prestress Force in Bottom Flange	e/h top	e/h bottom	Concrete Compressive Strength psi	Reinforcement Diameter in.	Reinforcement Yield Force kips	Reinforcement Distance from End in.	Reinforcement Number of Bars	Strand Diameter in.
A1	50	0.46	0.32	5050	--	--	--	--	1/4
A2	50	0.46	0.32	4125	--	--	--	--	1/4
A3	50	0.46	0.32	4625	--	--	--	--	1/4
A4	50	0.46	0.32	4145	--	--	--	--	1/4
A5	93	0.50	0.27	4900	--	--	--	--	1/4
A6	93	0.50	0.27	4560	--	--	--	--	1/4
A7	93	0.50	0.27	5095	--	--	--	--	1/4
A8	93	0.50	0.27	4580	--	--	--	--	1/4
A9	93	0.50	0.27	4520	--	--	--	--	1/4
A10	93	0.50	0.27	4520	--	--	--	--	1/4
B1	90	0.44	0.30	4580	#3 bar	4.9	1,2.25	2 at each	3/8
B2	90	0.44	0.30	4580	#2 bar	2.5	3.5,4.75	distance,	3/8
B3	80	0.44	0.32	7090	#3 bar	4.9	7.25,9.75	12 bars	3/8
B4	80	0.44	0.32	7090	#2 bar	2.5		total	3/8
B5	80	0.44	0.32	7190	#2 bar	2.5			3/8
B6	60	0.38	0.32	4855	#3 bar	4.9			3/8
B7	60	0.38	0.32	4855	#2 bar	2.5			3/8
B8	60	0.38	0.32	4995	#2 bar	2.5			3/8
B9	60	0.38	0.32	4290	#3 bar	4.9			1/4
B10	60	0.38	0.32	4290	#2 bar	2.5			1/4
B11	60	0.38	0.32	4475	#2 bar	2.5			1/4
B12	60	0.38	0.32	4415	#3 bar	4.9			1/2
B13	60	0.38	0.32	4415	#2 bar	2.5			1/2
B14	60	0.38	0.32	4200	#2 bar	2.5			1/2
B15	75	0.44	0.29	4030	#2 bar	2.5			1/4
B16	75	0.44	0.29	3715	#3 bar	4.9			1/4
B17	75	0.44	0.29	3715	#2 bar	2.5			1/4
B18	75	0.44	0.29	4450	#2 bar	2.5			3/8
B19	75	0.44	0.29	4575	#3 bar	4.9			3/8
B20	75	0.44	0.29	4575	#2 bar	2.5			3/8
B21	75	0.44	0.29	4090	#2 bar	2.5			1/2
B22	75	0.44	0.29	4975	#3 bar	4.9			1/2
B23	75	0.44	0.29	4975	#2 bar	2.5			1/2
B24	50	0.46	0.32	4660	#2 bar	2.5			1/4
B25	50	0.46	0.32	4660	#2 bar	2.5			1/4

e = eccentricity of prestress force measured from centroid of cross section.

h = height of cross section.

TABLE 12

PLAIN CONCRETE COLUMN HEADS, KRIZ AND RATHS

Mark	Cross Section b x h in. x in.	$\frac{t^*}{h}$	$\frac{b'^*}{b}$	$\frac{e^*}{h}$	Compressive Strength psi	Ultimate Load kips**
1	8x12	0.083	1	0.460	2850	20.5
2	12x8	0.125	1	0.438	4010	34.3
3	8x12	0.083	1	0.413	2850	30.6
4	8x8	0.125	1	0.312	3940	39.0
5	8x12	0.083	1	0.375	3230	36.2
6	12x8	0.125	1	0.312	4000	53.0
7	8x8	0.125	1	0.188	4000	44.2
8	8x12	0.083	1	0.291	2790	32.2
9	8x12	0.083	1	0.291	2820	40.0
10	8x12	0.083	1	0.291	6690	59.5
11	8x8	0.125	1	0	4060	56.7
12	8x12	0.083	1	0.167	3170	57.3
13	12x24	0.042	1	0.167	2900	94.8
14	12x24	0.042	1	0.042	2940	89.0
15	12x24	0.042	1	0	2750	116.5
16	8x12	0.167	1	0.413	3030	56.3
17	8x12	0.167	1	0.413	3110	53.0
18	12x8	0.250	1	0.375	4010	75.4
19	8x12	0.167	1	0.375	3230	65.6
20	12x8	0.250	1	0.250	4000	99.8
21	8x12	0.167	1	0.291	2790	60.3
22	8x12	0.167	1	0.291	3110	61.3
23	8x12	0.167	1	0.291	6490	95.0
24	8x12	0.167	1	0.291	6490	104.5
25	8x12	0.167	1	0.167	2970	68.0
26	12x12	0.167	1	0.167	3600	122.2
27	12x24	0.083	1	0	2280	147.1
28	12x24	0.083	1	0	2760	157.0
29	12x36	0.056	1	0	2810	177.1
30	8x12	0.250	1	0.375	2820	74.9
31	8x12	0.250	1	0.375	3030	80.2
32	12x12	0.250	1	0.313	3520	148.0
33	8x12	0.250	1	0.291	3170	94.8
34	8x12	0.250	1	0.291	6690	135.4
35	8x12	0.250	1	0.167	2970	90.5
36	12x24	0.125	1	0	2530	180.0
37	12x36	0.083	1	0	2870	230.0

*Refer to Figure B4.
**One-half total load on specimen.

TABLE 13

PROPERTIES OF PRETENSIONED BEAMS,
ARTHUR AND GANGULI

Mark*	e/h top	e/h bottom	7-Day Cube Strength psi
A1(1)	0.083	0.111	3950
A1(2)	0.083	0.111	4900
A1(3)	0.083	0.111	5400
A2(1)	0.083	0.111	5300
A2(2)	0.083	0.111	4900
A2(3)	0.083	0.111	4650
A3(5)	0.083	0.111	5650
A3(6)	0.083	0.111	5350
A3(7)	0.083	0.111	2250
B1(1)	0.083	0.083	5650
B1(2)	0.083	0.083	5000
B1(3)	0.083	0.083	4000
B2(1)	0.083	0.083	4950
B2(2)	0.083	0.083	5050
B2(3)	0.083	0.083	5050
B3(1)	0.083	0.083	6200
B3(2)	0.083	0.083	5950
B3(3)	0.083	0.083	5900
B3(4)	0.083	0.083	3900

*Refer to Figure B5.

TABLE 14

PROPERTIES OF END BLOCKS, ZIELINSKI AND ROWE

Test No.	Cross Section	Compressive Strength, Cube psi	Splitting Strength psi	Number of Loads	Positions of Loads*	Diameter of Loading Plate(s) in.
1+	I	7730	520	1	1	1.9(dia.)
2	I			1	1	
3	I			2	2,2'	
4	I			2	3,3'	
5	I	7200	505	2	1,3'	1.9(dia.)
6	I			2	2',5	
7	I			2	2,5	
8	I			3	4,6,1	
9+	I			3	4,6,2'	
10	R			1	1	5.5 x 3
11	R			1	1	6 x 4
12	R			1	e/h=0.224	5.5 x 3
13	R	7450	520	2	2,2'	1.9(dia.)
14	R			1	3/h=0.224	6 x 4
15	R			3	4,6,1	1.9(dia.)
16+	R			3	4,6,2'	1.9(dia.)
17+	R	7640	504	1	e/h=0.224	5.375(dia.)
18+	I	7640	561	2	2,5	1.9(dia.)
19+	I	10500	745	5	1,2',4,5,6	1.9(dia.)
20+	R	9980	762	5	1,2',4,5,6	1.9(dia.)

*Refer to Figure B6.

+ Test to failure.

the modulus of rupture specimen.

The second observation to be made about the values of the effective tensile strength is that the strength of the air-dried specimens was significantly less than that of the epoxy-coated specimens. This phenomenon can be explained on the basis of the relative magnitudes of the shrinkage strains measured in the two types of specimens. The ratio of the shrinkage strains in the air-dried specimens to those in the epoxy-coated specimens was about 2.5.

The variation of the effective tensile strength along the length of the beam is to be studied next. This distribution is important since it determines the relationship between the applied load and crack propagation. Theoretically, if the effective tensile strength is independent of the distance from the beam end, the spalling crack should propagate under the load that produces initial cracking. However, this behavior was not observed in the tests.

The average effective tensile strength envelopes for the air-dried and epoxy-coated specimens are shown in Figure 43. These envelopes were computed using Equation (34) and the average of the measured relationships between applied load and crack length. As would be expected in view of the nature of differential shrinkage, the curves show that the effective tensile strength increases with increasing distance from the beam end. Both curves approach a value close to the modulus of rupture for the epoxy-coated specimens. The reason the air-dried specimens approach an effective tensile strength equivalent to the modulus of rupture in a specimen without shrinkage is that the average shrinkage stress across a transverse section near the center of the air-dried specimens is zero. Thus, the magnitude of the shrinkage stresses in this region should not reduce the effective tensile strength.

The physical analog for the cracked beam can be used to calculate the spalling crack width from the crack length and effective tensile strength envelope. Since the stirrup force, F_1, is zero in a plain concrete specimen, Equation (C53) can be substituted into Equation (C55) to give the following relationship between crack length, crack width, and effective tensile strength:

$$\frac{Z^3 f_{te} b \sqrt{S}}{2} + 3Z^2 abf_{te} + Z\left(-\frac{Wk}{2} + 2f_{te}b + \frac{f_{te}bR}{\sqrt{S}}\right)\frac{-Wak}{S} = 0 . \qquad (35)$$

Solving Equation (35) for the crack width gives:

$$W = \frac{0.5Z^3 f_{te} b\sqrt{S} + 3Z^2 abf_{te} + Zbf_{te}\left(2 + \frac{R}{\sqrt{S}}\right)}{k\left(0.5Z + \frac{a}{\sqrt{S}}\right)} . \qquad (36)$$

Equation (36) can be solved using the relationship between f_{te} and Z given by the effective tensile strength envelope.

The crack widths at the beam end were computed from Equation (36), and are shown in Figure 44 for the air-dried and epoxy-coated specimens. The modulus of elasticity for the concrete was assumed to be 4×10^6 psi. Also shown in Figure 44 are the measured relationships between crack width at the beam

end and the applied load. It can be seen from this figure that the computed crack widths compare well with the measured values. It should be pointed out that below a load of 18 kips in the epoxy-coated beams and 7.5 kips in the air-dried beams, the curves in Figure 44 represent the deformation measured over a 2-in. gage length instead of the crack width. After cracking has occurred, however, the deformation over the 2-in. gage length can be assumed to be the crack width, since the concrete within a small distance from either side of the crack is not stressed in a direction normal to the crack.

As was mentioned in Section 3.2.4, the curves in Figure 44 refer to specimens with comparable concrete properties and yet the initial slopes differ measurably. The observed difference can be ascribed to differential shrinkage. For a given load, the total transverse stresses (applied stress pluss existing tensile shrinkage stress) in the air-dried specimens are considerably higher than those in the epoxy-coated specimens. If it is accepted that the apparent load-deformation curve for concrete in flexural tension is non-linear with a decreasing slope, it follows that the incremental deformation in the case of the air-dried specimens should be larger than that for the epoxy-coated specimens. The initial slopes of the curves in Figure 44 correspond to initial moduli of deformation in tension of 3.4×10^6 and 1.45×10^6 psi for the epoxy-coated and air-dried specimens. Considering that the initial modulus of deformation in compression as determined from compression tests on cylinders for the concrete in these specimens was about 3.8×10^6 psi, these values do not seem untenable.

It is of interest to calculate the effect of the epoxy coating on the strength of the specimens. The thickness of the epoxy layer on the beams ranged from about 0.005 in. to 0.025 in., with an average of approximately 0.012 in. The modulus of deformation of the epoxy was between 0.5×10^6 and 0.6×10^6 psi and its tensile strength was about 10,000 psi. If it is assumed that the strain in the epoxy is the same as the strain in the concrete, the epoxy layer can be converted to an equivalent layer of concrete using the ratio of the moduli of deformation for the two materials. The equivalent thickness of concrete would be about 0.002 in. This is negligible compared with the 6-in. beam width. Based on the above assumptions, the epoxy layer has a negligible structural effect on the specimen strength, since the concrete and the epoxy reach their maximum strengths at different strains. Even if the strength of the epoxy layer was fully effective and additive to the strength of the beam, it would increase the applied load at cracking by 2 kips (the average cracking load was 18 kips). Considering strain compatibility, it is estimated that the epoxy layer may have contributed about 2 per cent of the observed cracking load.

So far in the comparison of test results with analytical calculations it has been implied that the only phenomenon affecting the slow crack propagation is the transverse shrinkage. However, there are several other phenomena that must be investigated

before the above conclusion can be established. The four factors to be investigated are: (1) the possibility of a decay in the ratio of the transverse tensile stress to the applied load as the crack length increases, (2) inelasticity of the concrete along the trajectory of the crack, (3) inelasticity and cracking of the concrete in the longitudinal tension zone, and (4) instability of the crack with time.

Lenschow's physical analog cannot be used to study the possibility of a decay in the ratio of spalling stress to applied load with increasing distance from the beam end. His analysis assumes that the bending moment produced by the applied load is independent of the distance from the beam end, and it neglects the localized differences between an applied moment and a load concentrated at the beam end. Consequently, it is necessary to use one of the analytical methods based on the classical theory of elasticity to solve the problem. Therefore, the transverse stress at the end of a spalling crack was calculated from Guyon's[15] tables in the following way. It was assumed that the spalling crack was long enough so that a linear strain distribution was obtained at the end of the crack. Consequently, the force distribution applied to the uncracked portion of the beam could be computed from ordinary bending theory. It is shown in Figure 45. Using Guyon's tables it is possible to calculate the maximum spalling stress produced by a concentrated load and to compare it with that produced by a linear distribution of load. Using this procedure it was found that there was no significant difference in the spalling stress produced by the two loading conditions. Thus, a strong case cannot be made for a decay in the ratio of spalling stress to applied load with increasing distance from the beam end.

It has been mentioned in connection with Figure 44 that the concrete in the spalling zone acts inelastically. Although the inelastic behavior may affect the cracking load, it should not affect the propagation of the crack. If it can be assumed that the ratio of f_{te}/P remains constant along the beam, it follows that the inelastic behavior should also be independent of the distance from the beam end (neglecting shrinkage).

The effect of inelasticity or cracking in the longitudinal tension zone is illustrated in Figure 45. If large flexural cracks occur in a specimen, there is no longer a need for the applied load to flow to the upper part of the beam. Therefore, the spalling stresses are greatly reduced. To prevent this phenomenon from occurring in the test specimens, two No. 3 deformed bars were placed in the flexural zone. As in the case of inelasticity along the spalling crack, inelasticity of the concrete in the flexural zone cannot account fully for the slow propagation of the spalling crack. However, if the crack propagation is first slowed by some other phenomena, elasticity in the flexural zone may have a small effect.

It was noticed during the tests on the specimens that the crack propagated with time when the applied load was

above 30 kips. This phenomenon is related to the inability of concrete to carry a high sustained tensile stress. Since the rate of load application in the tests was fairly slow (approximately one five-kip increment per every 20 minutes), it is felt that the time instability of the crack was not a factor in the slow crack propagation.

From the above discussion, it appears that the only plausible reason for the increase in the applied load needed for propagation of the spalling crack is differential shrinkage. While the estimated effects of the factors discussed above appear to be negligible, the effects of differential shrinkage stresses can be shown to be high enough to explain the increase in load with crack propagation.

5.2.3 Tests to Determine the Bearing Strength of Concrete Column Heads by Kriz and Raths[23]

Kriz and Raths investigated the bearing strength of 37 plain concrete column heads subjected to two symmetrically placed loads. The test results are described in Section 4.2.2. The failure load for each specimen is given in Table 12.

The data from the tests are plotted in Figure 46 which shows the variation in measured bearing capacity with the eccentricity of each of the applied loads. Since bearing plates of various widths were used in the tests, the ultimate loads given in Table 12 were modified by Equation (21) before they were plotted. The effective tensile strength of the concrete was assumed to be $6\sqrt{f'_c}$ for all specimens.

If it is assumed that bursting failure occurs when the bursting stress equals the effective tensile strength of the concrete, Equation (18) can be used to calculate the bearing capacity of a specimen. Curve 1 in Figure 46 shows the relationship between bearing capacity and load eccentricity which is found when two symmetrically placed loads are applied to the specimen. Curve 2 shows the relationship that is found if the shear force on the reference plane produced by the distant load is neglected. It can be seen from Figure 46 that the combination of curves 1 and 2 which gives the lower ultimate load falls fairly close to the test results.

The mechanism of failure described by curve 2, however, does not match that observed in the tests. In the tests in which the eccentricity of the load was large, spalling cracks formed before the bursting failure occurred. Therefore, at the time of the bursting failure, the specimens were cracked in the spalling region. If it is assumed that no shear can be transferred across the spalling crack, the load at bursting failure can be calculated on the basis of a cracked section.

The location of the plane of maximum spalling stress for a rectangular section loaded with two symmetrical loads is:

$$h_b = h-2e \ , \qquad (37)$$

where h_b is the height of the reference plane above the bottom of the cross section, h is the height of the section, and e is the eccentricity of one of the applied loads measured from the centroid

of the beam. Equation (37) is valid only for e/h > 1/4. Curve 3 in Figure 46 shows the relationship between the theoretical load at the initiation of a spalling crack and the eccentricity of the load. However, the formation of a spalling crack was never the direct cause of failure in the tests. Therefore, the bursting strength was computed assuming that the specimen was cracked through the reference plane given by Equation (37). The relationship between bursting strength and load eccentricity for this condition is given by curve 4. The lower limit of curves 1 and 4 represent a safe estimate of the bursting strength. It is seen in Figure 46 that curves 1 and 4 represent the trend of the data reasonably well.

5.2.4 Tests at the Cement and Concrete Association Laboratories[48]

Zielinski and Rowe investigated the transverse and longitudinal strain distributions in three rectangular and four I-section end blocks. The results of these tests are described in Section 4.4. The calculation of the transverse-strain distributions before cracking requires numerical values for the transverse stress, the longitudinal stress, Poisson's ratio and modulus of deformation for concrete. As was mentioned in Section 5.1, Lenschow's analysis can be used to determine the transverse stresses but not the longitudinal stresses. Consequently, it is not an easy chore to compute the transverse-strain distributions produced by a load distributed over a small area, if the loads are applied to an I-section.

The chief concern of a designer, however, is not the elastic distribution of strains in the anchorage zone but is the calculation of the cracking or failure load. The analysis described in Chapter II can be used for this purpose. Therefore, in this section, the failure loads for the seven specimens tested by Zielinski and Rowe will be compared with the analytical predictions.

The modes of failure for the seven specimens were described in Section 4.4. The failure loads calculated for these modes of failure are given in Table 4. The effective tensile strength of the concrete in all specimens was assumed to be equal to the splitting strength as given in Table 14. The effect of the cable ducts in reducing the width of the concrete section at the location of the crack was taken into account. The effect of the bearing plate size was taken into consideration by Equation (21).

Table 4 shows that in all specimens the predicted ultimate load compared well with the observed ultimate load. The average ratio of $P_{test}/P_{calc.}$ was 1.22. Two observations, however, can be made about the information presented in Table 4. The first observation concerns the ratio of the measured failure load to cracking load. In test 9, cracking was observed in the failure zone at a load of 66.3 kips. The specimen carried 77.0 kips, however, before failing under short-time loading. Because concrete cannot sustain a high stress for a long period of time, especially if the concrete has cracked,

the practical failure load for a specimen failing in bearing may be taken as the load at first cracking in the bursting zone. If the failure load is defined as above, the ratio of P_{test} $P_{calc.}$ is given by the quantities in parentheses in Table 4.

One factor that may have had some effect on the ratio of the ultimate to cracking loads measured in the tests is the confinement of the concrete at the point of load application. When more than one load was applied to the specimens, the loading points were prevented from moving perpendicular to the axis of the load since the total load was transmitted to the loading points through a single plate. Rollers were not used to support the load in the tests. This testing procedure may have increased the failure load over the first cracking load. Since only the total load applied was measured during the test, it is not certain that the loads on all the individual loading plates were equal. This factor may also have had some influence on the measured value of the failure load.

The second observation to be made is that the predicted and observed modes of failure did not always agree. The specimens in tests 1, 18, and 19 failed in the manner predicted. The specimens in tests 9, 16, and 17, however, did not fail in precisely the manner that was assumed for the calculations. The loading pattern was the same for specimens 9 and 16, three loads applied some distance from each other. The failure mechanism assumed was a bursting failure along the common axis for two of the loads. The observed failure was a local bursting failure under one of the loads. In test 17 the failure started at the junction of the rectangular and I-shaped cross sections. The analysis for this specimen assumed failure to occur in the bursting zone.

5.2.5 Tests of Pretensioned Girders by Marshall and Mattock[28]

Tests on 35 pretensioned girders have been reported by Marshall and Mattock. In Table 5, the estimated cracking load for 29 specimens is compared with the observed behavior. The theoretical calculations were made from Equation (26) with the assumptions that the transfer length was 40 strand diameters and that the effective tensile strength of the concrete in the spalling zone was $4\sqrt{f'_c}$. It should be mentioned that an underestimate of the transfer length is on the safe side in the calculation of anchorage-zone stresses. The cracking loads for girders B1 through B25 have been calculated from the assumption that the transverse reinforcement had no effect on the cracking load. This assumption, although not strictly correct, is reasonable if the area of the transverse reinforcement is small compared with the concrete area.

With the exception of seven beams out of 29 (B1, 2, 15, 20, 21, 22, and 23) the predicted and observed behavior were the same. The failure of the theory to predict the correct behavior in seven beams may result partly from the assumptions for transfer length and effective concrete tensile strength

and partly from some scatter within the test results themselves. In all seven beams the theory was on the safe side since it predicted cracking while the test specimens did not crack.

An increase in the assumed values of the transfer length or effective tensile strength will increase the calculated cracking load. The correct behavior of girders B21, B22, and B23 would have been predicted if the transfer length was assumed to be 45 strand diameters and the effective concrete tensile strength was assumed to be $5.5\sqrt{f'_c}$. Neither of these values is untenable.

Girders B3 and B4, which had 80 per cent of the prestressing force concentrated in the bottom flange, developed forces in the transverse stirrups nearly equal to those in girders B7 and B8 which had only 60 per cent of the strand in the bottom flange. It appears from this observation that a small variation in the distribution of the prestressing force did not have much effect on the cracking of the anchorage zone. If this conclusion is valid, and experimental evidence suggests that it is, girders B1 and B2 which had 90 per cent of the prestressing force concentrated in the bottom flange should have behaved similarly to girders B3, B4, B5, B6, B7, and B8. Theoretically, the predicted cracking loads for these eight girders support the above statement. However, in the experiments girders B1 and B2 did not crack while the other six girders did. No reason for this behavior can be given.

In eight cases it is possible to determine from the tests the effect of web thickness on cracking. In seven of the eight comparisons, web thickness appeared to have no significant influence on the development of spalling cracks in the girders. In one comparison, the girder with the thinner web, B15, did not crack, while the two girders with the thicker web, B16 and B17, did. No explanation can be given for the behavior of girder B15 since it appears to be unexpected on the basis of both theoretical calculations and experimental evidence.

The remaining girder for which the theory failed to predict the correct behavior is girder B20. This girder was similar to girder B19 which cracked. The difference in the behavior of the two beams shows that the test results themselves were not always reproducible.

5.2.6 Tests of Pretensioned Girders by Arthur and Ganguli[1]

Nineteen pretensioned I-girders were tested by Arthur and Ganguli. These tests are described in Section 4.3 and the test results are presented in Table 2. The cracking loads for 13 of the specimens were calculated from Equation (26). The transfer length for the 0.2-in. diameter wires used in the tests was assumed to be ten in. (Figure 36.) The effective tensile strength of the concrete was assumed to be $4\sqrt{f'_c}$ or $3.7\sqrt{f_{cube}}$, if the cylinder strength is 85 per cent of the cube strength. The cracking loads for the six girders with the intermediate web thickness were not calculated, but theoretically they can be shown to lie between the value of the cracking load

for the girders with the thinnest web and that for the girders with the thickest web.

The computed and observed ratios of the cracking load to the effective prestressing force are given in Table 6. The measured ratios given in Table 6 are misleading, however. In six of the specimens listed, cracking occurred in only one of the anchorage zones. Thus, for these specimens the ratio of cracking load to effective prestressing force ranged from that value given in Table 6 to a value greater than 100 per cent. Consequently, the scatter within the test results is much larger than is implied by Table 6. Taking this into consideration, the computed ratios of cracking load to effective prestressing force appear to be consistent with the measured ratios.

5.3 CRACK PROPAGATION AND CALCULATION OF STIRRUP FORCE IN REINFORCED ANCHORAGE ZONES

5.3.1 Tests at the University of Illinois

The effect of transverse reinforcement on the propagation of a spalling crack was studied in two series of tests on post-tensioned specimens. The specimens in the first test series were fabricated with a preformed crack in the anchorage zone as described in Section 3.3.1. The specimens in the second test series were initially uncracked.

Consider first the calculation of the stirrup force for the specimens of the first test series. Since the effective tensile strength across the trajectory of the spalling crack was zero in these specimens, Equations (27) and (32) can be written as

$$W = \frac{-M_o}{k} \frac{\left(\frac{SZ^3}{3} + 2a\sqrt{S}\,Z^2 + Z(\sqrt{S} - R)\right)}{Z + \frac{2a}{\sqrt{S}}}, \qquad (38)$$

$$F_o = \frac{-M_o}{Z + \frac{2a}{\sqrt{S}}}. \qquad (39)$$

The relationships between stirrup force, crack width, and crack length computed from Equations (38) and (39) for the rectangular specimens described above are given in Figure 47 for applied loads of 10, 20, and 30 kips. Also shown in Figure 47 are the force-slip curves for the transverse reinforcement used in the specimens. It is assumed that the anchorage of the stirrups is the same on both sides of the crack. From this assumption, the crack width is found to be equal to twice the slip measured between the stirrup and the concrete on one side of the crack. It has also been assumed that the force-slip relationship for the reinforcement as determined from the twin-pull out test is equivalent to that for the reinforcement in a beam (see Sections A.4.3 and A.5.2 for description of twin pull-out test).

The intersection of the force-slip curve with the theoretical F_o vs. W curve gives the stirrup force and crack width to be expected at a given value of the applied load. The relationships between stirrup force and applied load determined from Figure 47 are plotted

in Figure 48 along with the measured relationships. From this figure it can be seen that the agreement between the calculated curves and the test curves is good.

Equations (38) and (39) have also been used to calculate the stirrup force, crack width, and crack length relationships for the I-specimens with preformed cracks. These relationships are given in Figure 49. Following the procedure described above, the relationships between stirrup force and applied load were computed for the I-specimens and are plotted in Figure 50. The agreement between the curves for the test results and the computed curves is not as good for the I-specimens as for the rectangular specimens. However, the computed curves for the I-specimens show the trends of the test results correctly.

Consider now the calculations of the crack propagation in the initially uncracked specimens during the short-time tests. The five specimens in this test series (R29a, R29b, R30, R36, and R37) were moist cured for five days. Since they were tested at 15 days, their effective tensile strength envelopes should lie somewhere between the envelopes given in Figure 43 for the air-dried and epoxy-coated specimens. It appears from the load-deformation curves shown in Figure A40 and A47 and from the longitudinal strains measured in the center of the specimens that the average cracking load for the reinforced specimens was approximately 12 kips. This is about halfway between the cracking loads for the air-dried and epoxy-coated specimens. Therefore, the effective tensile strength envelope for the reinforced specimens was assumed to be halfway between the two curves shown in Figure 43.

One the effective tensile strength envelope is known or assumed, Equations (27) and (32) can be used to calculate the relationships between crack length, crack width, and stirrup force for any given value of the applied load. These relationships are shown in Figure 51 for the specimens described above. The force-slip curves for the 1/4-in. and 1/8-in. plain stirrups used in the test specimens are also shown in Figure 51. The intersection of the force-slip curve with the theoretical curve gives the crack width to be expected at a given value of the applied load. The calculated relationships between crack width and applied load are compared with the average test results in Figure 52. The computed and measured curves show good agreement.

It should be pointed out that there are two sources of strength in a reinforced anchorage zone. The first source of strength is the effective tensile strength of the concrete itself. In a plain concrete specimen, the increase in the effective tensile strength with increasing distance from the beam end retards crack propagation. The second source of strength in a reinforced specimen is provided by the stirrup reinforcement. The contribution of the stirrups to the restraint of the crack is shown in Figure 52 as the difference between the curves for the specimens reinforced with 1/4-in. and 1/8-in. diameter bars and the curve for a specimen with no reinforcement. It is seen that the stirrups appear to

have little effect on the crack width measured during a short-time test as long as the crack remains below 0.001 in. in width. For larger crack widths the stirrups are effective in restraining the crack and as would be expected, the larger the area of the reinforcement the more effective the reinforcement is.

It is interesting to note the cracking phenomena observed in specimens tested over a short period of time but at advanced ages after casting. On the basis of the quantitative considerations discussed in this chapter, such specimens should have smaller cracks because of three effects: (1) increase of concrete strength with time, (2) increase of modulus of deformation with time, and (3) reduction of the differential shrinkage stresses. Figure 25 compares the load vs. transverse deformation (very close to the crack width) curves for specimens loaded at ages of 15, 240, and 430 days. The observed trend agrees with that expected.

5.3.2 Tests of Pretensioned Girders by Marshall and Mattock[28]

The results of the tests by Marshall and Mattock are described in Section 4.2.1 and summarized in Table 1. In 14 of the 25 specimens which were reinforced with stirrups in the anchorage zone, spalling cracks occurred in the lower part of the web close to the strain gages in the stirrups. The total stirrup force and the maximum stirrup stress measured in these specimens is given in Table 1. In this section the measured stirrup forces will be compared with the stirrup forces calculated from a modified version of Lenschow's analysis.

It is assumed in the analysis that all the stirrups are concentrated at the end of the girder. For a girder with a given length of spalling crack, the calculations based on this assumption will slightly underestimate the total stirrup force that would be produced if the stirrups were distributed over some length of the girder. It is also assumed that the total measured stirrup force given in Table 1 is the maximum stirrup force in the girder. This assumption may lead to an underestimate of the maximum total stirrup force if the spalling crack in the girder did not pass through the strain gages on the stirrups. The errors introduced by these two assumptions are small with compensating effects on the comparison of the measured and computed stirrup forces.

The relationship between applied load, effective tensile strength, crack length, and stirrup force given by Equation (32) for a post-tensioned beam can be written as follows for a pretensioned beam.

$$F_1 = \frac{b\left[\frac{-2aM_o}{bI} + \left(\frac{2aM_o}{bI} - \frac{M_o\sqrt{S}}{b}\right)\frac{Z}{I} - f_{te}\right]}{Z\sqrt{S} + 2a} \quad (40)$$

The first term in the brackets in Equation (40) is the applied spalling stress at the end of a pretensioned girder. The second term in the brackets represents a linear variation of the applied spalling stress from that at the girder end (equal to that at the end of a pretensioned girder) to that at the end of the transfer length

(equal to that for a post-tensioned girder). The third term in the brackets is the effective tensile strength of the concrete at the end of the crack.

The total stirrup force in each girder that cracked near the centroidal axis was calculated from Equation (40) and is compared with the measured stirrup force in Figure 53. The measured crack lengths in Table 1 were used in the calculations. The crack lengths were determined by Marshall and Mattock from the measured stirrup strain distributions. The point at which the vertical strain became equal to 125×10^{-6} was taken as the end of the spalling crack. The assumed effective tensile strength envelope varied linearly from $4\sqrt{f'_c}$ at the girder end to $10\sqrt{f'_c}$ at 5 in. (equal to the width of the thickest web in the series) from the end. This strength envelope is consistent with the strength envelopes found for specimens with approximately the same thickness, type of cement, and curing conditions tested at the University of Illinois (Figure 43).

The calculated stirrup forces compare fairly well with the measured stirrup forces as is shown in Figure 53. However, the calculations do not show as large a difference in the forces for the two sizes of reinforcement as is shown in the tests. This comparison could be improved by assuming a lower effective tensile strength envelope for the specimens with the larger reinforcement. The use of two strength envelopes would take into account the effect of the reinforcement on the development of shrinkage stresses. Although this procedure is reasonable, it is not justified in this case because the necessary data needed for a good estimation of the tensile strength envelopes are not provided.

5.4 TIME-DEPENDENT PHENOMENA IN REINFORCED ANCHORAGE ZONES

A series of six specimens were subjected to sustained prestressing forces and the development of the spalling cracks was studied over a period of eight months. The observed crack profiles are shown in Figures A50, A51, A53, and A54. All results indicated an increase in the widths and lengths of the cracks with time. A quantitative discussion of the test phenomena is provided in this section.

Four factors may influence the behavior of a cracked anchorage zone subjected to a sustained load.

(1) The resistance of concrete to tension decays with time if the concrete is subjected to a tensile stress close to its short-time tensile strength.[36]

(2) Deformations of the concrete in the anchorage zone will change as a result of creep in both tension and compression.

(3) There may be a decay in the bond between the stirrup and the concrete.

(4) Differential shrinkage stresses may change with time producing a change in the effective tensile strength envelope.

The effect of the first two factors may be estimated by modifying the effective tensile strength envelope

as shown in Figure 54 and reducing the modulus of deformation for the concrete.

If the analysis for short-time phenomena is modified as described above, the results shown in Figure 55 are obtained. The solid curves represent the relationship between stirrup force and crack width as derived from Equations (27) and (32), The solid curve marked "initial" is the result of the short-time tensile strength envelope (Figure 54) and $E_c = 3.8 \times 10^6$ psi. The solid curve for a time 20 days after the start of the test was obtained from the lower strength envelope in Figure 54 with $E_c = 1.9 \times 10^6$ psi. The reduction in the modulus of deformation is based on longitudinal strain readings in the specimens. Similarly, the curve for 200 days corresponds to $E_c = 1.3 \times 10^6$ psi.

Since the solution for the crack width is indicated by the intersection of the solid curve with the force-slip relationship for the reinforcement (indicated by broken curves), it can be seen from Figure 55 that the increase in crack width with time is considerable.

The computed and measured crack widths are compared in Figure 56. It is seen that the computed crack widths follow the trends observed in the tests. Although minor changes in the apparent modulus of deformation and in the variation in the shape of the effective tensile strength envelope with time could be made to improve the correlation between the measured and computed crack widths, a more detailed analysis is not warranted on the basis of the test results. Furthermore, modifications of the force-slip relationship for the reinforcement do not appear necessary.

The crack lengths calculated from the analysis presented above agree with the measured crack lengths. The rapid increase in the ratio of crack width to crack length measured in the sustained-load tests as compared with that measured in the short-time tests is consistent with the theoretical calculations. Thus, from the foregoing discussion, it appears that a modified version of Lenschow's analysis that takes into account the creep of the concrete and the decay of the concrete tensile strength can be used successfully to describe the test results.

VI. DESIGN RECOMMENDATIONS

6.1 INTRODUCTORY REMARKS

This chapter is devoted to the description and discussion of a design procedure for anchorage-zone reinforcement in prestressed concrete beams. The design procedure is based on a modified version of Lenschow's[24] analysis and on the interpretation of the experimental work described in this report. Several illustrative design examples are given at the conclusion of the chapter.

Longitudinal cracks in the anchorage zones of prestressed concrete beams have been reported in field studies[10,16] and in laboratory investigations.[1,12,23,28,48] The cracks have been observed in both post-tensioned and pretensioned girders with rectangular, I-shaped or T-shaped cross sections.

Longitudinal cracking in the anchorage zone results from the transverse tensile stresses produced by the "flow" of the prestress force from the region of force concentration to a region of linear distribution of the longitudinal stresses. Two zones of transverse tensile stress can be identified (Figure 1). The transverse tensile stresses across the axis of the applied force are referred to as bursting stresses. The bursting stress reaches its maximum a short distance from the beam end. The transverse tensile stresses across any other longitudinal section are called spalling stresses. The maximum spalling stress occurs at the end of the uncracked beam.

Transverse reinforcement can be used to restrain the development of longitudinal cracks in the spalling zone (spalling cracks) and to delay the formation of bursting cracks. The development of a longitudinal crack in the bursting zone may be considered as a failure criterion for the beam even if reinforcement is provided.[12,23,48] However, the presence of a longitudinal crack in the spalling zone is not detrimental to the performance of the beam as long as the width and extent of the crack is limited.[12,24,28,33] Transverse reinforcement should be provided to prevent the growth of the cracks with time.[1,16]

The factors which influence cracking in the anchorage zone can be divided into three groups:

(1) The factors which govern the flow of the prestressing force in the anchorage zone comprise the first group. These factors are: (1) eccentricity of the applied prestressing force, (2) ratio of loaded area to cross-sectional area, (3) inclination of the prestressing force to the plane of the

cross section, (4) vertical reaction from support, (5) shape of cross section, and (6) type (post- or pretensioned) and distribution of the prestressing force.

(2) The second group contains the factors which provide restraint against cracking. These factors are the concrete quality and the amount, location, and type of transverse reinforcement.

(3) Group three contains the time-dependent factors which influence both the prestress force flow and the restraint against cracking. These factors are: (1) creep of concrete in compression and tension, (2) decay in the tensile strength of conrete under a sustained stress, (3) increase in the concrete strength with time, (4) shrinkage, (5) decay in bond strength under a sustained stress, and (6) decay of the prestressing force.

The design procedure described below considers the effects of most of the factors mentioned above. It presents a method for the determination of the stresses in the anchorage zone of an uncracked section and indicates when these stresses may lead to longitudinal cracking or failure. It also provides a simple expression for the selection of transverse reinforcement to restrain the growth of spalling cracks.

6.2 THE CONTRIBUTION OF THE CONCRETE

6.2.1 The Concrete in the Spalling Zone

The basic expressions for the maximum spalling stress on a given longitudinal plane (called the reference plane) are presented in Chapter 2. When the reference plane is below the centroid of the cross section, the maximum spalling stress is given by the following.

For a post-tensioned beam:

$$\sigma_s = \frac{-M_o}{b}\sqrt{\frac{b_{eq}}{cI_b}} \quad . \tag{41}$$

For a pretensioned beam:

$$\sigma_s = \frac{-M_o}{bT}\sqrt{2\sqrt{\frac{b_{eq}}{cI_b}} + \frac{2.3\gamma b_{eq}}{c\,A_b}} \quad , \tag{42}$$

where A_b = area of the section below the reference plane,

b = width of the cross section at the reference plane,

b_{eq} = average effective width of the cross section over the distance c. The effective width is determined on the assumption that the transverse stresses spread out at a 45-degree angle wherever there is a change in section,

c = distance from the reference plane to the centroid of the section below the reference plane,

I_b = moment of inertia of the section below the reference plane,

T = transfer length of the strand,

γ = shape factor for shear deflection (1.5 for a rectangular section),

σ_s = spalling stress on any reference plane,

and

$$M_o = M_{pb} + M_v - M_t\frac{I_b}{I} \quad , \tag{43}$$

where M_{pb} = moment of the load applied to the section below the reference plane about the centroid of that section,

M_v = moment of the shear force on the reference plane about the centroid of the section below the reference plane,

M_t = total moment applied to the beam by the prestressing force,

I = moment of inertia of the whole cross section.

The sign convention for a portion of the beam below the reference plane is shown in Figure C1. The magnitude of the spalling stress computed from Equation (41) (post-tensioned beam) should be taken as an upper bound for the spalling stress given by Equation (42) (pretensioned beam).

For beams with rectangular cross sections ($b_{eq} = b$ and $c = h_b/2$), Equations (41) and (42) can be simplified to:

For post-tensioned beams:

$$\sigma_s = \frac{-4.9M_o}{bh_b^2} \quad . \tag{44}$$

For pretensioned beams:

$$\sigma_s = \frac{-4.1M_o}{bTh_b} \quad . \tag{45}$$

The term h_b is the height of the reference plane above the lower edge of the cross section.

If the reference plane is above the centroid of the cross section, the minus sign on the right-hand side of Equations (41), (42), (44), and (45) should be omitted. The terms b_{eq}, c, I_b, A_b, and h_b then refer to the properties of the section above the reference plane. For this case,

$$M_o = M_{pt} + M_v - \frac{M_t I_b}{I} \quad , \tag{46}$$

where M_{pt} is the moment of the load on the section above the reference plane about the centroid of that section.

The reference plane on which the spalling stress is maximum must be found by trial and error. For rectangular sections with a single group of prestressing forces, the following expression can be used to locate the plane of the maximum spalling stress:

$$h_b = \frac{h}{2} - \frac{1}{3}(7e - 2h), \tag{47}$$

where h is the height of the section and e is the eccentricity of the prestressing force measured from the centroid of the section. (See Section 2.3 for background to Equation (47).)

A spalling crack is assumed to form when the maximum spalling stress exceeds the effective tensile strength of the concrete. The effective tensile strength of the concrete in the spalling zone may be taken as $4\sqrt{f'_c}$. If the computed spalling stress in a beam exceeds this value, transverse reinforcement must be supplied. However, if the computed spalling stress does not exceed $4\sqrt{f'_c}$, the minimum amount of transverse reinforcement may be used.

6.2.2 The Concrete in the Bursting Zone

The maximum bursting stress produced by a concentrated prestressing force applied below the centroid of the cross section is:

$$\sigma_{bc} = \frac{M_o}{4.9b}\sqrt{\frac{b_{eq}}{cI_b}} \quad . \tag{48}$$

All terms in Equation (48) have been defined previously except for the term σ_{bc} which is the bursting stress produced by a concentrated prestressing force. For a beam with a rectangular section, Equation (48) can be simplified to:

$$\sigma_{bc} = \frac{M_o}{bh_b^2} . \qquad (49)$$

If the bursting stress is investigated under a prestressing force acting above the centroid of the cross section, a minus sign must be added to the right-hand side of Equation (48) and (49). The value of M_o is given by Equation (46) for this case.

The bursting stress produced by a distributed load can be found from the following:

$$\sigma_b = \sigma_{bc} \left[1 - \frac{bt}{A}(3 - 4\frac{A_b}{A})\right] , \qquad (50)$$

where σ_b = the bursting stress produced by a distributed load,

A = area of the whole cross section,

t = height of the loaded area.

The formation of a longitudinal crack in the bursting zone normally leads to immediate failure of the anchorage. The portion of the total bursting force provided by the concrete may be computed by taking the effective tensile strength of the concrete in the bursting zone as $6\sqrt{f'_c}$. If a longitudinal crack is admitted, however, the reinforcement should be designed to take the total bursting force.

It should be noted that the recommended value of the effective tensile strength of the concrete in the bursting zone ($6\sqrt{f'_c}$) is greater than that recommended for spalling stresses ($4\sqrt{f'_c}$). These values are consistent with the test results as discussed in Chapter V. The differences in the two recommended values can be ascribed to differential shrinkage. The transverse tensile stresses which result from differential shrinkage are a maximum at the end of a beam. Since the applied spalling stresses are also a maximum at the beam end, the total transverse stress (shrinkage plus applied stress) may be quite high. This is the reason behind the recommendation of a low value for the effective tensile strength in the spalling zone. The maximum bursting stress occurs some distance from the end of the beam. In this region the transverse tensile stress produced by differential shrinkage is smaller than that at the beam end. Accordingly, a higher value of the effective tensile strength may be used.

6.3 CONTRIBUTION OF THE TRANSVERSE REINFORCEMENT

6.2.1 Reinforcement in the Spalling Zone

The purpose of transverse reinforcement in the spalling zone is to restrain the development of the spalling cracks. The total stirrup force necessary to restrain the spalling crack to a given permissible crack width can be determined in two steps.

(1) In the first step, the contribution of the concrete in the

spalling zone is neglected. The following equation gives the total stirrup force in terms of the applied moment, permissible crack width, cross-sectional properties, and modulus of deformation of the concrete.

$$F_o = -M_o \sqrt{\frac{1}{3E_c I_b \left(\frac{6\gamma(1+\mu)}{A_b E_c} - \frac{W}{M_o}\right)}} \quad , \quad (51)$$

where E_c = modulus of deformation of the concrete,

W = permissible crack width,

μ = Poisson's ratio for the concrete.

The minus signs in Equation (51) apply when the reference plane is below the centroid of the cross section. When the reference plane is above the centroid of the cross section, the minus signs must be omitted.

(2) The second step in the calculation of the stirrup force is to recognize the contribution of the concrete in the spalling zone. If it is assumed that the effective tensile strength is constant along the length of the beam, the effect of the concrete tensile strength can be taken into account by modifying the value of F_o obtained from Equation (51) as follows:

$$F_1 = F_o \left[1 - \left(\frac{f_{te}}{\sigma_s}\right)^2\right] \quad , \quad (52)$$

where F_o = stirrup force neglecting the effect of the concrete tensile strength,

F_1 = stirrup force recognizing the effect of the concrete tensile strength,

f_{te} = effective concrete tensile strength in the spalling zone (may be taken as $4\sqrt{f'_c}$),

σ_s = spalling stress computed from Equations (41), (42), (44), or (45).

If the ratio of the tensile strength to the applied spalling stress in Equation (52) exceeds unity, theoretically no reinforcement is required. However, it is strongly recommended that a minimum amount of transverse reinforcement be provided even in the cases where spalling cracks are not expected. This minimum can best be determined by the designer. Consideration should be given to the quality and quality control of the concrete in the anchorage zone, to the curing procedures, to the possible formation of initial irregularities (cracks or voids) which could lower the strength, and to the intended use of the beam.

The selection of the size and number of stirrups needed to provide the total stirrup force computed from Equations (51) or (52) is based on the force-slip relationships for the reinforcement. The maximum force that can be provided by a single stirrup is the force that will produce a slip between the bar and the concrete equal to one-half of the permissible crack width in the beam, assuming that the crack is not close to the end anchorage, if any, of the stirrup. The total number of stirrups can be determined by dividing the total stirrup force by the maximum force that can be provided by one stirrup.

6.2.2 Reinforcement in the Bursting Zone

The formation of a longitudinal crack in the bursting zone occurs almost

simultaneously with the sudden failure of the anchorage. It is on the safe side to consider the formation of a bursting crack as a failure criterion for the anchorage zone. Therefore, the stress in the transverse reinforcement in the bursting zone is limited to that obtained at the time of cracking of the concrete.

The force in the transverse reinforcement per unit length of beam may be computed from the following equation if the prestressing force is concentrated on the beam end.

$$f_{oc} = (\sigma_{bc} - f_{te})b \ . \qquad (53)$$

If the prestressing force is distributed over a finite area, the stirrup force per unit length is

$$f_o = (\sigma_b - f_{te})b \ , \qquad (54)$$

where σ_{bc} = the bursting stress under a concentrated load as given by Equations (48) or (49),

σ_b = the bursting stress under a distributed load as given by Equation (50),

f_{te} = effective tensile strength of the concrete in the bursting zone which can be taken as $6\sqrt{f'_c}$.

6.4 SPACING, DISTRIBUTION, AND SHAPE OF THE TRANSVERSE REINFORCEMENT

The first stirrup in the spalling zone should be placed as close to the end of the specimen as possible. The spacing of the remaining stirrups should also be as small as practicable. As in other problems of crack control, the use of a large number of small-diameter stirrups is more effective than using a few stirrups with a large diameter.

The spacing of the transverse reinforcement in the bursting zone is critical if the reinforcement is needed to delay cracking. Stirrups too close or too far from the end of the beam will have little effect. Therefore, it may be desirable to use a large number of small bars at close spacing distributed uniformly over the length of the bursting zone. The length of the bursting zone may be taken as twice the distance between the plane of the prestressing force and the closed edge of the beam. The same reinforcement should be used in both the bursting and spalling zones.

Closed stirrups are recommended. If the stirrups are not closed, anchorage sufficient to develop the strength of the bar should be provided beyond the plane at which cracking is expected. The stirrups should extend from the top to the bottom of the section but they must meet the requirements for cover.

6.5 NUMERICAL EXAMPLES

6.5.1 Pretensioned I-Girder

In order to illustrate the application of the design procedures described in this chapter, the maximum spalling stress and the required transverse reinforcement for a permissible crack width of 0.005 in. will be determined for an AASHO Type III pretensioned girder. The cross section of the girder is shown in Figure 57. The given cross-sectional, material, and prestressing properties are:

$A = 560$ in.^{2}

$I = 125{,}000$ in.^{4}

$y_t = 24.7$ in.

$y_b = 20.3$ in.

$W = 0.005$ in.

$D_{strand} = 1/2$ in.

$P = 650$ kip

$e = 12$ in.

$f'_c = 5000$ psi

$T = 40$ strand diameters

The longitudinal stress distribution is:

$$\sigma_{bottom} = P\left(\frac{1}{A} + \frac{ey_b}{I}\right) = 2430 \text{ psi}$$

(compression),

$$\sigma_{top} = P\left(\frac{1}{A} - \frac{ey_t}{I}\right) = -380 \text{ psi}$$

(tension).

The neutral axis is 38.9 in. from the lower edge of the cross section.

The position of the critical reference plane (the longitudinal section on which the spalling stress is a minimum) must be found by trial and error.

Trial 1

For the first trial the reference plane is assumed to be 11.5 in. from the top of the cross section. This is at the junction of the web and the top flange. Since the reference plane is above the centroid of the cross section, all calculations must refer to the section above the reference plane.

$$c = \frac{\frac{7\times(4.5)^2}{2} + \frac{2\times(4.5)^2\times 3}{2} + 7\times 16\times(4.5+3.5)}{31.5+20.25+112} = 6.27 \text{ in.}$$

$$b_{eq} = \frac{\frac{(7+16)\times 4.5}{2} + 16\times 1.77}{6.27} = 12.77 \text{ in.}$$

$$I_b = \frac{16(7)^3}{12} + 112(1.73)^2 + \frac{7(4.5)^3}{12} + 31.5(4.02)^2 + \frac{(4.5)^4}{18} + (4.5)^2(3.27)^2 = 1589 \text{ in.}^4$$

The shear acting along the reference plane is:

$$V = \left(\frac{-380+57}{2}\right)\times 112 + 57\times 51.75 + \left(\frac{338-57}{2}\right)\times 31.5 + \left(\frac{338-57}{2}\right)\times 20.25$$

$V = -8820$ lb.

This shear produces a positive moment about the centroid of the section above the reference plane.

From Equation (46):

$M_{pt} = 0$, no prestressing force is applied to the section above the reference plane.

$M_v = 8820 \times 6.27 = 55{,}300$ in.-lb.

$$\frac{M_t I_b}{I} = \frac{-650{,}000 \times 12 \times 1589}{125{,}000} = -99{,}150 \text{ in.-lb.}$$

and

$M_o = 55{,}300 + 99{,}150 = 154{,}450$ in.-lb.

The spalling stress is computed from Equation (42). The shape factor for a rectangular section will be used, since the section is close to being rectangular.

$$\sigma_s = \frac{154,450}{7\times20}\sqrt{2\left(\frac{12.77}{6.27\times1589}\right)^{1/2} + \frac{2.3\times1.5\times12.77}{6.27\times163.75}} = 375 \text{ psi}$$

The effect of the shape factor is small. A variation of the shape factor from 1.5 to 1.3 changes the calculated spalling stress from 375 to 360 psi.

Trial 2

The reference plane is taken 13.0 in. below the top of the section in this trial. The calculations are similar to those in the first trial and will not be given here. The spalling stress obtained was 345 psi.

Reinforcement

The maximum spalling stress was obtained in the first trial. Since the maximum stress was greater than $4\sqrt{f'_c}$, transverse reinforcement must be supplied. A crack width of 0.005 in. will be assumed. If the tensile strength of the concrete is neglected, the force in the reinforcement is given by Equation (51). Assume that E_c is 4×10^6 psi.

$$F_o = 154,450\sqrt{\left[3\times4\times10^6\times1589\left(\frac{9\times1.15}{163.75\times4\times10^6} + \frac{0.005}{154,450}\right)\right]^{-1}} = 5100 \text{ lb.}$$

The allowable tensile strength of the concrete in the spalling zone is:

$4\sqrt{f'_c} = 4\sqrt{5000} = 283$ psi .

The stirrup force can be reduced using Equation (52):

$$F_1 = 5100\left[1 - \left(\frac{283}{375}\right)^2\right] = 2200 \text{ lb.}$$

The number of stirrups needed to supply this force may be determined as follows. If the bond force per unit length is assumed to be uniformly distributed, the stirrup force is related to the crack width as follows:

$$F = \sqrt{WE_sA_sg}\ , \qquad (55)$$

where W = the crack width,

E_s = modulus of deformation for steel,

A_s = area of one reinforcing bar,

g = unit bond force.

If the stirrups are to be made of No. 3 bars ($A_s = 0.11$ in.^{2}), the permissible force in one bar as computed from Equation (55) for a unit bond force of 250 lb/in. is:

$$F = \sqrt{0.005\times29\times10^6\times0.11\times250} = 2000 \text{ lb.}$$

One closed stirrup made from No. 3 bars is required to restrain the spalling crack to a width of 0.005 in.

The effect of creep of the concrete and loss of prestressing force will now be considered. Assume that the final crack width is to be 0.005 in. and that E_c is reduced to 1.3×10^6 psi. The prestressing loss may be taken as 20 per cent. From Equation (51)

$$F_o = 0.8\times154,450\sqrt{\left[3\times1.3\times10^6\times1589\left(\frac{9\times1.15}{1.3\times10^6\times163.75} + \frac{0.005}{0.8\times154,450}\right)\right]^{-1}}\ ,$$

$$F_o = 5100 \text{ lb.}$$

Assuming that the effective tensile strength under a sustained load is reduced by 30 per cent, Equation (52) gives:

$$F = 5100 \left[1 - \left(\frac{0.7 \times 283}{375}\right)^2\right] = 3700 \text{ lb.}$$

This would require one closed stirrup made from No. 3 bars.

6.5.2 Post-Tensioned Rectangular Girder

The maximum bursting and spalling stresses and the required transverse reinforcement will be determined for a post-tensioned beam with a rectangular cross section (Figure 58). The given data are:

$A = 900$ in.^{2}
$I = 152{,}000$ in.^{4}
$f'_c = 5000$ psi
$P = 400$ kip
$e = 14.2$ in.
$t = 4$ in. (height of loaded area)

The longitudinal stresses are:

$\sigma_{bottom} = 1290$ psi (compression)
$\sigma_{top} = -400$ psi (tension)

The neutral axis is 34.4 in. from the bottom edge of the section.

Spalling Stress

The position of the critical reference plane is found from Equation (47):

$$h_b = 22.5 - \frac{1}{3}(7 \times 14.2 - 2 \times 45) = 19.4 \text{ in.}$$

Since the critical reference plane is below the centroid of the section, all computations will be referred to the section below the reference plane. The shear on the reference plane is:

$$V = 400{,}000 - \left(\frac{1290+560}{2}\right)(20 \times 19.4)$$
$$= 41{,}000 \text{ lb.}$$

With reference to Equation (43):

$$M_{pb} = -400{,}000 \times 1.4 = -560{,}000 \text{ in.-lb}$$
$$M_v = -41{,}100 \times 9.7 = -399{,}000 \text{ in.-lb}$$
$$\frac{M_t I_b}{I} = -400{,}000 \times 14.2 \times \left(\frac{19.4}{45}\right)^3$$
$$= -452{,}000 \text{ in.-lb}$$
$$M_o = -560{,}000 - 399{,}000 + 452{,}000$$
$$= -507{,}000 \text{ in.-lb.}$$

The spalling stress is given by Equation (44).

$$\sigma_s = \frac{4.9 \times 507{,}000}{20 \times 19.4 \times 19.4} = 330 \text{ psi.}$$

The transverse reinforcement to restrain the spalling crack to a permissible width of 0.005 in. can be found from Equations (51) and (52).

$$F_o = 507{,}000 \sqrt{\left[3 \times 4 \times 10^6 \times 12{,}200 \left(\frac{9 \times 1.15}{4 \times 10^6 \times 388} + \frac{0.005}{507{,}000}\right)\right]^{-1}} = 10{,}300 \text{ lb,}$$

$$F_1 = 10{,}300 \left[1 - \left(\frac{283}{330}\right)^2\right] = 2800 \text{ lb.}$$

This requires one closed stirrup made from No. 3 bars.

Bursting Stress

The reference plane for the maximum bursting stress is along the axis of the applied load (8.3 in. above the bottom edge of the beam). The shear along the reference plane is:

$$V = 400{,}000 - \left(\frac{1290+970}{2}\right) (20 \times 8.3)$$

$$= 213{,}000 \text{ lb.}$$

The bending moment is given by Equation (43):

$$M_{pb} = 400{,}000 \times 4.15 = 1{,}660{,}000 \text{ in.-lb,}$$

$$M_v = -213{,}000 \times 4.15 = -885{,}000 \text{ in.-lb,}$$

$$\frac{M_t I_b}{I} = -400{,}000 \times 14.2 \times \left(\frac{8.3}{45}\right)^3$$

$$= -36{,}000 \text{ in.-lb,}$$

$$M_o = 1{,}660{,}000 - 885{,}000 + 36{,}000$$

$$= 811{,}000 \text{ in.-lb.}$$

The bursting stress is given by Equation (49):

$$\sigma_{bc} = \frac{811{,}000}{20 \times 8.3 \times 8.3} = 585 \text{ psi.}$$

The bursting stress under a distributed load is given by Equation (50). The load is assumed to be distributed over a 4-in.-high anchorage plate in this example.

$$\sigma_b = 585 \left\{1 - \frac{4}{45} \left[3 - 4\left(\frac{8.3}{45}\right)\right]\right\} = 465 \text{ psi.}$$

The effective tensile strength of the concrete in the bursting zone is:

$$6\sqrt{f'_c} = 425 \text{ psi.}$$

The stirrup force per unit length of the beam is given by Equation (54).

$$f_o = (465-425)20 = 800 \text{ lb/in.}$$

If the stirrups are spaced every three in., the total stirrup force is:

$$F_1 = 800 \times 3 = 2400 \text{ lb.}$$

Assuming that the stress in the steel is 5000 psi at the time of cracking in the concrete, the required area of steel is 0.48 sq. in. spaced every three in. over the length of the bursting zone.

VII. SUMMARY

7.1 OBJECT AND SCOPE

The object of this report is to present information on the initiation of cracking and the action of transverse reinforcement in the anchorage zone of prestressed concrete beams.

A total of 177 tests are reported. Sixty-six of the tests were conducted at the University of Illinois, Urbana. These included tests on 48 post-tensioned rectangular beams and 18 post-tensioned I-beams. Seventy-two tests were made at the Portland Cement Association Research and Development Laboratories (Skokie). These included 35 tests on pretensioned I-girders[28] and 37 tests on concrete column heads.[23] Nineteen tests on pretensioned I-girders were made at the University of Glasgow.[1] The remaining tests were made at the Cement and Concrete Association Laboratories.[48] These included nine tests on post-tensioned rectangular end blocks and eleven tests on post-tensioned I-sections.

The tests investigated a wide range of variables that influence the behavior of the anchorage zone. The major variables investigated were: (1) size and shape of cross section, (2) eccentricity of the prestressing force, (3) ratio of the loaded area to the cross-sectional area, (4) distribution of the prestressing force, (5) type of prestressing (post- or pretensioned), (6) concrete quality, (7) amount, type, and location of transverse reinforcement and, (8) time-dependent effects.

7.2 BEHAVIOR OF THE TEST SPECIMENS

Longitudinal cracks in the anchorage zone were observed in all investigations. The cracks occurred in both post-tensioned and pretensioned girders with rectangular or I-shaped cross sections.

The longitudinal cracks resulted from the transverse tensile stresses produced by the "flow" of the prestressing force from the region of force concentration to a region of linear distribution of the longitudinal stresses. Two zones in which longitudinal cracking was likely to occur were identified (Figure 1). The first zone is the bursting stress zone which lies along the axis of the prestressing force a short distance from the beam end. The formation of a longitudinal crack in this region occurred almost simultaneously with the failure of the anchorage zone. The second zone in which a longitudinal crack is likely to occur is the spalling stress zone. A crack in this zone starts on the end

face of the beam at some distance from the prestressing force. This type of cracking did not lead to failure as long as the cracks were small.

The tests at the University of Illinois emphasized the importance of differential-shrinkage stresses on the formation of spalling cracks. The tests also showed that the width and length of the spalling cracks increased with time under a sustained load and that the effectiveness of the transverse reinforcement in restraining the development of the crack was approximately proportional to the stirrup size.

The tests on pretensioned beams showed that the spalling stresses in an uncracked beam and the stirrup force in a cracked beam were inversely proportional to the strand transfer length.

Two regions of spalling stress were observed in the rectangular end blocks tested at the Cement and Concrete Association Laboratories. The first of these zones was on the loaded face of the end block; the second was at the junction of the rectangular end block and the I-beam. From this test series it was concluded that rectangular end blocks on I-section beams were not necessary and, in some instances, were even detrimental.

The tests on concrete column heads brought out the relative importance of cracking in the bursting and spalling zones on the strength of the anchorage zone. The spalling cracks which occurred before bursting failure only when the eccentricity of the applied load was large did not seriously affect the bearing strength. The bearing strength increased with an increase in the width of the loading plates and with a decrease in an eccentricity of the applied loads.

7.3 ANALYSIS OF THE TEST RESULTS

A modified version of Lenschow's analysis[24] was used to interpret the test results. Lenschow's analysis is based on a physical analog (Figure 2) which represents the anchorage zone. The derivation and solution of the basic equations for the physical analog are based on the bending of beams on elastic foundations. The magnitudes and trends indicated by the analysis compare favorably with those of classical solutions. The advantage of the physical analog is that it can be modified to admit cracks in the anchorage zone, the essential requirement for developing a reasonable design method.

The measured loads at the initiation of cracking in the bursting and spalling zones were compared with the calculated values. The measured and computed stirrup forces were also compared. The modified version of the analysis gave an intelligible interpretation of the test results.

A design procedure based on the analysis was proposed for the calculation of the transverse stresses and the selection of the transverse reinforcement. The proposed design procedure is practical as well as being general. Two numerical applications of the design procedure are included in Chapter VI.

VIII. APPENDICES

A. MATERIALS, FABRICATION, AND TEST PROCEDURES — TESTS AT THE UNIVERSITY OF ILLINOIS

A.1 MATERIALS

A.1.1 Cement

Marquette brand type III portland cement was used in all specimens.

A.1.2 Aggregates

Wabash River sand and pea gravel were used for all specimens. Both aggregates have been used in this laboratory for a number of years. The maximum size of the gravel was 3/8 in.

The origin of these aggregates is an outwash of the Wisconsin glaciation. The major constituents of the gravel were limestone and dolomite. The sand consisted mainly of quartz.

A.1.3 Concrete

The design of the concrete mix was based on the trial-batch method. One batch was used in each beam. Tables 8 and 9 list the compressive strength, tensile splitting strength, and age at the time of test for each beam. The compressive strength was measured on standard 6- by 12-in. cylinders. The splitting strength was found from tests on 6- by 6-in. cylinders. A compressive force was applied along opposite generators of the cylinder in the splitting test. Stiff strips of 1/8-in. thick fiber board were placed between the heads of the testing machine and the cylinder to distribute the load evenly along the length of the specimen.

Twelve groups of control cylinders were tested to determine the variation in the compressive and splitting strengths with the age of the concrete. The mix and batch size used for these cylinders were the same as those used for the beams. The results of the strength tests on the control cylinders are presented in Figures A1 and A2. The 15-day strength was used as a standard in these figures. The points shown are the average of three tests. Figure A1 shows that the compressive strength increased with concrete age. The splitting strength increased with age until 15 days. A sound conclusion cannot be drawn from these tests about the variation of the splitting strength with concrete age for concrete that was older than 15 days.

A.1.4 Reinforcement

Four kinds of reinforcing bar were used as transverse stirrups: (1) No. 2 deformed bars, (2) No. 7 USSWG wires, (3) 1/4-in. diameter plain bars, and (4) 1/8-in. diameter plain bars. The No. 2 bars had a nominal area of 0.05 sq. in. and an average yield force of 2.5 kips. The cross-sectional area of the No. 7 USSWG wires was 0.025 sq. in. They had an average yield force of 0.8 kips.

The 1/4-in. and 1/8-in. diameter plain bars were obtained in 12-ft. lengths of cold drawn wire. The bars were cut to size and then annealed at 1200°F for three hours. After the steel had cooled slowly in the oven, it was bent and welded as shown in Figure A4a. The nominal cross-sectional area and average yield force were 0.049 sq. in., 1.75 kips, and 0.012 sq. in., 0.50 kips, for the 1/4-in. and 1/8-in. bars, respectively.

No. 3 deformed bars were used as reinforcement in the longitudinal tension zone of the beam. The bars had a nominal area of 0.11 sq. in. and an average yield force of 5.7 kips.

A.1.5 Tensioning Rod

One-in. diameter STRESSTEEL rods were used to apply the external force. They had a proportional limit of 87 kips, an ultimate capacity of 126 kips, and a modulus of deformation of about 30,000 ksi.

A.1.6 Epoxy Resin

An epoxy resin was used to coat three of the test beams. The epoxy was mixed in small quantities in the proportions of ten parts resin to one part hardener by weight. The epoxy was painted on the beams. The thickness of the epoxy layer on the beams ranged from about 0.005 in. to 0.025 in. with an average of approximately 0.012 in. The tensile strength of the epoxy was about 10,000 psi. The modulus of deformation was between 500 and 600 ksi.

A.2 DESCRIPTION OF THE SPECIMENS

The principal part of the investigation involved tests on short beam specimens. A complementary program to determine the bond characteristics of the transverse reinforcement involved tests on twin pull-out specimens.

The beam specimens had either a rectangular or I-cross section. The overall dimensions of both sections were 6 by 12 in. The specimens were 4 ft long. Details pertaining to the specimen dimensions are shown in Figure A3 and a picture of a specimen is given in Figure A10.

The one-in.-diameter STRESSTEEL rod was cast 1.5 in. from the bottom of all specimens. It was lubricated to prevent bond. A crack starter, Figure A4b, was placed in some beams as shown in Figure A5. The crack starter was formed from 0.025-in.-thick steel binding tape. The bottom surface of the crack starter was lubricated to prevent bond and to ensure the formation of a crack at the desired location.

The specimens with the "precrack"

were cast in two layers which were separated by a thin plastic sheet. The period between the casting of the two layers varied from 20 minutes to 3 hours.

A typical stirrup used for the transverse reinforcement is shown in Figure A4a. One or two stirrups encircling the STRESSTEEL rod were placed in the ends of all reinforced beams. Identical stirrup arrangement was used at both ends of a specimen.

One or two No. 3 deformed bars were used in the longitudinal tension region of most specimens. These bars were positioned one in. from the top surface of the beam. The positions of the crack starter, tensioning rod, stirrup, and No. 3 bars in a typical beam specimen are shown in Figure A5.

The twin pull-out specimen used in the bond tests on the stirrup reinforcement is shown in Figures A9 and A10b. This specimen was designed to simulate the conditions in the end of a cracked beam. Hence, there was no compression of the concrete around the bar that could produce the confinement normally associated with pull-out specimens. The two symmetrically placed bars were pulled at the same time. A No. 3 bar was placed in the bottom of the specimen to prevent failure from the bending stresses.

A.3 CASTING AND CURING

All beams were cast in steel forms. The STRESSTEEL rod and crack starter, both lubricated to prevent bond, were positioned in the forms. Transverse stirrups, if used, were looped about the STRESSTEEL bar before the latter was put into the form. The stirrups were clamped in the desired positions to prevent movement during the placing of the concrete.

The concrete was mixed in a drum-type mixer of 6 cu ft capacity. Usually one batch of concrete was required for a beam. However, when a precracked beam was desired, two batches of concrete were used. Four 6- by 6-in. cylinders for compression tests and four 6- by 6-in. cylinders for splitting tests were cast for each beam. Two twin pull-out specimens were cast with each of the beams containing transverse reinforcement. All specimens were vibrated with an internal vibrator. Several hours after casting, the top surface of the beam was trowelled smooth and the compression cylinders were capped with neat cement.

One day after casting, the specimens and the cylinders were removed from their forms, placed under wet burlap, and covered with polyethylene. After five to seven days the burlap was removed. The specimens were stored in the laboratory until they were set up for testing.

The curing procedures described above were not followed in the case of six beams. Three of these beams received no moist curing at all. These specimens were stored in the laboratory immediately after they were removed from their forms. The other three specimens were painted with an epoxy resin immediately after they had been removed from their forms. The epoxy used is described in Section A.1.6. It was hoped that the epoxy would prevent moisture evaporation and therefore

prevent drying shrinkage. This expectation was not fully realized since the epoxy layer was thin. However, the epoxy did prevent a large amount of moisture loss and thereby reduced the drying shrinkage to about one-third of that which occurred in the specimens exposed to the air.

A continuous record of the temperature and relative humidity in the testing area of the laboratory was made with a Foxboro temperature-humidity recorder. Over the period of one year, the temperature ranged from 65 to 82° and the relative humidity from 50 to 90 per cent.

A.4 INSTRUMENTATION AND TEST PROCEDURE

A.4.1 Short-Time Tests

All beams were instrumented one day before testing. In four specimens, type A3 SR-4 electric strain gages were used to measure the strain distribution on the surface of the concrete. The gages had a nominal length of 3/4 in. A base layer of Duco cement was applied to the concrete which had already been smoothed with sandpaper. A second layer of cement was used to attach the gages about ten minutes later.

Ames dials were used to measure the crack width in most of the precracked specimens. The dials were mounted on the concrete above the precrack at 1, 3, 6, and 10 in. from the beam end. The plungers of the dials rested on aluminum angles glued to the concrete below the precrack. One dial division was equal to a deformation of 0.0001 in.

Specimens R19 through R48 were instrumented with steel plug for the measurement of crack width and longitudinal strain. The plug, 1/2 by 1/2 by 1/8 in., were mounted with Eastman 910 adhesive on the beams at the locations shown in Figures A6, A7, and A10. The plugs shown in Figure A6 were used for the measurement of the width of a longitudinal crack in the anchorage zone. Deformation readings were taken across the longitudinal crack with a two-in. Berry gage. One dial division on the berry gage corresonded to a deformation of 0.00017-in. measured over two in. Repeated measurements of the same length were reproducible within a range of plus or minus one dial division. A direct-reading 10-in. Whittemore gage was used with the plugs shown in Figure A7 to measure longitudinal deformations. The gage was equipped with a 0.0001-in. dial and measurements were reproducible within a range of plus or minus one dial division. The plug arrangement shown in Figure A7 was also used to measure longitudinal and transverse shrinkage deformations in specimens R43 through R48.

Strains were measured in the transverse reinforcement in 18 or the precracked beams. Type A7 SR-4 electric strain gages were applied to the stirrups in the following manner. The stirrup was filed smooth and sanded with with emery cloth. The gage was trimmed and then mounted on the bar with Eastman 910 adhesive. After the lead wires were soldered and the gage covered with

a layer of wax, a protective layer of epoxy was applied as an outer cover. The gages on the stirrups were positioned at the level of the precrack in the beam.

The loading arrangement was varied slightly depending upon whether the crack width was to be measured at one or both ends of the specimen. Steel bearing blocks with a bearing area of 6 by 1.5 in. were used at the ends where the crack widths were measured. Bearing blocks with a bearing area of 6 by 3 in. were used at the ends where the crack widths were not measured.

A 50-ton center-hole hydraulic jack was used to apply the load to the specimens. The dynamometer that measured the load had a calibration factor of 310 lb per dial division on the strain indicator. The position of the jack and the dynamometer on the specimens tested at both ends is shown in Figures A8 and A10. The steel yoke was designed to allow the load to be applied without removal of the nut immediately behind the loading block. The yoke was important in the sustained-load tests because the jack and dynamometer could not be left on one beam for a long period of time. When a specimen was tested at one end only, the jack and dynamometer were placed at opposite ends of the beam. In this case a shorter STRESSTEEL bar was used and the yoke omitted. Cracks were always measured at the end of the specimen where the dynamometer was placed.

Initial readings were made at all gage locations before the start of loading. The load was applied in about 15 increments. The process of applying an increment of load took about one minute. Gage readings were taken on the end face of the beam and then on the sides. If both ends of the beam were being tested, the above procedure was applied first to end C and then to end D. Ends C and D are defined in Figure A8. If the crack appeared to be propagating with time, a second set of gage readings was made approximately ten minutes after the conclusion of the first set.

The development of the cracks on the surface of the specimens was observed with a magnifying glass. A record was kept of all visible cracks in the specimens including the flexural cracks in the longitudinal-tension zone.

A.4.2 Sustained-Load Tests

The locations of the steel gage plugs used for the measurement of crack width and longitudinal deformation in the sustained-load specimens are shown in Figures A6, A7, and A10. This instrumentation is the same as that described for the short-time tests.

The loading arrangement for a sustained-load test is presented in Figures A8 and A10. The load was increased from zero to 10 kips in one step and then to 30 kips in 5-kip increments. Crack widths and longitudinal deformations were measured after each load increment.

The hydraulic pressure was left on the jack for the first week of the test. Periodically the load was checked and increased to 30 kips if it had decreased by more than 5 per cent. The maximum load decrease recorded was

10 per cent. The time period between checks was developed by trial on the first beam. It ranged from one hour between the end of the initial loading and the first check to six months between the last check and the end of the test.

After one week, the nut between the yoke and loading plate was tightened with a strap wrench and the yoke, dynamometer, and jack were removed. Subsequent load checks were made using the following procedure. (1) A set of gage readings was taken. (2) The jack, dynamometer, and yoke were put in place and the load was increased until the anchor nut could be loosened with the strap wrench. This load was recorded. (3) The load was increased to 30 kips and a set of gage readings was made. (4) The nut was tightened and the hydraulic pressure in the jack was released. The yoke, dynamometer, and jack were then removed. (5) A final set of gage readings was made.

A.4.3 Bond Tests

The test arrangement for the twin pull-out bond specimens is shown in Figures A9 and A10b. The load was applied to the bars by a small hydraulic jack placed between the steel plate and the specimen. The bearing area of the jack on the specimen was 6 in. in diameter. Anchor grips placed on the bars provided the reactions for the load on the steel plate.

The load in each bar was measured by an aluminum dynamometer. The dynamometers had a calibration factor of approximately ten lb per dial division on the strain indicator.

The attack-end slip for each bar was measured by two dial gages mounted on a sleeve that was fastened to the bar by three set screws. The attack end of a bar is defined as that end of the bar which first experiences a relative movement between the bar and the concrete. The plungers of the dial gages rested on thin aluminum plates glued to the surface of the concrete. The gages could be read to 0.0001 in. and had 0.30 in. of travel.

The load was applied in 50-lb increments to the 1/8-in. diameter bars and in 100-lb increments to the 1/4-in. diameter bars. About two minutes were allowed to elapse between the application of the load and the reading of the dial gages. The average reading of the two gages on each bar was computed for all loads. The slip at a given load was given by the difference between the average dial reading at that load and the average dial reading at zero load.

A.5 TEST RESULTS

A.5.1 Introductory Remarks

A general discussion pertaining to the behavior of the tests conducted at the University of Illinois is given in Chapter III. The purpose of this section is to present the large number of figures of individual test results that are the basis for the statements made in Chapter III.

A.5.2 Bond Tests

Figure A11 presents the load-slip curves for No. 2 deformed bars and No. 7 USSWG plain wires. The curves are the average of six tests on the bars and three tests on the wires. The range of the slips measured at a given load varied less than 15 per cent from the average for the No. 2 bar and 10 per cent from the average for the wire. Figure 11 shows twice the slip measured in order to indicate the magnitude of the total slip at a crack.

Figures A12 and A15 present the load-slip envelopes for the 1/4-in. and 1/8-in. diameter plain bars. The lower and upper extremes shown in the figures refer to the range of curves obtained in 32 tests for each size bar. Also shown in each figure is the average load-slip curve and the range covering two-thirds of the data. Some of the individual test results are shown in Figures A13 and A14 for the 1/4-in. diameter bars and in Figures A16 and A17 for the 1/8-in. diameter bars. If it is assumed that the distribution of bond stress along the embedded length of the bar is uniform, the average load-slip curves shown in Figures A12 and A15 could be closely approximated by a unit bond force of 240 lb/in. for the 1/4-in. bars and 140 lb/in. for the 1/8-in. bars.

A.5.3 Beam Tests

The results of the beam tests are presented in three types of graphs. The first is a crack profile (e.g., Figure A27) which gives the length and width of the spalling crack as determined from deformation readings made across the crack at some stage of the test. The second is a load-deformation curve (e.g., Figure A27) which shows the relationship between the load and the transverse deformation measured across the crack on the end of the beam. The third is a curve showing the distribution of the longitudinal deformations measured at the center of the beam (e.g., Figure A42).

Crack profiles and load-deformation curves are given for specimen R19 and Specimens R22 through R48. The distribution of the longitudinal deformations is given for specimens R31 through R35 and R38 through R42. Table 10 gives the figure numbers pertaining to the graphs which show the test results for each specimen.

B. MATERIALS, FABRICATION, AND TEST PROCEDURES — TESTS AT OTHER LABORATORIES

B.1 TESTS AT THE PORTLAND CEMENT ASSOCIATION RESEARCH AND DEVELOPMENT LABORATORIES (SKOKIE)

B.1.1 Pretensioned Girders by Marshall and Mattock [28]

The concrete used in the specimens was made with Type III portland cement and 3/4-in. maximum size aggregate. The compressive strengths of concrete cylinders taken from the batches of concrete placed in the webs of the specimens are given in Table 11. These strengths were measured at the time of

transfer and each value is the average of three tests on 6- by 12-in. cylinders.

The specimens and cylinders were moist cured under plastic sheets at 70°F for the first three days after casting. The plastic sheeting was then removed and the specimens were stored at 70°F and 50 per cent relative humidity until transfer at an age of seven days.

The stirrups used for the transverse reinforcement in the anchorage zone had two legs as shown in Figure B3. They were made from No. 2 or No. 3 deformed bars with yield points of 49.9 and 44.4 ksi. The cross piece at the top of the stirrups was welded to the two legs. Hooks pointing along the axis of the girder were provided at the bottom of the two legs to ensure satisfactory bond. Type A12 SR-4 electric strain gages were mounted on the stirrups as is shown in Figure B3.

The prestressing steel was seven-wire, stress-relieved strand of 1/4-, 3/8-, or 1/2-in. diameter. The cross-sectional areas, stress at one per cent extension and strengths of the strands were 0.0356 sq. in., 251 ksi, and 280 ksi for the 1/4-in. strand; 0.0799 sq. in., 259 ksi, and 286 ksi for the 3/8-in. strand., and 0.1438 sq. in., 231 ksi, and 254 ksi for the 1/2-in. strand. Except for the strand used in specimens A3, A4, A7, and A8, all strand was free of rust and was cleaned of surface oil before tensioning. The 1/4-in. strand used for specimens A3, A4, A7, and A8 was purposely rusted prior to use.

All test specimens were 10 ft long. The cross section for each specimen is shown in Figures B1 or B2. The specimens were fabricated and tested in groups of one to three girders. The strands were tensioned individually using a center-hole ram with a 20-in. stroke. The tension in the strand was measured by a load cell placed between the hydraulic ram and the temporary anchorage used to grip the strand during the tensioning operation. The strands were over-tensioned by an amount sufficient to compensate for the draw in of the permanent anchorages. The prestress remaining after permanent anchorage was measured in five strands. The initial prestress was kept very close to the chosen value of 175 ksi.

The specimens were cast one day after the strands were prestressed. Five days after casting Type A12 SR-4 electric strain gages were mounted at several points on the girders. Seven days after casting the prestress was transferred by torch-cutting the strands. Readings of all gages and the load cells behind the strand anchorages were taken before the cutting of the strand. The strands were cut in predetermined groups. Readings of all gages and load cells were taken after the cutting of each group of strand. In this way the prestress forces applied and the resulting strains in the concrete and stirrups were measured for each stage in the transfer.

B.1.2 Tests to Determine the Bearing Strength of Concrete Column Heads by Kriz and Rath [24]

Type I portland cement was used for concrete cylinder strengths below 5000 psi. Type III portland cement was

used for cylinder strengths above 5000 psi. The maximum size of the gravel in the mix was 1.5 in. The fine aggregate was Elgin sand. An airentraining agent was added to produce 4.4 to 6 per cent air in the concrete. All test specimens were cast in a horizontal position, moist cured for three days, and then stored at 73°F and 50 per cent relative humidity. All specimens were tested 12 days after casting. The average compressive strengths determined from three 6- by 12-in. cylinders taken from each batch of concrete are listed in Table 12.

The notation referring to the cross-sectional dimensions and the size and location of the bearing plates is defined in Figure B4. Table 12 lists the cross-sectional dimensions and expresses the width and eccentricity of each loading plate as a function of the cross-sectional height for each specimen.

Two symmetrically placed loads were applied to each specimen as is shown in Figure B4. The 3/4-in.-thick steel bearing plates were set in a thin layer of hydrocal and aligned with a level. A round and a half-round bar were placed at the centers of the bearing plates to locate the resultant forces at a distance "s" from the edges of the column and to prevent lateral restraint. The load was applied to the specimens in increments until failure occurred. The development of cracks was observed after each load increment.

B.2 TESTS AT THE UNIVERSITY OF GLASGOW (1)

Type III portland cement was used in all specimens. The maximum size of the gravel was 3/8 in. The average strengths of the three 4-in. cubes tested at seven days are given in Table 13 for each specimen.

The prestressing steel used in all the tests was 0.2-in.-diameter indented high-tensile steel wire with an ultimate tensile strength of 246 ksi and an initial modulus of deformation of 28,000 ksi. The wires were free from rust and oil at the time of tensioning.

The tests were carried out in two series, A and B. The cross sections of the specimens are shown in Figure B5. All the specimens were 9 ft 6 in. long. In series A specimens, the prestressing wires were mainly grouped near the bottom of the cross section. In series B specimens the wires were divided equally between the top and bottom flanges.

The test beams were manufacturered and tested singly. The wires were tensioned altogether by movement of the anchor plate. The total extension of the wires was measured by two one-in. dial gages reading against the movable anchor plate. The wires in series A specimens were tensioned to 150 ksi, while those used in series B specimens were tensioned to 168 ksi.

The concrete was cast one day after the stressing of the wires. The specimens were vibrated with an external vibrator bolted to the base of the form. After ten hours the sides of the forms were removed and the beam was then cured under damp burlap for three days. On the fifth day after casting, Demec

gage (mechanical gage) points were fixed to the beam.

The prestressing force was transferred in small increments, normally 16 in number, when the beams were seven days old. The wires were all released simultaneously and in equal amounts. Gage readings were taken on the concrete surface with a 2-in. Demec gage after each increment of the prestressing force was released.

B.3 TESTS AT THE CEMENT AND CONCRETE ASSOCIATION LABORATORIES [48]

The mix used for the specimens had an aggregate/cement ratio of 3.55 and a water/cement ratio of 0.45. The maximum size of the granite aggregate was 3/8 in. and the percentage of sand was 22. Table 14 lists the compressive and splitting strengths measured from control specimens cast with each end block.

Figure B6 shows the cross sections and loading positions for the various tests. The overall length of the specimen was 40 in. and the length of the rectangular end block was 16 in. There were eight 5/8-in. diameter cable holes parallel to the centroidal axis of each specimen.

Concrete surface strains were measured with a 2-in. Demec gage. The strain gage points were arranged at 1/2-in. centers near the loaded face and at one-in. centers away from the loaded face. A large number of gage points was used in each test.

Table 14 gives the positions of loading for each test. Eleven tests were carried out on the I-section specimens including four tests with symmetrical loading and seven tests with eccentric loading. Nine tests including three with symmetric loading were carried out on the rectangular end blocks.

The specimens were tested in a reinforced concrete testing frame which provided a maximum load of 112 kips. For loads in excess of 112 kips, 1/2-in. diameter strand was used to apply the load. The loading plates were positioned on thin layers of plaster on the ends of the specimens.

C. DERIVATION OF LENSCHOW'S ANALYSIS

C.1 BASIC EQUATIONS FOR A BEAM ON AN ELASTIC FOUNDATION

An element of a beam on elastic springs with a spring constant k is shown in Figure C1. The forces and moments acting on the element in Figure C1 are drawn in the positive directions. From the conditions of equilibrium:

$$\frac{dQ}{dx} = ky \ , \qquad (C1)$$

$$\frac{dM}{dx} = Q \ . \qquad (C2)$$

From Equations (C1) and (C2)

$$\frac{d^2M}{dx^2} = ky \ . \qquad (C3)$$

It is assumed that the beam is prismatic and linearly elastic. The deflection of the element is produced by shear and

moment. The deflection due to shear is

$$dy_{sh} = \frac{\gamma Q}{AG}\, dx \ , \qquad (C4)$$

where γ is the shape factor for the cross section assuming that warping is not restrained.

The deflection due to moment is

$$y_m = \int\int - \frac{M}{EI}\, dx^2 \ . \qquad (C5)$$

Calling the total deflection y and combining Equations (C1) through (C5) gives:

$$\frac{d^2y}{dx^2} = - \frac{M}{EI} + \frac{\gamma}{AG} \frac{dQ}{dx} \ , \qquad (C6)$$

$$\frac{d^2y}{dx^2} = - \frac{M}{EI} + \frac{\gamma k y}{AG} \ , \qquad (C7)$$

$$\frac{d^4y}{dx^4} = \frac{\gamma k}{AG} \frac{d^2y}{dx^2} - \frac{k}{EI}\, y \ . \qquad (C8)$$

Let $$S = \frac{k}{EI} \qquad (C9)$$

$$R = \frac{\gamma k}{AG} \ . \qquad (C10)$$

Substituting Equations (C9) and (C10) into Equation (C8) gives

$$\frac{d^4y}{dx^4} - R \frac{d^2y}{dx^2} + Sy = 0 \ . \qquad (C11)$$

The solution of this equation is:

$$y = C\, e^{\alpha x} \ . \qquad (C12)$$

Substituting Equation (C12) into Equation (C11) gives

$$Ce^{\alpha x} (\alpha^4 - R\alpha^2 + S) = 0 \qquad (C13)$$

or

$$\alpha^2 = \frac{R}{2} \pm \frac{1}{2} \sqrt{R^2 - 4S} \ . \qquad (C14)$$

The solution for $(R^2 - 4S) < 0$ is

$$\alpha^2 = \frac{R}{2} \pm \frac{i}{2} \sqrt{4S - R^2} \ . \qquad (C15)$$

Consider the η-axis as the "real" axis and the ξ-axis as the "imaginary" axis. If β is the angle measured from the η-axis, then from Equation (C15):

$$\tan\beta = \frac{\xi}{\eta} = \pm \frac{\sqrt{4S - R^2}}{R} \qquad (C16)$$

and

$$\alpha^2 = \sqrt{\eta^2 + \xi^2}\ (\cos\beta + i \sin\beta) \qquad (C17)$$

$$\alpha^2 = \sqrt{S}\ (\cos\beta + i \sin\beta) \qquad (C18)$$

$$\alpha^2 = e^{i\beta} \sqrt{S} \qquad (C19)$$

or

$$\alpha = \pm\, e^{0.5\, i\beta}\, S^{0.25} . \qquad (C20)$$

Expanding the exponential term in Equation (C20) in a trignometric function

$$\alpha = \pm\, S^{0.25} \left(\cos\frac{\beta}{2} + i \sin\frac{\beta}{2}\right) . \qquad (C21)$$

Values of cos β and sin β are found from the following:

$$\cos\beta = \sqrt{\frac{1}{1 + \tan^2\beta}} \ . \qquad (C22)$$

Substituting Equation (C16) into Equation (C22) gives

$$\cos\beta = \frac{R}{2\sqrt{S}} \ . \qquad (C23)$$

The half angles in Equation (C21) can be expressed in terms of cos β through the trignometric relationships,

$$\cos\frac{\beta}{2} = \pm\sqrt{\frac{1}{2}(1 + \cos\beta)}$$

$$= \pm\sqrt{\frac{2\sqrt{S} + R}{4\sqrt{S}}} \ , \qquad (C24)$$

$$\sin \frac{\beta}{2} = \pm\sqrt{\frac{1}{2}(1 - \cos \beta)}$$

$$= \pm\sqrt{\frac{2\sqrt{S} - R}{4\sqrt{S}}} \, . \qquad (C25)$$

Now let

$$a = \frac{1}{2}\sqrt{2\sqrt{S} + R} \, , \qquad (C26)$$

$$g = \frac{1}{2}\sqrt{2\sqrt{S} - R} \, . \qquad (C27)$$

Substitution of Equations (C24) through (C27) into Equation (C21) gives:

$$\alpha = \pm (a \pm ig). \qquad (C28)$$

Substituting Equation (C28) into Equation (C12)

$$y = C\, e^{\pm(a \pm ig)x} . \qquad (C29)$$

Expanding Equation (C29) in a trigonometric series gives:

$$y = e^{ax}(C_1 \cos gx + C_2 \sin gx) + e^{-ax}(C_3 \cos gx + C_4 \sin gx). \qquad (C30)$$

Choosing the origin at one end of the beam, the first term in Equation (C30) represents a deflection that increases steadily with increasing distance from the beam end. For a long beam this is impossible, therefore, C_1 and C_2 must be zero. Thus, Equation (C30) can be simplified as shown below for all cases in which the beam length is more than twice its height.

$$y = e^{-ax}(C_3 \cos gx + C_4 \sin gx). \qquad (C31)$$

The second solution for Equation (C14) is for $(R^2 - 4s) \geq 0$. The solution for α is

$$\alpha = \pm(a \pm r), \qquad (C32)$$

where

$$r = ig = \frac{1}{2}\sqrt{R - 2\sqrt{S}} \, , \qquad (C33)$$

and "a" is given by Equation (C26). Substituting Equation (C32) into Equation (C12) gives

$$y = e^{ax}(C_1 \cosh rx + C_2 \sinh rx) + e^{-ax}(C_3 \cosh rx + C_4 \sinh rx). \qquad (C34)$$

Equation (C34) has little practical importance because the value of $(R^2 - 4S)$ is negative in all practical cases for which the analog is used. The case for $(R^2 - 4S) \geq 0$, therefore, will not be considered further.

C.2 DETERMINATION OF THE CONSTANTS FROM THE BOUNDARY CONDITIONS

C.2.1 Post-Tensioned Beam

The applied forces at the end of a post-tensioned beam may consist of a moment M_o and a stirrup force F_1. Both M_o and F_1 are assumed to be positive according to the sign convention given in Figure C1. The boundary conditions at x = 0 are:

$$\frac{d^2y}{dx^2} = -\frac{M_o}{EI} + Ry \, , \qquad (C35)$$

$$\frac{d^3y}{dx^3} = -\frac{F_1}{EI} + R\frac{dy}{dx} \, . \qquad (C36)$$

Substituting Equation (C31) into Equation (C35)

$$(a^2 - g^2)C_3 - 2ag\, C_4 = -\frac{M_o}{EI} + R\, C_3 \, , \qquad (C37)$$

and Equation (C31) into Equation (C36)

$$(-a^3 + 3ag^2)\, C_3 + (3a^2g - g^3)C_4 = -\frac{F_1}{EI} - aRC_3 + gR\, C_4 \,. \qquad (C38)$$

Solving Equations (C37) and (C38) simultaneously gives C_3 and C_4

$$C_3 = -\frac{M_o}{EI\sqrt{S}} - \frac{2af_1}{EIS}\,, \qquad (C39)$$

$$C_4 = \frac{aM_o}{gEI\sqrt{S}} + \frac{RF_1}{2EISg}\,. \qquad (C40)$$

For an uncracked anchorage zone, the transverse reinforcement has little effect and F_1 can be set equal to zero. The maximum deflection in the physical analog corresponds to the maximum stress in the beam. It can be seen that Equation (C31) has a maximum at the beam end, x = 0. Substituting Equation (C39) into Equation (C31) with x = 0 gives:

$$y = \frac{-M_o}{EI\sqrt{S}}\,. \qquad (C41)$$

By definition the spring force is equal to the spring constant multiplied by the spring deflection. The transverse stress at the beam end is therefore:

$$\sigma_{end} = \frac{ky}{b} = \frac{-M_o}{b}\sqrt{S}. \qquad (C42)$$

The location of the maximum bursting stress is found by differentiation of Equation (C31). The distance x from the beam end to the point of maximum bursting stress is given by:

$$x = \frac{1}{g}\,\text{artan}\left(\frac{4ag}{R}\right). \qquad (C43)$$

Substitution of Equations (C39), (C40), and (C43) into Equation (C31) will give the maximum bursting stress.

C.2.2 Pretensioned Beams

The forces applied to the anchorage zone of a pretensioned beam are shown in Figure 4. It is assumed that both the prestress force and the shear on the reference plane are uniformly distributed over the transfer length T. The bending moment distribution along the reference plane is shown in Figure C2a. The applied moment is:

$$M = \frac{M_o x}{T} \text{ for } 0 \leq x \leq T \qquad (C44)$$

and

$$M = M_o \text{ for } x \geq T\,. \qquad (C45)$$

The moment M is equivalent to the moment produced by two equal transverse forces (Figure C2b). The transverse stress at the beam end may be found from Equations (C31), (C39) and (C40) using Maxwell's law of reciprocity. Maxwell's theorem of reciprocity states that the deflection at point 1 in the direction A due to a unit at point 2 in direction B is equal to deflection at 2 in the direction B produced by a unit load at point 1 in the direction A. Thus, the deflection at the end of the analog shown in Figure C2b can be divided into two parts: that from the load applied at the end of the beam and that from the load applied at x = T.

The deflection at the beam end produced by the load at the end of the beam is:

$$y_1 = \frac{-2aM_o}{kT}\,. \qquad (C46)$$

From Maxwell's law of reciprocity it can be found that the deflection at the beam end produced by the load at x = T is equal to the deflection at x = T produced by the load at the end. This deflection is

$$y_2 = \frac{-M_o e^{-aT}}{kT} \left(-2a \cos gT + \frac{R}{2g} \sin gT\right). \quad (C47)$$

The total deflection at the beam end is the sum of y_1 and y_2. Therefore, the transverse stress at x = 0 for a pretensioned beam is:

$$\sigma_{end} = \frac{ky}{b} = \frac{-M_o}{bT} \left[2a(1-e^{-aT} \cos gT) + \frac{R}{2g} e^{-aT} \sin gT\right]. \quad (C48)$$

Theoretically, the transverse stress at the end of a pretensioned beam should approach that of a post-tensioned beam as the transfer length approaches zero. However, the limit of Equation (C48) as T approaches zero is

$$\sigma_{end} = \frac{-M_o}{b} (\sqrt{S} + R), \quad (C49)$$

which is not equal to Equation (C42). The term R in Equation (C49) occurs because the boundary conditions introduced when the applied moment is assumed to be equivalent to that produced by two equal transverse forces are not the same as the boundary conditions for pure moment. For this reason Equation (C48) should not be used for T < h/2. If T is less than h/2, Equation (C42) should be used.

In many practical applications the effect of the force at x = T on the deflection at x = 0 will be small and can be neglected. Equation (C48) is then reduced to:

$$\sigma_{end} = \frac{-2aM_o}{bT}. \quad (C50)$$

The stress given by Equation (C42) for a post-tensioned beam, however, should be taken as an upper bound for the stress in a pretensioned beam as given by Equation (C50).

C.3 MODIFIED ANALOG FOR THE CRACKED BEAM

The modified analog representing the conditions in a cracked anchorage zone is shown in Figure 5. The springs along Z, the length of the crack, have been removed. However, the expressions derived in Section C.2.1 are valid for all positive values of x if the origin of the axis is moved to the end of the crack. The springs at the end of the crack represent the effective tensile strength of the concrete as described in Section 2.5.

The deflection at the stirrup or the centroid of the stirrups can be considered to be the sum of (sign convention given in Figure C1):

(a) Initial displacement at the end of the crack, C_3

(b) The effect of initial slope, $(aC_3 - gC_4)Z$

(c) Deflection produced by M_o, $M_o Z^2/2EI$

(d) Deflection produced by F_1, $F_1 Z^3/3EI$

(e) Shear deflection, $\gamma F_1^2 Z/GA$

(f) Deflection produced by concrete strain at stirrups.

The deflections given by (a) and (f) are small and have compensating effects

on the crack width. Therefore, they will be neglected.

Summing up (b) through (e) gives:

$$\frac{kW}{2} = \frac{-F_1 SZ^3}{3} - (2aF_1\sqrt{S} + \frac{M_o S}{2})Z^2 - (\frac{3}{2}RF_1 + 2a^2F_1 + 2aM_o\sqrt{S})Z \ , \quad (C51)$$

where W is the deflection at the end of the beam. In determining Equation (C51) from (b) through (e) it was recognized that the moment at the end of the crack should be used in evaluating the constants C_3 and C_4. The moment at the end of the crack is:

$$M_o^* = M_o + F_1 Z \ . \quad (C52)$$

The relationship between Z and F_1 is determined by the effective tensile strength of the concrete at the end of the crack.

$$f_{te} = \frac{-(M_o + F_1 Z)\sqrt{S}}{b} - \frac{2aF_1}{b} \quad (C53)$$

or

$$F_1 = \frac{-f_{te} b - M_o\sqrt{S}}{2a + Z\sqrt{S}} \ . \quad (C54)$$

Substituting Equation (C54) into Equation (C51) gives

$$d_1 Z^3 + d_2 Z^2 + d_3 Z + d_4 = 0, \quad (C55)$$

where

$$d_1 = \frac{f_{te} b\sqrt{S}}{3} - \frac{M_o S}{6} \quad (C56)$$

$$d_2 = 2f_{te} ba - M_o a\sqrt{S} \quad (C57)$$

$$d_3 = f_{te} b(\frac{2R + \sqrt{S}}{\sqrt{S}} - M_o(\sqrt{S} - R) - \frac{Wk}{2} \quad (C58)$$

$$d_4 = -\frac{W ak}{\sqrt{S}} \ . \quad (C59)$$

Equation (C55) gives the relationship between the crack width and crack length in the analog. The relationship between crack length and stirrup force is given by Equation (C54).

In Equation (C51) it was assumed that the shear forces could be transmitted across the crack. This assumption may be valid for small cracks but it is not for wide cracks. If it is assumed that no shear can be transmitted across the cracks, the coefficients d_1 and d_2 in Equation (C55) are modified to d_1^* and d_2^*, where

$$d_1^* = d_1 - M_v S/2 \quad (C60)$$

$$d_1^* = d_2 - M_v a\sqrt{S} \ . \quad (C61)$$

The term M_v is the moment on the section below the reference plane that is produced by the shear V.

A typical curve representing the relationship between crack width and length given by Equation (C55) is shown in Figure 6. This curve may be calculated by using either the crack width or length as the dependent variable. In most practical cases, the maximum allowable width of the crack will be the governing restriction and Equation (C55) is solved for the crack length. The stirrup force can then be found from Equation (C54).

The procedure described in the paragraph above for finding the stirrup force is complicated by the fact that Equation (C55) is a cubic equation. The following simplifications will permit the direct determination of the stirrup force from the allowable crack width. The procedure is to calculate the stirrup force on the assumption that the effective tensile strength of the concrete is zero, and then to modify the stirrup force to take into account

the effect of the concrete. Assuming that $f_{te} = 0$ and combining Equations (C54) and (C55) gives

$$F_o^2 = -M_o^3 S / \left[3Wk - 9M_o R + 4F_o a\left(\frac{\sqrt{S}-4R}{\sqrt{S}}\right)\right], \quad (C62)$$

where F_o is the stirrup force when $f_{te} = 0$. Equation (C62) can be solved by iteration. However, the last term in the denominator is usually relatively small and may be omitted. Hence, Equation (C62) can be reduced to

$$F_o = -M_o \sqrt{\frac{1}{3E_c I_b\left(\frac{3\gamma}{A_b G} - \frac{W}{M_o}\right)}} \quad . \quad (C63)$$

The effect of $f_{te} > 0$ must now be considered. Consider the coefficients of Equation (C55) and denote Z_1 the crack length and F_1 the stirrup force when $f_{te} > 0$, and Z_o the crack length and F_o the stirrup force when $f_{te} = 0$. For large values of Z the coefficient d_1 is most important and

$$\frac{Z_o}{Z_1} = \sqrt{\frac{M_o\sqrt{S} - 2b\, f_{te}}{M_o\sqrt{S}}} \quad . \quad (C64)$$

For small values of Z the coefficient d_3 becomes more important. The term $Wk/2$ is assumed to be relatively small when Z is small and therefore it is neglected. Furthermore, it is on the safe side to ignore the effect of shear deflection represented by the R-terms. Thus, for small values of Z:

$$\frac{Z_o}{Z_1} = \frac{M_o\sqrt{S} - b\, f_{te}}{M_o\sqrt{S}} \quad . \quad (C65)$$

Equation (C65) is more conservative than Equation (C64). Therefore, it will be used in the following.

From Equation (C54):

$$Z_o = \frac{-M_o\sqrt{S} - 2af_o}{F_o\sqrt{S}} \quad (C66)$$

and

$$Z_1 = \frac{-M_o\sqrt{S} - 2aF_o - bf_{te}}{F_o\sqrt{S}} \quad . \quad (C67)$$

Combining Equations (C65), (C66), and (C67) gives

$$\frac{F_1}{F_o} = \frac{(M_o\sqrt{S} - b\, f_{te})\,(M_o\sqrt{S} + 2aF_1 + b\, f_{te})}{(M_o\sqrt{S})\,(M_o\sqrt{S} + 2a\, F_o)} \quad . \quad (C68)$$

Since $M_o\sqrt{S} >> |2a\, F_o| > |2aF_1|$,

$$\frac{F_1}{F_o} \approx 1 - \left(\frac{b\, f_{te}}{M_o\sqrt{S}}\right)^2 \quad (C69)$$

or

$$F_1 \approx F_o\left[1 - \left(\frac{b\, f_{te}}{M_o\sqrt{S}}\right)^2\right] \quad . \quad (C70)$$

C.4 DERIVATION OF THE SPRING CONSTANT

The function of the fictitious springs is to simulate the action of the concrete. The derivation of a spring constant to achieve this result is described in the following paragraphs.

If it can be assumed that the spring constant does not vary with the distance from the beam end, the stress distribution on the reference plane as derived in Section C.1 is:

$$\sigma_t = \frac{k}{b} e^{-ax}\,(C_3 \cos gx + C_4 \sin gx) \quad . \quad (C71)$$

The spring constant k will be investigated for the cases of uniform, sinusoidal, and exponential stress distribution on the reference plane. It will be shown that k depends only on the modulus of elasticity and geometry of the beam element. As long as these values are constant, the value of k will remain constant along the length of the beam.

C.4.1 Uniform Stress Distribution

Consider the prismatic element shown in Figure C3a. When a uniform stress σ_1 is applied to one face, the distance c between the loaded edge and the centroid deforms by an amount Δ. The spring constant k corresponding to this deformation is

$$k = \sigma_1 / \Delta \ . \qquad (C72)$$

For a linearly elastic homogeneous system, the deformation Δ can be expressed as:

$$\Delta = \frac{1}{E} \int_0^c \sigma_y \, dy \ . \qquad (C73)$$

The transverse stress may be evaluated using Airy's stress function and the boundary conditions. The stress function must satisfy

$$\frac{\partial^4 \Phi}{\partial x^4} + \frac{2\partial^4 \Phi}{\partial x^2 dy^2} + \frac{\partial^4 \Phi}{\partial y^4} = 0 \ . \qquad (C74)$$

The transverse stress component is

$$\sigma_y = \frac{\partial^2 \Phi}{\partial x^2} \ . \qquad (C75)$$

It should be mentioned that the stress function used to determine the spring constant requires certain boundary conditions at the end of the beam. This requirement is not fulfilled in an actual beam; therefore, there will be some disturbance at the very end. It is assumed herein that the disturbance is small and it will be neglected. For the boundary conditions shown in Figure C3a, the transverse stress is:

$$\sigma_y = \frac{3\sigma_1}{4bc^3} \left(\frac{-y^3}{3} + c^2 y + \frac{2}{3} c^3 \right). \qquad (C76)$$

Combining Equations (C76) and (C72),

$$\Delta = \frac{39}{48} \frac{\sigma_1 c}{bE} \ ; \qquad (C77)$$

therefore,

$$k = \frac{48}{39} \frac{bE}{c} = 1.23 \frac{bE}{c} \ . \qquad (C78)$$

For an element subjected to a uniform stress distribution on two faces as shown in Figure C3b, the numerical constant, 1.23, in Equation (C78) is reduced to unity. Thus, for the case of uniform boundary stress, k depends only on the modulus of elasticity and the geometry of the element.

C.4.2 Sinusoidal Stress Distribution

Now consider a pure sinusoidal stress distribution on the boundaries of the element as shown in Figure C4. Let Airy's stress function be

$$\Phi = f(y) \sin \alpha x \ , \qquad (C79)$$

where $\alpha = \frac{\pi}{\lambda}$ and f(y) is a function of y only.

Substitution of Equation (C79) into Equation (C74) gives

$$\alpha^4 f(y) - 2\alpha^2 f''(y) + f''''(y) = 0. \quad (C80)$$

The general solution of Equation (C80) is

$$f(y) = A_1 \cosh \alpha y + A_2 \sinh \alpha y + A_3 y \cosh \alpha y + A_4 y \sinh \alpha y . \quad (C81)$$

If the particular case of equal stress distribution on the two opposite faces of the element is considered, the solution for σ_y is

$$\sigma_y = \frac{2A_m}{b}\left[\frac{(\alpha c \cosh \alpha c + \sinh \alpha c)\cosh \alpha y - (\alpha y \sinh \alpha y \sinh \alpha c)}{\sinh 2\alpha c + 2\alpha c}\right]\sin\alpha x . \quad (C82)$$

Substituting Equation (C82) in Equation (C73) gives

$$\Delta = \left[\frac{4A_m \sinh^2 \alpha c}{\alpha b E(\sinh 2\alpha c + 2\alpha c)}\right]\sin\alpha x . \quad (C83)$$

value the spring constant for sinusoidal load is practically the same as for a uniform load.

The variation of Δ with c/λ is plotted in Figure C4. The spring constant k which is an inverse function of Δ is plotted in Figure C5. Up to $c = 0.5\lambda$, k is close to the spring constant for a uniform load. It can also be seen that as c increases, Δ approaches a constant, and the ratio of k for a sinusoidal stress distribution to that for a uniform distribution approaches infinity.

It is interesting to note that the value of c/λ of the sinusoidal terms in Equation (C71) is approximately 0.14 for a rectangular beam. At this

C.4.3 Exponential Stress Distribution

The value of the spring constant for an exponential distribution of the boundary stress is to be determined next. The distribution considered is shown in Figure C6.

Let Airy's stress function be

$$\Phi = f(y)\, e^{-ax} . \quad (C84)$$

Substitution of Equation (C84) into Equation (C74) gives

$$a^4 f(y) + 2a^2 f''(y) + f''''(y) = 0 . \quad (C85)$$

The general solution is

$$y = D_1 e^{iay} + D_2 e^{-iay} + D_3 y e^{iay} + D_4 y e^{-iay} . \quad (C86)$$

Converting into trigonometric functions and substituting into Equation (C84) gives

$$\Phi = (B_1 \cos ay + B_2\, ay \cos ay + B_3 \sin ay + B_4\, ay \sin ay)e^{-ax} . \quad (C87)$$

The boundary conditions are as shown in Figure C6 and give

$$\sigma_y = \frac{2Be^{-ax}}{b}\left[\frac{(\sin ac + ac \cos ac)\cos ay + (\sin ac)ay \sin ay}{\sin 2ac + 2ac}\right]. \quad (C88)$$

Using Equation (C73)

$$\Delta = \frac{4B}{baE} e^{-ax} \left[\frac{\sin^2 ac}{\sin 2ac + 2ac}\right]. \qquad (C89)$$

The variation of Δ with ac is shown in Figure C6. In Figure C7 the value of k for an exponential boundary stress distribution is compared with that for a uniform stress distribution. The range in the value of "ac" for the exponential term in Equation (C71) is close to the value of "ac" that is shown in Figure C7 for a rectangular beam. Within this range the spring constant for an exponential distribution of the boundary stress is close to that for a uniform boundary stress distribution.

C.4.4 The Spring Constant

The exponential term in Equation (C71) is so dominant that the value of k in Figure C7 is a good approximation for the function described in Equation (C71). The final spring constant, k, which represents the total spring effect is:

$$\frac{1}{k} = \frac{1}{k_b} + \frac{1}{k_m}, \qquad (C90)$$

where k_b and k_m refer to the spring stiffnesses for the lower and middle parts of the analog.

The variation of the total spring stiffness with the ratio of the height of the reference plane to the height of the beam is given in Figure C8. It can be concluded that the spring constant can be considered as equal to that for a uniform load as long as the middle part of the analog is smaller than the lower part. As the lower part of the analog increases in excess of the mid-part, the spring constant increases rapidly. In plotting Figure C8 it was assumed that for small ratios of h_b/h the total spring stiffness could not exceed k_b.

The above discussion refers to rectangular beams. In fact, only the part between the centroids of the lower and middle parts of the analog are of importance for the spring constant. If these portions are rectangular, the equations derived above are applicable. Therefore, ordinary I-, T-, and inverted T-beams may be included. The "a" and "g" lines shown in Figures C5 and C7 for a rectangular beam would be moved to the left for I- and inverted T-beams. Thus, the value of k found for rectangular beams can be applied to beams with other cross sections if it is written as follows:

$$k = \frac{b_{eq} E}{c}, \qquad (C91)$$

where b_{eq} is the average width of the beam over the distance c, and c is the distance from the reference plane to the centroid of the section below the reference plane. The term b_{eq} may be found by assuming that the stress spreads out at a 45-degree angle at a change in section.

C.5 DISTRIBUTION OF SHEAR ALONG THE REFERENCE PLANE

The solution of the shear problem involves the use of infinite series or finite differences as in the solutions by Guyon,[15] Bleich,[3] Schleeh,[40]

and Gergely.[12] Although such solutions are interesting in themselves, they are tedious and are not practical to use in the case of the physical analog. For the physical analog it is sufficient to replace the shear stress on the reference plane with an equivalent force acting at some distance from the end of the beam.

Consider the section of the anchorage zone shown in Figure 45. From St. Venant's principle it is assumed that a linear longitudinal stress distribution exists at approximately a distance equal to h from the end of the beam. The sum of the shear forces on the reference plane can be found by considering a free body of a section below the reference plane. The total shear is:

$$V = \int_0^h \tau_{xy}\, b\, dx = P - \int_0^{\frac{h}{2}} \sigma_x\, b\, dx \,. \quad (C92)$$

The distribution of τ_{xy} is not known from the free body. However, it may be investigated with the use of the solution by Guyon. The centroid of the shear stresses on a longitudinal plane lie approximately on a line that intersects the end face at a 45-degree angle. Thus, if the reference plane is close to the applied load, it is a good approximation to consider the total shear force to be concentrated at the end of the beam. This will always be the case for bursting stresses.

Spalling stresses always occur some distance away from the applied load. Thus, the resultant shear force acts at some finite distance from the beam end and has less effect on the physical analog than a shear force concentrated at the very end. For a single applied load, however, it is on the safe side to assume that the shear force acts at the end of the beam.

If more than one load is applied, the influence of the shear forces from the distant loads must be considered in the calculation of both bursting and spalling stresses. The shear effect is small if the distant load is farther than h_b from the reference plane. Lenschow suggests that the shear force be modified to V_m where:

$$V_m = V \text{ for } y_v \leq \frac{h_b}{3} \quad (C93)$$

and

$$V_m = \frac{V\, h_b}{3\, y_v} \text{ for } y_v > \frac{h_b}{3} \,. \quad (C94)$$

The term y_v is the distance from the load to the reference plane.

IX. REFERENCES

1. P. D. Arthur and S. Ganguli, "Tests on End-Zone Stresses in Pretensioned Concrete I-Beams," *Magazine of Concrete Research*, Vol. 17, No. 51 (June, 1965).

2. S. Ban, H. Muguruma, and Z. Ogaki, "Anchorage Zone Stress Distribution in Post-Tensioned Concrete Members," *Proceedings, World Conference on Prestressed Concrete*, San Francisco, 1957.

3. F. Bleich, "Der gerade Stab mit Rechteckquerschnitt als ebenes Problem," *Der Bauingenieur*, Nos. 9 and 10, 1923.

4. S. P. Christodoulides, "A Two-dimensional Investigation of the End Anchorages of Post-Tensioned Concrete Beams," *The Structural Engineer*, Vol. 33 (1955).

5. _____, "The Distribution of Stresses Around the End Anchorages of Prestressed Concrete Beams," *International Association for Bridge and Structural Engineering, Publications*, Vol. 16 (1956).

6. _____, "Three-dimensional Investigation of Anchorage Zone Stresses," *The Structural Engineer*, Vol. 35 (1957).

7. A. Dodge, Discussion of a paper by P. K. Som and K. Ghosh, *Journal of the Structural Division*, ASCE, Vol. 91, No. ST2 (1965).

8. D. J. Douglas and N. S. Trahair, "An Examination of the Stresses in the Anchorage Zone of a Post-Tensioned Prestressed Concrete Beam," *Magazine of Concrete Research*, Vol. 12, No. 34 (March, 1960).

9. J. Fadle, "Die Selbstspannungs—Eigenwerfunktionen der quadratischen Scheibe," *Ingenieur-Archiv*, Vol. 11 (1940).

10. R. S. Fountain, "A Field Inspection of Prestressed Concrete Bridges," Structural Bureau, Portland Cement Association, 1963.

11. L. Garay, "Research on Prestressed Load-Bearing Structures in the Hungarian Scientific Institute for Structural Engineering," *Fourth Congress of the F.I.P.*, Rome-Naples, 1962, Vol. 1, Theme III.

12. P. Gergely, M. A. Sozen, and C. P. Siess, "The Effect of Reinforcement on Anchorage Zone Cracks in Prestressed Concrete Members," *Structural Research Series* No. 271, University of Illinois, 1963.

13. R. W. Gerstner and O. C. Zienkiewicz, "A Note on Anchorage Zone Stresses," *Journal of the ACI*, Vol. 59, (July, 1962).

14. Y. Guyon, "Contraintes dans les Pieces prismatiques soumises à des Forces appliquées sur leurs Bases, au Voisinage de ces Bases," *International Association for Bridge and Structural Engineering, Publications*, Vol. 11 (1951).

15. _____, *Prestressed Concrete*. 1st Ed. New York: John Wiley & Sons, Inc., 1953.

16. D. E. Halsted, "Precast and Prestressed -- But Not Permanent," *Civil Engineering Magazine* (August, 1963).

17. N. M. Hawkins, V. Srinivasagopalan, and M. A. Sozen, " Anchorage Zone Stresses in Prestressed Concrete Beams," *Structural Research Series* No. 207, University of Illinois, 1960.

18. R. Hiltscher and G. Florin, "Die Spaltzugkraft in einseitig eingespannten, am gegenüberliegenden Rande belasteten rechteckigen Schieben," *Die Bautechnik*, No. 10 (1962).

19. _____, "Spalt- und Abreisszugspannungen in rechteckigen Scheiben, die durch eine Last in verschiedenem Abstand von einer Scheibenecke belastet sind," *Die Bautechnik*, Vol. 40 No. 12 (1963).

20. T. Huang, "A Study of Stresses in End Blocks of Post-Tensioned Prestressed Beams," Thesis, University of Michigan, 1961.

21. _____, "Stresses in End Blocks of Post-Tensioned Prestressed Beam," *Proceedings, ACI*, Vol. 61 (1964).

22. K. T. Iyengar, "Two-dimensional Theories of Anchorage Zone Stresses in Post-Tensioned Beams," *Proceedings, ACI*, Vol. 59 (1962).

23. L. B. Kriz and C. H. Raths, "Connections in Precast Concrete Structures - Bearing Strength of Column Heads," *Journal of the Prestressed Concrete Institute*, Vol. 8, No. 6 (1963). Also PCA *Development Department Bulletin D73*.

24. R. J. Lenschow and M. A. Sozen, "Practical Analysis of the Anchorage Zone Problem in Prestressed Beams," *Proceedings, ACI*, Vol. 69 (1965).

25. G. Magnel, "Design of the Ends of Prestressed Concrete Beams," *Concrete and Constructional Engineering*, Vol. 44 (1949).

26. K. D. Mahajan, "Analysis of Stresses in a Prestressed Beam Using Araldite Models," *Indian Construction News* (August, 1958).

27. W. T. Marshall, "A Theory for End Zone Stresses in Pretensioned Concrete Beams," *Journal of the Prestressed Concrete Institute*, Vol. 11, No. 2 (April, 1966).

28. W. T. Marshall and A. H. Mattock, "Control of Horizontal Cracking in the Ends of Pretensioned Prestressed Concrete Girders," *Journal of the Prestressed Concrete Institute*, Vol. 7, No. 5 (1962). Also PCA *Development Department Bulletin D58*.

29. D. I. McNeely and S. D. Lash, "Tensile Strength of Concrete," *Proceedings, ACI*, Vol. 60 (1963).

30. K. H. Middendorf, "Practical Aspects of End Zone Bearing of Post-Tensioning Tendons," *Journal of the Prestressed Concrete Institute*, Vol. 8, No. 4 (1963).

31. E. Morsch, "Über die Berechnung der Gelenkquader," *Beton und Eisen*, No. 12 (1924).

32. G. S. Ramaswamy and H. Goel, "Stresses in End Blocks of Prestressed Beams by Lattice Analogy," *Proceedings, World Conference on Prestressed Concrete*, San Francisco, 1957.

33. E. E. Reis, Jr., J. D. Mozer, A. C. Bianchini, and C. E. Kesler, "Causes and Control of Cracking in Concrete Reinforced with High Strength Steel Bars -- A Review of Research," *T. & A. M. Report* No. 261, University of Illinois (1964).

34. A. D. Ross, "Some Problems in Concrete Construction," *Magazine of Concrete Research*, Vol. 12 (1960).

35. R. E. Rowe, "Endblock Stresses in Post-Tensioned Concrete Beams," *Structural Engineer*, Vol. 41, No. 2 (February, 1963).

36. H. Rusch and H. Hilsdorf, "Verformungseigenschaften von Beton unter zentrischen Zugspannungen," *Building Materials Testing Laboratory, Technical University of Munich*, Report No. 44 (1963).

37. H. Rusch and G. Rehm, "Versuche zur Bestimmung der Übertragungslänge von Spannstählen," *Deutscher Ausschuss für Stahlbeton*, Berlin No. 147 (1963).

38. M. Sargious, "Beitrag zur Ermittlung der Hauptzugspannungen am Endauflager vorgespannter Betonbalken," Thesis, Technische Hochschule, Stuttgart, 1960.

39. _____, Hauptzugkräfte am Endauflager vorgespannter Betonbalken," *Die Bautechnik*, Vol. 38, No. 3 (1961).

40. W. Schleeh, "Die Spannungszustände beim Auflager eines Spannbetonträgers," *Beton und Stahlbetonbau*, Berlin, Vol. 58, No. 7 (July, 1963).

41. H. Sievers, "Die Berechnung von Auflagerbänken und Auflagerquadern von Brückenpfeilern," *Der Bauingenieur*, Vol. 27 (1952).

42. _____, "Über den Spannungszustand im Bereich der Ankerplatten von Spanngliedern vorgespannter Stahlbetonkonstruktionen," *Der Bauingieur*, Vol. 31 (1956).

43. P. K. Som and K. Ghosh, "Anchor Zone Stresses in Prestressed Concrete Beams," *Journal of the Structural Division*, ASCE, Vol. 90 (August, 1964).

44. V. Srinivasagopalan, "An Investigation of the Anchorage Zone Stresses in Post-Tensioned Prestressed Concrete Beams," Thesis, Indian Institute of Technology, Kharagpur, India.

45. S. Timoshenko and J. N. Goodier, *Theory of Elasticity*. 2nd Ed. New York: McGraw-Hill Book Co., Inc., 1951.

46. G. E. Troxell and H. E. Davis, *Composition and Properties of Concrete*. New York: McGraw-Hill Book Co., Inc., 1956.

47. J. Zielinski and R. E. Rowe, "An Investigation of the Stress Distribution in the Anchorage Zones of Post-Tensioned Concrete Members," Cement and Concrete Association, Research Report 9, 1960.

48. _____, "The Stress Distribution Associated with Groups of Anchorages in Post-Tensioned Concrete Members," Cement and Concrete Association, Research Report 13, 1962.

This page is intentionally blank.

PUBLICATIONS OF THE COLLEGE OF ENGINEERING

Bulletins from the University of Illinois College of Engineering are detailed reports of research results, seminar proceedings, and literature searches. They are carefully reviewed before publication by authorities in the field to which the material pertains, and they are distributed to major engineering libraries throughout the world. They are available at a charge approximately equal to the cost of production.

The annual *Summary of Engineering Research* is available in the fall of each year. It contains a short report on every research project conducted in the College during the past fiscal year, including the names of the researchers and the publications that have resulted from their work.

Engineering Outlook, the College's monthly newsletter, contains short articles about current happenings, new research results, recent technical publications, and educational practices in the College of Engineering. Free subscriptions are available upon request.

The Seminar and Discussion Calendar, which is published and distributed weekly, lists current meetings, lectures, and other events on the engineering campus that are open to the public. Free subscriptions are available upon request.

Requests for a catalog of available technical bulletins or for any of the above publications should be addressed to the Engineering Publications Office, College of Engineering, University of Illinois, Urbana, Illinois 61801.

OTHER PUBLICATIONS IN RELATED FIELDS BY THE ENGINEERING EXPERIMENT STATION

Bulletin 452. *Investigation of Prestressed Concrete for Highway Bridges, Part I: Strength in Shear of Beams Without Web Reinforcement,* by M. A. Sozen, E. M. Zwoyer, and C. P. Siess. 1959. $1.00.

Bulletin 463. *Investigation of Prestressed Concrete for Highway Bridges, Part II: Analytical Studies of Relations Among Various Design Criteria for Prestressed Concrete,* by N. Khachaturian, I. Ali, and L. T. Thorpe. 1962. $1.00.

Bulletin 464. *Investigation of Prestressed Reinforced Concrete for Highway Bridges, Part III: Strength and Behavior in Flexure of Prestressed Concrete Beams,* by J. Warwaruk, M. A. Sozen, and C. P. Siess. 1962. $2.00.

Bulletin 493. *Investigation of Prestressed Reinforced Concrete for Highway Bridges, Part IV: Strength in Shear of Beams with Web Reinforcement,* by S. Ø. Olesen, M. A. Sozen, and C. P. Siess. 1967. $3.00.

These publications are available from:

Engineering Publications Office
112 Engineering Hall
University of Illinois
Urbana, Illinois 61801